BioMed Research International

# ECM-Like Scaffolds: Nature Drives Research

Guest Editors: Costantino Del Gaudio, Silvia Baiguera, Alessandra Bianco, and Luca Urbani

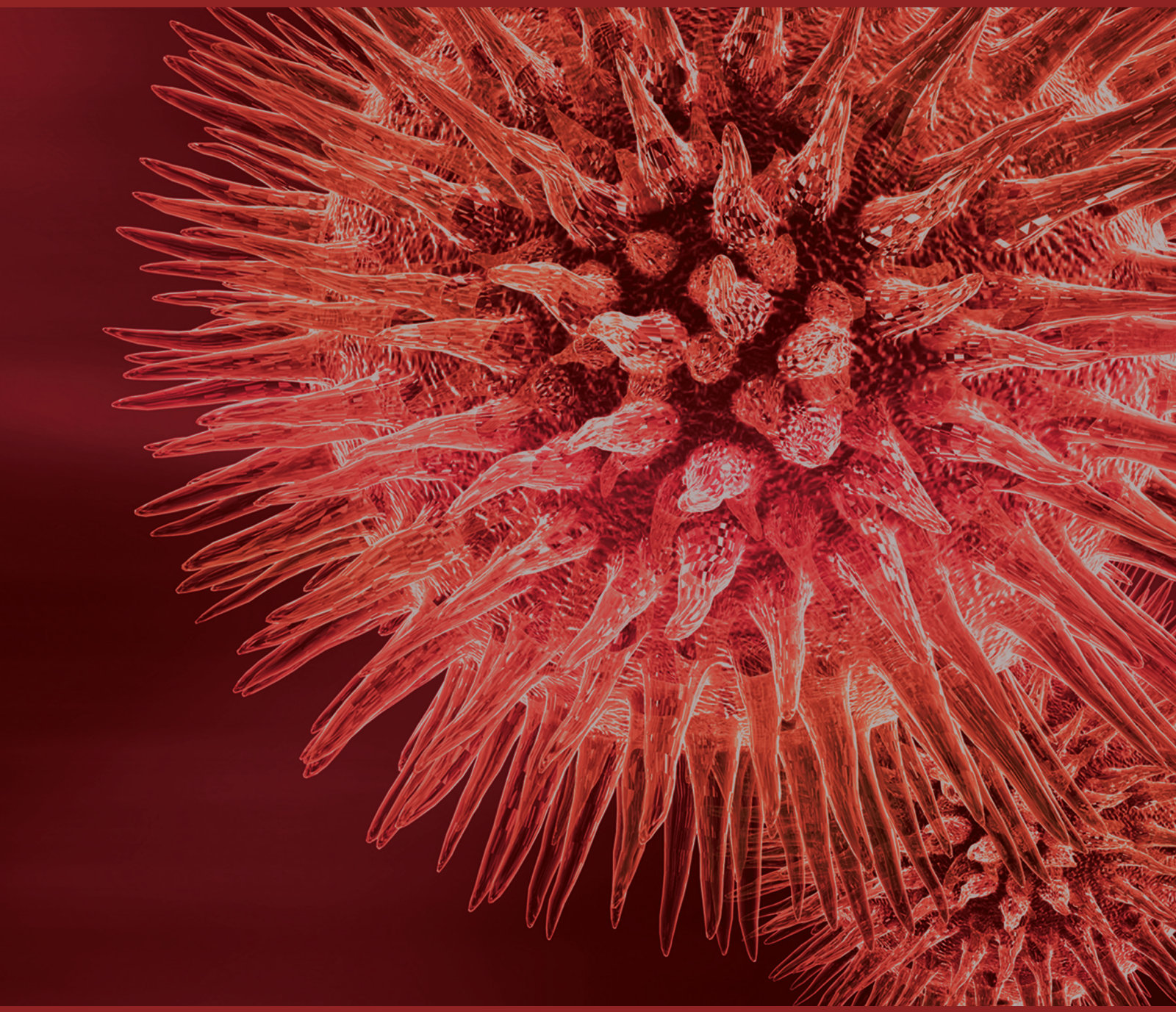

# ECM-Like Scaffolds: Nature Drives Research

BioMed Research International

# ECM-Like Scaffolds: Nature Drives Research

Guest Editors: Costantino Del Gaudio, Silvia Baiguera, Alessandra Bianco, and Luca Urbani

# Contents

Hindawi Publishing Corporation
BioMed Research International
Volume 2014, Article ID 298361, 2 pages
http://dx.doi.org/10.1155/2014/298361

# *Editorial*
# ECM-Like Scaffolds: Nature Drives Research

**Costantino Del Gaudio,[1] Silvia Baiguera,[2] Alessandra Bianco,[1] and Luca Urbani[3]**

[1]*Department of Enterprise Engineering, Intrauniversitary Consortium for Material Science and Technology (INSTM), Research Unit "Tor Vergata", University of Rome "Tor Vergata", Via del Politecnico 1, 00133 Rome, Italy*
[2]*INAIL-DIPIA, Via Alessandria 220E, 00198 Rome, Italy*
[3]*Surgery Unit, Institute of Child Health and Great Ormond Street Hospital, University College London, 30 Guilford Street, London WC1N 1EH, UK*

Correspondence should be addressed to Costantino Del Gaudio; costantino.delgaudio@uniroma2.it

Received 11 September 2014; Accepted 11 September 2014; Published 28 December 2014



The development of an *ad hoc* scaffold for effective tissue engineering applications plays a pivotal role in promoting and support the healing process. For this aim, an accurate morphological, biochemical, and mechanical replication of the tissue-specific extracellular matrix (ECM) to be regenerated can contribute to elicit a positive cell response, tissue formation and, therefore, a proper host integration after implantation. To further enhance this expected result, several technical strategies can be usefully planned, including innovative fabrication techniques, surface modification, incorporation of specific fillers, and/or addition of drugs or growth factors to be subsequently released to speed up the autologous tissue regeneration.

This special issue presents both original research and review articles aimed to investigate and underline the crucial role of an ECM-like scaffold. In order to present an overview on the *in vivo* results collected so far, according to tissue engineering guidelines, S. Baiguera et al. focused on the analysis of implanted orthotopic organ substitutes. Different clinical fields were considered, highlighting limitations and promising approaches when properly prepared scaffolds were used. M. G. de Morais et al. reviewed the potential role of *Spirulina*, a prokaryotic microalga, as a specific element to be included into electrospun polymeric fibers to mimic the architecture of natural ECM. A key topic for an effective tissue regeneration was considered by A. Neve et al., emphasizing the role played by ECM in the regulation of the angiogenic process. This is a well-known issue to be addressed in order to deal with a suitable tissue engineered construct, and the proposed review also shows that ECM molecules and fragments, resulting from proteolysis, can act directly as inflammatory stimuli and contribute to exacerbated angiogenesis.

Original research studies demonstrate the influence of natural cues for the fabrication of tailored constructs. E. Stocco et al. propose a hybrid scaffold made of polyvinyl alcohol hydrogel and ECM to promote cartilage regeneration. Similarly, H. Fan et al. combined human-like collagen and nanohydroxyapatite to fabricate a specific scaffold for bone tissue engineering. Both the approaches show that a scaffold not only is a "simple" (passive) structural support but plays an active part in the healing process, supporting cell adhesion, migration, and proliferation by means of different signalling cues. More directly, L. Dall'Olmo et al. address the relevant issue to fabricate functional small-diameter vascular grafts, evaluating the potential of decellularized rat iliac arteries. *In vivo* investigation led to unsatisfactory results since the lack of endothelial cells contributed to thrombus formation and intimal proliferation. Once again, this study supports the need (i) to deeply analyse the properties of the biomaterial to be used for tissue engineering scaffolding and (ii) to understand that several factors concur to a positive outcome.

Interestingly, two papers focus on the analysis of the morphological/structural properties of human trabecular bone tissue (F. Marinozzi et al.) and composite scaffolds made of chitosan/gelatin blend and bioactive glasses for bone tissue engineering (D. Massai et al.). The proposed studies can contribute to better investigate local features of ECM and,

therefore, to design biomimetic porous ECM-like scaffolds that resemble the tissue of interest.

Tissue engineering can positively improve clinical treatments, but the expected outcome is strictly dependent on the strategy to be adopted. The present special issue aims to underline this crucial aspect and, thanks to the authors participating in this project, we hope to offer a sound basis to enhance regenerative protocols.

*Costantino Del Gaudio*
*Silvia Baiguera*
*Alessandra Bianco*
*Luca Urbani*

Hindawi Publishing Corporation
BioMed Research International
Volume 2014, Article ID 398069, 27 pages
http://dx.doi.org/10.1155/2014/398069

*Review Article*

# Tissue Engineered Scaffolds for an Effective Healing and Regeneration: Reviewing Orthotopic Studies

**Silvia Baiguera,[1] Luca Urbani,[2] and Costantino Del Gaudio[3]**

[1] *INAIL-DIPIA, Via Alessandria 220E, 00198 Rome, Italy*
[2] *Surgery Unit, Institute of Child Health and Great Ormond Street Hospital, University College London, 30 Guilford Street, London WC1N 1EH, UK*
[3] *University of Rome "Tor Vergata", Department of Enterprise Engineering, Intrauniversitary Consortium for Material Science and Technology (INSTM), Research Unit "Tor Vergata", Via del Politecnico 1, 00133 Rome, Italy*

Correspondence should be addressed to Costantino Del Gaudio; costantino.delgaudio@uniroma2.it

Received 18 March 2014; Accepted 22 July 2014; Published 27 August 2014

Academic Editor: Alessandra Bianco



It is commonly stated that tissue engineering is the most promising approach to treat or replace failing tissues/organs. For this aim, a specific strategy should be planned including proper selection of biomaterials, fabrication techniques, cell lines, and signaling cues. A great effort has been pursued to develop suitable scaffolds for the restoration of a variety of tissues and a huge number of protocols ranging from *in vitro* to *in vivo* studies, the latter further differentiating into several procedures depending on the type of implantation (i.e., subcutaneous or orthotopic) and the model adopted (i.e., animal or human), have been developed. All together, the published reports demonstrate that the proposed tissue engineering approaches spread toward multiple directions. The critical review of this scenario might suggest, at the same time, that a limited number of studies gave a real improvement to the field, especially referring to *in vivo* investigations. In this regard, the present paper aims to review the results of *in vivo* tissue engineering experimentations, focusing on the role of the scaffold and its specificity with respect to the tissue to be regenerated, in order to verify whether an extracellular matrix-like device, as usually stated, could promote an expected positive outcome.

## 1. Introduction

A simple search on the PubMed website using the key "scaffold tissue engineering" gave 8948 results (July, 2014), the first two papers being published in 1993, characterized by a linear-like distribution starting from the year 2000 (Figure 1). This occurrence suggests that, after an initial pioneering period, tissue engineering has been rapidly developed as an emerging research field with relevant implications for the enhancement of clinical treatments and the improvement of quality of life of a patient. Clearly, this can be considered a rough and not targeted bibliographic research that can be surely refined in order to highlight subtle and specific aspects related to this innovative and promising multidisciplinary approach, but it can give an idea, at the same time, of the great effort in the field. Now, after 20 years, a critical consideration about the overall findings collected so far can support the questions "where are we now?" and "have we enough information to move toward this or that direction?". We hope to have a preliminary answer at the end of this review, since a definitive one would be unreasonable. For this aim, the present review focuses on the role of the scaffold in tissue engineering to be considered not just as a passive support for cell seeding but as an active platform that can effectively contribute to tissue regeneration and host integration. It is usually stated that such a scaffold should mimic the natural ECM of the tissue to be healed, but what this exactly means is the objective of this paper and, therefore, we will try to furnish a critical review of the literature data. One of the great expectations from tissue engineering is the potential to develop functional organs to overcome the current limitations related to the shortage of donor organs, incompatibility problems, and the detrimental effects of long-term use of immunosuppressive drugs after transplantation [1, 2]. The technical approach to address this issue is summarized into the well-known tissue engineering paradigm [3], and one of its key points specifically focuses

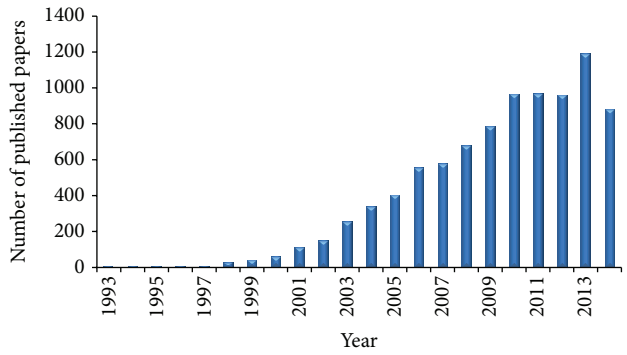


Figure 1: Timeline of published papers (number per year) from the PubMed website using the key "scaffold tissue engineering" (updated to July, 2014).

on the definition of a viable and instructive scaffold for cell seeding, proliferation, migration, and differentiation in the case of stem cells. This statement implies a careful selection of: (i) the material(s) for scaffold fabrication, either synthetic or naturally derived, (ii) the most suitable technique that allows to deal with a substrate morphologically and mechanically similar to the ECM to be replaced, thus avoiding any mismatch with the surrounding tissue, (iii) possible surface treatments that can confer a positive biochemical profile to elicit a significant biological response, and (iv) drugs and/or growth factors to be loaded into the scaffold and subsequently released to enhance the final performance, avoiding, for instance, any side effect that can limit the therapeutic efficacy, for example, prevention of platelet adhesion on the luminal surface of tissue engineered vascular grafts [4].

Reasonably, due to the wide range to be covered and in order to furnish a clear scenario of the potential of a proper scaffold for tissue engineering applications, the main inclusion (or exclusion) criteria that led to the paper selection, here critically presented, were strictly related to the *in vivo* studies, preferentially focusing on orthotopic implantations. The rationale for this choice is expected to underline the findings that have already demonstrated promising results for the clinical translation of the tissue engineering approach. To provide a comprehensive survey on the topic, this review will firstly introduce a section on the common features of the ECM. Thereafter, currently investigated tissue engineered approaches, reporting only *in vivo* experimentations on tissue/organ and focusing on the properties of the scaffolds involved in the healing process, will be presented. Finally, a general discussion will resume the results with the aim to identify, if possible, the most promising strategies that can prompt an effective clinical translation.

## 2. The Extracellular Matrix: A Model for Tissue Engineered Scaffolds?

The ECM is the basic microstructure of each tissue and organ. It is usually referred to as one of the pivotal elements when a reliable tissue engineering strategy is needed. This relies on the fact that the replication of its specificity represents a key factor for the development of a scaffold that could provide a suitable microenvironment for a functional physioanatomic district to substitute the failing one.

The ECM functions as a structural as well as a signaling scaffold for cells, influencing cell behavior in terms of differentiation, proliferation, survival, and migration. It is a heterogeneous composition of proteoglycans, proteins, and signaling molecules. Structural proteins, such as collagen, elastin, and reticular fibers, are organized in an interwoven network of fibers and fibrils and provide architectural rigidity and mechanical support [5]. This fibrous architecture has also an important role in mechanotransduction: it deforms viscoelastically to external and internal stresses allowing cells to respond to mechanical stresses [6]. The ECM nonfibrous components, mostly glycosaminoglycans, regulate turgor pressure, form intimate intracellular connections, and modulate the binding sites and activity of growth factors, acting also as a local factor reservoir [7]. The composition dictates matrix stiffness and rigidity (affecting cell differentiation, migration, and proliferation), permeability (affecting nutrient diffusion to tissues and cell function), and cell-matrix interactions (affecting cell adhesion and proliferation) [8].

The ECM spatial arrangement, composition, and interaction with cells and growth factors are tissue- and function-specific. The epithelial ECM, for example, is minimal (only the basement membrane), on the contrary of connective tissues, characterized by an abundant ECM, while bone ECM consists mostly of collagen type I structural proteins, apatite mineral and noncollagenous proteins, such as osteocalcin, fibronectin, and vitronectin [9]. As a consequence, tissue peculiar characteristics, defining the unique biochemical, biomechanical, and structural profile, should be the goal to be achieved when defining a tissue engineered scaffold. For this aim several cues concur, which can be summarily classified into (i) internal ones, for example, the type and ratio of the "materials" that constitute that particular ECM, the hierarchical structure, the morphology and stiffness, and the signalling cascade between cells and extracellular environment, and (ii) external ones, being, for instance, dependent on the mechanical load exerted for a specific function, for example, muscle contractility/distensibility for food propelling within esophagus, bladder distension, or heart activity.

The advantage of using natural scaffolds from innate organs allows to deal with substrates characterized by tissue-specific biochemistry (proteins and polysaccharides) and structural architecture, an intact and patent vasculature, and the presence of growth factors able to drive progenitor cell differentiation into organ-specific phenotypes [2]. In order to obtain a suitable ECM-like natural scaffold, the tissue should be preliminarily subjected to a decellularization process aimed to avoid any immunological response after implantation. However, it should be carefully considered that even if this strategy seems to be straightforward, the influence of the decellularization protocol adopted can harshly affect the final result leading to a structure that does not retain anymore the expected cues, specially the mechanical ones. Besides, the main limitation of native-derived scaffold is related to the shortage of cadaveric donor organs, which may significantly

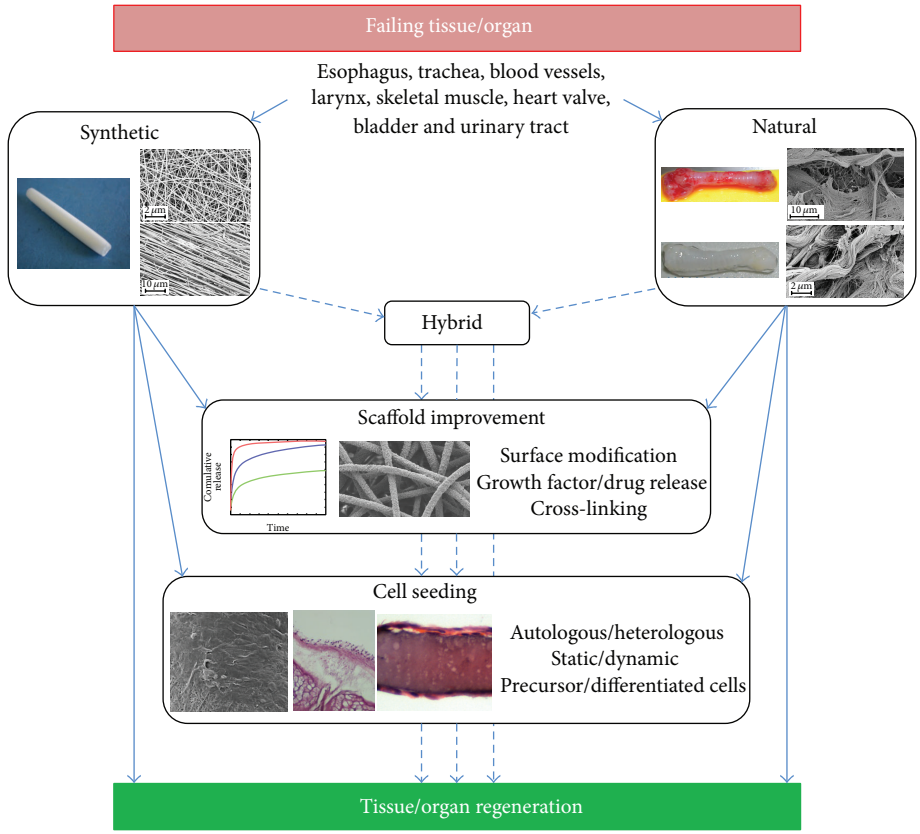


Figure 2: Strategies to develop a functional tissue engineered substitute for regeneration of failing tissues and organs. Synthetic, natural, or hybrid scaffolds can be treated to improve their features and performances, seeded with different cells types before implantation or directly *in vivo* implanted after the fabrication procedure.

delay the obtainment of biological substitutes and increase patients' waiting time [10]. In order to overcome these limitations, an alternative route has been developed based on the use of synthetic scaffolds. Reasonably, the need for a donor is eliminated, and scaffold dimensions and shape can be tailored to fit the anatomy of the recipient due to intrinsic possibility to deal with a number of fabrication techniques and to select the most appropriate one [11]. Obviously, materials must be biocompatible, nontoxic, nonimmunogenic, and noncarcinogenic, should facilitate cellular adhesion, proliferation, organization, and differentiation, should be characterized by a suitable degradation rate and resist bacterial colonization [12]. It should be underlined that the ideal material, to be modelled into the specific organ to be regenerated, is still to come, as a single material can hardly recapitulate all the needed characteristics. An integrated strategy including possible postfabrication treatments and addition of fillers or drugs/growth factors for a subsequent release can be a desirable option. Figure 2 summarizes possible strategies that can be considered for this aim, but at the same time this is only a macroscopic point of view since a detailed study of the tissue-specific ECM is necessary, especially referring to the intrinsic hierarchical nature. Clearly, the structure is strictly related to the final function and, in this regard, a nanoscale investigation of the characteristics composing each tissue can support the development of suitable scaffolds. As reported by Kim et al. [13], nanostructures in the human body can be classified into four categories dependent on the physiological environment: protective tissue (skin), mechanosensitive tissues (bone, ligament/tendon), electroactive tissues (neuron, skeletal muscle, and heart), and shear stress-sensitive tissue (blood vessel). This directly implies that the resulting mechanical properties play a crucial role in the expected tissue healing and regeneration, as rigidity can span in a wide range from few kPa to tens of GPa [14]. However, other features should be included when an ad hoc ECM-like scaffold has to be prepared. Metabolic activity is mainly based on a diffusion process of nutrients and removal of waste products and this is affected by porosity and permeability of the three-dimensional architecture; for instance, oxygen diffusion is limited to about 100 $\mu$m from a blood vessel. In addition, cell-matrix interaction plays a pivotal role in the definition of the typical ECM dynamical environment, being related to its degradation that changes the local modulus, decreases the number of cell-matrix adhesion sites, and results in ECM fragments that may possess biological activity [8].

In this context, a critical review of the *in vivo* tissue engineering results collected so far can elucidate the role of an ECM-like scaffold, to be indented not only as a three-dimensional architecture to accommodate cells, but also as

a complex and dynamic mixture of factors that concur to the expected target.

## 3. Tissue Engineered Orthotopic Approaches

In the last few years, there has been considerable progress in the clinical translation of tissue engineered organs, obtained using natural or synthetic scaffolds, repopulated with terminally differentiated cells or stem cells [15–21]. However, no gold standard strategy has been till now developed, possibly in relation to the fact that even "simple" organs, devoted only to transport functions (e.g., air, food, and liquids), represent a challenge.

The past strategies conducted to identify the ideal substitute for different organ/tissue will be here reported. As a guideline, Table 1 summarizes each biological district here considered in terms of (i) function, microstructure, histological features, and (ii) requirements that an ideal scaffold should provide. In order to understand which is the current real state of the art of the tissue engineering approach, the review will focus only on the most recent studies associated with relevant preclinical and clinical applications of natural and synthetic scaffolds.

## 4. Trachea

Being a relatively simple and hollow organ, the trachea was the ideal starting point for evaluating the possibility to obtain clinical relevant respiratory organ engineering. For more than 50 years, several approaches have been pursued to reconstruct the airways when conventional surgical approaches were unsuitable; however, the resulting clinical outcome was inconsistent, incomplete, and controversial [22, 23]. Most of the evaluated tissue engineering strategies resulted to be suitable only as patches for small airway repairs and were unable to resist collapse when used for whole long-segment (>6 cm) airway applications [24]. As a consequence, herein only the approaches focusing on tubular (for long circumferential defects) or trachea-like (bifurcated) scaffolds applied in preclinical and clinical studies will be reported.

### 4.1. Preclinical Studies

*4.1.1. Natural Approach.* Different approaches have been tried to decellularize native airway; however a functional tissue engineered substitute has not been developed, due mainly to the decellularization protocol used, which, causing damage and/or disruption to ECM components, compromised the ability of the scaffold to provide mechanical support during the remodeling process [25–29]. Recently a detergent-enzymatic method (DEM), originally developed for the isolation of basement membranes from several tissues [30], has been modified and applied to animal airways. Bioengineered tracheal matrices with ultrastructure and physical properties similar to native tissue [31, 32], able to support *in vitro* adhesion of auricular chondrocytes and tracheal epithelial cells [33] and not to elicit any rejection response, were obtained [31]. Decellularized rabbit tracheas, obtained using DEM approach and preseeded both statically and dynamically with ovine amniotic MSCs, have been implanted into fetal lambs (9 to 12 tracheal rings) [34]. At retrieval, all the implants were characterized by variable degree of stenosis, but the engineered constructs showed full epithelialization, increased levels of $\alpha$-elastin and collagen, and decreased GAG content pre- and postoperatively. The latter occurrence, as stated by the authors, was ascribed to the fact that cells were exposed to chondrogenic medium for 7 days before implantation, but GAG accumulation does not begin until the second or third week.

Porcine trachea matrices, decellularized by DEM, intraoperatively seeded with mononuclear cells (external surface) and epithelial cells (internal surface), and conditioned with a boosting factor treatment (transforming growth factor-$\beta$3, erythropoietin, and granulocyte colony stimulating factor), were tested in a porcine model. After 2 months, the implanted graft, even if not fully covered by cells, showed nearly native anatomic architecture and morphology [35].

*4.1.2. Synthetic Approach.* Tubular high density polypropylene (20 mm in length and 8 mm in diameter) or PLA/PGA fiber (15 mm in length and 6 mm in diameter) scaffolds, preseeded with chondrocytes, allowed the formation of cartilaginous-like tissue with native-like biomechanical properties and mitigated the inflammatory reaction [36, 37]. Using both nasal septal chondrocytes and fibroblasts, PGA scaffolds, wrapped around silicon helical tube, have been implanted in mice ($30 \times 40 \times 2$ mm) or in sheep (50 mm in length and 20 mm in diameter) [38, 39]. Tissue morphology and composition resulted to be similar to native tracheal tissue, even if the implanted constructs collapsed and tracheomalacia was observed in sheep after anastomosis [38]. A straight *Dacron* prosthesis, reinforced with spiral-shaped polypropylene monofilaments, has been firstly implanted subcutaneously into rabbits, to allow the infiltration of blood vessels and connective tissue, and then was vertically opened and conditioned, on the inner surface, with tracheal epithelial cell sheets. The resulting bioartificial trachea was implanted (3 cm length): after 1 month a mature columnar epithelium was revealed in the interior graft portions, highlighting the importance of a functional epithelium lining the lumen of a prosthetic trachea [40].

Being a polymer with a slow degradation profile and mechanical characteristics potentially able to maintain the long-term patency, PCL has been widely used to develop tracheal prosthesis. Highly porous (pore size 10–40 $\mu$m) hollow PCL tubular scaffolds, implanted in rabbits, were covered with epithelial cells, but animals died due to stenosis after 30 days from implantation. The same scaffolds, coated in the luminal surface with gelatin crosslinked with genipin, allowed a longer animal survival (43 days) and prevented the granulation tissue overgrowth. However, an epithelial lining was not revealed and the ingrowth of granulation tissue from the anastomotic sites into the lumen leads eventually to occlusion occurrences [41]. The same material was used to fabricate a scaffold (2 cm long) to be seeded with chondrocytes and bone marrow stem cells and implanted into

Table 1: Function and macroscopic structure of tissues and organs here considered, along with histological features and expected characteristics that an ideal tissue engineered substitute should provide for regeneration.

| Organ | Function | Structure | Histological features | Ideal scaffold properties |
|---|---|---|---|---|
| Trachea | Conduction of air from the nose or mouth to the lungs | Thin-walled, fibromuscular, airtight tube supported by C-shaped, cartilaginous rings, spans by the pars membranacea (fibroelastic ligament).<br>At its distal end, it bifurcates into the two main stem bronchi. | (i) Cartilaginous structure prevents collapse during respiration, provides flexibility, assures lumen patency;<br>(ii) muscular tissue reduces lumen size during the cough reflex, facilitates airway clearance;<br>(iii) mucosal membrane allows air conditioning, prevents epithelium dehydration | (i) lateral rigidity<br>(ii) longitudinal flexibility<br>(iii) impermeability to liquid and air<br>(iv) ability to induce functional ciliated respiratory epithelium resurfacing<br>(v) ability to induce blood vessel formation |
| Larynx | Orchestrate swallowing, breathing, coughing, and voice<br>Immunological organ | Tuned sphincter situated in the anterior portion of the neck | Mucosa-covered collection of cartilaginous framework (three single and two paired cartilages), ligaments, muscles, and vocal cords (covered by respiratory epithelium) | (i) whole laryngeal framework<br>(ii) low immunogenicity |
| Esophagus | Secretion of mucus to aid ingesta passage from the larynx to the stomach<br>Move of ingesta to the stomach through peristaltic movement | Muscular tube | (i) Mucosa: basal membrane consisting of nonkeratinized squamous epithelial cells, which produce the mucus.<br>(ii) Submucosa loose connective tissue (collagen types I and III, arranged in a criss-cross pattern), consisting of blood vessels and mucus glands.<br>(iii) Muscularis externa: contains inner circular and outer longitudinal muscle cells (skeletal and smooth).<br>(iv) Adventitia: composed of loose soft connective tissue, blood and lymph vessels, adipose tissue, and simple squamous cell epithelium | (i) tubular morphology and specific nanogeometry (four layers with different properties)<br>(ii) resistant the reflux of gastric juice from the stomach<br>(iii) appropriate mechanical properties (strength and viscoelasticity) to withstand peristaltic movements |
| Heart valves | Guarantee the unidirectional blood flow within the beating heart | Situated around a tendinous ring, possess three cusps, except for the mitral valve, only two. | Distinct complex layers composed of interstitial fibroblasts and connective tissue fibres and lined by valvular endothelial cells:<br>(i) ventricularis composed of mainly aligned elastic fibers (assist valve leaflet dynamics)<br>(ii) spongiosa consists mainly of proteoglycans and glycosaminoglycans (to absorb shear stress during cyclical valve motion)<br>(iii) fibrosa composed of mainly collagen (provide strength and stiffness to maintain coaptation in the diastolic phase) | (i) highly specialized three-dimensional (inhomogeneous) microstructure<br>(ii) anisotropic mechanical properties<br>(iii) dynamic behavior |

Table 1: Continued.

| Organ | Function | Structure | Histological features | Ideal scaffold properties |
|---|---|---|---|---|
| Vascular system (blood vessels) | Blood transport through the body | Fibromuscular tubular structure | Three layers (from the lumen outward):<br>(i) tunica intima composed of an endothelial cell monolayer (diffusion of oxygen and carbon dioxide)<br>(ii) tunica media composed of smooth muscle cells (regulate blood flow by altering vascular resistance through vasoconstriction and vasodilatation)<br>(iii) tunica adventitia composed of fibroblasts and elastic connective tissue (stretches and supports blood vessels) | (i) longitudinal and transversal elasticity<br>(ii) patency<br>(iii) impermeability to liquid and air<br>(iv) resistant to bacterial colonization<br>(v) thrombotic formation resistance |
| Kidney | Maintain body homeostasis by excreting excess water, regulating the chemical blood composition, removing waste products, and assuring endocrinologic functions | Bean-shaped structure made of approximately 0.5–1 million nephrons, consisting of a glomerulus, surrounded by a Bowman's capsule, a proximal tubule, a loop of Henle, and a distal tubule connected to a collecting duct | Composed of various different cell types, including parietal cells, podocytes, tubule brush border cells, capillary bed covered by visceral epithelial cells, endothelial cells, and basement membrane (collagen IV, laminin, and heparin sulfate proteoglycans) | (i) provide blood ultrafiltration<br>(ii) provide transport regulatory function<br>(iii) appropriate mechanical properties (strength and viscoelasticity) to withstand peristaltic movements |
| Bladder | Store urine at low pressure and allow voluntary micturition, acting as a pressure vessel subjected to mechanical stress | Musculomembranous sac | (i) adventitia: connective tissue<br>(ii) muscular layer: inner longitudinal, circular, and outer longitudinal layers of thick muscle bundles with intrafascicular connective tissue<br>(iii) submucosa or lamina propria: connective tissue (collagen I, III, elastic fibers)<br>(iv) mucosa: transitional epithelium (polyhedral flattened or large club-shaped cells), urothelial cells, and connective tissue (collagen IV and laminin)<br>(v) serosa: simple squamous epithelium overlying connective tissue | (i) allow for even and constant attachment of mature epithelial cell layer on the luminal surface and harbor multiple cell layers of smooth muscle cells on the outside<br>(ii) provide adequate mechanical support<br>(iii) prevent collapse prematurely before new tissue *in vivo* formation |
| Urinary tracts | Propel urine from the kidneys to the bladder (ureters) and from the bladder to the outside of the body (urethra) | Narrow fibromuscular tubular structure | | |
| Skeletal muscle | Locomotion, maintenance of posture, respiration (diaphragm and intercostal), communication, and production of body heat. | Composed of muscle cells (fibers), connective tissue, blood vessels, and nerves. | Muscle fibers form a long multinucleated syncytium grouped in bundles surrounded by connective tissue sheaths and extending from the site of origin to their insertion.<br>Connective tissue covering:<br>(i) epimysium: dense connective tissue ensheathing the entire muscle<br>(ii) perimysium: surrounding bundles of muscle fibers<br>(iii) endomysium: layer of reticular fibers and ECM surrounding individual muscle fibers. | (i) appropriate mechanical properties, such as contraction, stiffness, force, and elasticity<br>(ii) provide orientation fiber guiding<br>(iii) provide adequate porosity |

rabbit abdominal wall for vascularization. Three weeks after tracheal replacement, the transplanted constructs retained good airway patency, did not collapse following removal of a silicone stent, and adequate vascularisation and muscular and epithelial regeneration were revealed in the neotrachea luminal surface. However, inflammatory changes and sputum accumulation occurred in the regions without epithelium-like tissue coating [42]. Tubular PGA fiber scaffolds, seeded with chondrocytes and implanted into sternohyoid muscle for 4 weeks, have been used, with or without muscle pedicle, to repair segmental defect of trachea with a silicon tube as stent (removed after 2 months). Six out of ten animals, implanted with vascularisation, survived over six months, while all the animals in the control group (without vascularization) died within two months after reconstruction, due to mucus impaction. 6 months after implantation, vascularised constructs retained structures and features of cartilage-like tissue and developed a continuous ciliated columnar epithelium layer, suggesting the importance of the prevascularization for the development of a suitable airway graft [43]. A copolymer of L-lactide and ε-caprolactone was synthesized to fabricate a sponge-like tubular structure (80% porosity; 20–100 $\mu$m pore size; 6 cm length), reinforced by a woven fabric of PGA and coated with gelatin, to be implanted into sheep. After 9 months, only stent implanted substitutes (silicone stent, 7 cm length) had positive outcomes, even if a complete and spontaneous reconnection of the native trachea was not observed [44]. The same copolymer has been used to coat the luminal surface of a tubular scaffold, consisting of two collagen layers separated by a polypropylene framework and reinforced with 5 rings of polypropylene monofilament (30 mm long, 15 mm internal diameter) and implanted in dog left main bronchus [45]. After 14 days, the luminal surface resulted to be completely epithelialised with ciliated columnar and squamous epithelium, suggesting that the polymeric coating promoted an effective epithelialisation protecting the collagen layer.

Naito et al. [46] developed a tracheal prosthesis using a different approach: fibroblast and collagen hydrogels, mechanically supported by osteogenically induced MSCs in ring-shaped 3D-hydrogels, were implanted into rats (length 5-mm). The negative outcome (only three animals survived for 24 h and died the day after), due to strictures in the anastomotic regions, was mainly associated with the lack of an epithelial layer.

Regarding Y-shaped tubular scaffolds, a limited experimentation has been conducted till now. Sekine et al. [47] implanted into dogs Y-shaped scaffolds made of *Marlex* mesh (260 $\mu$m pore size), reinforced with polypropylene spiral and coated with collagen. 14 out of 20 dogs died after experimentation due to obstruction of the main bronchus, omental necrosis, and air leakage. The same construct (60 mm long and 18 mm outer diameter) was tested as tracheobronchial bifurcation replacement: after 5 years, the prosthesis resulted to be completely incorporated by the host trachea and bronchus, neither stenosis nor dehiscence was observed, and a functional airway was revealed [48].

### 4.2. Clinical Studies

*4.2.1. Natural Approach.* Using DEM approach, decellularized human tracheal matrices, characterized by structural and mechanical properties similar to native trachea, lack of immunogenicity, sufficient length for clinical application, containing proangiogenic factors, and supporting *in vivo* recellularization, have been developed [32, 49]. A bioengineered airway (7 cm long), dynamically preseeded with autologous epithelial respiratory cells and mesenchymal stem cell-derived chondrocytes, has been successfully used to replace left main bronchus (stenosed from tuberculosis) [18]. After 5 years, the patient is well, active, and, more importantly, has not shown neither an adverse immunological response nor serological signs of rejection, even without any immunosuppressive treatment [50]. Unfortunately, a recurrent cicatricial stenosis occurred at the native trachea closest to the transplanted trachea anastomosis, probably due to reduced mucosal blood flow, particularly when associated with lung inflammatory or infectious diseases.

In order to fast the obtainment of a suitable scaffold to be implanted and based on the experience performed with porcine model, decellularized human tracheas have been intraoperatively seeded with autologous bone marrow stromal cells, conditioned with growth and boosting factors and implanted to treat both benign ($n = 5$) and malignant ($n = 3$) airway diseases. The *in vivo* engineered transplanted tracheas resulted to be vascularised and lined with complete respiratory neomucosa; however a partial collapse of the most proximal part of the graft was observed in about 30% of patients [50]. This result could be probably due to an oxygen concentration gradient developing throughout the engineered trachea with consequent transmembrane cell migration from the outer (chondrocyte compartment) to the internal scaffold lumen (epithelial compartment). However, it is also possible that the decellularization process, slightly affecting the scaffold properties and surface topography, could have an effect on the long-term graft properties [10]. A short follow-up of 2 years verified the clinical outcome of this procedure [51]. The graft revascularised 1 week postoperatively, but an evidence of epithelium restoration was not observed before 1 year, which was verified after 15 months. The analysis of the decellularized scaffold showed the presence of 166 proteins relevant for regenerative medicine (e.g., angiogenesis and immunity), confirming the suitability of the proposed tissue engineering approach.

Recently, decellularized human trachea, repopulated with autologous stem cells, has been implanted into a 76-year-old patient with tracheal stenosis including the lower part of the larynx. After 23 days, the patient died due to cardiac arrest; however, the implanted construct resulted to be patent, also showing the presence of a squamous epithelium, neovascularization, muscular cells, serous glands, nerve fibers, and intact chondrocytes [52]. These clinical experiences demonstrated that functional tissue engineering natural-derived airway scaffolds can be obtained and are safe and promising. However, means to improve the biomechanical long-term stability of such grafts have to be developed before this technology can be translated into routine clinical practice.

*4.2.2. Synthetic Approach.* A *Marlex* mesh tube (pore size 260 $\mu$m; 50 mm long; 18, 20 or 24 mm inner diameter), covered with collagen sponge and reinforced with a supporting polypropylene ring and injected with autologous venous blood, was implanted into 4 patients affected by airway stenosis or cancer invasion [53]. During the postoperative observation period (8–34 months), a good epithelialisation was revealed in all the patients, and only in one case air leakage was observed.

A tracheobronchial graft made of POSS-PCU, both in casted form, for the cartilage "U" shaped rings, and in coagulated form, for the "connective" tracheal part, was implanted into a 36-year-old male patient affected by a recurrence of a primary tracheal mucoepidermoid carcinoma involving the distal trachea and both main bronchi [19]. Before implantation, the bioartificial scaffold was dynamically cellularized with autologous bone marrow mononuclear cells for 36 h. 1 week after operation a normal and patent airway was revealed, while biopsy samples showed the presence of necrotic connective tissue associated with fungi contamination and neovessels. After 2 months from transplantation, biopsy revealed large granulation areas associated with smooth epithelialisation and some organised vessels formation; bacterial or fungi contamination was not observed. An almost normal airway and improved lung function were assessed at 5 months.

## 5. Larynx

Attempts to construct an entire larynx have involved several approaches, and so far, tissue engineering has only been used for partial laryngeal reconstruction. The main problem is how to construct a bioartificial larynx with whole complex laryngeal framework, low immunogenicity, and dynamic function which requires combination of sphincter and breathing functions. Moreover, from a surgical point of view, the restoration of a laryngeal defect by means of a scaffold is challenging, because of vocal fold movement and the restriction to provide sufficient space for tissue regeneration [54].

### 5.1. Preclinical Studies

*5.1.1. Natural Approach.* Tissue engineered cartilage grafts, obtained by seeding chondrocytes on hyaluronic acid (Hyalograft C) *via* a bioreactor, have been implanted in rabbits: despite no animals showed signs of respiratory distress, implanted grafts revealed marked signs of an unspecific foreign body reaction, leading to a complete degradation of the neocartilage and graft failure [55]. Cartilage sheets, obtained by seeded autologous cells on fibronectin-conditioned semipermeable polyester membrane *via* a bioreactor, have been implanted in rabbits for laryngotracheal reconstruction: the grafts showed no signs of degradation or inflammatory reaction, were covered with mucosal epithelium, but showed evidence of mechanical failure through migration and buckling [56].

Natural-derived scaffolds, obtained by tissue decellularizing, have been shown to allow a laryngeal repair superior to that observed using control standard procedure [57–59]. The regeneration of thyroid cartilage, epithelium, connective tissue, glandular structures, and some skeletal muscles has been obtained in dog by implanting porcine decellularized urinary bladder matrix [57]. Rabbit tracheas have been decellularized using a perfusion decellularization protocol to simultaneously reach all parts of the larynx and to create a low-immune whole-larynx scaffold comprising decellularized laryngeal muscles, a reserved decellularized matrix, and an integrated cartilage framework. The grafts, reseeded with MSCs and implanted in rabbits, allowed the regeneration of muscle bundles and vessels, even if a severe immunological reaction was observed [60]. A recent study evaluated the regenerative effects of acellular porcine urinary bladder matrix on hemilarynx, using a canine model. After one month, all animals showed good reepithelialization with minimum complication, while after 6 months postoperatively, cartilaginous structures, normal (or near normal) phonation threshold pressure, and mucosal wave amplitude were assessed. Even if the regenerated vocal fold mucosa resulted to be scarred, the acellular urinary bladder scaffold can be regarded as a potential means for a functional tissue regeneration of the hemilarynx [61].

*5.1.2. Synthetic Approach.* *Marlex* mesh (pore size of 260 $\mu$m), reinforced with a polypropylene supporting ring, coated with collagen, and preclotted with arterial blood, has been used in dogs for the treatment of subglottic stenosis: the scaffold resulted to be well integrated and covered by epithelial cells; however the presence of granulation tissue and mesh exposure were reported [62]. The same synthetic scaffold has then been developed based on the replication of the luminal canine larynx and was used to perform a hemilaryngectomy. The scaffold has been preclotted with a mixture of peripheral blood and bone marrow-derived stromal cells and implanted in dogs: soft tissue regeneration (after 8 days) and the presence of mucosal cells (after 3 weeks) were observed [63]. Recently, *Marlex* mesh, coated with collagen and wrapped with autologous fascia, resulted to be a viable alternative for the regeneration of laryngeal defects. However, scar-like tissue with consequent reduction of the treated vocal fold, exposure, or dislocation of the mesh was revealed, suggesting that additional approaches are required to regenerate a normal and functional vocal fold [54].

### 5.2. Clinical Studies

*5.2.1. Natural Approach.* A free-tissue transfer and an autologous tracheal segment have been successfully used for partial laryngeal replacement preserving one muscle-nerve-joint unit, providing vocal and sphincter functions [64]. Good breathing results were reported, while, due to the lack of a truly laryngeal architecture, voice and swallowing remain to date suboptimal. The availability of substitutes displaying equivalent anatomical, physiological, and biomechanical properties compared to normal human larynxes

would provide the right, complex architecture, and dynamics for normal voice production and sphincter action.

*5.2.2. Synthetic Approach.* Considering the efficacy evaluated in preclinical studies, *Marlex* meshes, coated with collagen and injected with autologous venous blood, have been implanted into 4 patients affected by airway stenosis ($n$ = 1 subglottis stenosis) or cancer invasion ($n$ = 3 thyroid cancers) [53]. A good epithelialisation occurred in all patients during the postoperative observation period, and air leak was revealed in only one case. These promising results demonstrate the ability to regenerate cricoid cartilage using scaffolds composed of polypropylene and collagen sponge in clinical applications.

## 6. Esophagus

Esophageal substitution is generally required in presence of several pathological conditions, for example, esophageal atresia, acquired constriction esophagitis, esophagotomy, or cancer, becoming the world's sixth leading cause of death [65, 66]. Surgical resection is regarded as a standard treatment in the early stage of the disease, involving gastrointestinal segments as potential substitutes to repair the esophageal defect. However, this procedure is not free of drawbacks, as the incidence of complications is relatively high, and the mortality rate is up to 4% [67]. In this regard, the development of a suitable alternative according to the tissue engineering approach might represent the desired option, as the following reported studies suggest.

To the best of our knowledge, no clinical studies have been till now performed following the synthetic route, highlighting, once again, the complexity of designing a reliable scaffold even for a tubular organ mainly characterized by a transport function.

### 6.1. Preclinical Studies

*6.1.1. Natural Approach.* Natural-derived matrices have been used both as esophageal patches and as tubular scaffolds. Porcine-derived, xenogeneic ECM obtained from SIS, seeded with autologous oral mucosal epithelial cells, has been used as patch to repair an esophageal defect (5 cm length and 2.5 cm width) in a canine model [68]. The seeded scaffolds showed a better healing process compared to the control group (unseeded scaffolds): a complete reepithelialization was observed 4 weeks after surgery, while extension of the muscular bundles and appearance of island muscle cells in the connective tissue were revealed after 8 weeks (muscle cells generation was not observed in the control group). Patches made of porcine SIS or urinary bladder submucosa were characterized by a positive outcome when implanted into adult dogs to repair a defect of approximately 5 cm in length and encompassing 40%–50% of the circumference of the esophagus [69]. The naturally derived material resorbed within 2 months, and the presence of organized skeletal muscle bundles and of a confluent squamous epithelium was observed. Following a similar approach, acellular porcine SIS, seeded with bone marrow MSCs, has been used to replace a section of canine cervical esophagus (5 cm in length and 50% in circumference). After 12 weeks from surgery, a complete construct reepithelialization, revascularization, and muscular regeneration were revealed, with almost no inflammation signs [70]. The use of matrices derived by SIS gave similar promising results for the treatment of esophageal semicircumferential defects in rats [71], used as an animal model also to test the gastric acellular matrix, an alternative naturally derived material [65]. In this latter case, rat gastric acellular matrix was prepared to recover a defect (5 mm length and 3-4 mm width) in the abdominal esophagus of the same animal model. Two weeks after implantation, the regeneration of keratinized stratified squamous mucosa was assessed, but no ingrowth of the inner or outer muscle layer was detected after 18 months. Interestingly, a decellularized esophagus was tested as a potential scaffold to repair an esophageal defect, which seems to be a logical approach due to the intrinsic similarity of the "artificial" patch-organ microstructures [72]. A 2 cm defect in the tunica muscularis of the thoracic pig esophagus was covered with an esophageal homologous matrix, seeded or not with autologous SMCs. At 3 weeks from surgery, both patches were infiltrated by mononuclear cells and fibroblasts without signs of rejection, even if unseeded scaffolds showed a severe inflammatory response and were negative for $\alpha$-smooth muscle actin immunostaining. On the contrary, seeded implants were characterized by SMC ingrowth, with an early organization into small fascicules.

A tubular scaffold for esophageal regeneration was evaluated by Badylak et al. [73]. Porcine urinary bladder matrix was shaped into a tubular construct to be used in conjunction or not with muscle tissue to recover a canine esophageal circumferential resection of 5 cm. For this aim, four groups were considered: ECM scaffold alone, muscle tissue alone, and ECM plus either a partial (30%) or complete (100%) covering with muscle tissue. Animals of the first two groups developed severe strictures within the 3 weeks, while a constructive remodelling was verified in the last two groups. Also matrices derived from SIS have been tested as tubular scaffolds and implanted in the cervical esophagus of piglets (about 4 cm in length) [74]. However, implanted matrices lead to a high rate of esophageal stenosis, suggesting that, dealing with a decellularized ECM could not assure the desired results, even if a similar microstructure is provided to the surrounding tissue. More specifically, dynamically decellularized rat oesophagi were seeded with allogeneic mesenchymal stromal cells which spontaneously differentiated into epithelial- and muscle-like cells. The reseeded scaffolds were then implanted to orthotopically replace the entire cervical oesophagus in immunocompetent rats. All animals survived the 14-day study period, with patent and functional grafts, and gained significantly more weight than sham-operated animals. At retrieval, explanted grafts showed regeneration of all the major cell and tissue components of the oesophagus, including functional epithelium, muscle fibres, nerves, and vasculature [75].

*6.1.2. Synthetic Approach.* To repair semicircular esophageal defects (0.5 × 1 cm), both absorbable (*Polyglactin 910*, Vicryl) and nonabsorbable (polyvinylidene fluoride) meshes were implanted in rabbits [76]. Mucosal regeneration was observed, with the nonabsorbable meshes leading to better results. The absorbable scaffolds lead indeed to early degradation with consequent ulceration, abscess formation, and diffuse inflammation. To improve tissue regeneration, the implantation of cell seeded scaffold has been evaluated. PGA/PLA scaffolds, seeded with rat adipose smooth muscle-like cells, were implanted in rats in order to repair a defect (3 mm width; 5 mm length) created in the abdominal esophagus [77]. A complete reepithelialisation of the esophageal lumen was observed after 10 weeks, while muscularis layer regeneration was detected at 16 weeks. PCL meshes, seeded with smooth muscle and epithelial cells, have been implanted in the abdominal part of rabbit esophagus (0.6 × 1 cm). Fifteen rabbits survived the trial period (30 days), and 6 out of 20 animals had no complications. The synthetic mesh was almost completely degraded and replaced by a layered continuum of epithelium and SMCs, organized in varying degrees [78].

In order to provide a more complex and anatomical-like engineered substitute, a typical surgical approach to promote esophagus scaffold-guided regeneration consists in wrapping a selected material around a tube to impart and retain the tubular shape after implantation; the tube is then removed and the resulting scaffold should act as a functional device. This strategy was followed by Takimoto et al. [79]: a 5 mm thick freeze-dried collagen sponge was wrapped around a silicone tube and implanted into dogs to recover a 10 cm defect. Two animals died after tube removal (6 weeks), while after 6 months a completely epithelialized luminal surface, normal esophagus glands, and immature muscle tissue were revealed. Similarly, a PLA : PCL (50 : 50) mat, reinforced with PGA fibers, supported by a nasopharyngeal airway tube, was used to repair an esophageal oval-shaped defect (4 × 2 cm) in a pig model [80]. The tube was used only as temporarily support and was sutured to the scaffold with short-term sutures in order to allow the tube falling off into the intestine. After 4 weeks squamous epithelium was regenerated, and after 12 weeks the muscular layer was similar to the native tissue. However, the main limit of this strategy is the dislodgment of the stent which might cause bowel obstruction. A scaffold, made of nonwoven PGA used as a substrate for human amniotic membrane seeded with canine oral keratinocytes and fibroblasts, rolled around a polypropylene tube (3 cm in length and 2 cm in diameter) and previously implanted in dog abdomen for 3 weeks, was used to replace a 3 cm esophageal resection [81]. Unseeded grafts developed strictures, with consequent complete esophageal obstruction, while seeded ones showed the regeneration of squamous epithelium, muscularis mucosa, and smooth muscle tissue and a good distensibility. However, the presence of esophageal glands and peristalsis was not detected.

A more sophisticated approach considered 2 mm thick nonwoven tubular PGA (15 $\mu$m fiber diameter) scaffolds (1 cm length; 0.5 cm outer diameter, 0.2 cm inner diameter), seeded with neonatal or adult rat esophagus organoid units (mesenchymal cores surrounded by epithelial cells), sealed with poly-L-lactic acid, and implanted in syngeneic hosts [82]. Esophageal architecture with keratinized squamous epithelium and an actin-positive muscularis was revealed and no signs of deterioration were observed for 42 days.

### 6.2. Clinical Studies

*6.2.1. Natural Approach.* To treat a cervical esophageal perforation in an 82-year-old man, Clough et al. [83] implanted an acellular matrix (Surgisis) derived from porcine SIS. A patch of 5 × 3 cm was used to repair the defect and after 6 days from surgery no leakage was detected, allowing commencing oral intake. At 4 weeks, the healing process was confirmed displaying a normal calibre esophagus; the patient was discharged after 61 days and remains well 4 months postoperatively, even if a normal swallowing was not reestablished. The same scaffold was also used to treat Barrett's esophagus with high-grade dysplasia and mucosal adenocarcinoma by means of a minimally invasive endoscopic procedure [66]. Five male patients (average age 62.0 ± 5.3) were subjected to circumferential, long segment sleeve resection of mucosa and submucosa and placement of the biological scaffold, secured into position with a radially expanding stent, resulting in gentle compression against the muscularis externa, removed after 9–18 days postoperatively. During the follow-up (4–24 months) a progressive tissue restoration was observed with the formation of squamous epithelium.

## 7. Heart Valves

Currently, the failure of pathological heart valves is surgically treated by means of an artificial prosthesis, either mechanical or biological, the latter being a porcine-derived heart valve or made of bovine pericardium. However, none of these two models is free of drawbacks that can concur to limit the performance of the implanted valve. Due to the nature of the materials and the nonphysiologic hemodynamics, mechanical valves require a lifelong anticoagulant therapy that can expose the recipient to hemorrhagic events. On the other hand, biologic valves, due to a degenerative calcific process, are characterized by a limited temporal functionality [84]. A novel alternative is therefore desirable and tissue engineering might furnish the solution to the problem. Reasonably, this is not expected in the very next future since a reliable safe heart valve has not been developed yet and a large number of research groups have been focused on different aspects of the issue and, as a consequence, multiple routes have been traced. It is interesting to notice that most of the pivotal studies focusing on the assessment of a functional tissue engineered heart valve prosthesis are based on the use of naturally derived decellularized heart valves, and an entire synthetic polymeric heart valve tested in an *in vivo* model is still to come. This might be due to the peculiar features of this anatomical district, implying the development of a proper strategy to fabricate a valid substitute that closely matches the natural one. Several synthetic approaches can be cited that moved along this route, but the related evaluation has been

mainly conducted *in vitro* [85]. Therefore, a decellularized scaffold seems to be a suitable choice at present, since it offers a morphology, binding sites, and three-dimensional architecture that is naturally designed for the expected function.

### 7.1. Preclinical Studies

*7.1.1. Natural Approach.* Decellularized allogenic pulmonary valve conduits were orthotopically implanted into a sheep model after being reseeded with autologous myofibroblasts and endothelial cells [86]. Transplantation of unseeded acellular valves (control group) leads to only a minimal immigration of myofibroblasts without matrix reorganization or procollagen synthesis, but both cell seeded or unseeded valves were characterized by a confluent endothelial cell lining after 3 months. The latter result, according to the authors, could be influenced by the animal model used in the study and may be more limited in human beings without preseeding. A heart valve completely made of fibrin was proposed by Flanagan et al. [87]. Fibrin-based valves were cast in customized molds by mixing fibrinogen solution, saline solution containing carotid artery ovine SMCs and fibroblasts, and calcium chloride. Polymerization was started by adding thrombin solution. After being conditioned in a bioreactor for 28 days, valves were subsequently implanted into cell-donor animals in the pulmonary trunk, leaving intact the native pulmonary valve to prevent acute volume load of the right ventricle due to a possible incompetence of tissue engineered valves. At 3 months after surgery, all valve conduits were patent, covered by a confluent layer of endothelial-like cells with viable interstitial-like cells throughout the entire valve thickness. Moreover, the production of autologous collagen and ECM proteins, replacing the fibrin, was also assessed.

The *in vivo* spontaneous recellularization of acellular matrix was evaluated by implanting decellularized porcine aortic valves in the descending thoracic aorta of lambs and providing subcutaneous injections of G-CSF, as boosting factor to mobilize early bone marrow progenitor cells [88]. However, this treatment did not improve scaffold recolonization but, rather, induced accelerated valve deterioration, enhanced inflammatory cell infiltration, and neovessel formation in the adventitia, myointimal proliferation, and calcifications, both in leaflets and the aortic wall. The *in vivo* reendothelialization of decellularized ovine aortic valve allografts, implanted as an aortic root in lambs, has been evaluated also by Baraki et al. [89]. At retrieval (3 and 9 months postoperatively), partial luminal endothelialisation, neovasculogenesis at the adventitial side, trivial regurgitation, and normal morphology with no signs of graft dilatation, degeneration, or rejection were reported. On the contrary, marked calcification/degeneration and advanced valve insufficiency were revealed in control valves group (fresh native ovine aortic valve conduits). In order to improve graft recellularization, cells have been seeded on natural-derived scaffolds before implantation. Canine myofibroblasts and endothelial cells have been seeded on acellular porcine aortic valve leaflets, which, after a 7-day incubation period, have been implanted into the lumens of canine abdominal aortas [90]. After 70 days from surgery, histochemistry confirmed that myofibroblasts grew within the matrix, while valve leaflets were partially covered by endothelial cells. In addition, no evidence of calcification was observed. A similar technical approach has been presented by Kim et al. [91]: canine endothelial and myofibroblast cells, derived from allogenic BMCs, have been seeded on decellularized porcine heart valves, before being implanted into canine abdominal aorta and pulmonary valve. At retrieval (1 and 3 weeks postoperatively), grafts showed a normal morphology, but an incomplete endothelialization and regeneration were observed, due to a nonhomogenous cell seeding and the subsequent detachment after implantation. Cell seeding before implantation represents a crucial issue to be addressed. It is well known that, based on the complete tissue engineering paradigm, a proper tissue engineered scaffold is the concurrent result of an effective cell-matrix interaction. Tudorache et al. [92] further proved this point dealing with an ovine decellularized aortic valve conduit, reseeded with autologous endothelial cells, conditioned *in vitro* into a bioreactor, and then implanted in orthotopic position into sheep (cryopreserved valves were used as control). The proposed constructs were not affected by valvular insufficiency, stenosis, and cusp thickening, differently from the control group. In particular, the degeneration of the cryopreserved valves was related to the presence of allogenic cells and disorganization of ECM components as a result of storage and mechanical stress.

On the other hand, cell seeding can be considered a time-consuming procedure and can be overcome planning a specific strategy. In this regard, decellularized porcine pulmonary valves, conjugated with CD133 antibody, were transplanted in the pulmonary position into sheep, while unconjugated and autologous endothelial cell-reseeded valves were used as control [93]. This study proved that a more cell-rich valve can be obtained: the production of matrix proteins improved, as collagen and GAGs increased from 1 to 3 months postoperatively, and the biomechanical properties were similar to those of a normal valve, compared to the control cases. However the functional remodelling was not assessed.

*7.1.2. Synthetic Approach.* An interesting use of resorbable polymers for tissue engineering heart valves was proposed by Wu et al. [94] fabricating a hybrid heart valve made of decellularized porcine aortic valves coated with PHBHHx, which belongs to polyhydroxyalkanoates, a class of polymers of microbial origin. The resulting scaffold was implanted in pulmonary position in sheep and, even if the polymeric surface covered the ECM beneath, a positive outcome (16 weeks postoperatively) was assessed as it contributed to prevent the activation of thrombogenic matrix components, protected ECM from the potential harmful influence of host fluids, and supported repopulation with recipient's myofibroblasts and endothelial cells. An example of the performance of a synthetic valve conduit was presented by Gottlieb et al. [95], assembling nonwoven sheets containing PGA and PLA fibers (50% : 50%). Firstly, grafts have been seeded with MSCs from neonatal sheep bone marrow, then

cultured for 1 month, and finally implanted in pulmonary position, after having excised the native valve cusps and 1-2 cm main pulmonary artery segment. The diameter of the implanted valve conduits remained unchanged for 20 weeks; however cusp dimensions decreased leading to pulmonary regurgitation after 6 weeks. In order to improve the clinical outcome of congenital cardiac defects, prenatal heart valve interventions can be a valuable strategy [96]. Trileaflet heart valve scaffold, made of nonwoven PGA meshes, integrated into radially self-expandable nitinol stents, and coated with poly-4-hydroxybutyrate, was seeded with ovine amniotic fluid cells and implanted orthotopically into the pulmonary position using an in-utero closed-heart hybrid approach. Tissue engineered valves showed intact and mobile leaflets with no thrombus formation or impairment of substitute integrity. The same materials and the same valve design were used for pulmonary valve substitution in nonhuman primates, either considering autologous bone marrow-derived mononuclear cell seeding [97] and the decellularization approach [98]. In the latter case, scaffolds were firstly seeded with human fibroblasts, dynamically cultured for 4 weeks, and decellularized to be implanted into baboons in orthotopic pulmonary valve position by means of an antegrade transapical approach. Postoperatively, the implanted valves were characterized by a mild-moderate insufficiency, leaflet shortening, and rapid cellular repopulation, compared to decellularized native human heart valve control.

## 8. Vascular System

The most common treatment for cardiovascular diseases is the use of an autologous vascular graft, retrieved from the internal mammary arteries and saphenous veins; however this approach can be limited by patient's age and pathology [99]. Endothelium restoration/regeneration is one of the major aims of vascular tissue engineering, since it plays a crucial role in vascular biology regulating permeability, inflammation, thrombosis, and fibrinolysis [100, 101]. Endothelial growth can be supported *in vivo* with appropriate scaffolds with mechanical stability and remodelling potential. Several scaffolds have been developed for vascular tissue engineering; among these, it is possible to distinguish between three categories that have been *in vivo* tested: decellularized matrices, self-assembling vessels, and electrospun synthetic scaffolds.

### 8.1. Preclinical Studies

*8.1.1. Natural Approach.* In an early study, porcine iliac blood vessels were decellularized with 1% TritonX-100 and 0.1% ammonium hydroxide for 72 h, seeded with EPCs, and tested in a sheep common carotid artery substitution model [102]. EPC-seeded grafts remained patent for 130 days, whereas nonseeded grafts occluded within 15 days. The seeded grafts exhibited contractile activity and nitric-oxide-mediated vascular relaxation. The study did not show analysis of dilation, thrombogenesis, or intima hyperplasia. The same decellularization protocol was used also in other works to fabricate acellular canine and porcine carotid arteries [103, 104]. Canine matrices were seeded with bone marrow derived cells, differentiated toward smooth muscle and endothelial cells, and implanted in cell donor dogs in a carotid artery interposition model [103]. The acellular scaffold was primarily composed of elastin and collagen and exhibited porous structure. Cell seeded vascular grafts remained patent for up to 8 weeks, whereas unseeded grafts occluded within 2 weeks. Matrix remodelling was evident with maintenance of the 3 layers and the graft demonstrated appropriate mechanical strength to endure forces exerted by sutures during surgery. Longer time points (4 months) in a similar approach in pig showed no structural failures, aneurysms, or infectious complications [104].

Decellularized veins have been developed using also other detergents, such as SDS: decellularized canine external jugular veins have been transplanted in a carotid interposition model in dogs [105]. No graft deterioration, in terms of rupture, anastomotic complication, or dilation, was observed 8 weeks after implantation, with minimal inflammation, transmural repopulation of vascular cells, and a compact fibrin layer formed along the lumen. Unfortunately, no longer time points were analysed. Decellularized porcine saphenous arteries have been implanted into rabbit carotid arteries: after 3 months grafts showed 60% patency rates, regeneration of vascular elements, with no aneurysm and intimal hyperplasia events, suggesting their potential as small-diameter grafts [106]. Decellularized equine carotid arteries, coated with a matricellular protein (CCN1) and implanted as cervical arteriovenous shunts, showed, 14 weeks after implantation, smooth muscle regeneration, complete endothelialisation, and immunologic tolerance, suggesting CCN1 coating as a promising tool for generation of bioartificial vascular prostheses [107].

Acellular human umbilical cord arteries have also been evaluated *in vivo* as vascular tissue engineered graft [108]. These vessels, decellularized with CHAPS buffer and SDS buffer for 4 days, were incubated for 2 days in endothelial growth media-2. The acellular arteries retained the majority of the ECM components (collagen and elastin) and similar mechanical properties (maximum burst pressure and maximum modulus) to the native vessels. To evaluate the mechanical strength of decellularized umbilical arteries *in vivo*, vessels were implanted into nude rats as abdominal aorta interposition grafts. The scaffolds were mechanically robust *in vivo* for 8 weeks with no dilation or aneurysm formation, but the absence of a cellular compartment in the construct seemed to cause occlusions within 24 h after implantation and various levels of thrombosis. Furthermore, no cell infiltration was observed within the scaffold, probably due to the short time observation period.

Cell self-assembling scaffolds are composed by cell-derived ECM sheets developed *in vitro* to produce vascular grafts of arbitrary lengths. Cells are normally autologous in order to obtain a total biocompatible graft [109–113]. A pioneering study has been published in 1999 where smooth muscle and endothelial cells, derived from a biopsy of a vascular tissue, were cultured for 8 weeks in a pulsatile perfusion system [109]. These engineered vessels were composed of alive and functional cells, secreting ECM, mainly

collagen. The grafts showed rupture strength greater than native human saphenous veins and contractile responses to pharmacological agents. Tissue engineered arteries were implanted in swine into the right saphenous artery, showing patency up to 24 days after transplantation, without evidence of stenosis or dilatation. The xenograft had also unchanged contractile responses to prostaglandin and there was no evidence of bleeding at the anastomoses or mechanical breakdown at explantation. A similar approach used a combination of human vascular SMC-derived sheets and human fibroblasts sheets to provide the adventitia. After maturation, the tubular support was removed and endothelial cells were seeded in the lumen [110]. Histological analysis revealed well-defined tissues (intima, media, and adventitia) and a complex and naturally organized ECM, although single components were not quantified and characterized. Short-term grafting experiment in a canine model demonstrated good handling and suturability characteristics, mechanical stability, and blood compatibility. Human fibroblast sheet-derived vascular grafts were also tested in nude rats (long-term study) and primates (for up to 8 weeks), showing physiological mechanical strength and positive scaffold remodelling with activation of resident cells [111]. Another similar study confirmed the applicability of this technique using MSC-derived sheets organised to produce a vascular graft [113]. Here, the constructs were implanted into common carotid artery defects of rabbits and analysed after 4 weeks, evidencing excellent patency and good integration with the native vessel. No stenosis, thrombus formation, or inflation occurred in this short time point.

Alternatively, allogeneic cells can be cultured on degrading tubular scaffolds and then decellularized to eliminate the cellular compartment maintaining the cell-secreted ECM as an acellular scaffold. This hybrid approach has been proposed to fabricate human allogeneic, porcine or canine smooth muscle cell-derived constructs, starting from tubular PGA scaffolds [114, 115]. The acellular grafts, subsequently seeded with autologous cells (endothelial or endothelial progenitor cells) on the lumen, have been then transplanted *in vivo* in porcine, baboon, or canine vessel transposition models. Scaffolds demonstrated excellent patency for up to 1 year, resistance to dilatation, calcification, and intima hyperplasia. Infiltration of smooth muscle positive cells, endothelial cells, and elastin formation were observed near anastomoses. Endothelial cell-seeded scaffolds showed capacity to better maintain patency after *in vivo* implantation with respect to synthetic constructs [115]. The combination of natural and synthetic materials was also assessed using decellularized umbilical arteries, coated with polyelectrolyte multilayers (3.5 bilayers of poly(styrene sulfonate)/poly(allylamine hydrochloride)), seeded with endothelial cells, and cultured *in vitro*. The constructs were successfully implanted as rabbit carotid substitute, demonstrating that preconditioning is a crucial factor for graft patency [116].

*8.1.2. Synthetic Approach.* PCL micro- and nanofiber-based vascular grafts were evaluated in a rat abdominal aorta replacement model for up to 18 months [117]. No dilatation or thrombosis and limited intimal hyperplasia were shown together with endothelialisation, cell invasion, and neovascularisation of the scaffold. Neverthless, after 18 months, the graft was remodeled, even if blood capillaries were not present and a calcification process was detected in the layers. PCL showed poor compliance before transplantation and did not improve throughout the time points. The same authors implanted in a rat model as an aortic replacement a PCL vascular graft with increased hydrophilicity (obtained by plasma treatment). After 3 weeks, a recellularized graft was revealed, suggesting that plasma treatment could be a strategy to easily increase the biocompatibility of a scaffold and accelerate tissue regeneration without compromising mechanical strength [118]. When compared to ePTFE electrospun grafts, transplanted in the same rat model, PCL scaffolds showed significantly better endothelial coverage, macrophage and fibroblast ingrowth, ECM deposition and angiogenesis, and no stenotic lesions up to 24 weeks [119]. In these experiments, however, chondroid metaplasia occurred after 6 weeks and was then replaced by calcification. A combination of PCL and collagen was used to improve cell adhesion and growth into the graft in a rabbit arterial bypass model [120]. This work indicates that the construct supported *in vitro* cell adherence and maintained structural integrity and patency over 1 month of implantation, but no cell invasion or evident endothelialisation was shown after this short time point. A scaffold composed of $\varepsilon$-caprolactone and lactic acid [P(CL/LA)], 50 : 50 ratio, was seeded with bone marrow cells and implanted in the inferior vena cava of dogs [121]. Analyses were more focused on cell proliferation and differentiation after 8 weeks after implantation, but histology showed graft remodelling with new ECM deposition. Natural and synthetic polymers were blended into an electrospun scaffold composed of chitosan and PCL to combine the bioactive functions of the first one (biocompatibility, low toxicity, and antibacterial properties) with the good mechanical properties of latter one [122]. The scaffold was seeded with autologous outgrowth endothelial cells harvested from canine peripheral blood and expanded *in vitro* and then implanted into carotid arteries of cell-donor dogs for 3 months. Chitosan/PCL scaffolds were characterized by nanofiber average diameter ($550 \pm 120$ nm), porosity (more than 80%), and tensile strength proper for vascular tissue engineering. Seeded scaffolds remained patent as compared with unseeded grafts 3 months after implantation, with tissue remodelling (presence of collagen and elastin) and regeneration of a functional endothelium. Furthermore, biomechanical properties were close to native carotid arteries when grafts were collected 3 months after transplantation, with no blood leaking or deformation. In Hoerstrup et al. [123], PGA meshes were coated with a thin layer of poly-4-hydroxybutyrate, seeded with myofibroblasts and endothelial cells, and surgically implanted as main pulmonary artery replacement in lambs for up to 100 weeks. The animals more than doubled their body weight during the 2-year period. Regular echocardiography and angiography showed good functional performance and absence of thrombus, calcification, stenosis, suture dehiscence, or aneurysm. There was a significant increase in diameter by 30% and length by 45%, cellular engraftment, and new ECM deposition in all

the groups, but the mechanical profiles of the graft were lower than native pulmonary arteries.

Cell-free PGA vascular graft, reinforced with P(CL/LA) monofilaments on the outer surface to maintain the shape for the initial crucial period following implantation, was implanted in a canine model of substitution of inferior vena cava (24 months) and pulmonary artery (12 months) [124, 125]. In both cases, histological examinations revealed a well-formed vessel-like vasculature without calcification and similarities to native vessels in terms of patency and biomechanical properties. The slower degradation rate of P(CL/LA) guaranteed constant construct elasticity during the tissue-remodelling process, resulting in prevention of stenosis and endothelialisation improvement. However, vascular SMCs were not well-developed 12 months after implantation in the pulmonary artery model [125]. Recently, the authors demonstrated that after 24 months, this biodegradable scaffold can gradually regenerate and develop into a mature vessel characterized by histological and biochemical properties similar to the native tissues [126]. The same combination of PGA and P(CL/LA) (80% porosity; 20–50 $\mu$m diameter) has been used with bone marrow derived cell seeding in an inferior vena cava substitution in dogs, showing higher remodelling and endothelial and smooth muscle cell invasion of the graft with respect to unseeded scaffolds, even though the latest time point was 4 weeks [127]. Tissue engineered PGA and P(CA/LA) scaffolds, seeded with bone marrow cells and implanted in an immune competent mouse model, demonstrated that this type of constructs, functionalized by mobilizing resident cells, allows the activation of the innate healing process, more than an active participation of the cells delivered concurrently with the scaffold [128–130].

Reinforced multiple layer scaffolds, created using polymers, like poly(ester urethane)urea, and obtained by thermally induced phase separation and electrospinning (for the outer layer) procedure, have shown higher resistance with lower mechanical failure and dilatation [131]. Multilayer tubular conduits, made of collagen fiber networks and elastin-like protein polymers, characterized by collagen ultrastructure (internal diameters: 1 and 4 mm) and mechanical properties similar to native blood vessels with limited platelet adhesion, were implanted in a rat aortic interposition model. After 14 days after implantation, grafts appeared patent with minimal adhesive response and with a limited early inflammatory response, suggesting that engineered collagen-elastin composites could represent a promising strategy for fabricating synthetic tissues with defined ECM content, composition, and architecture [132].

In order to accelerate construct remodelling and integration, a fast degrading elastomer, poly(glycerol sebacate), has been recently used in rat abdominal aorta substitution model [133]. The graft, coated with heparin to enhance thromboresistance, showed mechanical properties able to promote vascular cell differentiation and avoid stress shielding, being also characterized by high porosity with interconnected pores. Three months after transplantation, these cell-free grafts resembled native arteries in terms of pulsation, endothelium and smooth muscle layer development, expression of elastin, collagen and GAGs, and compliant mechanical properties. Scaffold integration and remodelling were almost complete after 3 months, suggesting that rapid graft degradation may be helpful for cell infiltration, positive inflammation, and new matrix production.

### 8.2. Clinical Studies

*8.2.1. Natural Approach.* Autologous human fibroblast and endothelial cell derived grafts were evaluated in a clinical trial including ten patients implanted with a completely biological and autologous tissue engineered vascular graft [112]. Self-assembling vessels, giving natural cell-produced ECM with established mechanical properties and *in vivo* applicability, showed promising results in early clinical applications. However, extensive *in vitro* culture and high costs are required [134].

## 9. Kidney

Even if kidney is the most commonly transplanted organ, its availability is limited [135]. Hemodialysis represents a real contribution to the survival of patients with end-stage renal disease, but transplantation is the only available curative treatment [136]. Clearly, the ultrastructure and function of this organ pose a significant challenge for the definition of a valuable tissue engineered substitutes. This concurs to explain the degree of the development of a viable alternative in terms of materials selected and *in vivo* experimentation. Ideally, a tissue engineered kidney should be able to replace all the functions, including endocrine and metabolic activities and removal of uremic protein-bound waste products [137]. The attention was therefore focused on those studies dealing with the whole organ, treated with specific protocols aimed to preserve the anatomical integrity and assess the potential to restore its peculiar physiology.

### 9.1. Preclinical Studies

*9.1.1. Natural Approach.* Using SDS, Orlando et al. [138] demonstrated an effective decellularization of porcine kidneys, preserving organ structure (including vascular network) and function. A particular care was adopted in the selection of the most suitable decellularization protocol. SDS may disrupt the native tissue architecture and damage some ECM components, but it was preferred to an enzymatic method, due to the adverse effect that enzymes may exert on digestion-sensitive molecules in the ECM, or to snap freezing because exposure to extremely low temperatures may alter the three-dimensional architecture of the scaffolds. The obtained decellularized kidney scaffolds were implanted for two weeks in pigs, matched for age and weight to the scaffold donors. The surgical procedure was technically feasible as the mechanical properties of the vasculature deprived of the endothelial layer supported the surgical reconnection of the vessel stumps of the scaffold to the recipient's aorta and vena cava. This study showed that the organ was reperfused and the scaffold implantation was well tolerated with no adverse reaction. However, according to the authors,

the lack of endothelium elicited the formation of massive thrombi within the renal artery and vein. Interestingly, the ureter was ligated and not reconnected to the bladder to reduce morbidity; moreover, it was also stated that no urine production was expected. Another interesting result, considering the whole organ for orthotopic transplantation and verifying its main function of urine production, was obtained by harvesting rat kidneys and preserving the intact and perfusable vascular, glomerular, and tubular compartments [136]. Kidneys, decellularized by a perfusion approach, were *in vitro* repopulated with endothelial and epithelial cells with consequent formation of a functional graft. Urine production was observed *in vitro* and this led the authors to test *in vivo* the engineered organ after orthotopic transplantation. Kidneys were anastomosed to the recipient's renal artery and vein and no evidence of bleeding was observed; ureter remained cannulated for collection of urine production, verified shortly after the unclamping of recipient vasculature. In addition $\beta$-1 integrin expression in engrafted podocytes suggested site-specific cell adhesion to physiologic ECM domains. This report highlighted the role of native ECM proteins, as laminins and collagen IV, the major ECM proteins of the glomerular basement membrane necessary for podocyte adhesion, slit diaphragm formation, and glomerular barrier function.

## 10. Bladder

Native nonurologic tissues, like gastrointestinal segments, are usually employed in reconstructive surgery [139, 140]. However, these tissues are lined by an absorptive and mucus-secreting epithelium that is incompatible with long-term exposure to urine [141]. This consideration further supports the need of a specific engineered scaffold that could properly replace the function of the organ, critically considering the microstructure of the native bladder which is then related to its specific action. Reported findings suggest that urothelium presents mechanosensitive sodium ion channels as transducers of the parasympathetic nervous system involved in bladder sensation and that cyclical deformation induces connective tissue synthesis [142]. The urothelium is one of the three major layers that constitute the bladder wall along with the lamina propria and the detrusor muscle. The different structures suggest that each component of this composite organ plays a peculiar role to assure the final function. In fact, an *ex vivo* study on the deformation characteristics of rat bladder wall showed that the organ can accommodate very large stretches prior to activation of neurological signals that trigger voiding and before collagen coils are fully distended, confirming that the lamina propria is the major structural capacitance layer, while the detrusor limits the total volume to avoid overdistention [143].

### 10.1. Preclinical Studies

*10.1.1. Natural Approach.* SIS has been implanted in rat and canine bladder augmentation models, resulting in the regeneration of full thickness bladder tissue, including urothelium, muscularis, nerves, and blood vessels, characterized by physical properties, such as contractility, similar to native bladder [144]. Moreover, it has been demonstrated that terminally differentiated urothelium is the first portion of the bladder to completely regenerate after SIS implantation [145]. However, SIS, derived from different segments (proximal small bowel or distal ileum), resulted to have different regenerative potential and further investigation resulted to be necessary to identify the effective SIS regenerative potential [146].

Rabbit or sheep decellularized gallbladders (2 cm × 2 cm), either alone or seeded with autologous detrusor muscle small fragments, have been implanted on rabbit bladder mucosa for bladder augmentation. No evidence of inflammatory response was revealed 12 weeks postoperatively, and after 24 weeks seeded grafts resulted in whole bladder and muscular layer regeneration and in new micro vessel formation, suggesting that fragment-seeded cholecyst-derived ECM can enhance the properties of acellular gallbladder in terms of bladder wall regeneration [147]. Even if a decellularized scaffold seems to be the direct and straightforward solution for tissue engineering of tissues and organs, several issues need to be addressed as well. Probably, the most critical one is related to neovascularization, which is pivotal in promoting tissue formation and should be therefore favoured by developing ad hoc strategies. Kanematsu et al. [148] dealt with a rat bladder acellular matrix, as a model, incorporating bFGF by a reswelling procedure of the growth factor solution. When tested for a possible bladder augmentation in rats (diameter 15–20 mm), it was observed that bFGF significantly enhanced angiogenesis, probably inhibiting the graft shrinkage at 4 weeks in a dose dependent manner, which was not suppressed after 12 weeks. The authors reported that this occurrence could be related to regression of immature vessels formed by bFGF or unclear characteristics of the infiltrating cells. The strategy to include relevant chemical cues into the tested matrix was also verified by using VEGF, a well-known angiogenic factor. In this regard, porcine bladder was firstly decellularized and treated either with HA or with HA-VEGF and then implanted into pigs for bladder augmentation (4 × 4 $cm^2$) [149]. The incorporation of HA significantly decreased the matrix porosity, preventing urine seepage and possible inflammation, while the presence of VEGF contributed to a great infiltration of microvessels. Moreover, the highest epithelialization was detected for the HA-VEGF scaffolds, as demonstrated by the presence of UPIII, a urothelium-specific protein. Subsequently, Chen et al. [150] proposed an acellular porcine bladder matrix preseeded with modified endothelial progenitor cells (transfected with VEGF gene carried by adenovirus). The scaffolds were then implanted into pigs which underwent partial cystectomy (about 40%); unseeded scaffolds were implanted as control. Postoperatively, treated grafts showed an enhanced neovascularization and prevented tissue shrinkage and scar formation.

Another possible concern on the use of naturally derived scaffolds is generally related to their limited temporal stability, but it has been rarely assessed *in vivo*. In this regard, $^{14}C$ labelled piglet SIS sheets were implanted into dogs to replace between 35 and 45% of the dome of native bladders [151].

Liquid scintillation assays showed that less than 10% of the radioactivity remained at 3 months after surgery, in addition the excretion of the scaffold was mainly via a hematogenous route with subsequent urinary excretion.

*10.1.2. Synthetic Approach.* According to the whole tissue engineering paradigm, an engineered scaffold can be cell seeded and conditioned, dynamically or not, before implantation. This option is not always followed as the implantation of the nude scaffold can be an alternative route to overcome the *in vitro* period that might expose the device to a possible contamination, also allowing reducing the waiting time before surgery. In this regard, the potential of noncell seeded gel spun silk matrices was assessed for murine bladder augmentation [152]. Silk fibroin solutions were prepared from *Bombyx mori* silkworm cocoons to obtain tubes by using the gel spinning technique. Tubular scaffolds were bisected along the central axis before implantation into an immune competent mouse strain model. Bladder reconstruction with silk led to an 82% survival rate, comparable to that with PGA (71%), and substantially higher than SIS implants (66%), the latter two being the reference cases. Connective tissue ingrowth was observed along the periphery of the silk matrix and traversed the defect site (day 21); the regenerated tissue was lined with a luminal multilayer epithelium bordered by a lamina propria with fibroblastic cell populations and a gradual increase in the degree and distribution of uroplakin expression was detected up to 70 days following implantation. However, a microscopic analysis of the implanted tube was not reported in the cited paper, as it was presented in a previous one [153]. As stated by the authors, no modifications occurred in the fabrication process and the final scaffold appeared to be like a dense structure without a fibrous architecture similar to the bladder ECM. The positive result presented seemed not to be affected by this occurrence, and probably an *in vivo* experimentation in larger animal models could further elucidate the point. Seeded polymeric scaffolds were evaluated in beagle dogs, undergone trigone-sparing cystectomy, by implanting PGA matrices (15 $\mu$m average fiber diameter) coated with PLGA [154]. Urothelial and muscle cells were harvested, expanded separately, and, within 5 weeks, seeded onto biodegradable polymer matrices. Three different groups were considered for the study: (i) animals that were primarily closed gained a minimal amount of reservoir volume without regaining the precystectomy values, (ii) unseeded grafts led to a slight increase in volume, a well-developed urothelial layer and a deficient muscular architecture, (iii) seeded scaffolds allowed to approach and surpass the precystectomy bladder capacities, showing a normal cellular organization. Bladder cystoplasty was performed into mongrel dogs by implanting PLGA based scaffolds with or without autologous UCs and SMCs to assess the resulting outcome as affected by the presence of seeded cells [155]. In this regard, a regenerative process was observed when UCs and SMCs were seeded onto the implant, while a reparative healing occurred for the unseeded scaffolds (e.g., mucosal growth, but an incomplete tissue layer development). However, this study was not focused on the characteristics of the implanted scaffolds, thus not allowing evaluating the possible influence of the three-dimensional architecture on the final result. The influence of seeded or unseeded PGA scaffolds on urothelial proliferation was also previously assessed by using 3T3 mouse fibroblasts for rat bladder augmentation [156]. Seeded cells acted as a "feeder layer" confirming an improved outcome compared to the control case. Different cell types were also evaluated for this aim, as tested by Lai et al. [157] comparing bladder SMCs and intestinal SMCs seeded onto unwoven PGA sheets covered with PLGA for urinary bladder wall replacement in a rabbit model. However, a real improvement in bladder regeneration is strictly related to the nervous tissue regeneration. This issue was addressed by implanting PGA grafts, covered with fibroblast-seeded chitosan and modified with chitosan, to allow nerve growth within the bladder wall [158]. No complications were noticed and immunostaining results showed the presence of neuronal cells, suggesting that chitosan could improve scaffold abilities not only as a cell matrix, but also in guiding neurons into the graft.

In order to be as close as possible to the morphological structure of the bladder ECM, the fibrous architecture was considered by Del Gaudio et al. [159] evaluating an electrospun scaffold made of PCL and PHBV (50 : 50 ratio). The collected mats were composed of randomly arranged fibers, free of defects (3.0 ± 0.1 $\mu$m average fiber diameter), and, due to the dynamic function of the here considered organ, characterized by means of dynamic mechanical analysis in a frequency range representative of the time scales of the physiological dynamics of the bladder wall. The electrospun scaffolds were implanted into rats for bladder augmentation and retrieved at 15, 30, and 90 days for the subsequent histological assays. The regenerative process was poorly evident in specimens 15 days after surgery, evident after 30 days and complete three months after. A progressive reconstitution of the entire bladder wall on the top of the scaffold to build a "new dome" was observed, with moderate scars along the suture lines. The bladder wall was reconstituted with the growth of both normal urothelium and fibrils of smooth muscle cells. The electrospinning approach was also followed to fabricate a hybrid scaffold composed of pig BAM substrates covered by PGA or PGA-PEG fibers [160]. An *in vivo* evaluation was carried out by implanting bladder SMC-seeded scaffolds into rats subjected to partial cystectomy (>50%): both types of substitutes supported the formation of a bladder wall-like structure, even if a significant shrinkage was observed for the PGA scaffold and an increased microvessel density characterized the PGA-PEG scaffold. Previously, the same group started this study including PLGA only and evaluating three different electrospinning procedures, that is, continuous spinning of PLGA microfibers on dry BAM, continuous spinning of PLGA microfibers on wet BAM, and layer-by-layer spinning of PLGA fibers on continuously rehydrated BAM [161]. After *in vivo* implantation, urothelium, smooth muscle, and collagen rich layers infiltrated with host cells and microvessels were detected. Furthermore, hybrid scaffolds maintained normal bladder capacity, whereas BAM recipients showed a significant distension of the bladder, demonstrating that

adaptable hybrid scaffold supports bladder regeneration and holds potential for engineering of bladder.

A dome-shaped scaffold composed of electropulled PLGA mat (inner surface) and PLGA sponge, made by solvent casting and salt leaching, (outer surface) was evaluated as a potential substrate for amniotic stem cell differentiation into SMCs for rat bladder augmentation [162]. The composite had a final diameter of 10 mm and thickness of 0.8 mm; the inner surface was composed of polymeric fibers characterized by a large distribution (0.5–10 $\mu$m). Postoperatively, bladder capacity and compliance were maintained in the cell-seeded group throughout the 12 weeks, while the acellular scaffold group (control group) showed a sequential deterioration with time. In addition, the contractile response was observed after 12 weeks, probably due, according to the authors, to the time for PLGA to be completely resorbed, as well as for the time required for the smooth muscle to gain significant mass.

Finally, to improve the *in vivo* outcome of the regenerative strategy, postfabrication treatments or scaffolds with nanostructured surface have been tested. Modified silk scaffolds have been implanted in a murine model for bladder augmentation and different results have been obtained, demonstrating that selective alterations in fabrication parameters can enhance the degradation rate of gel spun silk scaffolds *in vivo* while preserving their ability to support bladder tissue regeneration and function [163]. Nanometric (less than 100 nm) PLGA/PU scaffolds, treated with NaOH or $HNO_3$ [164] and/or functionalized with IKVAV and YIGSR peptides, to improve cellular responses [165], have been tested for bladder tissue regeneration in a minipig model. After 11 weeks, both the urothelium and smooth muscle were consistently and continuously formed on the new bladder wall tissue with the polymer incorporation. These studies suggested that nanostructured resorbable synthetic scaffolds could be promising replacement materials for partial bladder and urogenital repair as well as neobladder replacement.

### 10.2. Clinical Studies

*10.2.1. Synthetic Approach.* Moving to clinical applications, a viable engineered substitute should be fabricated based on the composite nature and properties of the bladder. This approach was followed by Atala et al. [17] to treat seven patients with myelomeningocele. Urothelial and muscle cells, obtained by a biopsy from each patient, were cultured and then seeded onto biodegradable bladder-shaped scaffold made of collagen (from homologous decellularized bladder submucosa), or collagen and PGA, to be implanted with or without omental wrap. In the follow-up no complications were noted and the renal function was preserved. Moreover, the mean maximum capacity in the collagen engineered bladders without omental wrap showed a 30% decrease, the one with omental wrap showed a 1.22-fold increase in volume, while the composite engineered bladders wrapped with omentum showed a 1.58-fold increase. These results supported the conclusion that PGA contributed to structural integrity, while collagen to cell growth and survival.

## 11. Urinary Tracts

In this section tissue engineering applications to both ureter and urethra reconstruction are considered. These structures are mainly characterized by a transport function that can be severely impaired by several disorders such hypospadias, epispadias, and strictures, specifically referring to urethra [166]. In this regard, the implanted scaffold should promptly concur to recover the natural function offering a suitable environment that does not elicit any adverse reaction, particularly due to the toxic nature of the fluids in contact with the scaffold surface. The role of a functional epithelium is therefore crucial and this might suggest planning ad hoc strategy for the development of a proper tissue engineered conduit.

### 11.1. Preclinical Studies

*11.1.1. Natural Approach.* A possible improvement for urethral reconstruction, firstly based on the use of oral keratinocytes seeded onto BAM [167], was proposed by the same group considering oral keratinocyte and TGF-$\beta$1 siRNA transfected fibroblast seeded onto BAM in order to minimize the inflammatory response and avoid graft contraction and shrinkage [168]. For this aim, a mucosal defect (2 cm length and 0.8 cm width) was created in the anterior rabbit urethra obtaining 3 groups: oral keratinocyte and TGF-$\beta$1 siRNA transfected fibroblast-seeded BAM, autologous oral keratinocyte-seeded grafts, and unseeded grafts. All the animals survived to the postoperative observational period (up to 6 months), being characterized by a severe fibrosis and shrinkage (control group), intact epidermal cellular layer (increasing to 5–7 layers) with no evidence of the formation of capillary in the lower layer (autologous oral keratinocyte-seeded grafts), or by a well-developed 5 to 7 layers of stratified keratinocytes associated with the formation of capillary in the epithelial lower layer at 6 months after implantation (TGF-$\beta$1 siRNA group). This approach showed that TGF-$\beta$1 siRNA can inhibit the expression of TGF-$\beta$1 and significantly reduce the secretion of type I collagen and scar formation. The concept to use two different cell lines was already explored by Feng et al. [169], stating that this approach can accelerate the regenerative process and avoid strictures. In this regard, porcine ACSMs were seeded with lingual keratinocytes or with autologous CSMCs and lingual keratinocytes and transplanted into rabbits to recover a urethral defect. After 6 months, fibrosis, inflammation, and the absence of epithelium were observed in animals treated with ACSMs, simple epithelial layer regeneration was revealed in the case of ACSMs seeded with CSMCs, while stratified epithelial layer and organized muscle fiber bundles were evident in animal treated with ACSMs seeded with both cellular types. Even if a naturally derived material seems to be the most appropriate choice for a tissue engineered specific scaffold, several drawbacks can be highlighted as well. In fact, in this study a sever inflammatory response was highlighted due to (i) a slight retention of cellular compounds within the ACSM, that might cause chronic immunoreactions and fibrosis, (ii) the long urethral defect length (1.5 cm) that limited the regeneration of native

urothelium, and (iii) the thickness of the scaffold that hindered the penetration of a vascular network into the matrix. A nude substrate can be hardly considered as a suitable means to promote tissue regeneration, since the lack of a functional epithelium concurs to the high rate urethral reconstruction failure. For this aim, Li et al. [170] assessed whether Epith-rASCs seeded onto rabbit bladder acellular matrix could aid the regeneration of a defect (2 cm length and 0.8 cm width) in rabbits' ventral anterior urethra. A remarkable stricture was detected into two control groups (undifferentiated adipose-derived stem cells grafts and unseeded grafts), differently from the treated case. Epith-rASCs showed the capability to differentiate into epithelium due to the contribution of *in vivo* urethral microenvironment. On the other hand, in the undifferentiated group, the contracture of grafts did not ameliorate even if epithelial differentiation of the implanted cells occurred, but this relatively slow process could not prevent inflammatory cell infiltration and fibrosis of lumen. The role of the epithelium was underlined by a comparable approach for the urethral reconstruction by using bone marrow MSCs and SMCs into a bladder acellular matrix [171]. Bladder was firstly explanted from rabbits and, after being decellularized, seeded with those two cell lines, wrapped around a catheter (MSCs on the luminal side), and covered with omentum has been implanted into rabbits to recover a 4 cm ureter defect. Multilayered urothelium covered the entire lumen with central visible neovascularization after 8 and 16 weeks postoperatively. This result further underlined the role of a proper scaffold, as the bladder acellular matrix, which provides at least 10 different biological factors (including, e.g., VEGF, TGF-$\beta$1, and bFGF), supporting a good microenvironment for cell migration, proliferation, and differentiation [172].

*11.1.2. Synthetic Approach.* An example of urethral reconstruction by using a collagen tubular scaffold was proposed by Micol et al. [166]. According to this approach a high density collagen gel tube was fabricated including autologous SMCs from bladder biopsy to repair a 1 cm defect in the rabbit urethra. Spontaneous urothelial regeneration was observed that can be ascribed to colonization from the edges of native urothelium adjacent to the graft, or by seeding, during voiding, of urine-derived progenitor cells.

### *11.2. Clinical Studies*

*11.2.1. Synthetic Approach.* Clinical urethral reconstruction was performed in five boys (median age 11 years) by using tubularised fibrous polyglycolic acid:poly(lactide-coglycolide acid) scaffolds seeded with muscle (outer surface) and epithelial (inner surface) cells from a biopsy of each patient [20]. Scanning electron microscopy revealed that all scaffold surfaces were covered with cells at day 6 of culture. The size of the engineered urethras ranged from 4 to 6 cm (median 5 cm), with a 16 French diameter, and the construction of the implantable scaffolds took 4–7 weeks. All patients were continent and the absence of fistulae or urinary tract infections was verified during the follow-up (range 36–76 months).

## 12. Skeletal Muscle

Skeletal muscle has a remarkable inherent ability to regenerate and self-repair in response to limited and not severe injury and stress [173, 174]. Damage caused by crush injury or blunt trauma is typically associated with a host response that leads to the activation and differentiation of a population of resident muscle stem cells named satellite cells [175]. Therapeutic options for severe and extensive muscle injury (such as VML) are currently limited and reconstruction of skeletal muscle in these injuries remains a complex and unsolved task. Typical therapeutic procedures include autologous tissue transfer, muscle transposition, or amputation, but they show minimal success and extensive donor site morbidity [176–181]. Repair technologies have been focusing in the last few years on tissue engineering to reconstruct and restore structural and functional deficit of the skeletal muscle after VML. Several synthetic and natural-derived scaffolds have been developed and studied *in vitro* with the aim of mimicking the muscle ECM structure and properties; however, very few have been tested in reliable muscle injury animal models, mainly after total or partial muscle ablation and substitution [182].

### *12.1. Preclinical Studies*

*12.1.1. Natural Approach.* Several ECM proteins have been adopted for scaffold fabrication for skeletal muscle tissue engineering. Collagen electrospun scaffolds, seeded with C2C12 cells, were implanted in the mouse gastrocnemius. After different time points, a slow degradation of the scaffold has been showed, with activation of vascularization and the regeneration of muscle fibers [183]. These constructs, however, had low biocompatibility since only immune-compromised mice were able to integrate the 3D tissue graft into their host tissue. Also, the development of a fibrotic tissue has been shown and this is known to lead to healing problems and potential tissue/organ dysfunction during the final healing stages.

Fibrin, collagen, and other ECM proteins are used also to form scaffolds in commercially available gel forms or can be suspended for the creation of functional engineered musculoskeletal tissue [184]. These ECM-derived gels provide natural-like microenvironment for MSC proliferation and differentiation, but scale-up of these scaffolds is a major limitation.

A fibrin-based scaffold, seeded with adult human myoblasts, has been studied *in vivo* in a partial-thickness tibialis anterior muscle injury model in mouse [185]. Cell engraftment was observed 10 weeks after implantation, with reduced collagen deposition and mean tetanic force of the tibialis anterior recovered to approximately 90% of uninjured values. In a quite innovative approach, dual layered collagenous scaffolds were constructed with a radial pore orientation or with round pores. Unseeded scaffolds were implanted into a surgically created diaphragm defect in rats and explanted

after 12 weeks. While new collagen deposition was more oriented in radial scaffolds with respect to round pores, cells and vessel migration within the scaffolds was similar between the two constructs [186].

Skeletal muscle regeneration and reconstruction are improved when native-derived scaffolds are used because of their content in cytokines that are released by means of matrix degradation. Furthermore, macrophage activation and polarization to M2 phenotype have been identified as an important mechanism determining proregenerative response after ECM-derived scaffold transplantation [187–191]. Acellular tissue scaffolds for skeletal muscle tissue engineering have been developed with several protocols starting from a wide variety of tissues and evaluated in a large number of animal models. ECM-derived scaffolds have been transplanted with and without muscle precursor cells since the early studies. An abdominal wall defect model has been used to test muscle-derived matrices obtained with different decellularization protocols and transplanted to correct the defect in rats and rabbits [192–194]. Matrices were also seeded with myoblasts and showed support to fibroblast migration, deposition of newly formed collagen, and neovascularization. However, evidence of skeletal-muscle-cell ingrowth was very poor and muscular electrophysiologic activity was minimum, with more encouraging results with myoblasts-seeded patches. Fibrosis development seems to be the major limitation of this approach using muscle-derived matrices after decellularization. Although acellular muscle ECM conserve chemical and architectural features of the original tissue, few papers highlighted strong myogenesis activation and de novo formation of muscle fibers derived from local activated muscle precursor cells [195–197].

As recently shown, the use of scaffolds originated from skeletal muscle tissue is not exclusive for muscle regeneration and different matrices can have equal or stronger benefits. SIS-derived acellular scaffolds have been compared *in vivo* to muscle ECM-derived matrices in a rat abdominal wall injury model [198]. Composition in growth factor content, GAGs, and basement membrane structural proteins were different between the two matrices, but *in vivo* results showed similar effects on constructive remodelling outcome and myogenesis in the implanted area, suggesting that superior muscle regeneration is not universally dependent upon homologous tissue derived ECM scaffolds [198, 199]. SIS-derived scaffolds have been largely tested in muscle defects in rodents and dogs, generally showing formation of vascularized skeletal muscle with different degrees of functional restoring (when tested) [181, 200, 201].

Porcine bladder-derived acellular matrix has also been tested in a mouse VML model with similar outcomes: 2 months postinjury and implantation of the scaffold seeded with muscle progenitor cells demonstrated remodelling of the construct and formation of new desmin-positive myofibers with and without striations, blood vessels, and neurovascular bundles in the site of implantation, but neuromuscular junction function has not been demonstrated [202]. Engineered acellular bladder seeded with muscle precursor cells and transplanted in a VML defect in tibialis anterior muscle exhibited variable capacity to restore *in vivo* function of injured muscles 12 weeks after injury [203]. In this work, cell seeded matrices promoted muscle fiber regeneration within the initial defect area, indicating that engineered constructs, including a cellular component, can improve the *in vivo* functional capacity of the injured musculature generating functional skeletal muscle fibers.

*12.1.2. Synthetic Approach.* Several biodegradable synthetic scaffolds have been developed to support muscle regeneration and regrowth. Despite several attempts, cell engraftment, and proliferation within the synthetic construct is generally limited by low early adhesion. These scaffolds also tend to be more rigid than a biological matrix, interfering with functional muscle force development and transmission [184, 204]. Nevertheless, synthetic scaffolds are largely studied in literature for muscle tissue engineering application [184, 185, 205, 206].

Among several types of polymers used as a construct for muscle replacement and support, electrospun synthetic polymer mats, made of uniformly aligned fibers, resembling skeletal muscle ECM, are the scaffolds most evaluated in *in vivo* studies. Electrospun fibrous matrices have been fabricated of different single or combinations of polymers and promote cell adhesion and proliferation and nutrient diffusion and provide favourable mechanical properties [184, 205, 206]. These sheets of fibres from polymers, and sometimes biological proteins (elastin and collagen), are cost-effective and can be customized for pore size and fiber diameter and length and density. These characteristics affect muscle cell adhesion, migration, functional differentiation, and nutrient and oxygen availability in the engineered muscle [184, 205–207].

*In vivo*, unseeded biodegradable fibers of PEUU deposited with electrosprayed serum-based culture medium have been used in a rat model for abdominal wall replacement [208]. This wet electrospinning resulted in scaffolds with softer mechanical properties and a distinct morphology with fiber tortuosity (looping) that might ease cell migration by more readily locally distended fibers. 8 weeks after implantation, PEUU substrate showed a healing result that developed toward approximating physiologic mechanical behaviour. Extensive cellular infiltrate with smooth muscle and endothelial positive cells was observed together with ECM (collagens, elastin) elaboration. The functional result, however, seemed to be an effect of scaffold replacement by a fibrotic scar tissue improving only passive mechanical properties rather than active functionality of any new muscle tissue.

Zhao et al. [209] used an electrospun PCL/collagen hybrid scaffold for diaphragmatic muscle reconstruction. The aligned fibrous scaffold was fabricated to mimic muscle organization and to guide muscle cell orientation. Furthermore, these scaffolds, combining both synthetic polymer and naturally derived material, effectively supported cell adhesion, proliferation, and differentiation. The hybrid scaffolds were implanted into a central left hemidiaphragmatic defect in rats, showing muscle ingrowth into the scaffold up to 6 months after implantation. The mechanical properties of

the retrieved diaphragmatic scaffolds were similar to those of normal tissue: electrospun PCL/collagen hybrid scaffolds exhibited initial elastic behaviour followed by stiffening, a behaviour which is similar to the tensile behaviour of native tissues. The *in vivo* remodelling process evidenced organized skeletal muscle cells, vascularization, and deep cell infiltration into the scaffold. Coaxial electrospun scaffolds, made of PCL, multiwalled carbon nanotubes and a (83/17 or 40/60) poly(acrylic acid)/poly(vinyl alcohol) hydrogel, capable of movement with electrical stimulation, have been implanted into a cavity (5 mm × 5 mm) created within the vastus lateralis muscle of rats for four weeks to determine *in vivo* biocompatibility. No significant clinical adverse effects and complications were revealed, and both scaffold types displayed evidence of muscle regeneration and neovascularisation after 28 days postimplantation. Although initial results are encouraging, authors commented that longer studies are necessary to determine if the two hydrogel concentrations will critically affect the body including local and systemic effects [210].

## 13. Concluding Remarks

The need for a suitable scaffold that can (i) accommodate cells, (ii) be instructive, (iii) mimic the natural ECM to be replaced, and (iv) promote an effective tissue regeneration is mandatory for tissue engineering applications. As already stated, this is only a partial vision of the whole problem because the term/concept "scaffold" needs to be understood in detail. The analysis of the results here reported, that was strictly focused on orthotopic implants with the aim to provide the state of the art for a reliable bench-to-bedside translation, clearly shows that multiple solutions have been proposed that still need to be properly refined for the desired outcome. Obviously, the *in vivo* approach does not guarantee a safe and viable technique to treat degenerative pathologies but is a necessary step to furnish relevant findings on the possible response of a tissue engineered scaffold. This approach helps to overcome the inherent limitations of the *in vitro* model but should not be considered as the only resource to test or verify an idea. On the contrary, it must be clearly stated that the animal experimentation is the last step to functionally assess a device when all the preliminary characterizations have given a positive response. As here demonstrated, dealing with scaffolds structurally similar to the anatomic site to be recovered, like the ones derived from a decellularization process, does not necessarily improve the host response since the key factor is the delicate interplay among different factors that concur to define a specific tissue. Morphology, three-dimensional architecture, mechanical and chemical properties, selection of the most appropriate cell type (i.e., stem cells or already differentiated cells), surface treatments, combination of multiple materials to fabricate a composite, loading and release of drugs and/or growth factors, and *in vitro*/*in vivo* models are to be critically evaluated and require a deep knowledge of all the aspects of the tissue or organ to be healed. The complexity of the problem is strictly dependent on the resulting outcome obtained by combining two or more of these starting elements, and a proper observational period after implantation can support the critical assessment of the investigated approach. Long follow-ups are therefore needed, like the one, for instance, ranging from 22 to 61 months considered to evaluate the response of tissue engineered bladders for patients needing cystoplasty [17] or the one (5 years) regarding the tissue engineered trachea transplantation to replace an end-staged left main bronchus with malacia [50].

Regarding the starting questions of this review, it is possible to conclude that clinical investigations effectively support the bench-to-bedside translation of the tissue engineering approach for some tissues/organs, allowing enhancing and proposing novel strategies toward a desired outcome. However, for complex organs more detailed studies are still necessary to develop a suitable engineered solution. A critical improvement of the knowledge of the host response to an implanted scaffold, which is dependent on all the features discussed in this review, is essential in order to accurately design a viable device aimed to readily promote the healing process.

## Acronyms

| | |
|---|---|
| ACSM: | Acellular corpus spongiosum matrix |
| ASCs: | Adipose stem cells |
| BAM: | Bladder acellular matrix |
| bFGF: | Basic fibroblast growth factor |
| BMCs: | Bone marrow cells |
| CSMCs: | Corporal smooth muscle cells |
| ECM: | Extracellular matrix |
| EPCs: | Epithelial precursor cells |
| Epith-rASCs: | Epithelial-differentiated rabbit adipose-derived stem cells |
| G-CSF: | Granulocyte colony-stimulating factor |
| GAGs: | Glycosaminoglycans |
| HA: | Hyaluronic acid |
| MSCs: | Mesenchymal stem cells |
| PCL: | Poly($\varepsilon$-caprolactone) |
| PCU: | Poly(carbonate-urea)urethane |
| PEG: | Poly(ethylene glycol) |
| PEUU: | Poly(ester urethane)urea |
| PGA: | Polyglycolic acid |
| PHBHHx: | Poly(3-hydroxybutyrate-co-3-hydroxyhexanoate) |
| PHBV: | Poly(3-hydroxybutyrate-co-3-hydroxyvalerate) |
| PLA: | Polylactic acid |
| PLGA: | Poly(lactic-*co*-glycolic acid) |
| POSS: | Polyhedral oligomeric silsesquioxane |
| PU: | Poly(ether urethane) |
| ePTFE: | Expanded polytetrafluoroethylene |
| SDS: | Sodium dodecyl sulphate |
| SIS: | Small intestine submucosa |
| SMCs: | Smooth muscle cells |
| TGF-$\beta$1: | Transforming growth factor-$\beta$1 |
| UCs: | Urothelial cells |
| VEGF: | Vascular endothelial growth factor |
| VML: | Volumetric muscle loss. |

## Conflict of Interests

The authors declare that there is no conflict of interests regarding the publication of this paper.

## References


[1] C. Del Gaudio, S. Baiguera, F. Ajalloueian, A. Bianco, and P. Macchiarini, "Are synthetic scaffolds suitable for the development of clinical tissue-engineered tubular organs?" *Journal of Biomedical Materials Research A*, vol. 102, no. 7, pp. 2427–2447, 2013.

[2] G. Orlando, S. Soker, and R. J. Stratta, "Organ bioengineering and regeneration as the new holy grail for organ transplantation," *Annals of Surgery*, vol. 258, no. 2, pp. 221–232, 2013.

[3] H. Shin, S. Jo, and A. G. Mikos, "Biomimetic materials for tissue engineering," *Biomaterials*, vol. 24, no. 24, pp. 4353–4364, 2003.

[4] C. Del Gaudio, E. Ercolani, P. Galloni et al., "Aspirin-loaded electrospun poly(ε-caprolactone) tubular scaffolds: potential small-diameter vascular grafts for thrombosis prevention," *Journal of Materials Science: Materials in Medicine*, vol. 24, no. 2, pp. 523–532, 2013.

[5] C. T. Laurencin and L. S. Nair, *Nanotechnology and Tissue Engineering: The Scaffold*, CRC Press, Boca Raton, Fla, USA, 2008.

[6] J. A. Pedersen and M. A. Swartz, "Mechanobiology in the third dimension," *Annals of Biomedical Engineering*, vol. 33, no. 11, pp. 1469–1490, 2005.

[7] T. M. Handel, Z. Johnson, S. E. Crown, E. K. Lau, M. Sweeney, and A. E. Proudfoot, "Regulation of protein function by glycosaminoglycans: as exemplified by chemokines," *Annual Review of Biochemistry*, vol. 74, pp. 385–410, 2005.

[8] S. C. Owen and M. S. Shoichet, "Design of three-dimensional biomimetic scaffolds," *Journal of Biomedical Materials Research A*, vol. 94, no. 4, pp. 1321–1331, 2010.

[9] G. Khang, S. J. Lee, M. S. Kim et al., "Scaffolds; tissue engineering," in *Webster's Biomedical Engineering Handbook*, S. Webster, Ed., pp. 366–383, John & Wiley Press, New York, NY, USA, 2006.

[10] S. Baiguera, C. Del Gaudio, M. O. Jaus et al., "Long-term changes to in vitro preserved bioengineered human trachea and their implications for decellularized tissues," *Biomaterials*, vol. 33, no. 14, pp. 3662–3672, 2012.

[11] Y. Gustafsson, J. Haag, P. Jungebluth et al., "Viability and proliferation of rat MSCs on adhesion protein-modified PET and PU scaffolds," *Biomaterials*, vol. 33, no. 32, pp. 8094–8103, 2012.

[12] H. Naderi, M. M. Matin, and A. R. Bahrami, "Review paper: Critical issues in tissue engineering: biomaterials, cell sources, angiogenesis, and drug delivery systems," *Journal of Biomaterials Applications*, vol. 26, no. 4, pp. 383–417, 2011.

[13] H. N. Kim, A. Jiao, N. S. Hwang et al., "Nanotopography-guided tissue engineering and regenerative medicine," *Advanced Drug Delivery Reviews*, vol. 65, no. 4, pp. 536–558, 2013.

[14] H. N. Kim, D. H. Kang, M. S. Kimet et al., "Patterning methods for polymers in cell and tissue engineering," *Annals of Biomedical Engineering*, vol. 40, no. 6, pp. 1339–1355, 2012.

[15] N. Hibino, E. McGillicuddy, G. Matsumura et al., "Late-term results of tissue-engineered vascular grafts in humans," *Journal of Thoracic and Cardiovascular Surgery*, vol. 139, no. 2, pp. 431–436, 2010.

[16] N. L'Heureux, T. N. McAllister, and L. M. de la Fuente, "Tissue-engineered blood vessel for adult arterial revascularization," *New England Journal of Medicine*, vol. 357, no. 14, pp. 1451–1453, 2007.

[17] A. Atala, S. B. Bauer, S. Soker, J. J. Yoo, and A. B. Retik, "Tissue-engineered autologous bladders for patients needing cystoplasty," *The Lancet*, vol. 367, no. 9518, pp. 1241–1246, 2006.

[18] P. Macchiarini, P. Jungebluth, T. Go et al., "Clinical transplantation of a tissue-engineered airway," *The Lancet*, vol. 372, no. 9655, pp. 2023–2030, 2008.

[19] P. Jungebluth, E. Alici, S. Baiguera et al., "Tracheobronchial transplantation with a stem-cell-seeded bioartificial nanocomposite: a proof-of-concept study," *The Lancet*, vol. 378, no. 9808, pp. 1997–2004, 2011.

[20] A. Raya-Rivera, D. R. Esquiliano, J. J. Yoo, E. Lopez-Bayghen, S. Soker, and A. Atala, "Tissue-engineered autologous urethras for patients who need reconstruction: an observational study," *The Lancet*, vol. 377, no. 9772, pp. 1175–1182, 2011.

[21] T. H. Petersen, E. A. Calle, L. Zhao et al., "Tissue-engineered lungs for in vivo implantation," *Science*, vol. 329, no. 5991, pp. 538–541, 2010.

[22] H. C. Grillo, "Tracheal replacement: a critical review," *Annals of Thoracic Surgery*, vol. 73, no. 6, pp. 1995–2004, 2002.

[23] A. E. Doss, S. S. Dunn, K. A. Kucera, L. A. Clemson, and J. B. Zwischenberger, "Tracheal replacements: part 2," *ASAIO Journal*, vol. 53, no. 5, pp. 631–639, 2007.

[24] K. Kojima, R. A. Ignotz, T. Kushibiki, K. W. Tinsley, Y. Tabata, and C. A. Vacanti, "Tissue-engineered trachea from sheep marrow stromal cells with transforming growth factor $\beta 2$ released from biodegradable microspheres in a nude rat recipient," *Journal of Thoracic and Cardiovascular Surgery*, vol. 128, no. 1, pp. 147–153, 2004.

[25] J. W. Park, D. Pavcnik, B. T. Uchida et al., "Small intestinal submucosa covered expandable Z stents for treatment of TrachEal injury: an experimental pilot study in swine," *Journal of Vascular and Interventional Radiology*, vol. 11, no. 10, pp. 1325–1330, 2000.

[26] S. P. Gubbels, M. Richardson, D. Trune, D. A. Bascom, and M. K. Wax, "Tracheal reconstruction with porcine small intestine submucosa in a rabbit model," *Otolaryngology: Head and Neck Surgery*, vol. 134, no. 6, pp. 1028–1035, 2006.

[27] L. Zhang, Z. Liu, P. Cui, D. Zhao, and W. Chen, "SIS with tissue-cultured allogenic cartilages patch tracheoplasty in a rabbit model for tracheal defect," *Acta Oto-Laryngologica*, vol. 127, no. 6, pp. 631–636, 2007.

[28] T. W. Gilbert, S. Gilbert, M. Madden, S. D. Reynolds, and S. F. Badylak, "Morphologic assessment of extracellular matrix scaffolds for patch tracheoplasty in a canine model," *Annals of Thoracic Surgery*, vol. 86, no. 3, pp. 967–974, 2008.

[29] N. T. Remlinger, C. A. Czajka, M. E. Juhas et al., "Hydrated xenogeneic decellularized tracheal matrix as a scaffold for tracheal reconstruction," *Biomaterials*, vol. 31, no. 13, pp. 3520–3526, 2010.

[30] E. Meezan, J. T. Hjelle, K. Brendel, and E. C. Carlson, "A simple, versatile, nondisruptive method for the isolation of morphologically and chemically pure basement membranes from several tissues," *Life Sciences*, vol. 17, no. 11, pp. 1721–1732, 1975.

[31] P. Jungebluth, T. Go, A. Asnaghi et al., "Structural and morphologic evaluation of a novel detergent-enzymatic tissue-engineered tracheal tubular matrix," *Journal of Thoracic and Cardiovascular Surgery*, vol. 138, no. 3, pp. 586–593, 2009.

[32] S. Baiguera, P. Jungebluth, A. Burns et al., "Tissue engineered human tracheas for in vivo implantation," *Biomaterials*, vol. 31, no. 34, pp. 8931–8938, 2010.

[33] M. T. Conconi, P. de Coppi, R. di Liddo et al., "Tracheal matrices, obtained by a detergent-enzymatic method, support in vitro the adhesion of chondrocytes and tracheal epithelial cells," *Transplant International*, vol. 18, no. 6, pp. 727–734, 2005.

[34] F. L. Gray, C. G. Turner, A. Ahmed, C. E. Calvert, D. Zurakowski, and D. O. Fauza, "Prenatal tracheal reconstruction with a hybrid amniotic mesenchymal stem cells-engineered construct derived from decellularized airway," *Journal of Pediatric Surgery*, vol. 47, no. 6, pp. 1072–1079, 2012.

[35] P. Jungebluth, A. Bader, S. Baiguera et al., "The concept of in vivo airway tissue engineering," *Biomaterials*, vol. 33, no. 17, pp. 4319–4326, 2012.

[36] B. H. I. Ruszymah, K. Chua, M. A. Latif, F. Nor Hussein, and A. Bin Saim, "Formation of in vivo tissue engineered human hyaline cartilage in the shape of a trachea with internal support," *International Journal of Pediatric Otorhinolaryngology*, vol. 69, no. 11, pp. 1489–1495, 2005.

[37] X. Luo, G. Zhou, W. Liu et al., "In vitro precultivation alleviates post-implantation inflammation and enhances development of tissue-engineered tubular cartilage," *Biomedical Materials*, vol. 4, no. 2, Article ID 025006, 2009.

[38] K. Kojima, L. J. Bonassar, A. K. Roy, C. A. Vacanti, and J. Cortiella, "Autologous tissue-engineered trachea with sheep nasal chondrocytes," *Journal of Thoracic and Cardiovascular Surgery*, vol. 123, no. 6, pp. 1177–1184, 2002.

[39] K. Kojima, L. J. Bonassar, A. K. Roy, H. Mizuno, J. Cortiella, and C. A. Vacanti, "A composite tissue-engineered trachea using sheep nasal chondrocyte and epithelial cells," *FASEB Journal*, vol. 17, no. 8, pp. 823–828, 2003.

[40] M. Kanzaki, M. Yamato, H. Hatakeyama et al., "Tissue engineered epithelial cell sheets for the creation of a bioartificial trachea," *Tissue Engineering*, vol. 12, no. 5, pp. 1275–1283, 2006.

[41] C. H. Lin, S. H. Hsu, J. M. Su, and C. Chen, "Surface modification of poly(ε-caprolactone) porous scaffolds using gelatin hydrogel as the tracheal replacement," *Journal of Tissue Engineering and Regenerative Medicine*, vol. 5, no. 2, pp. 156–162, 2011.

[42] C. K. Tsao, C. Y. Ko, S. R. Yang et al., "An ectopic approach for engineering a vascularized tracheal substitute," *Biomaterials*, vol. 35, no. 4, pp. 1163–1175, 2014.

[43] X. Luo, Y. Liu, Z. Zhang et al., "Long-term functional reconstruction of segmental tracheal defect by pedicled tissue-engineered trachea in rabbits," *Biomaterials*, vol. 34, no. 13, pp. 3336–3344, 2013.

[44] H. Tsukada, S. Gangadharan, R. Garland, F. Herth, M. Decamp, and A. Ernst, "Tracheal replacement with a bioabsorbable scaffold in sheep," *Annals of Thoracic Surgery*, vol. 90, no. 6, pp. 1793–1797, 2010.

[45] T. Sato, M. Araki, N. Nakajima, K. Omori, and T. Nakamura, "Biodegradable polymer coating promotes the epithelization of tissue-engineered airway prostheses," *Journal of Thoracic and Cardiovascular Surgery*, vol. 139, no. 1, pp. 26–31, 2010.

[46] H. Naito, T. Tojo, and M. Kimura, "Engineering bioartificial tracheal tissue using hybrid fibroblast-mesenchymal stem cell cultures in collagen hydrogels," *Interactive Cardiovascular and Thoracic Surgery*, vol. 12, no. 2, pp. 156–161, 2011.

[47] T. Sekine, T. Nakamura, H. Ueda et al., "Replacement of the tracheobronchial bifurcation by a newly developed Y-shaped artificial trachea," *ASAIO Journal*, vol. 45, no. 3, pp. 131–134, 1999.

[48] T. Nakamura, M. Teramachi, T. Sekine et al., "Artificial trachea and long term follow-up in carinal reconstruction in dogs," *International Journal of Artificial Organs*, vol. 23, no. 10, pp. 718–724, 2000.

[49] T. Go, P. Jungebluth, S. Baiguero et al., "Both epithelial cells and mesenchymal stem cell-derived chondrocytes contribute to the survival of tissue-engineered airway transplants in pigs," *The Journal of Thoracic and Cardiovascular Surgery*, vol. 139, no. 2, pp. 437–443, 2010.

[50] A. Gonfiotti, M. O. Jaus, and D. Barale, "The first tissue-engineered airway transplantation: 5-year follow-up results," *The Lancet*, vol. 383, no. 9913, pp. 238–244, 2014.

[51] M. J. Elliott, P. de Coppi, S. Speggiorin et al., "Stem-cell-based, tissue engineered tracheal replacement in a child: a 2-year follow-up study," *The Lancet*, vol. 380, no. 9846, pp. 994–1000, 2012.

[52] M. Berg, H. Ejnell, A. Kovács et al., "Replacement of a tracheal stenosis with a tissue-engineered human trachea using autologous stem cells: a case report," *Tissue Engineering Part A*, vol. 20, no. 1-2, pp. 389–397, 2014.

[53] K. Omori, Y. Tada, T. Suzuki et al., "Clinical application of in situ tissue engineering using a scaffolding technique for reconstruction of the larynx and trachea," *Annals of Otology, Rhinology and Laryngology*, vol. 117, no. 9, pp. 673–678, 2008.

[54] Y. Kitani, S. Kanemaru, H. Umeda et al., "Laryngeal regeneration using tissue engineering techniques in a canine model," *Annals of Otology, Rhinology and Laryngology*, vol. 120, no. 1, pp. 49–56, 2011.

[55] M. Weidenbecher, J. H. Henderson, H. M. Tucker, J. Z. Baskin, A. Awadallah, and J. E. Dennis, "Hyaluronan-based scaffolds to tissue-engineer cartilage implants for laryngotracheal reconstruction," *Laryngoscope*, vol. 117, no. 10, pp. 1745–1749, 2007.

[56] D. A. Gilpin, M. S. Weidenbecher, and J. E. Dennis, "Scaffold-free tissue-engineered cartilage implants for laryngotracheal reconstruction," *Laryngoscope*, vol. 120, no. 3, pp. 612–617, 2010.

[57] J. E. Huber, A. Spievack, A. Simmons-Byrd, R. L. Ringel, and S. Badylak, "Extracellular matrix as a scaffold for laryngeal reconstruction," *Annals of Otology, Rhinology and Laryngology*, vol. 112, no. 5, pp. 428–433, 2003.

[58] R. L. Ringel, J. C. Kahane, P. J. Hillsamer, A. S. Lee, and S. F. Badylak, "The application of tissue engineering procedures to repair the larynx," *Journal of Speech, Language, and Hearing Research*, vol. 49, no. 1, pp. 194–208, 2006.

[59] C. C. Xu, R. W. Chan, and N. Tirunagari, "A biodegradable, acellular xenogeneic scaffold for regeneration of the vocal fold lamina propria," *Tissue Engineering*, vol. 13, no. 3, pp. 551–566, 2007.

[60] N. Hou, P. Cui, J. Luo, R. Ma, and L. Zhu, "Tissue-engineered larynx using perfusion-decellularized technique and mesenchymal stem cells in a rabbit model," *Acta Oto-Laryngologica*, vol. 131, no. 6, pp. 645–652, 2011.

[61] M. Kitamura, S. Hirano, and S. I. Kanemaru, "Glottic regeneration with a tissue-engineering technique, using acellular extracellular matrix scaffold in a canine model," *Journal of Tissue Engineering and Regenerative Medicine*, 2014.

[62] T. Nakamura, A. Magrufov, K. Omori et al., "Cricoid regeneration using in situ tissue engineering in canine larynx for the treatment of subglottic stenosis," *Annals of Otology, Rhinology and Laryngology*, vol. 113, no. 8, pp. 623–627, 2004.

[63] M. Yamashita, K. Omori, S. Kanemaru et al., "Experimental regeneration of canine larynx: a trial with tissue engineering techniques," *Acta Oto-Laryngologica*, vol. 127, no. 557, pp. 66–72, 2007.

[64] P. Delaere, A. Goeleven, V. V. Poorten, R. Hermans, R. Hierner, and J. Vranckx, "Organ preservation surgery for advanced unilateral glottic and subglottic cancer," *The Laryngoscope*, vol. 117, no. 10, pp. 1764–1769, 2007.

[65] Y. Urita, H. Komuro, G. Chen et al., "Regeneration of the esophagus using gastric acellular matrix: an experimental study in a rat model," *Pediatric Surgery International*, vol. 23, no. 1, pp. 21–26, 2007.

[66] S. F. Badylak, T. Hoppo, A. Nieponice, T. W. Gilbert, J. M. Davison, and B. A. Jobe, "Esophageal preservation in five male patients after endoscopic inner-layer circumferential resection in the setting of superficial cancer: a regenerative medicine approach with a biologic scaffold," *Tissue Engineering A*, vol. 17, no. 11-12, pp. 1643–1650, 2011.

[67] A. Gallo and C. Cha, "Updates on esophageal and gastric cancers," *World Journal of Gastroenterology*, vol. 12, no. 20, pp. 3237–3242, 2006.

[68] R. Wei, B. Tan, M. Tan et al., "Grafts of porcine small intestinal submucosa with cultured autologous oral mucosal epithelial cells for esophageal repair in a canine model," *Experimental Biology and Medicine*, vol. 234, no. 4, pp. 453–461, 2009.

[69] S. Badylak, S. Meurling, M. Chen, A. Spievack, and A. Simmons-Byrd, "Resorbable bioscaffold for esophageal repair in a dog model," *Journal of Pediatric Surgery*, vol. 35, no. 7, pp. 1097–1103, 2000.

[70] B. Tan, R. Q. Wei, M. Y. Tan et al., "Tissue engineered esophagus by mesenchymal stem cell seeding for esophageal repair in a canine model," *Journal of Surgical Research*, vol. 182, no. 1, pp. 40–48, 2013.

[71] M. F. Lopes, A. Cabrita, J. Ilharco, P. Pessa, and J. Patrício, "Grafts of porcine intestinal submucosa for repair of cervical and abdominal esophageal defects in the rat," *Journal of Investigative Surgery*, vol. 19, no. 2, pp. 105–111, 2006.

[72] M. Marzaro, S. Vigolo, B. Oselladore et al., "In vitro and in vivo proposal of an artificial esophagus," *Journal of Biomedical Materials Research A*, vol. 77, no. 4, pp. 795–801, 2006.

[73] S. F. Badylak, D. A. Vorp, A. R. Spievack et al., "Esophageal reconstruction with ECM and muscle tissue in a dog model," *Journal of Surgical Research*, vol. 128, no. 1, pp. 87–97, 2005.

[74] T. Doede, M. Bondartschuk, C. Joerck, E. Schulze, and M. Goernig, "Unsuccessful alloplastic esophageal replacement with porcine small intestinal submucosa," *Artificial Organs*, vol. 33, no. 4, pp. 328–333, 2009.

[75] S. Sjöqvist, P. Jungebluth, M. L. Lim et al., "Experimental orthotopic transplantation of a tissue-engineered oesophagus in rats," *Nature Communications*, vol. 5, article 3562, 2014.

[76] P. L. Jansen, U. Klinge, M. Anurov, S. Titkova, P. R. Mertens, and M. Jansen, "Surgical mesh as a scaffold for tissue regeneration in the esophagus," *European Surgical Research*, vol. 36, no. 2, pp. 104–111, 2004.

[77] J. Basu, K. L. Mihalko, R. Payne et al., "Extension of bladder-based organ regeneration platform for tissue engineering of esophagus," *Medical Hypotheses*, vol. 78, no. 2, pp. 231–234, 2012.

[78] P. Diemer, S. Markoew, D. Q. Le, and N. Qvist, "Poly-ε-caprolactone mesh as a scaffold for in vivo tissue engineering in rabbit esophagus," *Diseases of the Esophagus*, 2014.

[79] Y. Takimoto, T. Nakamura, M. Termachi, T. Kiyotani, and Y. Shimizu, "Replacement of long segments of the esophagus with a collagen-silicone composite tube," *ASAIO Journal*, vol. 41, no. 3, pp. M605–M608, 1995.

[80] M. Aikawa, M. Miyazawa, K. Okamoto et al., "A bioabsorbable polymer patch for the treatment of esophageal defect in a porcine model," *Journal of Gastroenterology*, vol. 48, no. 7, pp. 822–829, 2013.

[81] Y. Nakase, T. Nakamura, S. Kin et al., "Intrathoracic esophageal replacement by in situ tissue-engineered esophagus," *Journal of Thoracic and Cardiovascular Surgery*, vol. 136, no. 4, pp. 850–859, 2008.

[82] T. C. Grikscheit, E. R. Ochoa, A. Srinivasan, H. Gaissert, and J. P. Vacanti, "Tissue-engineered esophagus: experimental substitution by onlay patch or interposition," *Journal of Thoracic and Cardiovascular Surgery*, vol. 126, no. 2, pp. 537–544, 2003.

[83] A. Clough, J. Ball, G. S. Smith, and S. Leibman, "Porcine small intestine submucosa matrix (Surgisis) for esophageal perforation," *Annals of Thoracic Surgery*, vol. 91, no. 2, pp. e99–e100, 2011.

[84] Y. S. Morsi, I. E. Birchall, and F. L. Rosenfeldt, "Artificial aortic valves: an overview," *International Journal of Artificial Organs*, vol. 27, no. 6, pp. 445–451, 2004.

[85] C. Del Gaudio, M. Grigioni, A. Bianco, and G. de Angelis, "Electrospun bioresorbable heart valve scaffold for tissue engineering," *International Journal of Artificial Organs*, vol. 31, no. 1, pp. 68–75, 2008.

[86] G. Steinhoff, U. Stock, N. Karim et al., "Tissue engineering of pulmonary heart valves on allogenic acellular matrix conduits: in vivo restoration of valve tissue," *Circulation*, vol. 102, supplement 3, no. 19, pp. III50–III55, 2000.

[87] T. C. Flanagan, J. S. Sachweh, J. Frese et al., "In vivo remodeling and structural characterization of fibrin-based tissue-engineered heart valves in the adult sheep model," *Tissue Engineering A*, vol. 15, no. 10, pp. 2965–2976, 2009.

[88] F. Juthier, A. Vincentelli, J. Gaudric et al., "Decellularized heart valve as a scaffold for in vivo recellularization: deleterious effects of granulocyte colony-stimulating factor," *Journal of Thoracic and Cardiovascular Surgery*, vol. 131, no. 4, pp. 843–852, 2006.

[89] H. Baraki, I. Tudorache, M. Braun et al., "Orthotopic replacement of the aortic valve with decellularized allograft in a sheep model," *Biomaterials*, vol. 30, no. 31, pp. 6240–6246, 2009.

[90] D. Zhao, R. Li, W. Liu et al., "Tissue-engineered heart valve on acellular aortic valve scaffold: in-vivo study," *Asian Cardiovascular and Thoracic Annals*, vol. 11, no. 2, pp. 153–156, 2003.

[91] S. Kim, S. Lim, Y. Hong et al., "Tissue engineering of heart valves in vivo using bone marrow-derived cells," *Artificial Organs*, vol. 30, no. 7, pp. 554–557, 2006.

[92] I. Tudorache, A. Calistru, H. Baraki et al., "Orthotopic replacement of aortic heart valves with tissue-engineered grafts," *Tissue Engineering A*, vol. 19, no. 15-16, pp. 1686–1694, 2013.

[93] J. E. Jordan, J. K. Williams, S. Lee, D. Raghavan, A. Atala, and J. J. Yoo, "Bioengineered self-seeding heart valves," *Journal of Thoracic and Cardiovascular Surgery*, vol. 143, no. 1, pp. 201–208, 2012.

[94] S. Wu, Y. L. Liu, B. Cui, X. Qu, and G. Chen, "Study on decellularized porcine aortic valve/poly (3-hydroxybutyrate-co-3-hydroxyhexanoate) hybrid heart valve in sheep model," *Artificial Organs*, vol. 31, no. 9, pp. 689–697, 2007.

[95] D. Gottlieb, T. Kunal, S. Emani et al., "In vivo monitoring of function of autologous engineered pulmonary valve," *Journal of*

*Thoracic and Cardiovascular Surgery*, vol. 139, no. 3, pp. 723–731, 2010.

[96] B. Weber, M. Y. Emmert, L. Behr et al., "Prenatally engineered autologous amniotic fluid stem cell-based heart valves in the fetal circulation," *Biomaterials*, vol. 33, no. 16, pp. 4031–4043, 2012.

[97] B. Weber, J. Scherman, M. Y. Emmert et al., "Injectable living marrow stromal cell-based autologous tissue engineered heart valves: first experiences with a one-step intervention in primates," *European Heart Journal*, vol. 32, no. 22, pp. 2830–2840, 2011.

[98] B. Weber, P. E. Dijkman, J. Scherman et al., "Off-the-shelf human decellularized tissue-engineered heart valves in a non-human primate model," *Biomaterials*, vol. 34, no. 30, pp. 7269–7280, 2013.

[99] D. Pankajakshan and D. K. Agrawal, "Scaffolds in tissue engineering of blood vessels," *Canadian Journal of Physiology and Pharmacology*, vol. 88, no. 9, pp. 855–873, 2010.

[100] G. M. Rubanyi, "The role of endothelium in cardiovascular homeostasis and diseases," *Journal of Cardiovascular Pharmacology*, vol. 22, supplement 4, pp. S1–S14, 1993.

[101] V. W. M. van Hinsbergh, "The endothelium: vascular control of haemostasis," *European Journal of Obstetrics, Gynecology, and Reproductive Biology*, vol. 95, no. 2, pp. 198–201, 2001.

[102] S. Kaushal, G. E. Amiel, K. J. Guleserian et al., "Functional small-diameter neovessels created using endothelial progenitor cells expanded ex vivo," *Nature Medicine*, vol. 7, no. 9, pp. 1035–1040, 2001.

[103] S. W. Cho, S. H. Lim, I. K. Kim et al., "Small-diameter blood vessels engineered with bone marrow-derived cells," *Annals of Surgery*, vol. 241, no. 3, pp. 506–515, 2005.

[104] L. P. Neff, B. W. Tillman, S. K. Yazdani et al., "Vascular smooth muscle enhances functionality of tissue-engineered blood vessels in vivo," *Journal of Vascular Surgery*, vol. 53, no. 2, pp. 426–434, 2011.

[105] N. D. Martin, P. J. Schaner, T. N. Tulenko et al., "In vivo behavior of decellularized vein allograft," *Journal of Surgical Research*, vol. 129, no. 1, pp. 17–23, 2005.

[106] Y. Xiong, W. Y. Chan, A. W. C. Chua et al., "Decellularized porcine saphenous artery for small-diameter tissue-engineered conduit graft," *Artificial Organs*, vol. 37, no. 6, pp. E74–E87, 2013.

[107] U. Böer, C. Spengler, D. Jonigk et al., "Coating decellularized equine carotid arteries with CCN1 improves cellular repopulation, local biocompatibility, and immune response in sheep," *Tissue Engineering A*, vol. 19, no. 15-16, pp. 1829–1842, 2013.

[108] L. Gui, A. Muto, S. A. Chan, C. K. Breuer, and L. E. Niklason, "Development of decellularized human umbilical arteries as small-diameter vascular grafts," *Tissue Engineering A*, vol. 15, no. 9, pp. 2665–2676, 2009.

[109] L. E. Niklason, J. Gao, W. M. Abbott et al., "Functional arteries grown in vitro," *Science*, vol. 284, no. 5413, pp. 489–493, 1999.

[110] N. L'Heureux, S. Pâquet, R. Labbé, L. Germain, and F. A. Auger, "A completely biological tissue-engineered human blood vessel," *FASEB Journal*, vol. 12, no. 1, pp. 47–56, 1998.

[111] N. L'Heureux, N. Dusserre, G. Konig et al., "Human tissue-engineered blood vessels for adult arterial revascularization," *Nature Medicine*, vol. 12, no. 3, pp. 361–365, 2006.

[112] T. N. McAllister, M. Maruszewski, S. A. Garrido et al., "Effectiveness of haemodialysis access with an autologous tissue-engineered vascular graft: a multicentre cohort study," *The Lancet*, vol. 373, no. 9673, pp. 1440–1446, 2009.

[113] J. Zhao, L. Liu, J. Wei et al., "A novel strategy to engineer small-diameter vascular grafts from marrow-derived mesenchymal stem cells," *Artificial Organs*, vol. 36, no. 1, pp. 93–101, 2012.

[114] C. Quint, Y. Kondo, R. J. Manson, J. H. Lawson, A. Dardik, and L. E. Niklason, "Decellularized tissue-engineered blood vessel as an arterial conduit," *Proceedings of the National Academy of Sciences of the United States of America*, vol. 108, no. 22, pp. 9214–9219, 2011.

[115] S. L. Dahl, A. P. Kypson, J. H. Lawson et al., "Readily available tissue-engineered vascular grafts," *Science Translational Medicine*, vol. 3, no. 68, Article ID 68ra9, 2011.

[116] E. Paternotte, H. Kerdjoudj, T. Kokten et al., "Endothelialized and preconditioned natural umbilical arteries with long term patency open the route for future human uses," *Clinical Hemorheology and Microcirculation*, vol. 54, no. 3, pp. 223–234, 2013.

[117] S. de Valence, J. Tille, D. Mugnai et al., "Long term performance of polycaprolactone vascular grafts in a rat abdominal aorta replacement model," *Biomaterials*, vol. 33, no. 1, pp. 38–47, 2012.

[118] S. de Valence, J. C. Tille, C. Chaabane et al., "Plasma treatment for improving cell biocompatibility of a biodegradable polymer scaffold for vascular graft applications," *European Journal of Pharmaceutics and Biopharmaceutics*, vol. 85, no. 1, pp. 78–86, 2013.

[119] E. Pektok, B. Nottelet, J. C. Tille et al., "Degradation and healing characteristics of small-diameter poly(ε-caprolactone) vascular grafts in the rat systemic arterial circulation," *Circulation*, vol. 118, no. 24, pp. 2563–2570, 2008.

[120] B. W. Tillman, S. K. Yazdani, S. J. Lee, R. L. Geary, A. Atala, and J. J. Yoo, "The in vivo stability of electrospun polycaprolactone-collagen scaffolds in vascular reconstruction," *Biomaterials*, vol. 30, no. 4, pp. 583–588, 2009.

[121] G. Matsumura, S. Miyagawa-Tomita, T. Shin'Oka, Y. Ikada, and H. Kurosawa, "First evidence that bone marrow cells contribute to the construction of tissue-engineered vascular autografts in vivo," *Circulation*, vol. 108, no. 14, pp. 1729–1734, 2003.

[122] M. Zhou, W. Qiao, Z. Liu et al., "Development and in vivo evaluation of small-diameter vascular grafts engineered by outgrowth endothelial cells and electrospun chitosan/poly(ε-caprolactone) nanofibrous scaffolds," *Tissue Engineering A*, vol. 20, no. 1-2, pp. 79–91, 2014.

[123] S. P. Hoerstrup, I. Cummings, M. Lachat et al., "Functional growth in tissue-engineered living, vascular grafts: follow-up at 100 weeks in a large animal model," *Circulation*, vol. 114, no. 1, pp. I159–I166, 2006.

[124] G. Matsumura, N. Nitta, S. Matsuda et al., "Long-term results of cell-free biodegradable scaffolds for in situ tissue-engineering vasculature: in a canine inferior vena cava model," *PLoS ONE*, vol. 7, no. 4, Article ID e35760, 2012.

[125] G. Matsumura, N. Isayama, S. Matsuda et al., "Long-term results of cell-free biodegradable scaffolds for in situ tissue engineering of pulmonary artery in a canine model," *Biomaterials*, vol. 34, no. 27, pp. 6422–6428, 2013.

[126] N. Isayama, G. Matsumura, H. Sato et al., "Histological maturation of vascular smooth muscle cells in in situ tissue-engineered vasculature," *Biomaterials*, vol. 35, no. 11, pp. 3589–3595, 2014.

[127] N. Hibino, T. Shin'oka, G. Matsumura, Y. Ikada, and H. Kurosawa, "The tissue-engineered vascular graft using bone marrow without culture," *Journal of Thoracic and Cardiovascular Surgery*, vol. 129, no. 5, pp. 1064–1070, 2005.

[128] N. Hibino, G. Villalona, N. Pietris et al., "Tissue-engineered vascular grafts form neovessels that arise from regeneration of

the adjacent blood vessel," *FASEB Journal*, vol. 25, no. 8, pp. 2731–2739, 2011.

[129] T. L. Mirensky, N. Hibino, R. F. Sawh-Martinez et al., "Tissue-engineered vascular grafts: does cell seeding matter?" *Journal of Pediatric Surgery*, vol. 45, no. 6, pp. 1299–1305, 2010.

[130] J. D. Roha, R. Sawh-Martinez, M. P. Brennan et al., "Tissue-engineered vascular grafts transform into mature blood vessels via an inflammation-mediated process of vascular remodeling," *Proceedings of the National Academy of Sciences of the United States of America*, vol. 107, no. 10, pp. 4669–4674, 2010.

[131] A. Nieponice, L. Soletti, J. Guan et al., "*In Vivo* assessment of a tissue-engineered vascular graft combining a biodegradable elastomeric scaffold and muscle-derived stem cells in a rat model," *Tissue Engineering A*, vol. 16, no. 4, pp. 1215–1223, 2010.

[132] V. A. Kumar, J. M. Caves, C. A. Haller et al., "Acellular vascular grafts generated from collagen and elastin analogs," *Acta Biomaterialia*, vol. 9, no. 9, pp. 8067–8074, 2013.

[133] W. Wu, R. A. Allen, and Y. Wang, "Fast-degrading elastomer enables rapid remodeling of a cell-free synthetic graft into a neoartery," *Nature Medicine*, vol. 18, no. 7, pp. 1148–1153, 2012.

[134] T. N. McAllister, N. Dusserre, M. Maruszewski, and N. L'Heureux, "Cell-based therapeutics from an economic perspective: primed for a commercial success or a research sinkhole?" *Regenerative Medicine*, vol. 3, no. 6, pp. 925–937, 2008.

[135] G. Orlando, C. Booth, Z. Wang et al., "Discarded human kidneys as a source of ECM scaffold for kidney regeneration technologies," *Biomaterials*, vol. 34, no. 24, pp. 5915–5925, 2013.

[136] J. J. Song, J. P. Guyette, S. E. Gilpin, G. Gonzalez, J. P. Vacanti, and H. C. Ott, "Regeneration and experimental orthotopic transplantation of a bioengineered kidney," *Nature Medicine*, vol. 19, no. 5, pp. 646–651, 2013.

[137] P. Y. Dankers, J. M. Boomker, E. W. Meijer, E. R. Popa, and M. J. A. Van Luyn, "From kidney development to drug delivery and tissue engineering strategies in renal regenerative medicine," *Journal of Controlled Release*, vol. 152, no. 1, pp. 177–185, 2011.

[138] G. Orlando, A. C. Farney, S. S. Iskandar et al., "Production and implantation of renal extracellular matrix scaffolds from porcine kidneys as a platform for renal bioengineering investigations," *Annals of Surgery*, vol. 256, no. 2, pp. 363–370, 2012.

[139] B. Brehmer, D. Rohrmann, C. Becker, G. Rau, and G. Jakse, "Different types of scaffolds for reconstruction of the urinary tract by tissue engineering," *Urologia Internationalis*, vol. 78, no. 1, pp. 23–29, 2007.

[140] S. Y. Chung, "Bladder tissue-engineering: a new practical solution?" *The Lancet*, vol. 367, no. 9518, pp. 1215–1216, 2006.

[141] A. Atala, "Tissue engineering for the replacement of organ function in the genitourinary system," *The American Journal of Transplantation*, vol. 4, supplement 6, pp. 58–73, 2004.

[142] S. Korossis, F. Bolland, E. Ingham, J. Fisher, J. Kearney, and J. Southgate, "Tissue engineering of the urinary bladder: considering structure-function relationships and the role of mechanotransduction," *Tissue Engineering*, vol. 12, no. 4, pp. 635–644, 2006.

[143] A. Parekh, A. D. Cigan, S. Wognum, R. L. Heise, M. B. Chancellor, and M. S. Sacks, "Ex vivo deformations of the urinary bladder wall during whole bladder filling: contributions of extracellular matrix and smooth muscle," *Journal of Biomechanics*, vol. 43, no. 9, pp. 1708–1716, 2010.

[144] B. P. Kropp, "Small-intestinal submucosa for bladder augmentation: a review of preclinical studies," *World Journal of Urology*, vol. 16, no. 4, pp. 262–267, 1998.

[145] C. C. Roth, C. H. Bell, B. Woodson et al., "Temporal differentiation and maturation of regenerated rat urothelium," *BJU International*, vol. 103, no. 6, pp. 836–841, 2009.

[146] B. P. Kropp, E. Y. Cheng, H. Lin, and Y. Zhang, "Reliable and reproducible bladder regeneration using unseeded distal small intestinal submucosa," *Journal of Urology*, vol. 172, no. 4, pp. 1710–1713, 2004.

[147] A. M. Kajbafzadeh, S. Sabetkish, R. Heidari et al., "Tissue-engineered cholecyst-derived extracellular matrix: a biomaterial for in vivo autologous bladder muscular wall regeneration," *Pediatric Surgery International*, vol. 30, no. 4, pp. 371–380, 2014.

[148] A. Kanematsu, S. Yamamoto, T. Noguchi, M. Ozeki, Y. Tabata, and O. Ogawa, "Bladder regeneration by bladder acellular matrix combined with sustained release of exogenous growth factor," *Journal of Urology*, vol. 170, no. 4, pp. 1633–1638, 2003.

[149] Y. Loai, H. Yeger, C. Coz et al., "Bladder tissue engineering: tissue regeneration and neovascularization of HA-VEGF-incorporated bladder acellular constructs in mouse and porcine animal models," *Journal of Biomedical Materials Research A*, vol. 94, no. 4, pp. 1205–1215, 2010.

[150] B. Chen, H. Xie, S. Zhang et al., "Tissue engineering of bladder using vascular endothelial growth factor gene-modified endothelial progenitor cells," *International Journal of Artificial Organs*, vol. 34, no. 12, pp. 1137–1146, 2011.

[151] R. D. Record, D. Hillegonds, C. Simmons et al., "In vivo degradation of $^{14}$C-labeled small intestinal submucosa (SIS) when used for urinary bladder repair," *Biomaterials*, vol. 22, no. 19, pp. 2653–2659, 2001.

[152] J. R. Mauney, G. M. Cannon, M. L. Lovett et al., "Evaluation of gel spun silk-based biomaterials in a murine model of bladder augmentation," *Biomaterials*, vol. 32, no. 3, pp. 808–818, 2011.

[153] M. L. Lovett, C. M. Cannizzaro, G. Vunjak-Novakovic, and D. L. Kaplan, "Gel spinning of silk tubes for tissue engineering," *Biomaterials*, vol. 29, no. 35, pp. 4650–4657, 2008.

[154] F. Oberpenning, J. Meng, J. J. Yoo, and A. Atala, "De novo reconstitution of a functional mammalian urinary bladder by tissue engineering," *Nature Biotechnology*, vol. 17, no. 2, pp. 149–155, 1999.

[155] M. J. Jayo, D. Jain, B. J. Wagner, and T. A. Bertram, "Early cellular and stromal responses in regeneration versus repair of a mammalian bladder using autologous cell and biodegradable scaffold technologies," *Journal of Urology*, vol. 180, no. 1, pp. 392–397, 2008.

[156] T. Drewa, J. Sir, R. Czajkowski, and A. Wozniak, "Scaffold seeded with cells is essential in urothelium regeneration and tissue remodeling in vivo after bladder augmentation using in vitro engineered graft," *Transplantation Proceedings*, vol. 38, no. 1, pp. 133–135, 2006.

[157] J. Lai, P. Chang, and J. Lin, "A comparison of engineered urinary bladder and intestinal smooth muscle for urinary bladder wall replacement in a rabbit model," *Journal of Pediatric Surgery*, vol. 41, no. 12, pp. 2090–2094, 2006.

[158] T. Drewa, J. Adamowicz, J. Lysik, J. Polaczek, and J. Pielichowski, "Chitosan scaffold enhances nerve regeneration within the in vitro reconstructed bladder wall: an animal study," *Urologia Internationalis*, vol. 81, no. 3, pp. 330–334, 2008.

[159] C. Del Gaudio, A. Vianello, G. Bellezza et al., "Evaluation of electrospun bioresorbable scaffolds for tissue-engineered urinary bladder augmentation," *Biomedical Materials*, vol. 8, no. 4, Article ID 045013, 2013.

[160] M. Horst, V. Milleret, S. Nötzli et al., "Increased porosity of electrospun hybrid scaffolds improved bladder tissue regeneration,"

*Journal of Biomedical Materials Research A*, vol. 102, no. 7, pp. 2116–2124, 2014.

[161] M. Horst, S. Madduri, V. Milleret, T. Sulser, R. Gobet, and D. Eberli, "A bilayered hybrid microfibrous PLGA-Acellular matrix scaffold for hollow organ tissue engineering," *Biomaterials*, vol. 34, no. 5, pp. 1537–1545, 2013.

[162] G. S. Jack, R. Zhang, M. Lee, Y. Xu, B. M. Wu, and L. V. Rodríguez, "Urinary bladder smooth muscle engineered from adipose stem cells and a three dimensional synthetic composite," *Biomaterials*, vol. 30, no. 19, pp. 3259–3270, 2009.

[163] P. Gomez, E. S. Gil, M. L. Lovett et al., "The effect of manipulation of silk scaffold fabrication parameters on matrix performance in a murine model of bladder augmentation," *Biomaterials*, vol. 32, no. 30, pp. 7562–7570, 2011.

[164] M. Pattison, T. J. Webster, J. Leslie, M. Kaefer, and K. M. Haberstroh, "Evaluating the *in vitro* and *in vivo* efficacy of nanostructured polymers for bladder tissue replacement applications," *Macromolecular Bioscience*, vol. 7, no. 5, pp. 690–700, 2007.

[165] C. Yao, M. Hedrick, G. Pareek et al., "Nanostructured polyurethane-poly-lactic-co-glycolic acid scaffolds increase bladder tissue regeneration: an in vivo study," *International Journal of Nanomedicine*, vol. 8, pp. 3285–3296, 2013.

[166] L. A. Micol, L. F. Arenas da Silva, P. J. Geutjes et al., "In-vivo performance of high-density collagen gel tubes for urethral regeneration in a rabbit model," *Biomaterials*, vol. 33, no. 30, pp. 7447–7455, 2012.

[167] C. Li, Y. Xu, L. Song, Q. Fu, L. Cui, and S. Yin, "Urethral reconstruction using oral keratinocyte seeded bladder acellular matrix grafts," *Journal of Urology*, vol. 180, no. 4, pp. 1538–1542, 2008.

[168] C. Li, Y. M. Xu, Z. S. Liu, and H. Li, "Urethral reconstruction with tissue engineering and RNA interference techniques in rabbits," *Urology*, vol. 81, no. 5, pp. 1075–1080, 2013.

[169] C. Feng, Y. Xu, Q. Fu, W. Zhu, and L. Cui, "Reconstruction of three-dimensional neourethra using lingual keratinocytes and corporal smooth muscle cells seeded acellular corporal spongiosum," *Tissue Engineering A*, vol. 17, no. 23-24, pp. 3011–3019, 2011.

[170] H. Li, Y. Xu, H. Xie et al., "Epithelial-differentiated adipose-derived stem cells seeded bladder acellular matrix grafts for urethral reconstruction: an animal model," *Tissue Engineering Part A*, vol. 20, no. 3-4, pp. 774–784, 2014.

[171] W. Liao, S. Yang, C. Song, X. Li, Y. Li, and Y. Xiong, "Construction of ureteral grafts by seeding bone marrow mesenchymal stem cells and smooth muscle cells into bladder acellular matrix," *Transplantation Proceedings*, vol. 45, no. 2, pp. 730–734, 2013.

[172] S. Y. Chun, G. J. Lim, T. G. Kwon et al., "Identification and characterization of bioactive factors in bladder submucosa matrix," *Biomaterials*, vol. 28, no. 29, pp. 4251–4256, 2007.

[173] A. Mauro, "Satellite cell of skeletal muscle fibers," *The Journal of Biophysical and Biochemical Cytology*, vol. 9, pp. 493–495, 1961.

[174] S. B. P. Chargé and M. A. Rudnicki, "Cellular and molecular regulation of muscle regeneration," *Physiological Reviews*, vol. 84, no. 1, pp. 209–238, 2004.

[175] M. Hill, A. Wernig, and G. Goldspink, "Muscle satellite (stem) cell activation during local tissue injury and repair," *Journal of Anatomy*, vol. 203, no. 1, pp. 89–99, 2003.

[176] M. Deutinger, R. Kuzbari, T. Paternostro-Sluga et al., "Donor-site morbidity of the gracilis flap," *Plastic and Reconstructive Surgery*, vol. 95, no. 7, pp. 1240–1244, 1995.

[177] Y. Kimata, K. Uchiyama, S. Ebihara et al., "Anterolateral thigh flap donor-site complications and morbidity," *Plastic and Reconstructive Surgery*, vol. 106, no. 3, pp. 584–589, 2000.

[178] S. H. Lin, D. C. Chuang, Y. Hattori, and H. Chen, "Traumatic major muscle loss in the upper extremity: reconstruction using functioning free muscle transplantation," *Journal of Reconstructive Microsurgery*, vol. 20, no. 3, pp. 227–235, 2004.

[179] C. Fan, P. Jiang, L. Fu, P. Cai, L. Sun, and B. Zeng, "Functional reconstruction of traumatic loss of flexors in forearm with gastrocnemius myocutaneous flap transfer," *Microsurgery*, vol. 28, no. 1, pp. 71–75, 2008.

[180] M. D. Vekris, A. E. Beris, M. G. Lykissas, A. V. Korompilias, A. D. Vekris, and P. N. Soucacos, "Restoration of elbow function in severe brachial plexus paralysis via muscle transfers.," *Injury*, vol. 39, pp. S15–22, 2008.

[181] B. M. Sicari, V. Agrawal, B. F. Siu et al., "A murine model of volumetric muscle loss and a regenerative medicine approach for tissue replacement," *Tissue Engineering A*, vol. 18, no. 19-20, pp. 1941–1948, 2012.

[182] N. J. Turner and S. F. Badylak, "Biologic scaffolds for musculotendinous tissue repair," *European Cells and Materials*, vol. 25, pp. 130–143, 2013.

[183] J. Ma, K. Holden, J. Zhu, H. Pan, and Y. Li, "The application of three-dimensional collagen-scaffolds seeded with myoblasts to repair skeletal muscle defects," *Journal of Biomedicine and Biotechnology*, vol. 2011, Article ID 812135, 9 pages, 2011.

[184] J. P. Mertens, K. B. Sugg, J. D. Lee et al., "Engineering muscle constructs for the creation of functional engineered musculoskeletal tissue," *Regenerative Medicine*, vol. 9, no. 1, pp. 89–100, 2014.

[185] R. L. Page, C. Malcuit, L. Vilner et al., "Restoration of skeletal muscle defects with adult human cells delivered on fibrin microthreads," *Tissue Engineering A*, vol. 17, no. 21-22, pp. 2629–2640, 2011.

[186] K. M. Brouwer, W. F. Daamen, N. van Lochem, D. Reijnen, R. M. H. Wijnen, and T. H. van Kuppevelt, "Construction and in vivo evaluation of a dual layered collagenous scaffold with a radial pore structure for repair of the diaphragm," *Acta Biomaterialia*, vol. 9, no. 6, pp. 6844–6851, 2013.

[187] S. F. Badylak, J. E. Valentin, A. K. Ravindra, G. P. McCabe, and A. M. Stewart-Akers, "Macrophage phenotype as a determinant of biologic scaffold remodeling," *Tissue Engineering A*, vol. 14, no. 11, pp. 1835–1842, 2008.

[188] B. N. Brown, J. E. Valentin, A. M. Stewart-Akers, G. P. McCabe, and S. F. Badylak, "Macrophage phenotype and remodeling outcomes in response to biologic scaffolds with and without a cellular component," *Biomaterials*, vol. 30, no. 8, pp. 1482–1491, 2009.

[189] J. E. Valentin, A. M. Stewart-Akers, T. W. Gilbert, and S. F. Badylak, "Macrophage participation in the degradation and remodeling of extracellular matrix scaffolds," *Tissue Engineering A*, vol. 15, no. 7, pp. 1687–1694, 2009.

[190] M. B. Ariganello, D. T. Simionescu, R. S. Labow, and J. Michael Lee, "Macrophage differentiation and polarization on a decellularized pericardial biomaterial," *Biomaterials*, vol. 32, no. 2, pp. 439–449, 2011.

[191] J. M. Fishman, M. W. Lowdell, L. Urbani et al., "Immunomodulatory effect of a decellularized skeletal muscle scaffold in a discordant xenotransplantation model," *Proceedings of the National Academy of Sciences of the United States of America*, vol. 110, no. 35, pp. 14360–14365, 2013.

[192] P. G. Gamba, M. T. Conconi, R. Lo Piccolo, G. Zara, R. Spinazzi, and P. P. Parnigotto, "Experimental abdominal wall defect repaired with acellular matrix," *Pediatric Surgery International*, vol. 18, no. 5-6, pp. 327–331, 2002.

[193] V. Vindigni, F. Mazzoleni, K. Rossini et al., "Reconstruction of ablated rat rectus abdominis by muscle regeneration," *Plastic and Reconstructive Surgery*, vol. 114, no. 6, pp. 1509–1515, 2004.

[194] M. T. Conconi, P. D. Coppi, S. Bellini et al., "Homologous muscle acellular matrix seeded with autologous myoblasts as a tissue-engineering approach to abdominal wall-defect repair," *Biomaterials*, vol. 26, no. 15, pp. 2567–2574, 2005.

[195] E. K. Merritt, M. V. Cannon, D. W. Hammers et al., "Repair of traumatic skeletal muscle injury with bone-marrow-derived mesenchymal stem cells seeded on extracellular matrix," *Tissue Engineering A*, vol. 16, no. 9, pp. 2871–2881, 2010.

[196] B. Perniconi, A. Costa, P. Aulino, L. Teodori, S. Adamo, and D. Coletti, "The pro-myogenic environment provided by whole organ scale acellular scaffolds from skeletal muscle," *Biomaterials*, vol. 32, no. 31, pp. 7870–7882, 2011.

[197] B. T. Corona, X. Wu, C. L. Ward, J. S. McDaniel, C. R. Rathbone, and T. J. Walters, "The promotion of a functional fibrosis in skeletal muscle with volumetric muscle loss injury following the transplantation of muscle-ECM," *Biomaterials*, vol. 34, no. 13, pp. 3324–3335, 2013.

[198] M. T. Wolf, K. A. Daly, J. E. Reing, and S. F. Badylak, "Biologic scaffold composed of skeletal muscle extracellular matrix," *Biomaterials*, vol. 33, no. 10, pp. 2916–2925, 2012.

[199] J. E. Valentin, N. J. Turner, T. W. Gilbert, and S. F. Badylak, "Functional skeletal muscle formation with a biologic scaffold," *Biomaterials*, vol. 31, no. 29, pp. 7475–7484, 2010.

[200] N. J. Turner, A. J. Yates, D. J. Weber et al., "Xenogeneic extracellular matrix as an inductive scaffold for regeneration of a functioning musculotendinous junction," *Tissue Engineering A*, vol. 16, no. 11, pp. 3309–3317, 2010.

[201] K. A. Daly, M. Wolf, S. A. Johnson, and S. F. Badylak, "A rabbit model of peripheral compartment syndrome with associated rhabdomyolysis and a regenerative medicine approach for treatment," *Tissue Engineering C: Methods*, vol. 17, no. 6, pp. 631–640, 2011.

[202] M. A. MacHingal, B. T. Corona, T. J. Walters et al., "A tissue-engineered muscle repair construct for functional restoration of an irrecoverable muscle injury in a murine model," *Tissue Engineering A*, vol. 17, no. 17-18, pp. 2291–2303, 2011.

[203] B. T. Corona, C. L. Ward, H. B. Baker, T. J. Walters, and G. J. Christ, "Implantation of in vitro tissue engineered muscle repair constructs and bladder acellular matrices partially restore in vivo skeletal muscle function in a rat model of volumetric muscle loss injury," *Tissue Engineering A*, vol. 20, no. 3-4, pp. 705–715, 2014.

[204] L. E. Freed, F. Guilak, X. E. Guo et al., "Advanced tools for tissue engineering: scaffolds, bioreactors, and signaling," *Tissue Engineering*, vol. 12, no. 12, pp. 3285–3305, 2006.

[205] K. J. Aviss, J. E. Gough, and S. Downes, "Aligned electrospun polymer fibres for skeletal muscle regeneration," *European Cells and Materials*, vol. 19, pp. 193–204, 2010.

[206] M. R. Ladd, S. J. Lee, J. D. Stitzel, A. Atala, and J. J. Yoo, "Co-electrospun dual scaffolding system with potential for muscle-tendon junction tissue engineering," *Biomaterials*, vol. 32, no. 6, pp. 1549–1559, 2011.

[207] D. Klumpp, R. E. Horch, U. Kneser, and J. P. Beier, "Engineering skeletal muscle tissue—new perspectives in vitro and in vivo," *Journal of Cellular and Molecular Medicine*, vol. 14, no. 11, pp. 2622–2629, 2010.

[208] R. Hashizume, K. L. Fujimoto, Y. Hong et al., "Morphological and mechanical characteristics of the reconstructed rat abdominal wall following use of a wet electrospun biodegradable polyurethane elastomer scaffold," *Biomaterials*, vol. 31, no. 12, pp. 3253–3265, 2010.

[209] W. Zhao, Y. M. Ju, G. Christ, A. Atala, J. J. Yoo, and S. J. Lee, "Diaphragmatic muscle reconstruction with an aligned electrospun poly(ε-caprolactone)/collagen hybrid scaffold," *Biomaterials*, vol. 34, no. 33, pp. 8235–8240, 2013.

[210] K. D. McKeon-Fischer, J. H. Rossmeis, A. R. Whittington et al., "*In vivo* skeletal muscle biocompatibility of composite, coaxial electrospun, and microfibrous scaffolds," *Tissue Engineering A*, vol. 20, no. 13-14, pp. 1961–1970, 2014.

Hindawi Publishing Corporation
BioMed Research International
Volume 2014, Article ID 762189, 12 pages
http://dx.doi.org/10.1155/2014/762189

*Research Article*

# Tailored PVA/ECM Scaffolds for Cartilage Regeneration

**Elena Stocco,[1] Silvia Barbon,[1,2] Daniele Dalzoppo,[1] Silvano Lora,[2] Leonardo Sartore,[3] Marcella Folin,[4] Pier Paolo Parnigotto,[1,2] and Claudio Grandi[1]**

[1] *Department of Pharmaceutical and Pharmacological Sciences, University of Padua, Via Marzolo 5, 35131 Padua, Italy*
[2] *Foundation for Biology and Regenerative Medicine, Tissue Engineering and Signaling (TES) ONLUS, Via De Sanctis 10, Caselle di Selvazzano Dentro, 35030 Padua, Italy*
[3] *Operative Unit of Plastic Surgery, Sant'Anna Hospital, Via Ravona 20, 22020 Como, Italy*
[4] *Department of Biology, University of Padua, Viale Colombo 3, 35121 Padua, Italy*

Correspondence should be addressed to Claudio Grandi; claudio.grandi@unipd.it

Received 28 March 2014; Revised 8 July 2014; Accepted 8 July 2014; Published 24 July 2014

Academic Editor: Luca Urbani



Articular cartilage lesions are a particular challenge for regenerative medicine due to cartilage low self-ability repair in case of damage. Hence, a significant goal of musculoskeletal tissue engineering is the development of suitable structures in virtue of their matrix composition and biomechanical properties. The objective of our study was to design *in vitro* a supporting structure for autologous chondrocyte growth. We realized a biohybrid composite scaffold combining a novel and nonspecific extracellular matrix (ECM), which is decellularized Wharton's jelly ECM, with the biomechanical properties of the synthetic hydrogel polyvinyl alcohol (PVA). Wharton's jelly ECM was tested for its ability in promoting scaffold colonization by chondrocytes and compared with polyvinyl alcohol itself and the more specific decellularized cartilage matrix. Our preliminary evidences highlighted the chance of using Wharton's jelly ECM in combination with PVA hydrogels as an innovative and easily available scaffold for cartilage restoration.

## 1. Introduction

Cartilage degeneration, due to congenital abnormalities or disease and trauma, represents a major health problem of great clinical consequence [1, 2]. In case of damage, cartilage is not capable of healing as it is an avascular and aneural tissue; moreover, its cellular components, chondrocytes, have low mitotic ability [3, 4]. Cartilage lesions are generally believed to progress to severe forms of osteoarthritis [5, 6], leading to pathologic changes in the joints with consequent pain, inflammation, and functional disability [7, 8]. Injuries which reach the subchondral bone may induce a systemic reaction and generate reparative tissue. Although type II collagen may be produced by this reparative tissue, it consists predominantly of type I collagen, resulting in the formation of fibrocartilage which does not have the biomechanical properties of articular cartilage [9].

The poor regenerative potential of cartilage and the unsatisfactory current clinical therapies have led to the research of strategies providing solutions to the treatment of focal defects [10, 11]. An emerging and promising field for the generation of tissue substitutes is tissue engineering. The basic approach to tissue engineering depends upon the interaction between cells, scaffolds, and signalling factors to create *in vitro* a biological tissue construct to implant *in vivo* mimicking the tissue of interest; engineering cartilage is no exception to this approach [1, 12, 13].

Implanting the patient's own chondrocytes into the cartilage defect is a method called "matrix-associated autologous chondrocyte transplantation" (MACT): it is performed with either natural or synthetic polymer-based scaffolds [14]. Amongst synthetic biomaterials, hydrogels have demonstrated their ability to simulate human tissue better than any other class. In particular, physically cross-linked poly(vinyl alcohol) (PVA) hydrogels are attractive tools in cartilage tissue engineering as they have a viscoelastic behaviour comparable with that of articular and meniscal cartilage. PVA hydrogels are physically cross-linked through freeze-thaw (FT) cycles: exposing the polymer solution to cold

temperatures, water freezes and PVA is expelled forming areas of high PVA concentration. PVA chains come into close contact with each other and crystallite formation as well as hydrogen bonding occurs. These interactions remain intact after thawing and create a nondegradable 3D hydrogel network. It is possible to tailor mechanical properties of the hydrogel acting on the number of FT cycles [15]. However, despite PVA biocompatibility, its low protein adsorption property results in low cell adhesion compared with other hydrogels [3].

In the body, cells are embedded in the extracellular matrix (ECM) which is made up of protein fibres interwoven in a network of glycosaminoglycan (GAG) chains. The ECM influences cellular responses like survival, development, and behaviour by interacting with cellular adhesion molecules, growth factors, binding proteins, proteolytic enzymes, and enzyme inhibitors [16]. Hence, ECM has been successfully used as a scaffold for constructive remodelling of multiple tissues in both preclinical studies and in human clinical applications [17]. However, despite ECM, derived scaffolds offer promising regenerative responses in many settings; in some applications, more robust and long lasting mechanical properties are necessary [18]. A composite scaffold, strong and bioactive, may represent an interesting solution to this problem. In this work, we have investigated how to realize a scaffold able to sustain articular cartilage regeneration. We have combined mechanical properties of PVA and bioactive ones of ECM. In particular, our attention focused on the investigation of an alternative ECM tissue derived from the umbilical cord Wharton's jelly in comparison with the more specific cartilage matrix.

## 2. Materials and Methods

*2.1. Culture Media and Reagents.* All chemicals and reagents were obtained from Sigma-Aldrich Chemical Company (St. Louis, MO, USA), except for phosphate-buffered saline (PBS) tablets, Dulbecco's modified Eagle's medium/F12 (DMEM/F12) (2 : 1) (Gibco Invitrogen Corporation, Paisley, UK), sodium chloride (Fluka, Basel, Switzerland), the Vectashield Mounting medium for fluorescence with DAPI (Vector Laboratories, Burlingame, CA, USA), Movat pentachromic staining kit (Diapath, Bergamo, Italy), Masson trichrome staining kit (Bio-Optica, Milano, Italy), and collagenase B (Roche, Basel, Switzerland). MilliQ grade water was prepared with a MilliQ Academic system (Millipore, Bedford, MA, USA).

*2.2. Scaffold Manufacture.* Three different scaffold groups were investigated to analyse their ability in sustaining chondrocytes adhesion and proliferation: the PVA hydrogel alone and the PVA hydrogel combined with Wharton's jelly (W's J) derived matrix; the PVA hydrogel combined with articular cartilage (AC) derived matrix.

For the first group, an aqueous solution of 16 wt% PVA (Mw 146,000–186,000 Da, 99+% hydrolysed) was prepared by heating the polymer suspension for 48 hours at 90°C, under stirring, until complete dissolution. The PVA solution was then slowly cooled down to room temperature. Finally, a volume of 0.7 mL of the PVA solution was cast into each well of a 24-well tissue culture plate (mould) (BD Falcon, Franklin Lakes, NJ, USA).

For composite scaffolds, ECMs were gained from umbilical cord and cartilage samples collected after obtaining informed consent of donors. All tissue samples were rinsed several times in PBS containing 2% penicillin/streptomycin solution in order to remove any residual blood.

After taking off blood vessels from umbilical cords, Wharton's jelly and cartilage were minced into small fragments that were all gathered in a 50 mL tube (BD Falcon). Fragments were then decellularized according to the detergent-enzymatic method by Meezan and collaborators [19]. Briefly, samples were soaked in distilled water for 72 h at 4°C, changing the aqueous solution every 2 h, 4% sodium deoxycholate for 4 h at room temperature (RT), and 2,000 KU (Kunitz Units) DNase-I in 1 M NaCl for 2 h at RT. After decellularization, 1 g of W's J or cartilage was soaked with 15 mL of 10% acetic acid solution (2.5 M) in deionized water ($dH_2O$) and homogenized at 0°C using Ultra-Turrax homogenizer (Janke & Kunkel GmbH, Staufen, Germany) 8 times/20 sec with intervals of 5 min. This stage was led in an ice bath. For total protein quantitation, 1 mL of each homogenate was analysed as described in Section 2.5. In parallel, 400 $\mu$L of matrix solution was cast into each well of a 24-well cell culture plate (mould) and frozen at −20°C before being lyophilized overnight using an under-vacuum evaporator (Speed Vac Concentrator Savant, Instruments Inc., Farmingdale, NJ, USA). Composite scaffolds of PVA and ECM were prepared setting down carefully a thin matrix layer upon PVA solution poured in 24-well plates. A freeze-thaw treatment was used to physically cross-link the hydrogel and to embed the lyophilized matrix upon it. Briefly, the coated plate was frozen at −20°C and slowly thawed at −2.5°C for 5 times. At the end of the freeze-thawing treatment, composite scaffolds were kept at −20°C until use.

*2.3. Mechanical Testing of PVA Hydrogels.* Hydrated 16 and 25 wt% PVA hydrogels underwent tensile tests. Analyses were performed in a universal testing machine Bose (Electroforce, Eden Prairie, MN, USA), at RT and with a crosshead speed of 0.5 mm/sec. The samples were cut with a rectangular shape and size of 5 mm × 25 mm × 1 mm. The samples were fixed to the machine by means of clamps.

*2.4. Morphological Analysis by Scanning Electron Microscopy (SEM).* PVA and PVA composite scaffold morphology before and after chondrocytes seeding was investigated by SEM. Samples were fixed with 2.5% glutaraldehyde in 0.1 M cacodylate buffer (pH 7.2) for 24 h and then dehydrated with a graded ethanol series. After critical point drying and gold sputtering, they were observed by a scanning electron microscope (Stereoscan-205 S; Cambridge instruments, Pine Brook, NJ, USA).

*2.5. Protein Quantitation Assay of Decellularized ECMs.* Total ECM proteins were quantitated by bicinchoninic acid (BCA)

method using the Pierce BCA Protein assay kit (Thermoscientific, Rockford, IL, USA) and following the manufacturer's instructions for protein detection on microplate wells. The analysis was performed on five different donor samples of W's J and AC matrix homogenates, obtained as described previously. Acetic acid homogenates (1 mL) were centrifuged at 12000 rpm for 5 min at 4°C and protein pellets were dissolved in 1 mL of 1% sodium dodecyl sulphate (SDS). The colorimetric reactions were analyzed at 562 nm using a Microplate autoreader EL 13 (BIO-TEK Instruments Inc., Winooski, Vermont, USA). The total protein amount was determined using a standard curve for bovine serum albumin (BSA).

*2.6. Quality Assessment of ECM after Decellularization Treatment.* For histological analysis, Wharton's jelly and articular cartilage fragments were soaked in cold isopentane and frozen in liquid nitrogen fumes and then kept at −80°C for 24 h. Samples were then ice-included and sliced in 7 $\mu$m serial slices using a cryomicrotome (Leica CM 1850 UV). These sections were fixed with acetone and mounted with Vectashield mounting medium for fluorescence with DAPI (Vector Laboratories, Burlingame, CA, USA) to ascertain complete decellularization after each detergent-enzymatic cycle. In parallel, acellular samples were stained with Movat pentachromic and Masson trichromic kits to assess the maintenance of structural properties. As control, native W's J and AC samples were used.

*2.7. Cartilage Harvest and Chondrocyte Isolation.* Noncalcified human articular cartilage samples were collected from 3 donors who underwent total knee arthroplasty; only tissue from joints without signs of degenerative changes was used. The cartilage specimens were kept in basal medium DMEM and Nutrient Mixture F12, ratio 2 : 1, until further processed (within 24 h of sample collection). For chondrocyte isolation, cartilage was washed in PBS containing 2% of penicillin/streptomycin, minced finely, and digested with 0.1% collagenase B in basal medium at 37°C for 22 hours. The resulting cell suspension was collected and centrifuged at 1500 rpm for 5 min. Isolated cells were then seeded on 25 $cm^2$ flasks (BD Falcon) at high density with complete medium as described below.

*2.8. Chondrocyte Culture.* Chondrocytes were cultured at 37°C in humidified atmosphere containing 5% $CO_2$ with complete medium: DMEM/F12 (2 : 1) was added with 10% fetal bovine serum (FBS), 0.4 $\mu$g/mL hydrocortisone, 8 ng/mL cholera toxin, 5 $\mu$g/mL insulin, 24 $\mu$g/mL adenine, 0.5 $\mu$g/mL transferrin, 136 pg/mL triiodothyronine, and 1% penicillin/streptomycin solution. The medium was changed at the sixth day and then every 3-4 days.

*2.9. Optical Microscopy Analysis.* Cell cultures were daily observed by optical microscope DM/IL (Leica), and pictures were taken with a camera Nikon Digital Sight Ds-SMCc (Nikon Corporation).

*2.10. RT-PCR.* To investigate gene expression profile of chondrocyte primary cultures, mRNAs of specific cartilage markers were analysed using reverse transcription polymerase chain reaction (RT-PCR). Total RNA of cultured chondrocytes was first isolated using Trizol and quantified by NanoDrop 2000 (Thermo Fisher Scientific, Waltham, MA, USA) at 260 and 280 nm. Reverse transcription and specific amplification were performed in a single tube using QIAGEN OneStep RT-PCR Kit (Qiagen, Hilden, Germany, EU) according to the manufacturer's instructions. Specific oligoprimers (Life technologies, Carlsbad, CA, USA) designed on Gene Bank sequences (Table 1) were used and the expression of HPRT was considered as internal control. Finally, PCR products were separated by 7% polyacrylamide gel electrophoresis and visualized by silver nitrate staining. Pictures were taken using 3000 VersaDoc Gel Imaging System (Bio-Rad, Hercules, California, USA) and Quantity One software (Bio-Rad). Finally, band intensities were quantitated by densitometry, using *Image J* software.

*2.11. Immunophenotype Characterization.* Flow cytometry analysis was performed to identify chondrocyte specific immunophenotype. Cells were first harvested by treatment with trypsin-EDTA and resuspended in PBS and 0.2% BSA. Hence, chondrocytes were stained with phycoerythrin-conjugated antibodies, CD26, CD49c, CD44, and CD73; fluorescein isothiocyanate-conjugated antibodies, CD49e and CD151; and PerCP-Cyanine5-conjugated antibody, CD49f. Labeling occurred in 15 minutes at RT, in the dark. Isotypic antibodies served as controls. All the antibodies were purchased from BioLegend (San Diego, CA, USA), with the exception of CD151 and its isotype, purchased from Millipore (Billerica, MA, USA) (Table 2). For each sample, at least 10,000 events were analysed by a FACS Canto II cytometer (Becton Dickinson, Franklin Lakes, NJ, USA). Data were analysed by Flowing Software 2 and results were expressed as percentage of positive cells compared to the isotype negative control.

*2.12. Chondrocyte Culture on Scaffolds.* Primary human chondrocytes from passage 1, isolated and cultured as previously described, were used for seeding on scaffolds. PVA/W's J and PVA/AC scaffolds were washed 4 times of 2 h each in PBS solution containing 2% penicillin/streptomycin and then incubated at 37°C in basal medium overnight. Scaffolds were placed in a 24-well cell culture plate, seeded with chondrocytes (20,000 cells/$cm^2$), and incubated at 37°C in a 5% $CO_2$ humidified atmosphere.

*2.13. Evaluation of Proliferative Activity.* After 24 h and 7 and 14 days from seeding on scaffolds, cells were treated with 3-(4,5-dimethylthiazol-2-yl)-2,5-dimethyltetrazolium bromide (MTT) (0.5 mg/mL) for 4 h. Formazan precipitates were dissolved in 2-propanol acid (0.04 M HCl in 2-propanol) and optical density was measured at 570 nm, using a Microplate autoreader EL 13. Results were expressed as number of cells grown on seeded surface.

Table 1: Primers for RT-PCR.

| Gene | Forward primer 5′ → 3′<br>Reverse primer 3′ → 5′ | GenBank accession | Base pair (bp) |
|---|---|---|---|
| Collagen, type II, alpha 1 (COL2A1) | F: CCGGGCAGAGGGCAATAGCAGGTT<br>R: CAATGATGGGGAGGCGTGAG | NM_001844.4 | 127 |
| Collagen, type IX, alpha 3 (COL9A3) | F: AATCAGGCTCTCGAAGCTCATAAAA<br>R: CCTGCCACACCCCCGCTCCTTCAT | NM_001853.3 | 99 |
| Collagen, type X, alpha 1 (COL10A1) | F: GAACTCCCAGCACGCAGAATCC<br>R: GTGTTGGGTAGTGGGCCTTTTATG | NM_000493.3 | 144 |
| Cartilage oligomeric matrix protein (COMP) | F: CCGGAGGGTGACGCGCAGATTGA<br>R: TGCCCTCGAAGTCCACGCCATTGAA | NM_000095.2 | 132 |
| Aggrecan (ACAN) | F: GGCTGCTGTCCCCGTAGAAGA<br>R: GGGAGGCCAAGTAGGAAGGAT | NM_001135.3 | 162 |
| Transcription factor SOX9 (SOX9) | F: CTGGGCAAGCTCTGGAGA<br>R: ATGTGCGTCTGCTCCGTG | NM_000346.3 | 178 |
| Hyaluronan synthase 1 (HAS1) | F: CAGACCCACTGCGATGAGAC<br>R: CCACCAGGTGCGCTGAAA | NM_001523.2 | 217 |
| Hypoxanthine phosphoribosyltransferase 1 (HPRT1) | F: ATGGACAGGACTGAACGTCTTGCT<br>R: TTGAGCACACAGAGGGCTACAATG | NM_000194.2 | 79 |

Table 2: Antibodies used for flow cytometry.

| Antigen recognized | Isotype | Fluorochrome | Category |
|---|---|---|---|
| CD26 (peptidase IV) | IgG2a | PE | Ectoenzyme |
| CD44 | IgG1 | PE | Adhesion molecule |
| CD49c ($\alpha$3 integrin chain) | IgG1 | PE | Adhesion molecule |
| CD49e ($\alpha$5 integrin chain) | IgG2b | FITC | Adhesion molecule |
| CD49f ($\alpha$6 integrin chain) | IgG2a | PerCP/Cy5.5 | Adhesion molecule |
| CD73 (5′-nucleotidase) | IgG1 | PE | Ectoenzyme |
| CD151 | IgG1 | FITC | Tetraspanin |

*2.14. Statistical Analysis.* We performed Student's $t$-test to determine the statistical significance of the data.

## 3. Results

*3.1. Mechanical Properties of PVA Hydrogel.* Resilience is a measure of a material's ability to deform reversibly without loss of energy. To examine the possibility of using PVA as a mechanical support for cartilage regeneration, the resilience of 16% and 25% hydrogels was measured. Briefly, an electromechanical transducer exerted a traction force, stretching the specimen up to 100% of the initial length, while registering the applied strength. The stretching and relaxation curves of both biomaterials are represented by stress-strain profiles in Figure 1. Graphs show stress values relative to a 100% elongation and equal to 0.35 MPa for 16% PVA (Figure 1(a)) and 0.5 MPa for 25% PVA (Figure 1(b)).

*3.2. Characterization of Scaffold Morphology (SEM).* SEM micrographs were obtained to characterize the superficial morphology of scaffolds before chondrocyte seeding (Figure 2). PVA scaffolds showed a quite homogenous porous distribution with pore size ranging from 4 to 10 $\mu$m (Figure 2(a)). PVA/W's J and PVA/AC scaffolds have a different surface morphology: the first is quite regular and smooth with convolution-like structures (Figure 2(b)); the second has a more irregular spongy appearance (Figure 2(c)).

*3.3. Protein Quantitation of Decellularized ECMs.* After ECM decellularization treatment, BCA assay was performed to control contingent sample-to-sample variations in total protein amount. Matrix homogenates of W's J and AC, gained from different donors, were compared. Total protein content for W's J and AC ECMs resulted in 29.2 and 24.8 mg per gram of tissue, respectively (mean values). No statistically

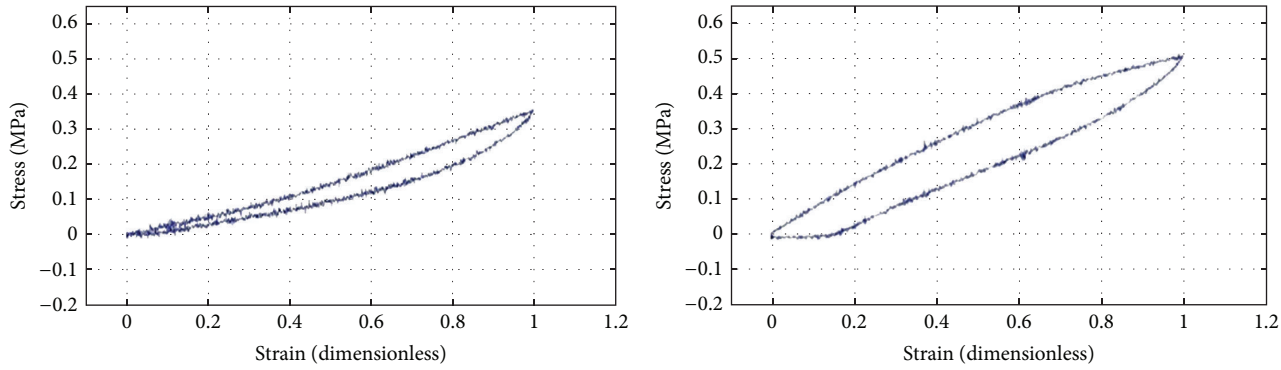


Figure 1: Stress-strain curves of PVA 16% (a) and PVA 25% (b) hydrogels.

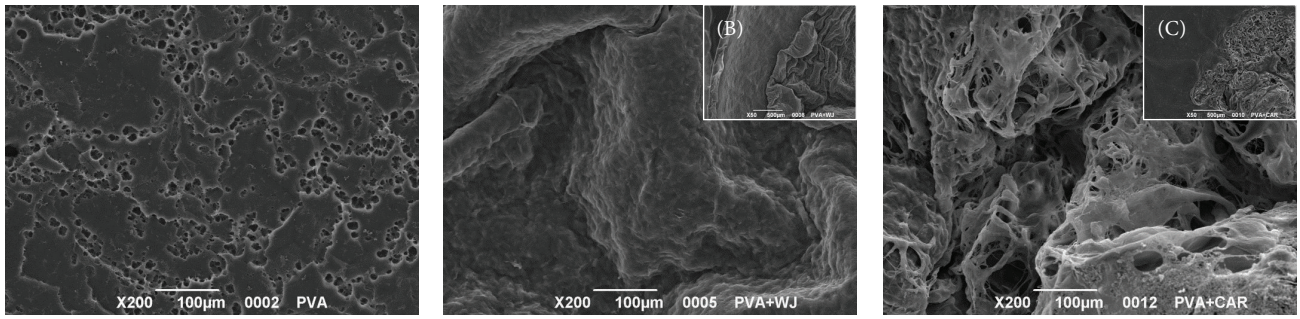


Figure 2: SEM investigation of PVA (a), PVA/W's J (b), and PVA/AC (c) scaffold surface morphology. The edge of PVA scaffold not covered by W's J and AC matrix is represented in (b) and (c), respectively. Magnification: ×200 (a, b, c); ×50 (b, c).

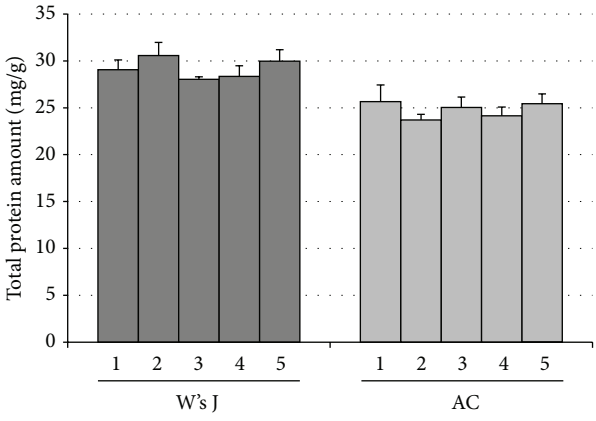


Figure 3: Total protein quantitation by BCA assay in decellularized Wharton's jelly and articular cartilage.

significant difference was found between samples of each study group (Figure 3).

*3.4. Evaluation of Acellular ECMs.* Umbilical cord Wharton's jelly and articular cartilage were completely decellularized with 3 and 7 detergent-enzymatic cycles, respectively; DAPI staining was used to assure decellularization degree after each cycle. Cartilage tissue resulted in more resistance to cell removal compared to Wharton's jelly; already one cycle induced an appreciable disappearance of cellular elements in the umbilical cord derived matrix. The histological sections of native and decellularized ECMs stained with DAPI are presented in Figures 4(a) and 4(g) and Figures 4(b) and 4(h), respectively.

ECMs morphology before and after the decellularization treatment was evaluated by means of Masson trichromic staining, which demonstrated a similar protein content of W's J and AC samples. In particular, both matrices mainly consist of collagen fibers and mucus, as shown by the green staining of native (Figures 4(c) and 4(i)) and decellularized (Figures 4(d) and 4(l)) tissues.

Movat pentachromic staining allowed us to detect red fibrin and yellow collagen components in native W's J (Figure 4(e)). Moreover, in native AC (Figure 4(m)) and acellular ECMs (Figures 4(f) and 4(n)), blue and yellow colors indicate the presence of mucins and collagen fibers, respectively.

*3.5. Chondrocyte Monolayer Cultures.* Freshly isolated chondrocytes were small and round and they were initially grown as a suspension culture. Six days after AC enzymatic digestion, adherent cells were observed to spread across the

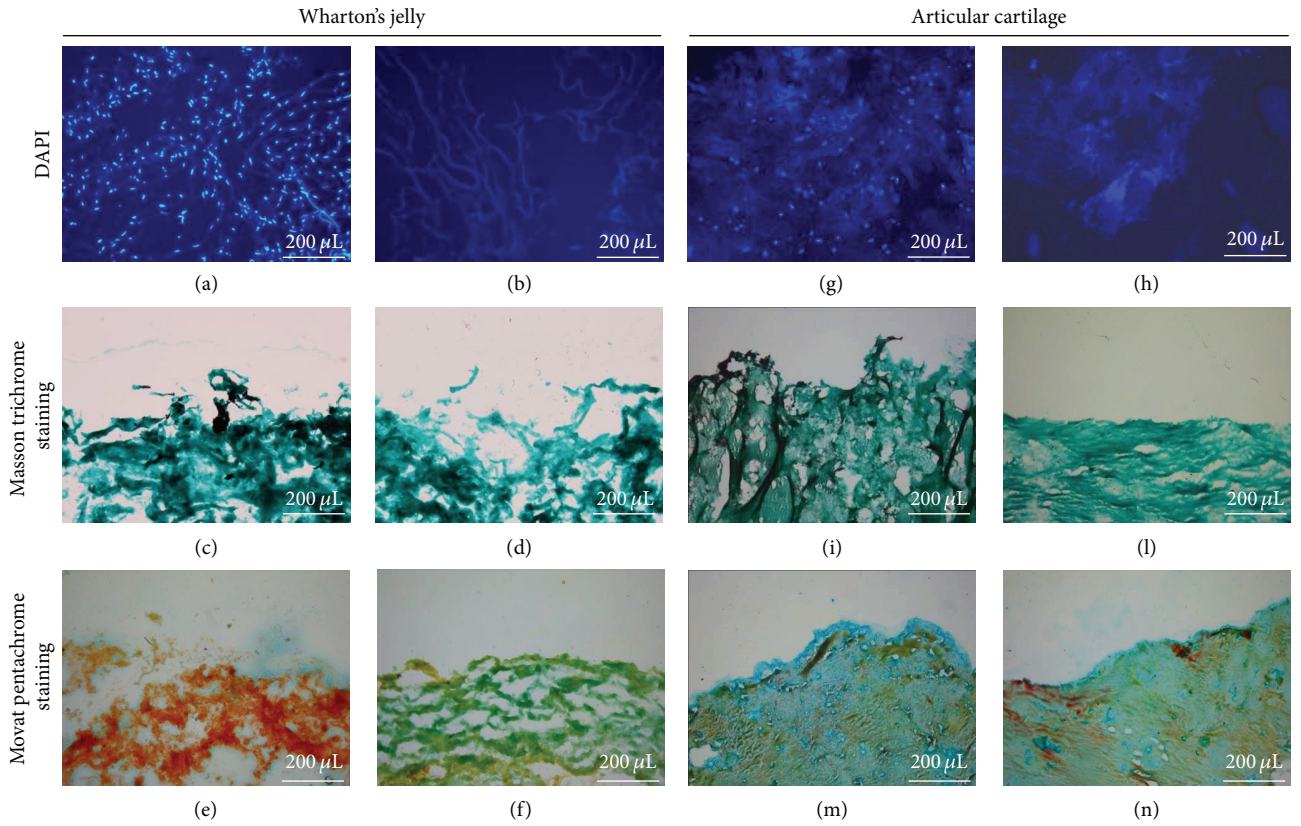


FIGURE 4: Histological evaluation of decellularized ECMs (b, d, f, h, l, and n) versus native tissues (a, c, e, g, i, and m). Magnification: ×100.

flask and demonstrated clear boundaries and distinct nuclei (Figure 5(a)). In the subcultures, at a subconfluence state, chondrocytes showed the classic round or polygonal shape with small membrane extroflessions (Figure 5(b)). Once monolayer cultures reached 100% confluence, cells appeared to be smaller but maintained their characteristic morphology (Figures 5(c) and 5(d)). Chondrocytes were expanded in culture up to passage 4; hereafter, their proliferation rate started to decrease and their morphology changed to elongated fibroblast-like phenotype.

*3.6. Characterization of Isolated Chondrocytes.* Before seeding on 3D scaffolds, isolated human chondrocytes were characterized for the expression of specific cartilage markers. Gene expression analysis by RT-PCR showed that AC-derived cell populations are active in the transcription of typical chondrocyte mRNAs: collagen types II, IX, and X, cartilage oligomeric matrix protein, aggrecan, SOX9, and hyaluronan synthase (Figure 6(a)). As shown in Figure 6(b), densitometry quantitated band intensities were corrected for loading using housekeeping gene HPRT1 as a control and graphed as a ratio of HPRT1.

To define the immunophenotype of AC chondrocytes, cell surface molecules expressed on cells obtained from 3 different donors (age range 32–85; mean 58.9) were evaluated by flow cytometry. Chondrocytes of each donor were cultured for 2 weeks in monolayer and passages 1 and 2 were investigated. The analysed cell surface molecules were classified into different categories according to their function: adhesion molecules (CD44; CD49c; CD49e; CD49f), receptors (CD151), and other surface molecules as ectoenzyme molecules (CD26; CD73). Chondrocytes subcultures were positive for CD44 (95.5%), CD73 (86.0%), CD151 (85.0%), CD49c (20.7%), and CD49e (34.5%); they showed low and negative expression of CD49f (3.7%) and CD26 (0.3%), respectively (Figure 7).

*3.7. Chondrocytes Growth on 3D Scaffolds.* Chondrocyte's distribution and proliferative activity on scaffolds were evaluated by SEM and MTT assay.

According to SEM micrographs (Figure 8), on PVA scaffolds, any cell was visible since 24 h from seeding (Figure 8(a)); even at days 7 and 14 (Figures 8(d) and 8(g)), no cell adhesion and proliferation was observable. On the contrary, chondrocytes are visible both on PVA/W's J and on PVA/AC scaffolds. Twenty-four hours from seeding, on PVA/AC scaffolds, chondrocytes appeared well distributed with their typical round-shaped morphology (Figure 8(c)); cell organization on PVA/W's J scaffolds was less tidy (Figure 8(b)). At day 7, cells' limits on PVA/AC were still visible (Figure 8(e)), unlike ones of chondrocytes seeded on PVA/W's J scaffolds (Figure 8(f)). At day 14, chondrocytes extensively colonised both scaffold surfaces, forming a homogeneous monolayer (Figures 8(h) and 8(i)).

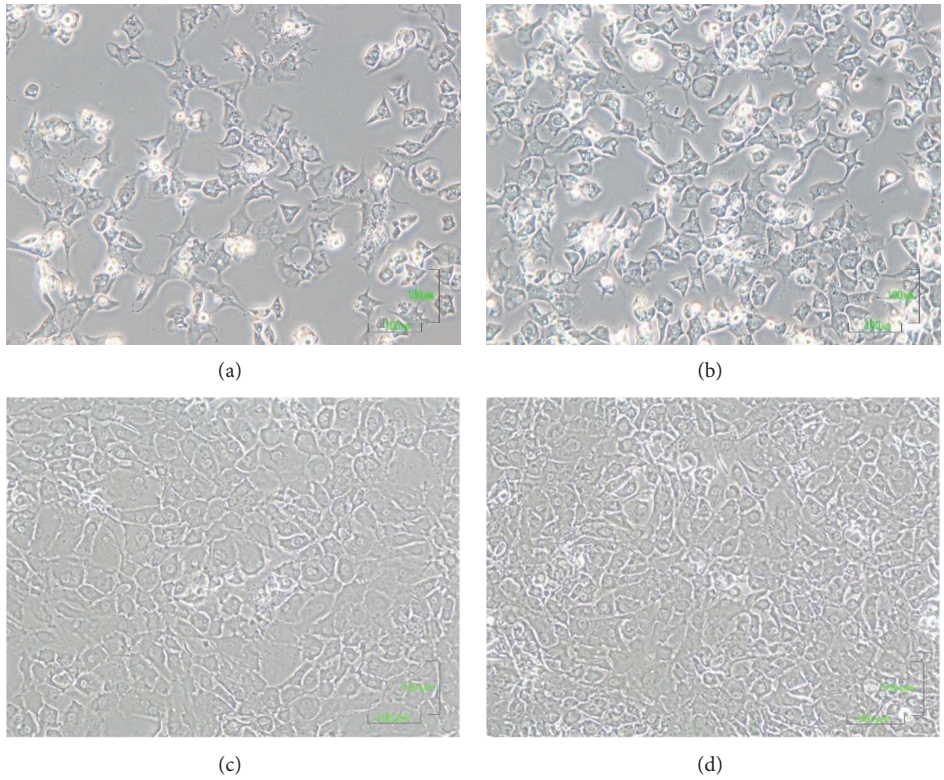

(a) (b) (c) (d)

Figure 5: Morphological analysis by optical microscopy of human AC chondrocytes at passages 0 (a, c) and 4 (b, d) at a subconfluent (a, b) and confluent (c, d) state. Magnification: ×100.

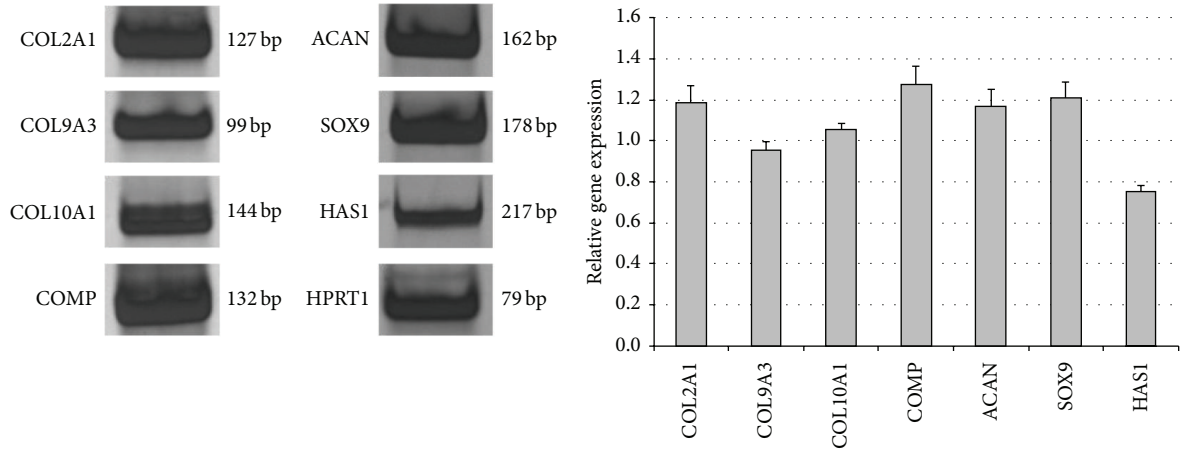


(a) (b)

Figure 6: (a) Gene expression profile of isolated chondrocytes identified by RT-PCR. (b) Band intensities quantitation by densitometry. Relative expression of target genes is referred to HPRT1 expression.

According to MTT assay (Figure 9), PVA did not sustain cell adhesion and proliferation, as previously demonstrated by SEM. Twenty-four hours from seeding, colonization of PVA/ECM scaffolds occurred, and cell number on composite supports was significantly higher ($P \leq 0.01$) than that on native PVA. A progressive increase of cell number was observable from day 7 to day 14 on PVA/ECM scaffolds, where chondrocyte proliferation remained significantly higher ($P \leq 0.01$) in comparison with PVA itself. Cell growth on tissue culture-treated polystyrene plates was considered as internal proliferation control (Ctrl).

## 4. Discussion

Articular hyaline cartilage is a soft tissue; it sustains the pressure between the hard ends of bones and it is subjected

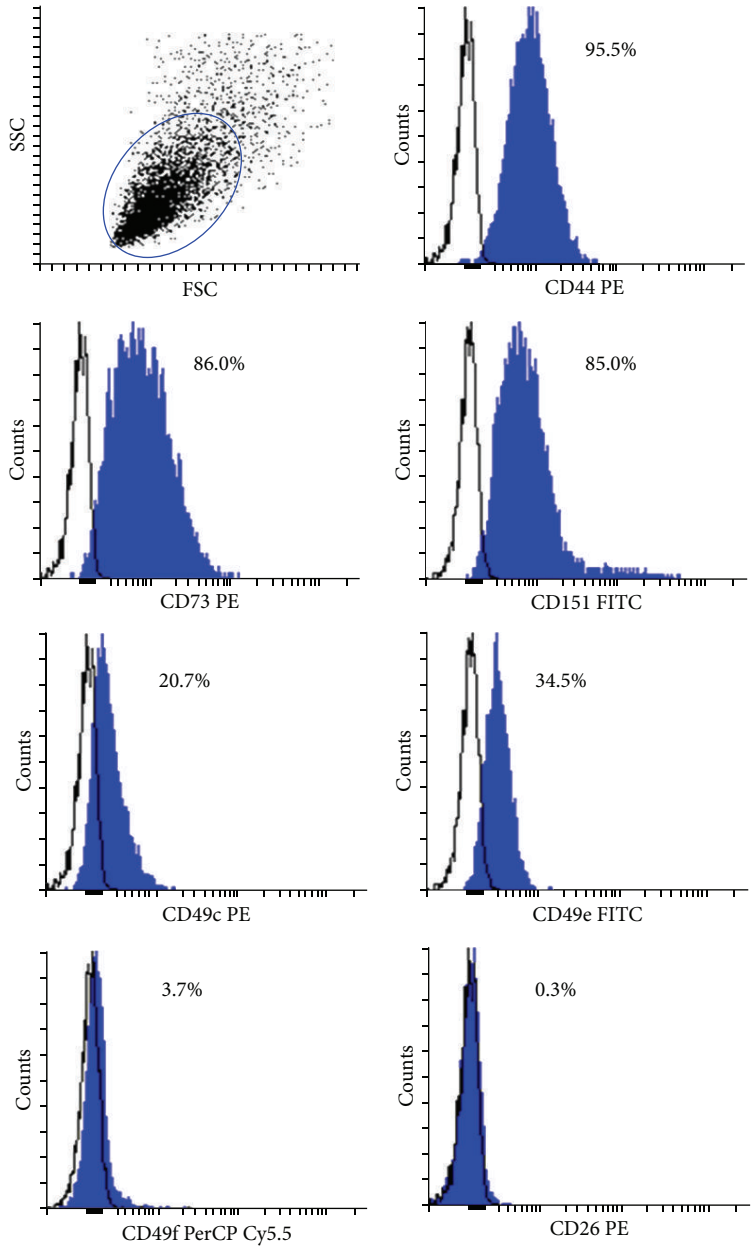


Figure 7: Immunophenotype evaluation of AC chondrocytes by flow cytometry. Data are expressed as percentage of positive cells (blue profile) compared to isotypic control (black profile).

to particularly complex loads affecting its development and maintenance in the body [20, 21]. Because of its limited self-healing capacity, as it is an avascular and aneural tissue, even minor cartilage defects lead to mechanical joint instability and progressive damage [21, 22]. Cartilage damage is difficult to treat. Until now, many approaches have been investigated: arthroscopic repair procedures, soft tissue grafts, osteochondral transfer, autologous chondrocytes transplantation, and marrow stimulation [23], but average long-term results are unsatisfactory. A general drawback of these therapeutic strategies is that the newly formed tissue lacks the structural organization of cartilage; it has inferior mechanical properties compared to native tissue, and it is, therefore, prone to failure [21, 24]. Hence, the goal is to produce a repair tissue that has the same functional and mechanical properties of hyaline articular cartilage [25]. Cartilage restoration represents a challenge of musculoskeletal tissue engineering; despite that, the use of matrix scaffolds has paved the way for the use of functional tissue substitutes in the treatment of cartilage defects [22]. A wide range of natural and synthetic materials have been investigated as scaffolding for cartilage repair [26]. Natural scaffolds may face problems of immunogenic compatibility and batch inconsistency, while the properties offered by synthetic matrices provide much promise in the future of articular cartilage repair [25]. Amongst synthetic biomaterials, physically cross-linked PVA hydrogels become

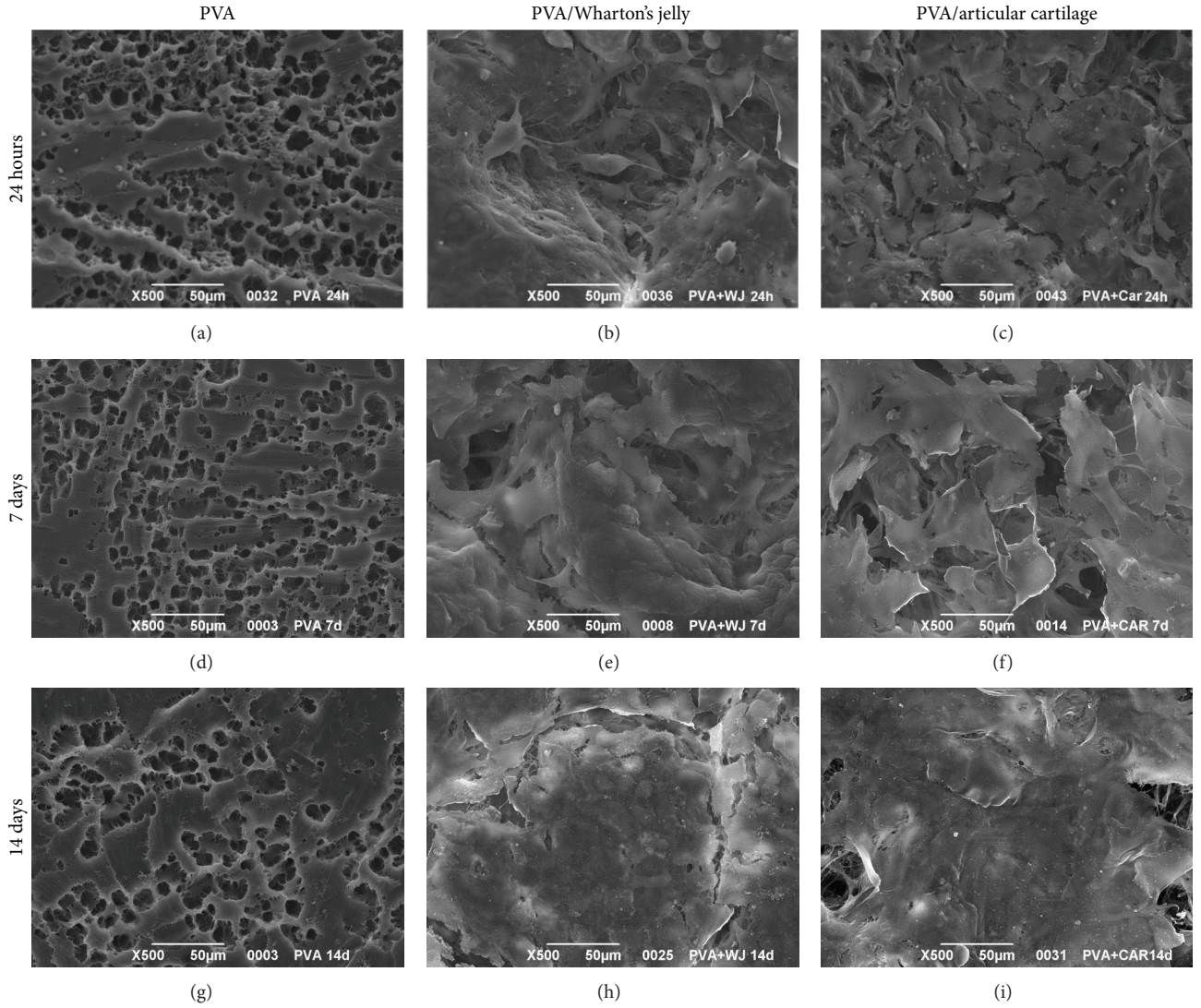


Figure 8: Evaluation of AC chondrocyte growth on 3D scaffolds by scanning electron microscopy. Cell cultures were analysed 24 h (a, b, c), 7 d (d, e, f), and 14 d (g, h, i) from seeding. Magnification: ×500.

suitable for soft tissue applications: thanks to their biocompatibility and mechanical properties, they have been proposed for many biomedical applications, even as cartilage substitutes [15]. Mechanical properties of the gel can be modulated acting on different variables: polymer molecular weight, number of freezing/thawing cycles, and polymer solution concentration [27]. Varying the polymer wt%, we realized two different PVA hydrogels (PVA 16 wt% versus PVA 25 wt%), which were tested for their tensile strength. PVA 16 wt% hydrogel is more elastic than 25 wt% one. As proved by stress-strain profiles presented, it did not maintain the residual strain when subjected to tensile strength, revealing high elasticity. However, cell adherence on PVA hydrogels is inhibited by its highly hydrophilic nature [28]. Many authors demonstrated ECM-based scaffold efficacy in creating a more suitable microenvironment to sustain cellular adhesion. Extracellular matrix is a reservoir of structural and functional proteins like collagens, glycoproteins, proteoglycans, mucins, and elastic fibres as well as a known repository for a variety of growth factors. As *in vivo* it is progressively degraded by proteinases, it can result in the exposure of new recognition sites with potent bioactivity [29]. In this work, we decided to combine PVA mechanical properties with ECM features. Our aim was to provide a supportive biomimetic microenvironment for chondrocytes to produce articular cartilage, taking advantage of both PVA and ECM. In particular, we considered an alternative matrix source: we focused our attention on a new ECM represented by decellularized Wharton's jelly, in comparison with decellularized cartilage matrix.

The research of a new biological ECM useful in cartilage restoration arises from the need to identify an easily available resource suitable in sustaining chondrocytes adhesion and proliferation, even if not specific. Every tissue and organ

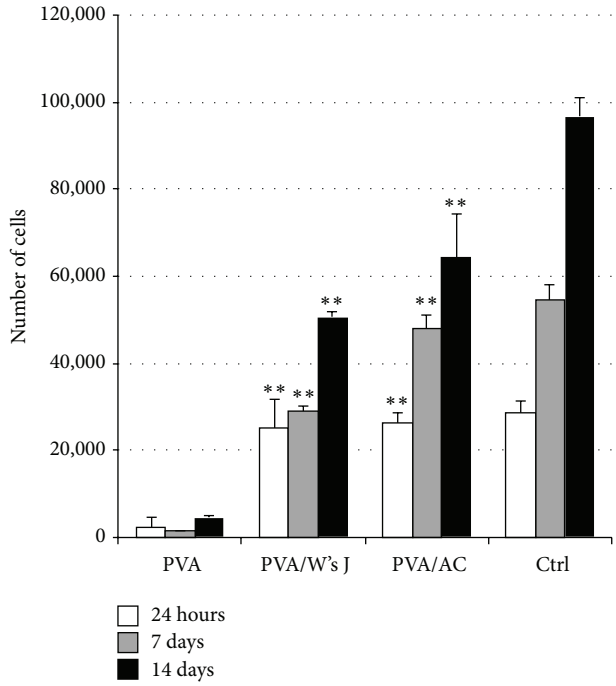


Figure 9: Cell proliferation following seeding on PVA, PVA/W's J, and PVA/AC scaffolds. Data are average of three independent experiments ($^{**}P \leq 0.01$: PVA/ECMs versus the corresponding PVA scaffold).

contains an ECM with unique composition that consists of the secreted products of resident cells [29]. The main components of Wharton's jelly were ECM proteins such as collagen and fibronectin. Previous studies demonstrated that Wharton's jelly contains growth factors such as insulin-like growth factor I (IGF-1), fibroblast growth factor (FGF), transforming growth factor $\beta$ (TGF$\beta$), platelet-derived growth factor (PDGF), epidermal growth factor (EGF), and ECM proteins [30]. These peptides and growth factors induce Wharton's jelly cells to produce large amounts of collagen and glycosaminoglycans [31], also typical components of cartilage matrix [32]. The aim of decellularization treatment is to decrease the antigenicity of matrices, through an efficient removal of cellular and nuclear material, preserving its composition [33]. Histological analysis of decellularized Wharton's jelly and articular cartilage ECM demonstrated the effectiveness of the treatment. A different number of detergent-enzymatic cycles, 3 and 7 cycles, respectively, were performed. According to DAPI staining, native Wharton's jelly showed a higher cellular density in comparison with native articular cartilage; nevertheless, its complete decellularization was easier to achieve. This may be related to a different tissue macroscopic aspect: while chondrocytes are deeply embedded in matrix, Wharton's jelly permits a better exposure of its cellular elements to sodium deoxycholate and DNase-I, as well as to the osmotic effect of deionized water. To control and quantify W's J and AC batch-to-batch variations, decellularized ECMs were analysed in regard to their total protein levels. Matrix homogenates, gained from different donors, showed a similar profile to BCA assay: no significant difference was detected between samples of the same group. According to this data, sample-to-sample variations are negligible. Extracellular matrix characterization before and after detergent-enzymatic treatment was also achieved by means of Masson trichrome and Movat pentachrome staining. According to Masson trichrome, both Wharton's jelly and articular cartilage maintain their collagen and mucus content (deeply green appearance). Movat pentachrome staining confirmed the concomitant presence of collagen and mucus, even after the treatment. The resulting green leading colour is due to the overlapping between yellow (referred to collagen and reticular fibres) and blue (referred to mucus). However, the detergent-enzymatic treatment seemed to remove or reduce fibrinoid elements' expression. This ECMs characterization highlighted a similar histomorphology for Wharton's jelly and cartilage, supporting our theory.

The chief aim of many authors is to preserve tissue or organ histoarchitecture from a too aggressive decellularization treatment; on the contrary, we approached ECMs in a different manner. We take advantage of matrices macromolecules instead of their superstructure. ECM homogenates are an interesting and innovative manner of working with matrices. Choosing an adequate mould and modulating the needed quantity, the liquid suspension obtained can be used to create tailored scaffolds. Furthermore, the lyophilization process they subsequently undergo makes them easy to store. The two different lyophilized matrices realized were examined by SEM for their fine structure: the cartilage derived one appeared spongier than the Wharton's jelly analogue.

Physical cross-linking of lyophilized matrices with PVA solutions led to three-dimensional composite scaffolds. As chondrocytes usually tend to dedifferentiate to fibroblasts when grown in a monolayer culture, a three-dimensional culture system can be used to maintain the chondrogenic phenotype [34]. Before seeding on scaffolds, we isolated cells from human articular cartilage; we confirmed their chondrocyte gene expression profile and phenotype through RT-PCR and flow cytometry analysis.

The viscoelastic properties of articular cartilage arise from the composition of its ECM, which consists primarily of type II collagen but also of collagen types IX and X and a proteoglycan termed aggrecan (ACAN) [35]. Aggrecan is retained in cartilage by binding to long filaments of another glycosaminoglycan, hyaluronan (HA), which is synthesized at the plasma membrane level by an enzyme called hyaluronan synthase (HAS) [36]. Moreover, one of the major noncollagenous proteins in the cartilage is COMP, which represents a useful marker of differentiation state of primary chondrocytes [37]. The synthesis of this cartilage-specific ECM requires the expression of genes associated with the specific chondrocyte phenotype, controlled by the transcription factor SOX9 [35]. According to RT-PCR analysis, cells isolated for this study express specific cartilage markers at the mRNA level, showing a gene expression profile typical of articular chondrocytes.

Expanded chondrocytes were, thus, assessed by flow cytometry. We purchased antibodies against several CDs, typically used to characterize the phenotype of mesenchymal progenitor cells [38, 39] and recently introduced to determine

the stage of differentiation of human articular chondrocytes [39, 40]. In this study, we confirmed the previously reported expression of several articular chondrocyte surface markers: the hyaluronan receptor CD44, the ectoenzyme CD73, the integrins $\alpha 3$ (CD49c), $\alpha 5$ (CD49e), and the tetraspanin CD151 [39, 40]. According to Grogan and colleagues [39], chondrocytes with marked chondrogenic capacity express high levels of the hyaluronan receptor CD44, the $\alpha 3$ integrin subunit CD49c, and the tetraspanin CD151. They are surface molecules involved in the early stages of cartilage development; all of them were present in the chondrocytes we investigated. Moreover, these proteins are responsible for establishing cell-cell and cell-matrix interactions. These processes are known to be important mediators of mesenchymal condensation, which is in turn necessary for initiation of chondrogenesis [41]. Hence, high expression levels of these membrane proteins might increase the propensity of the cells to differentiate and produce cartilage ECM. Markers characteristics of mesenchymal progenitor cells, that is, CD44 and CD73 [38], have been shown to be expressed in high-chondrogenic-capacity populations [39]. This suggests that, within a chondrocyte culture, subpopulations with higher capacity to form cartilage might correspond to those with progenitor characteristics.

After characterization of scaffold histomorphology and chondrocyte gene expression profile and specific immunophenotype, we seeded a known cell amount of 20,000 cells/cm$^2$ on PVA, PVA/W's J, and PVA/AC supports. We evaluated chondrocyte adhesion and proliferation at three different end-points: 24 h and 7 and 14 days. If PVA itself clearly demonstrated its absolute inability to sustain chondrocyte proliferation, cells on composite scaffolds revealed a progressive increasing growth trend. At 24 h from seeding, cells adhered on PVA/ECMs, which were able to sustain cell proliferation up to the last end-point considered (14 days). According to SEM micrographs, chondrocytes on PVA/AC showed a more specific morphology and a more tidy orientation on the scaffold surface. In parallel, PVA/W's J revealed a singular attitude to sustain cell proliferation despite its aspecific origin. Hence, as stressed also by MTT proliferation assay, our *in vitro* model confirmed the starting hypothesis regarding the possibility to use Wharton's jelly in composite scaffolds that mimic articular cartilage.

## 5. Conclusions

Decellularized Wharton's jelly matrix is an attractive reservoir of macromolecules. Our preliminary results proved that it promotes chondrocyte adhesion, representing an idoneous biomimetic microenvironment despite its aspecific nature. Further investigations are necessary to evaluate phenotype maintenance of chondrocytes grown upon PVA/W's J scaffolds. As a future goal, these composite supports will be tested *in vivo* using rabbit models of articular joint defects.

## Conflict of Interests

The authors declare that there is no conflict of interests regarding the publication of this paper.

## Authors' Contribution

Elena Stocco and Silvia Barbon contributed equally to this work.

## Acknowledgments

The authors would like to thank Professor Andrea Bagno for technical support in mechanical tests and Professor Marina Bortolami and Dr. Chiara Carlotto for collaboration in molecular biology analysis.

## References

[1] R. Tuli, W. Li, and R. S. Tuan, "Current state of cartilage tissue engineering," *Arthritis Research and Therapy*, vol. 5, no. 5, pp. 235–238, 2003.

[2] P. C. Kreuz, S. Müller, C. Ossendorf, C. Kaps, and C. Erggelet, "Treatment of focal degenerative cartilage defects with polymer-based autologous chondrocyte grafts: four-year clinical results," *Arthritis Research and Therapy*, vol. 11, no. 2, article R33, 2009.

[3] M. I. Baker, S. P. Walsh, Z. Schwartz, and B. D. Boyan, "A review of polyvinyl alcohol and its uses in cartilage and orthopedic applications," *Journal of Biomedical Materials Research B Applied Biomaterials*, vol. 100, no. 5, pp. 1451–1457, 2012.

[4] J. Y. Chung, D. H. Lee, T. H. Kim, K. S. Kwack, K. H. Yoon, and B. H. Min, "Cartilage extra-cellular matrix biomembrane for the enhancement of microfractured defects," *Knee Surgery, Sports Traumatology, Arthroscopy*, vol. 22, no. 6, pp. 1249–1259, 2014.

[5] S. Giovannini, J. Diaz-Romero, T. Aigner, P. Heini, P. Mainil-Varlet, and D. Nesic, "Micromass co-culture of human articular chondrocytes and human bone marrow mesenchymal stem cells to investigate stable neocartilage tissue formation in vitro," *European Cells and Materials*, vol. 20, pp. 245–259, 2010.

[6] J. D. Harris, R. A. Siston, X. Pan, and D. C. Flanigan, "Autologous chondrocyte implantation: a systematic review," *Journal of Bone and Joint Surgery A*, vol. 92, no. 12, pp. 2220–2233, 2010.

[7] J. Farr Ii, L. E. Miller, and J. E. Block, "Quality of life in patients with knee osteoarthritis: a commentary on nonsurgical and surgical treatments," *The Open Orthopaedics Journal*, vol. 13, no. 7, pp. 619–623, 2013.

[8] C. C. Yang, C. Y. Lin, H. S. Wang, and S. R. Lyu, "Matrix metalloproteases and tissue inhibitors of metalloproteinases in medial plica and pannus -like tissue contribute to knee osteoarthritis progression," *PLoS ONE*, vol. 8, no. 11, Article ID e79662, 2013.

[9] M. Ochi, Y. Uchio, K. Kawasaki, S. Wakitani, and J. Iwasa, "Transplantation of cartilage-like tissue made by tissue engineering in the treatment of cartilage defects of the knee," *Journal of Bone and Joint Surgery B*, vol. 84, no. 4, pp. 571–578, 2002.

[10] C. W. Archer, S. Redman, I. Khan, J. Bishop, and K. Richardson, "Enhancing tissue integration in cartilage repair procedures," *Journal of Anatomy*, vol. 209, no. 4, pp. 481–493, 2006.

[11] D. Nesic, R. Whiteside, M. Brittberg, D. Wendt, I. Martin, and P. Mainil-Varlet, "Cartilage tissue engineering for degenerative joint disease," *Advanced Drug Delivery Reviews*, vol. 58, no. 2, pp. 300–322, 2006.

[12] K. Kim, J. Lam, S. Lu et al., "Osteochondral tissue regeneration using a bilayered composite hydrogel with modulating dual

growth factor release kinetics in a rabbit model," *Journal of Controlled Release*, vol. 168, no. 2, pp. 166–178, 2013.

[13] RS. Nirmal and PD. Nair, "Significance of soluble growth factors in the chondrogenic response of human umbilical cord matrix stem cells in a porous three dimensional scaffold," *Journal of European Cells and Materials*, vol. 26, pp. 234–251, 2013.

[14] S. Nuernberger, N. Cyran, C. Albrecht, H. Redl, V. Vécsei, and S. Marlovits, "The influence of scaffold architecture on chondrocyte distribution and behavior in matrix-associated chondrocyte transplantation grafts," *Biomaterials*, vol. 32, no. 4, pp. 1032–1040, 2011.

[15] J. L. Holloway, K. L. Spiller, A. M. Lowman, and G. R. Palmese, "Analysis of the in vitro swelling behavior of poly(vinyl alcohol) hydrogels in osmotic pressure solution for soft tissue replacement," *Acta Biomaterialia*, vol. 7, no. 6, pp. 2477–2482, 2011.

[16] J. S. Choi, H. Yang, B. S. Kim et al., "Human extracellular matrix (ECM) powders for injectable cell delivery and adipose tissue engineering," *Journal of Controlled Release*, vol. 139, no. 1, pp. 2–7, 2009.

[17] B. Brown, K. Lindberg, J. Reing, D. B. Stolz, and S. F. Badylak, "The basement membrane component of biologic scaffolds derived from extracellular matrix," *Tissue Engineering*, vol. 12, no. 3, pp. 519–526, 2006.

[18] K. Takanari, Y. Hong, R. Hashizume et al., "Abdominal wall reconstruction by a regionally distinct biocomposite of extracellular matrix digest and a biodegradable elastomer," *Journal of Tissue Engineering and Regenerative Medicine*, vol. 9, no. 3, 2013.

[19] E. Meezan, J. T. Hjelle, K. Brendel, and E. C. Carlson, "A simple, versatile, nondisruptive method for the isolation of morphologically and chemically pure basement membranes from several tissues," *Life Sciences*, vol. 17, no. 11, pp. 1721–1732, 1975.

[20] H. Ahn, K. J. Kim, S. Y. Park, J. E. Huh, H. J. Kim, and W. R. Yu, "3D braid scaffolds for regeneration of articular cartilage," *Journal of the Mechanical Behavior of Biomedical Materials*, vol. 34, pp. 37–46, 2014.

[21] Y. Jung, M. S. Park, J. W. Lee, Y. H. Kim, S. H. Kim, and S. H. Kim, "Cartilage regeneration with highly-elastic three-dimensional scaffolds prepared from biodegradable poly(l-lactide-co-ε-caprolactone)," *Biomaterials*, vol. 29, no. 35, pp. 4630–4636, 2008.

[22] M. Demoor, D. Ollitrault, T. Gomez-Leduc et al., "Cartilage tissue engineering: molecular control of chondrocyte differentiation for proper cartilage matrix reconstruction," *Biochimica et Biophysica Acta*, vol. 1840, no. 8, pp. 2414–2440, 2014.

[23] J. Farr, B. Cole, A. Dhawan, J. Kercher, and S. Sherman, "Clinical cartilage restoration: evolution and overview," *Clinical Orthopaedics and Related Research*, vol. 469, no. 10, pp. 2696–2705, 2011.

[24] L. Kock, C. C. van Donkelaar, and K. Ito, "Tissue engineering of functional articular cartilage: the current status," *Cell and Tissue Research*, vol. 347, no. 3, pp. 613–627, 2012.

[25] S. N. Redman, S. F. Oldfield, and C. W. Archer, "Current strategies for articular cartilage repair," *European Cells and Materials*, vol. 9, pp. 23–32, 2005.

[26] C. Chung and J. A. Burdick, "Engineering cartilage tissue," *Advanced Drug Delivery Reviews*, vol. 60, no. 2, pp. 243–262, 2008.

[27] E. Fathi, N. Atyabi, M. Imani, and Z. Alinejad, "Physically crosslinked polyvinyl alcohol-dextran blend xerogels: Morphology and thermal behavior," *Carbohydrate Polymers*, vol. 84, no. 1, pp. 145–152, 2011.

[28] Y. Liu, L. M. Geever, J. E. Kennedy, C. L. Higginbotham, P. A. Cahill, and G. B. McGuinness, "Thermal behavior and mechanical properties of physically crosslinked PVA/Gelatin hydrogels," *Journal of the Mechanical Behavior of Biomedical Materials*, vol. 3, no. 2, pp. 203–209, 2010.

[29] B. N. Brown and S. F. Badylak, "Extracellular matrix as an inductive scaffold for functional tissue reconstruction," *Translational Research*, vol. 163, no. 4, pp. 268–285, 2014.

[30] H. Hao, G. Chen, J. Liu et al., "Culturing on Wharton's jelly extract delays mesenchymal stem cell senescence through p53 and p16INK4a/ pRb pathways," *PLoS ONE*, vol. 8, no. 3, Article ID e58314, 2013.

[31] K. Sobolewski, A. Małkowski, E. Bańkowski, and S. Jaworski, "Wharton's jelly as a reservoir of peptide growth factors," *Placenta*, vol. 26, no. 10, pp. 747–752, 2005.

[32] A. R. Poole, T. Kojima, T. Yasuda, F. Mwale, M. Kobayashi, and S. Laverty, "Composition and structure of articular cartilage: a template for tissue repair," *Clinical Orthopaedics and Related Research*, no. 391, pp. S26–S33, 2001.

[33] C. Grandi, S. Baiguera, F. Martorina et al., "Decellularized bovine reinforced vessels for small-diameter tissue-engineered vascular grafts," *International Journal of Molecular Medicine*, vol. 28, no. 3, pp. 315–325, 2011.

[34] J. Klangjorhor, P. Nimkingratana, J. Settakorn et al., "Hyaluronan production and chondrogenic properties of primary human chondrocyte on gelatin based hematostatic spongostan scaffold," *Journal of Orthopaedic Surgery and Research*, vol. 7, article 40, 2012.

[35] Y. Ono, T. Sakai, H. Hiraiwa et al., "Chondrogenic capacity and alterations in hyaluronan synthesis of cultured human osteoarthritic chondrocytes," *Biochemical and Biophysical Research Communications*, vol. 435, no. 4, pp. 733–739, 2013.

[36] N. Takahashi, C. B. Knudson, S. Thankamony et al., "Induction of CD44 cleavage in articular chondrocytes," *Arthritis and Rheumatism*, vol. 62, no. 5, pp. 1338–1348, 2010.

[37] F. Zaucke, R. Dinser, P. Maurer, and M. Paulsson, "Cartilage oligomeric matrix protein (COMP) and collagen IX are sensitive markers for the differentiation state of articular primary chondrocytes," *Biochemical Journal*, vol. 358, no. 1, pp. 17–24, 2001.

[38] M. F. Pittenger, A. M. Mackay, S. C. Beck et al., "Multilineage potential of adult human mesenchymal stem cells," *Science*, vol. 284, no. 5411, pp. 143–147, 1999.

[39] S. P. Grogan, A. Barbero, J. Diaz-Romero et al., "Identification of markers to characterize and sort human articular chondrocytes with enhanced in vitro chondrogenic capacity," *Arthritis and Rheumatism*, vol. 56, no. 2, pp. 586–595, 2007.

[40] J. Diaz-Romero, J. P. Gaillard, S. P. Grogan, D. Nesic, T. Trub, and P. Mainil-Varlet, "Immunophenotypic analysis of human articular chondrocytes: Changes in surface markers associated with cell expansion in monolayer culture," *Journal of Cellular Physiology*, vol. 202, no. 3, pp. 731–742, 2005.

[41] A. M. DeLise, L. Fischer, and R. S. Tuan, "Cellular interactions and signaling in cartilage development," *Osteoarthritis and Cartilage*, vol. 8, no. 5, pp. 309–334, 2000.

Hindawi Publishing Corporation
BioMed Research International
Volume 2014, Article ID 762705, 9 pages
http://dx.doi.org/10.1155/2014/762705

*Review Article*

# Biological Effects of *Spirulina* (*Arthrospira*) Biopolymers and Biomass in the Development of Nanostructured Scaffolds

**Michele Greque de Morais,[1] Bruna da Silva Vaz,[1] Etiele Greque de Morais,[2] and Jorge Alberto Vieira Costa[2]**

[1] *Laboratory of Microbiology and Biochemical, College of Chemistry and Food Engineering, Federal University of Rio Grande, P.O. Box 474, Avenida Itália, Km 8, 96203-900 Rio Grande, RS, Brazil*
[2] *Laboratory of Biochemical Engineering, College of Chemistry and Food Engineering, Federal University of Rio Grande, P.O. Box 474, 96203-900 Rio Grande, RS, Brazil*

Correspondence should be addressed to Michele Greque de Morais; migreque@yahoo.com.br

Received 2 April 2014; Revised 14 June 2014; Accepted 10 July 2014; Published 23 July 2014

Academic Editor: Costantino Del Gaudio



*Spirulina* is produced from pure cultures of the photosynthetic prokaryotic cyanobacteria *Arthrospira*. For many years research centers throughout the world have studied its application in various scientific fields, especially in foods and medicine. The biomass produced from *Spirulina* cultivation contains a variety of biocompounds, including biopeptides, biopolymers, carbohydrates, essential fatty acids, minerals, oligoelements, and sterols. Some of these compounds are bioactive and have anti-inflammatory, antibacterial, antioxidant, and antifungal properties. These compounds can be used in tissue engineering, the interdisciplinary field that combines techniques from cell science, engineering, and materials science and which has grown in importance over the past few decades. *Spirulina* biomass can be used to produce polyhydroxyalkanoates (PHAs), biopolymers that can substitute synthetic polymers in the construction of engineered extracellular matrices (scaffolds) for use in tissue cultures or bioactive molecule construction. This review describes the development of nanostructured scaffolds based on biopolymers extracted from microalgae and biomass from *Spirulina* production. These scaffolds have the potential to encourage cell growth while reducing the risk of organ or tissue rejection.

## 1. Introduction

Tissue engineering, the interdisciplinary field that combines techniques from cell science, engineering, and materials science, has the potential to reconstitute damaged tissues and organs using cells that are supported on scaffolds where the components of the extracellular matrix can segregate during tissue and organ formation. It is important to choose a scaffold material that stimulates cells to produce structures [1]; therefore, much research has been carried out on natural organic materials. The natural compounds that are incorporated into the scaffolds can act as a substratum for cellular growth by stimulating cell growth and anchoring with lower risk of tissue rejection when compared with synthetic sources.

*Spirulina* is a prokaryotic microalga, order Cyanophyceae, division Cyanophyta (Cyanobacteria). It has a distinctive arrangement of multicellular cylindrical trichomes in an open helix throughout its length. The helical shape of the trichomes is characteristic of the genus, but the length and size of the helix vary with species [2]. In 1981, the Food and Drug Administration (FDA) declared "*Spirulina* is source of protein and contains several vitamins and minerals. It can be legally marketed as a food or a food supplement if it is precisely defined and free from contaminants and adulterants" and is categorized by the FDA as "Generally Recognized as Safe" (GRAS) [3].

*Spirulina* biomass stimulates important biological processes and exhibits antiallergenic, antibacterial, antifungal, anti-inflammatory, antioxidant, and immunomodulating

properties [4]. Thus, *Spirulina* LEB 18 biomass incorporated into scaffolds stimulates cell growth and tissue regeneration [5–7].

Nanofiber scaffolds have the potential to be used in tissue engineering because they can reproduce the structure and function of the native extracellular matrix [8]. Electrospun scaffolds have attracted attention because of their characteristics: they have a high surface area in relation to fiber diameter, a high porosity that stimulates cell growth and connections between cells, and good nutrient diffusion and they encourage angiogenesis/vascularization during tissue regeneration [9].

The synthetic polymers normally used to produce nanofiber scaffolds can be replaced by *Spirulina* biopolymers, which are biodegradable and biocompatible with cells and tissues [5]. *Spirulina* biomass can be added to the polymer solutions used in nanofiber production to produce scaffolds that incorporate *Spirulina's* properties; this is possible because electrospinning does not involve extreme temperatures or pH that would reduce the biological activity of the biomass or its nutrients. Depending on the solvent used to prepare the polymer, the internal components (proteins, fatty acids, and biopolymers) of the biomass can be made available within the scaffolds to stimulate cells or tissues [4].

Polyhydroxyalkanoates (PHAs), a family of biopolymers that includes polyhydroxybutyrate (PHB), can be extracted from various microorganisms, including *Spirulina*, and used to provide atoxic biocompatible scaffolding for human tissue and organ culture. Low molecular weight PHB has been detected bound to human serum albumin and low-density lipoproteins. It degrades into (R)-$\beta$-hydroxybutyric acid, a naturally occurring mammalian metabolite present at serum concentrations of 3 mg $dL^{-1}$ to 10 mg $dL^{-1}$ in adult humans and presents no health risks. The fact that PHB degrades into such atoxic compounds may explain its biocompatibility with cultured cells and tissues. Not only do *Spirulina* biopolymer nanofiber scaffolds have a lower risk of rejection in human tissue culture but they also contain advantageous bioactive compounds that are present in the *Spirulina* biomass [10, 11].

This review describes the progress made in tissue engineering when *Spirulina* biomass and biopolymers are used in the production of nanostructured scaffolds that promote cell growth while decreasing the risk of tissue and organ rejection.

## 2. Tissue Engineering

Since its beginnings, this field has focused on the development of biological substitutes for the recuperation, regeneration, or substitution of defective tissues [12]. Permanent implants often result in chronic inflammation, which can lead to severe clinical complications. Implants developed using biomaterials could be a viable alternative to reestablish the normal functions of damaged tissues and organs [13].

The process of using tissue engineering to restore or substitute tissues or organs damaged by accidents, congenital defects, or diseases involves the *in vitro* propagation of viable cells attached to biological or synthetic supports, known as scaffolds [6]. After cellular cultivation, the scaffold is implanted into the patient and degrades when the new organ or tissue is formed [13–15].

*2.1. Scaffolds.* Scaffolds are three-dimensional structures that guide tissue development *in situ* at the site of interest depending only on the growth of the surrounding tissue [16]. The scaffold should be selected according to the type of repair and the tissues or organs to be reconstituted, and the scaffold surface is selected according to the desired interactions between the cells and the scaffold [13, 17].

For effective tissue reconstruction, scaffolds must conform to specific requirements. High porosity and pore interconnectivity are fundamental characteristics for increasing the available specific surface area, which is important not only for cell anchorage and the internal growth of tissues but also for facilitating the distribution and transportation of oxygen, nutrients, and cellular residues [18].

The degradability is a parameter closely related to the solubility of the molds. If the solubility is too high, the scaffolds will be reabsorbed by the body fluids too quickly without accompanying tissue regeneration. However, if the solubility is too low, it will remain for too long in the body and impede regeneration. Therefore, the degradability is associated with the stability of the biomaterial *in vivo* and an appropriate time is extremely important for proper regeneration [6].

The nature of the scaffold's surface can also affect cellular responses that influence the speed of formation and quality of new tissue [17]. The most appropriate scaffold material should be biocompatible and biodegradable, so that it is nonimmunogenic to avoid further surgical intervention when tissue regeneration is complete [19]. Scaffolds are designed to have a cell structure that is similar to the natural ECM and therefore have characteristics that are suitable for cell culture.

## 3. Extracellular Matrix

The extracellular matrix (ECM) is a component of the connective tissue. It is produced by cells and supports the morphological organization and physiological functions that occur during tissue formation [20, 21]. ECM produces the biochemical and biomechanical signals necessary for tissue morphogenesis, differentiation, and homeostasis [22].

Due to their versatile properties, decellularized extracellular matrices have been widely used as a source of biological scaffolds in tissue engineering and regenerative medicine [23–29]. The most important limitations in regenerative medicine are the shortage of autologous tissue and organ donors and the negative immunological responses and pathogen transfer whenever allogeneic or xenogeneic tissues or organs are used [30, 31]. Another advantage of scaffolds obtained from decellularized tissues and organs is the retention of the structure of the original tissue and organs.

Scaffolds made using the electrospinning process mimic the natural extracellular matrix's mechanical and architectural characteristics, enabling the anchoring and migration of cells. Growth factors, drugs, viruses, and proteins can be incorporated in the matrix. The microalga *Spirulina* is a good choice for incorporation in the production of scaffolds [6].

It is important to choose a scaffold material that stimulates cells to produce structures of the correct format and size. Such scaffolds are generally developed from synthetic polymers, which can be incompatible with human cells [1]. Therefore, much research has been carried out on natural organic materials.

*3.1. Extracellular Matrices Made of Natural or Synthetic Polymers.* Polymers are the raw materials for scaffold production in tissue engineering, and several types of biodegradable polymers are utilized in the development of artificial skin, surgical sutures, vascular grafts, bone joining devices, and controlled-release pharmaceuticals [32].

These materials can be classified as natural polymers (including polysaccharides such as alginate, chitin and chitosan, and starch and hyaluronic acid derivatives); proteins (such as collagen, fibrin gel, and soy and silk proteins); synthetic polymers (such as poly(lactic acid) (PLA), poly(glycolic acid) (PGA), and polycaprolactone (PCL)) [1, 33]; and microbial polymers (biopolymers) (such as polyhydroxyalkanoates (PHAs)).

Synthetic polymers are available in potentially unlimited amounts. Their physicochemical properties can be controlled, with their degradation rates and mechanical properties subject to chemical modification [34]. However, many synthetic scaffolds have hydrophobic surfaces that hinder cell recognition by native cells. Natural and microbial polymers are biologically recognized, which makes it easier to reproduce the properties of the tissues to be regenerated, such as their mechanical and cellular anchoring properties [18].

## 4. Nanotechnology and Scaffold Development

Cells interact with their environment via thousands of nanometric interactions. In tissues and organs, cells are located in three-dimensional microenvironments surrounded by other cells and the extracellular matrix. The ECM contains collagen and elastin, which are organized in nanostructures with specific bioactive functions that regulate cellular homeostasis. An essential stage of scaffold development is the creation of synthetic microenvironments that facilitate the formation of a three-dimensional structure to control cell behavior and promote specific cell interactions [35].

Nanotechnology has been used in several biomedical applications, including pharmaceutical transport, biological detection, disease diagnosis, clinical images resolution, and scaffold development [36]. Nanometric tissue engineering can produce biomaterials that regulate the interactions between cells and their microenvironments by the emission of molecular signals [37, 38]. The biometric and physicochemical properties of nanomaterials enable them to stimulate cell growth and regenerate injured tissue [39].

Developing nanofiber scaffolds using the electrospinning process enables the reproduction of the principal extracellular architecture and makes it easy for the cells to unite to tissue because such scaffolds have similar mechanical properties to natural structures [5]. Several authors have studied the application of nanofiber scaffolds in various processes, including the rebuilding of nerves [40] and brain tissue [41], the transport of pharmaceuticals through oral mucosa [42], and the cultivation of stem cells [6].

*4.1. Production of Nanostructured Scaffolds via Electrospinning.* The greatest challenge in the area of tissue engineering is the development of scaffolds that reproduce nanometric tissue architecture. The electrospinning process is the most widely adopted technique for the formation of polymer nanofibers [39], due to the repeatability of this method and the simplicity of scaling it up.

Nanostructured scaffolds obtained via electrospinning have been attracting attention due to their high porosity. They contain interlinked voids that can increase both cellular development and the connections between cells as well as nutrient diffusion, angiogenesis, and vascularization during tissue regeneration [9]. Electrospinning produces nanofibers with a diameter of between 3 nm and 1000 nm and it can be used to process several types of polymers [15, 43].

Electrospinning is carried out by applying a high voltage to a polymer solution in a process that results in nanofiber formation and lengthening due to electrostatic repulsion. The polymer solution is fed at a constant flow rate through a capillary charged with a high voltage (10 kV to 30 kV). When the electric field attains enough energy to overcome surface tension at the tip of the capillary, a "Taylor Cone" forms and the nanofibers are deposited in a stationary or rotating collector where the solvent evaporates and the nanofibers collect [44, 45].

Many parameters influence this process, including the properties of the polymers, the solvent, and the environment. Some of these parameters are viscosity, elasticity, conductivity, solution flow rate, surface tension, capillary diameter, distance between the capillary tip and the collector, polymer concentration, temperature, humidity, and air flow rate [33]. In addition, the manner in which the nanofibers are collected can influence their orientation, with the fibers being deposited either randomly or in alignment [8]. Electrospinning can be accomplished under laboratory conditions to produce a sterile product and can easily be scaled up [46]. Another advantage is the possibility of incorporating growth factors, drugs, viruses, proteins, and other properties into the nanofibers. Thus, *Spirulina* is a good candidate for incorporation into scaffolds [6].

## 5. The *Spirulina* (*Arthrospira*) Microalga

Phytoplankton are aquatic photosynthetic photoautotrophs characterized by the presence of various colored pigments [47]. Photosynthetic phytoplankton include the eukaryotic algae and the prokaryotic cyanobacteria. Biotechnological processes based on phytoplankton have come to the fore due to their potential to produce a wide range of byproducts, including carbohydrates, lipids, minerals, pigments, proteins, and vitamins [48], many of which are natural products, have a high nutritional value, and are commercially important [47].

(a) (b)

Figure 1: *Spirulina* LEB 18 (a) and culture at the Laboratory of Biochemical Engineering (b).

*Spirulina* is the common name for the product produced from pure cultures of the photosynthetic prokaryotic cyanobacteria *Arthrospira*, the natural habitat of which is alkaline lakes. *Spirulina* was originally given this name due to the spiral nature of its filaments (Figure 1(a)) and was thought to be eukaryotic algae. However, it was later found to be a prokaryotic cyanobacterium belonging to the genus *Arthrospira*. In South America, it has been cultivated as a food supplement since the time of the Aztecs, about 400 years ago [49].

Medical and nutritional studies about *Spirulina* have proliferated since the 1970s, because it is a good source of high quality protein (the concentration of which can reach 70% of the biomass), vitamins (B12 and provitamin A), minerals (especially iron), phenolics, and essential fatty acids [50]. For many years, *Spirulina* has been investigated for application in several fields, especially for use in foods and medicine. It is thus frequently used as a nutritional supplement and is generally regarded as safe when cultivated under conditions of appropriate hygiene. Toxicological studies have demonstrated that *Spirulina* is safe for human consumption.

*Spirulina* has been produced on a large scale in several countries for application as a food supplement and a pharmaceutical product [5]. In Germany (BlueBiotech International GmbH) and the United States (Cyanotech, Eathrise Nutritionals, and Phycobiologics) *Spirulina* is cultivated on a commercial scale for use as dietary supplement [2]. Clinical studies have demonstrated that *Spirulina* biomass has therapeutic properties and that it may be used to treat allergies [51], cancer [52], and HIV [53] and for the reduction of LDL cholesterol [54, 55]. It has also been reported to stimulate the immune system and intestinal lactobacilli, reduce hyperlipidemia and obesity, and counteract the effects of radiation, drugs, and heavy metals [48, 56]. Noninsulin dependent diabetics have shown a reduction in hypoglycemia when *Spirulina* was added to their diet [55].

Since 1996, the Laboratory of Biochemical Engineering (LEB) of the Federal University of Rio Grande (FURG), Brazil, has been running a research program on the cultivation of microalgae and other phytoplankton (Figure 1(b)).

*5.1. Spirulina LEB 18 Biopolymers Used in Nanostructured Scaffolds.* The first step in tissue reconstruction consists of the selection of the support material for the cells. During this phase, consideration must be made regarding the type of lesion being repaired along with its location in the body and the extension of the lesion. Permanent implants can cause inflammation, which, although a normal response to a foreign body, can result in more severe clinical complications such as tissue contraction [13].

Collagen-based scaffolds are currently substituted by supports produced from biodegradable polymers [57]. Biodegradable microbial polymers have potential application in the formation of nanostructured scaffolds. Such polymers include the polyhydroxyalkanoates (PHAs), a group of about 150 polymers that has been attracting medical interest. This group includes polyhydroxybutyrate (PHB), poly(3-hydroxybutyrate) (P3HB) and its copolymers, poly(4-hydroxybutyrate) (P4HB), 3-hydroxyvalerate (PHBV), and 3-hydroxyhexanoate (PHBHHx) [58]. The most studied polymer of the group is PHB, which is biodegradable, thermoplastic, and easily processed, making it a good candidate for the development of biodegradable scaffolds [59].

Human biocompatibility is one of the advantages of biopolymers compared with synthetic biodegradable polymers, and they can be used to produce scaffolds that facilitate the anchoring of implanted cells to the tissue that is being regenerated [60]. The United States Food and Drug Administration (FDA) has approved PHB for food packaging. Furthermore, because PHB is biocompatible with cells and tissues and is easily absorbed by the human body it can be used in the medical-pharmaceutical field for sutures, bone prostheses, cardiovascular grafts, orthopedic pins, and implants, as well as in tissue regeneration and repair [61]. Formulations of PHB biopolymer can be used as a matrix for the development of controlled-release medications such as hormones and other pharmaceuticals. The sodium salt of PHB can also be used as an anesthetic [62]. Neural stem cells have been produced in PHB scaffolds and have the potential to repair central nervous system lesions. PHB can also be used to regenerate bones, cartilage [58], and nervous and cardiovascular tissues [63].

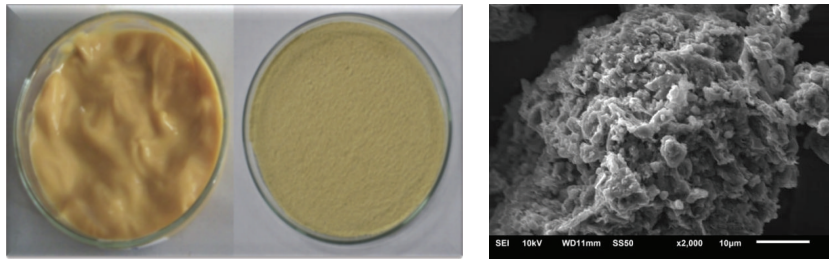


(a) (b)

Figure 2: Polyhydroxybutyrate biopolymer produced from the biomass of *Spirulina* strain LEB 18. Biopolymer before and after drying (a) and scanning electron microscopy of the surface of PHB with 2,000x magnification (b).

PHAs are biodegradable and therefore they do not produce any toxic substances during their metabolism. In the environment, bacteria and fungi secrete an extracellular depolymerase that readily degrades polymeric PHAs into their monomers. In mammalian tissues, degradation products are absorbed through the cellular wall and metabolized [64]. The degradation rate of PHAs depends on many factors. Some factors, such as temperature, humidity, pH, and nutrient supply, are related to the environment, while other factors, such as additives composition, crystallinity, and surface area, are intrinsic to the biopolymer [65].

During PHB synthesis, two acetyl-CoA molecules are joined in a condensation reaction catalyzed by the enzyme 3-($\beta$-ketothiolase) to form acetoacetyl-CoA. This enzyme competes for acetyl-CoA with several other metabolic pathways, such as acetate and citrate formation and fatty acid synthesis [66].

The product is reduced to 3-hydroxybutyryl-CoA in a reaction catalyzed by acetoacetyl NADPH-dependent reductase. High concentrations of NADPH and NADH inhibit the enzyme citrate synthase, which is responsible for feeding acetyl-CoA into the tricarboxylic (TCA) cycle, making acetyl-CoA available to 3-$\beta$-ketothiolase and enabling PHB to be synthesized by the polymerisation of 3-hydroxybutyryl-CoA units of by PHA synthase. The biosynthesis of PHB-HV proceeds with precursors such as acetic, itaconic, propionic, oleic, or valeric acid. Propionic acid is the valerate precursor that is most commonly employed in PHB-HV biosynthesis [66].

Polyhydroxybutyrate can be produced by prokaryotic microorganisms such as *Spirulina*, where it functions as carbon and energy reserve [67].

Since 2007, our team has studied PHB from microalgae. These studies investigated different genera and species of microalgae that produce this biopolymer, as well as physicochemical characterization (scanning electron microscopy, gas chromatography, thermal analysis, differential scanning calorimetry, color, and opacity), optimization of the extraction/purification process, and applications of the biopolymer in the development of biofilms, nanofibers, and nanocapsules (Figure 2).

*5.2. Physicochemical and Biological Properties and Stem Cell Cultivation of the Scaffolds Made with the Incorporation of Spirulina (Arthrospira) Biomass or Biopolymers Obtained from the Microalgal Biomass.* Since 2007, our team has studied the development of nanofibers produced from PLA, polyethylene oxide (PEO), and PHB extracted from LEB 18 and the incorporation of LEB 18 biomass or some of its metabolites (such as C-phycocyanin).

The formation of nanofibers via electrospinning is dependent upon the properties of the solution used and the electrical set-up. Morais et al. [5] observed that the addition of *Spirulina* LEB 18 biomass to nanofibers results in a strong increase in conductivity. Nanofibers with *Spirulina* LEB 18 biomass free of beads were produced with diameters of 107 nm (Figure 3(a)) [5].

The elasticity, tensile strength, and breaking elongation of *Spirulina* LEB 18 PHB nanofibers were higher than those of commercial PHB samples. The general finding is that nanofibers composed of *Spirulina* LEB 18 PHB have surprisingly enhanced mechanical properties when compared with nanofibers composed of commercial PHB. These nanofibers had high porosity, and the cells filled the matrix structure, thus enabling the arrival of nutrients and growth factors and removal of metabolic products (data not published) (Figure 3(b)) [68].

The PHB extracted from *Spirulina* and commercial PHB-HV5 and PHB-HV12 were electrospun with and without the addition of sodium chloride or LEB 18 biomass. Electrospinning of 22% w/w *Spirulina* PHB without the addition of sodium chloride or LEB 18 biomass produced uniform nanofibers with a diameter of about 750 nm, while the addition of sodium chloride reduced the diameter to about 480 nm, and the addition of 5% w/w LEB 18 biomass reduced it to about 310 nm. It is important to note that if biomass is added to the spinning solution, PHB nanofibers can be spun with PHB concentrations as low as 7% w/w.

This produces nanofibers with markedly reduced fiber diameters, which could be of importance for membranes produced from such nanofibers. One reason for the reduced nanofiber diameter in the presence of LEB 18 biomass may be that the biomass also contained some PHB, although this cannot be the main reason because the amount of biomass

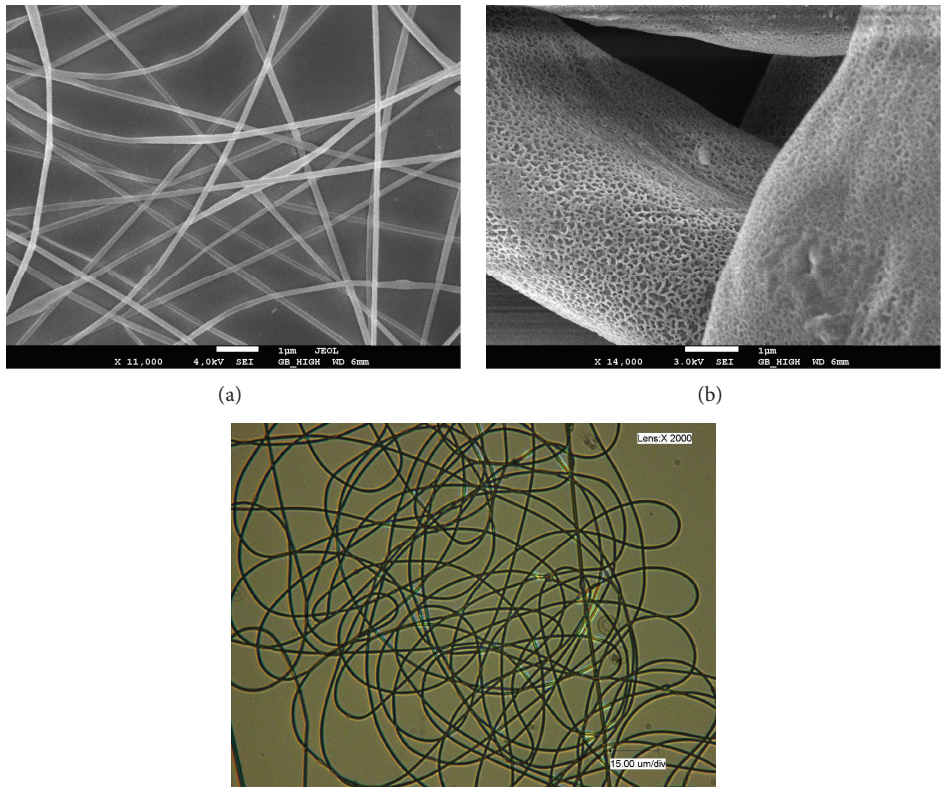


(a) (b)

(c)

Figure 3: Nanofibers produced with 65% polyethylene oxide and 35% *Spirulina* LEB 18 biomass (a), nanofibers incorporating 25% LEB 18 polyhydroxybutyrate and 5% LEB 18 biomass (b), and optical image of PHB nanofibers incorporating *Spirulina* LEB 18 biomass. 2,000x magnification (c).

was small. This phenomenon needs further research. Spinning nanofibers using lower concentrations of PHB would reduce production costs.

In another study carried out by our team, all of the electrospinning conditions used for the development of nanofibers with PHB extracted from *Spirulina* sp. LEB 18 were tested for commercial PHB. The commercial biopolymer did not form fibers under any of the conditions, forming only drops, while the PHB extracted from LEB 18 produced nanofibers with a diameter of 470.1 nm. The conditions that formed the smallest diameters were PHB polymer solution extracted from LEB 18 with a concentration of 20% (w/v), flow rate of 150 $\mu L \cdot h^{-1}$, capillary diameter of 0.45 mm, and voltage of 24.1 kV.

The addition of LEB 18 biomass can provide additional optical functionalization of the nanofibers and affect the transmission of light because it produces a nanofiber with a strong green color (Figure 3(c)).

In recent studies where nanofibers incorporating phycocyanin were developed, resistance to the thermal degradation of this biopigment increased when compared with the phycocyanin alone. This showed that the nanofibers produced via electrospinning may protect the added bioactive compounds (data not published) [69].

Scaffolds of poly-D,L-lactic acid (PDLLA) associated (or not) with *Spirulina* LEB 18 biomass (PDLLA/Sp) were developed with the aim of closely mimicking the natural ECM [6]. This resulted in nanofibers ranging from 163 to 581 nm in the PDLLA matrices and from 91 to 576 nm in the PDLLA/Sp scaffolds [6]. The physicochemical and biological properties of the nanofibers produced with PDLLA/Sp showed that these scaffolds had a high porosity and a large number of interconnected pores. They also had a greater and faster wettability when compared with the PDLLA matrix, and the cells had greater adhesion to PDLLA/Sp scaffolds than to PDLLA alone. The results of the cytotoxic assay showed there was not an increase in cell death. The degradability test showed that the PDLLA/Sp scaffolds had a rapid degradation rate (50% degraded within 60 days). Steffens et al. [6] observed that *Spirulina* LEB 18 biomass was released from the nanofiber while the fiber was being degraded. The authors showed that the PDLLA/Sp was capable of increasing the number of viable cells when compared with scaffolds made of PDLLA alone [6].

In another study, Steffens et al. [70] promoted the cultivation of stem cells with the PDLLA/Sp scaffold produced for testing in an animal model of skin injury. The PDLLA/Sp scaffolds were more moldable and had better adherence to the wound when compared with the PDLLA. The authors

observed that PDLLA/Sp was adequate for use in animals because it supported the suture and the mechanical stress, all of the animals survived, and there were no complications related to the procedure [70].

Scaffolds made from 0–25 $\mu$g/mL of *Spirulina* nanofibers have been used to produce artificial tissue and *Spirulina* enabled the proliferation of mouse fibroblasts. No cytotoxic effects were encountered [71].

Antibacterial and anti-inflammatory effects are critical when scaffolds are used in humans. This is especially true in patients with serious burns where the external protective skin barrier has been completely lost [6]. The application of 0.1% *Spirulina* extract reduces the levels of the bacteria *Escherichia coli* and *Staphylococcus aureus* to insignificant levels within 30 minutes. A methanolic extract of *Arthrospira platensis* had higher antimicrobial activity than dichloromethane, petroleum ether or ethyl acetate extracts, and volatile antibacterial compounds [7].

*Spirulina* stimulates lymphocytes and other cells involved in the immune response. Phycocyanin, a blue pigment associated with the chlorophyll of this organism, exhibits antioxidant and anti-inflammatory properties (due to the inhibition of the release of histamine) [72].

Biomass containing phycocyanin increased the immunity of mice and stimulated haematopoiesis by affecting the glycoprotein hormone erythropoietin and increasing the production of white blood cells. *Spirulina* C-phycocyanin can eliminate free radicals because it is a cyclooxygenase-2 inhibitor that induces apoptosis in the macrophages of mouse via the activation of lipopolysaccharide- (LPS-) induced macrophage [73].

## 6. Conclusion

The development of nanostructured scaffolds using polyhydroxybutyrate biopolymer and the incorporation of *Spirulina* biomass is a significant advance in the field of tissue engineering. This progress is exemplified by the nanofiber architecture, which reproduces the extracellular matrix while reducing tissue and organ rejection during restructuring because of the biocompatible nature of the matrix. This matrix also stimulates cell growth, better nutrient diffusion, and specific cellular interactions due to the properties of LEB 18 biomass. The use of this technology may result in the development of scaffolds that do not require tissue or organ donors.

## Conflict of Interests

The authors declare that there is no conflict of interests regarding the publication of this paper.

## Acknowledgment

The authors would like to thank the National Council of Technological and Scientific Development (CNPq) for their Scholarship.

## References

[1] E. Sachlos and J. T. Czernuszka, "Making tissue engineering scaffolds work. Review: the application of solid freeform fabrication technology to the production of tissue engineering scaffolds," *European Cells & Materials*, vol. 30, no. 5, pp. 29–39, 2003.

[2] J. A. C. Costa and M. G. Morais, "Microalgae for food production," in *Fermentation Process Engineering in the Food Industry*, C. R. Soccol, A. Pandey, and C. Larroche, Eds., p. 486, Taylor & Francis, 2013.

[3] R. Fox, *Spirulina Production & Potencial*, Edisud, Aix-en-Provence, France, 1996.

[4] Z. Khan, P. Bhadouria, and P. S. Bisen, "Nutritional and therapeutic potential of *Spirulina*," *Current Pharmaceutical Biotechnology*, vol. 6, no. 5, pp. 373–379, 2005.

[5] M. G. de Morais, C. Stillings, R. Dersch et al., "Preparation of nanofibers containing the microalga *Spirulina (Arthrospira)*," *Bioresource Technology*, vol. 101, no. 8, pp. 2872–2876, 2010.

[6] D. Steffens, M. Lersch, A. Rosa et al., "A new biomaterial of nanofibers with the microalga spirulina as scaffolds to cultivate with stem cells for use in tissue engineering," *Journal of Biomedical Nanotechnology*, vol. 9, no. 4, pp. 710–718, 2013.

[7] M. A. Qureshi, N. T. Kidd, and R. A. Ali, "Spirulina platensis extract enhances chicken macrophage functions after in vitro exposure," *Journal of Nutritional Immunology*, vol. 3, no. 4, pp. 35–45, 1995.

[8] S. A. Sell, P. S. Wolfe, K. Garg, J. M. McCool, I. A. Rodriguez, and G. L. Bowlin, "The use of natural polymers in tissue engineering: a focus on electrospun extracellular matrix analogues," *Polymers*, vol. 2, no. 4, pp. 522–553, 2010.

[9] J. Ramier, T. Bouderlique, O. Stoilova et al., "Biocomposite scaffolds based on electrospun poly(3-hydroxybutyrate) nanofibers and electrosprayed hydroxyapatite nanoparticles for bone tissue engineering applications," *Materials Science and Engineering: C*, vol. 38, pp. 161–169, 2014.

[10] K. Sudesh, H. Abe, and Y. Doi, "Synthesis, structure and properties of polyhydroxyalkanoates: biological polyesters," *Progress in Polymer Science*, vol. 25, no. 10, pp. 1503–1555, 2000.

[11] M. Jau, S. Yew, P. S. Y. Toh et al., "Biosynthesis and mobilization of poly(3-hydroxybutyrate) [P(3HB)] by *Spirulina platensis*," *International Journal of Biological Macromolecules*, vol. 36, no. 3, pp. 144–151, 2005.

[12] B. P. Chan and K. W. Leong, "Scaffolding in tissue engineering: general approaches and tissue-specific considerations," *European Spine Journal*, vol. 17, no. 4, pp. S467–S479, 2008.

[13] S. H. Barbanti, C. A. C. Zavaglia, and E. A. R. Duek, "Polímeros Bioreabsorvíveis na Engenharia de Tecidos," *Polímeros: Ciência e Tecnologia*, vol. 15, no. 1, pp. 13–21, 2005.

[14] H.-Y. Cheung, K.-T. Lau, T.-P. Lu, and D. Hui, "A critical review on polymer-based bio-engineered materials for scaffold development," *Composites B*, vol. 38, no. 3, pp. 291–300, 2007.

[15] R. Vasita and D. S. Katti, "Nanofibers and their applications in tissue engineering," *International Journal of Nanomedicine*, vol. 1, no. 1, pp. 15–30, 2006.

[16] N. Pallua and C. V. Suscheck, *Tissue Engineering-From Lab to Clinic*, Springer, 2010.

[17] I. O. Smith, X. H. Liu, L. A. Smith, and P. X. Ma, "Nanostructured polymer scaffolds for tissue engineering and regenerative medicine," *Wiley Interdisciplinary Reviews: Nanomedicine and Nanobiotechnology*, vol. 1, no. 2, pp. 226–236, 2009.

[18] I. Armentano, M. Dottori, E. Fortunati, S. Mattioli, and J. M. Kenny, "Biodegradable polymer matrix nanocomposites for tissue engineering: a review," *Polymer Degradation and Stability*, vol. 95, no. 11, pp. 2126–2146, 2010.

[19] J. M. Holzwarth and P. X. Ma, "Biomimetic nanofibrous scaffolds for bone tissue engineering," *Biomaterials*, vol. 32, no. 36, pp. 9622–9629, 2011.

[20] Z. Xiao, J. Blonder, M. Zhou, and T. D. Veenstra, "Proteomic analysis of extracellular matrix and vesicles," *Journal of Proteomics*, vol. 72, no. 1, pp. 34–45, 2009.

[21] C. Frantz, K. M. Stewart, and V. M. Weaver, "The extracellular matrix at a glance," *Journal of Cell Science*, vol. 123, no. 24, pp. 4195–4200, 2010.

[22] H. Järveläinen, A. Sainio, M. Koulu, T. N. Wight, and R. Penttinen, "Extracellular matrix molecules: potential targets in pharmacotherapy," *Pharmacological Reviews*, vol. 61, no. 2, pp. 198–223, 2009.

[23] F. Bolland, S. Korossis, S. Wilshaw et al., "Development and characterisation of a full-thickness acellular porcine bladder matrix for tissue engineering," *Biomaterials*, vol. 28, no. 6, pp. 1061–1070, 2007.

[24] R. Chen, H. Ho, Y. Tsai, and M. Sheu, "Process development of an acellular dermal matrix (ADM) for biomedical applications," *Biomaterials*, vol. 25, no. 13, pp. 2679–2686, 2004.

[25] T. Hoshiba, H. Lu, N. Kawazoe, and G. Chen, "Decellularized matrices for tissue engineering," *Expert Opinion on Biological Therapy*, vol. 10, no. 12, pp. 1717–1728, 2010.

[26] H. C. Ott, T. S. Matthiesen, S. K. Goh et al., "Perfusion-decellularized matrix: using nature's platform to engineer a bioartificial heart," *Nature Medicine*, vol. 14, no. 2, pp. 213–221, 2008.

[27] T. H. Petersen, E. A. Calle, L. Zhao et al., "Tissue-engineered lungs for in vivo implantation," *Science*, vol. 329, no. 5991, pp. 538–541, 2010.

[28] B. E. Uygun, A. Soto-Gutierrez, H. Yagi et al., "Organ reengineering through development of a transplantable recellularized liver graft using decellularized liver matrix," *Nature Medicine*, vol. 16, no. 7, pp. 814–820, 2010.

[29] P. W. Whitlock, T. L. Smith, G. G. Poehling, J. S. Shilt, and M. van Dyke, "A naturally derived, cytocompatible, and architecturally optimized scaffold for tendon and ligament regeneration," *Biomaterials*, vol. 28, no. 29, pp. 4321–4329, 2007.

[30] H. Lu, T. Hoshiba, N. Kawazoe, and G. Chen, "Autologous extracellular matrix scaffolds for tissue engineering," *Biomaterials*, vol. 32, no. 10, pp. 2489–2499, 2011.

[31] H. Lu, T. Hoshiba, N. Kawazoe, I. Koda, M. Song, and G. Chen, "Cultured cell-derived extracellular matrix scaffolds for tissue engineering," *Biomaterials*, vol. 32, no. 36, pp. 9658–9666, 2011.

[32] R. L. Órefice, M. M. Pereira, and H. S. Mansur, *Biomateriais: fundamentos e aplicações*, Cultura Médica, Guanabara Koogan, Rio de Janeiro, Brazil, 1st edition, 2012.

[33] S. Bose, M. Roy, and A. Bandyopadhyay, "Recent advances in bone tissue engineering scaffolds," *Trends in Biotechnology*, vol. 30, no. 10, pp. 546–554, 2012.

[34] J. J. Song and H. C. Ott, "Organ engineering based on decellularized matrix scaffolds," *Trends in Molecular Medicine*, vol. 17, no. 8, pp. 424–432, 2011.

[35] C. Cunha, S. Panseri, and S. Antonini, "Emerging nanotechnology approaches in tissue engineering for peripheral nerve regeneration," *Nanomedicine: Nanotechnology, Biology, and Medicine*, vol. 7, no. 1, pp. 50–59, 2011.

[36] N. Barkalina, C. Charalambous, C. Jones, and K. Coward, "Nanotechnology in reproductive medicine: emerging applications of nanomaterials," *Nanomedicine: Nanotechnology, Biology and Medicine*, vol. 10, no. 5, pp. 921–938, 2014.

[37] I. Wheeldon, A. Farhadi, A. G. Bick, E. Jabbari, and A. Khademhosseini, "Nanoscale tissue engineering: spatial control over cell-materials interactions," *Nanotechnology*, vol. 22, no. 21, Article ID 212001, 2011.

[38] B. D. Fahlman, *Materials Chemistry*, Springer, Dordrecht, The Netherlands, 2007.

[39] M. Zhang and J. Gunn, "Polyblend nanofibers for biomedical applications: perspectives and challenges," *Trends in Biotechnology*, vol. 28, no. 4, pp. 189–197, 2010.

[40] X. Zhan, M. Gao, Y. Jiang et al., "Nanofiber scaffolds facilitate functional regeneration of peripheral nerve injury," *Nanomedicine: Nanotechnology, Biology and Medicine*, vol. 9, pp. 305–315, 2013.

[41] G. K. K. Leung, Y. C. Wang, and W. Wu, "Peptide nanofiber scaffold for brain tissue reconstruction," *Methods in Enzymology*, vol. 508, pp. 177–190, 2012.

[42] D. C. Aduba Jr., J. A. Hammer, Q. Yuan, W. Andrew Yeudall, G. L. Bowlin, and H. Yang, "Semi-interpenetrating network (sIPN) gelatin nanofiber scaffolds for oral mucosal drug delivery," *Acta Biomaterialia*, vol. 9, no. 5, pp. 6576–6584, 2013.

[43] S. Ramakristna, W. Teo, T. Lim, and Z. Ma, *An Introduction to Electrospinning and Nanofibers*, World Scientific, River Edge, NJ, USA, 2005.

[44] T. J. Sill and H. A. von Recum, "Electrospinning: applications in drug delivery and tissue engineering," *Biomaterials*, vol. 29, no. 13, pp. 1989–2006, 2008.

[45] B. M. Baker, R. P. Shah, A. M. Silverstein, J. L. Esterhai, J. A. Burdick, and R. L. Mauck, "Sacrificial nanofibrous composites provide instruction without impediment and enable functional tissue formation," *Proceedings of the National Academy of Sciences of the United States of America*, vol. 109, no. 35, pp. 14176–14181, 2012.

[46] C. P. Barnes, S. A. Sell, E. D. Boland, D. G. Simpson, and G. L. Bowlin, "Nanofiber technology: designing the next generation of tissue engineering scaffolds," *Advanced Drug Delivery Reviews*, vol. 59, no. 14, pp. 1413–1433, 2007.

[47] R. B. Derner, S. Ohse, M. Villela, S. M. de Carvalho, and R. Fett, "Microalgae, products and applications," *Ciencia Rural*, vol. 36, no. 6, pp. 1959–1967, 2006.

[48] J. A. Vieira Costa, L. M. Colla, and P. F. Duarte Filho, "Improving Spirulina platensis biomass yield using a fed-batch process," *Bioresource Technology*, vol. 92, no. 3, pp. 237–241, 2004.

[49] A. Vonshak, *Spirulina platensis (Athrospira) Physiology, Cell-Biology and Biotechnoloby*, Taylor & Francis, New York, NY, USA, 1997.

[50] J. A. V. Costa, M. G. Morais, and M. R. Andrade, "Microalgal engineering: the metabolic products and the bioprocess," in *Microalgae Biotechnology, Microbiology and Energy—Marine Biology*, M. N. Johansen, Ed., chapter 4, p. 475, Nova Science, 2012.

[51] T. K. Mao, J. van de Water, and M. E. Gershwin, "Effects of a Spirulina-based dietary supplement on cytokine production from allergic rhinitis patients," *Journal of Medicinal Food*, vol. 8, no. 1, pp. 27–30, 2005.

[52] B. Mathew, R. Sankaranarayanan, P. P. Nair et al., "Evaluation of chemoprevention of oral cancer with *Spirulina fusiformis*," *Nutrition and Cancer*, vol. 24, no. 2, pp. 197–202, 1995.

[53] T. Hirahashi, M. Matsumoto, K. Hazeki, Y. Saeki, M. Ui, and T. Seya, "Activation of the human innate immune system by *Spirulina*: augmentation of interferon production and NK cytotoxicity by oral administration of hot water extract of *Spirulina platensis*," *International Immunopharmacology*, vol. 2, no. 4, pp. 423–434, 2002.

[54] N. Nakaya, Y. Homa, and Y. Goto, "Cholesterol lowering effect of *Spirulina*," *Atherosclerosis*, vol. 37, no. 6, pp. 1329–1337, 1988.

[55] U. V. Mani, S. Desai, and U. Iyer, "Studies on the long-term effect of spirulina supplementation on serum lipid profile and glycated proteins in NIDDM patients," *Journal of Nutraceuticals, Functional and Medical Foods*, vol. 2, no. 3, pp. 25–32, 2000.

[56] C. Jiménez, B. R. Cossío, and F. X. Niell, "The feasibility of industrial production of *Spirulina* (Arthrospira) in southern Spain," *Aquaculture*, vol. 221, pp. 331–345, 2003.

[57] M. Okamoto and B. John, "Synthetic biopolymer nanocomposites for tissue engineering scaffolds," *Progress in Polymer Science*, vol. 38, pp. 1487–1503, 2013.

[58] D. Puppi, F. Chiellini, A. M. Piras, and E. Chiellini, "Polymeric materials for bone and cartilage repair," *Progress in Polymer Science*, vol. 35, no. 4, pp. 403–440, 2010.

[59] T. Freier, C. Kunze, C. Nischan et al., "In vitro and in vivo degradation studies for development of a biodegradable patch based on poly(3-hydroxybutyrate)," *Biomaterials*, vol. 23, no. 13, pp. 2649–2657, 2002.

[60] J. M. B. T. Cavalheiro, R. S. Raposo, M. C. M. D. de Almeida et al., "Effect of cultivation parameters on the production of poly(3-hydroxybutyrate-co-4-hydroxybutyrate) and poly(3-hydroxybutyrate-4-hydroxybutyrate-3-hydroxyvalerate) by *Cupriavidus necator* using waste glycerol," *Bioresource Technology*, vol. 111, pp. 391–397, 2012.

[61] A. Shrivastav, S. K. Mishra, and S. Mishra, "Polyhydroxyalkanoate (PHA) synthesis by *Spirulina subsalsa* from Gujarat coast of India," *International Journal of Biological Macromolecules*, vol. 46, no. 2, pp. 255–260, 2010.

[62] A. Althuri, J. Mathew, R. Sindhu, R. Banerjee, A. Pandey, and P. Binod, "Microbial synthesis of poly-3-hydroxybutyrate and its application as targeted drug delivery vehicle," *Bioresource Technology*, vol. 145, pp. 290–296, 2013.

[63] G. Adamus, W. Sikorska, H. Janeczek, M. Kwiecień, M. Sobota, and M. Kowalczuk, "Novel block copolymers of atactic PHB with natural PHA for cardiovascular engineering: synthesis and characterization," *European Polymer Journal*, vol. 48, no. 3, pp. 621–631, 2012.

[64] E. Rudnik, "Biodegradability testing of compostable polymer materials," in *Handbook of Biopolymers and Biodegradable Plastics: Properties, Processing and Applications*, pp. 213–263, 2013.

[65] S. K. Sharma and A. A. Mudhoo, *Handbook of Applied Biopolymer Technology: Synthesis, Degradation and Applications*, 2011.

[66] S. Khanna and A. K. Srivastava, "Recent advances in microbial polyhydroxyalkanoates," *Process Biochemistry*, vol. 40, no. 2, pp. 607–619, 2005.

[67] L. Sharma, A. Kumar Singh, B. Panda, and N. Mallick, "Process optimization for poly-$\beta$-hydroxybutyrate production in a nitrogen fixing cyanobacterium, Nostoc muscorum using response surface methodology," *Bioresource Technology*, vol. 98, no. 5, pp. 987–993, 2007.

[68] M. G. Morais, "Bioengenharia microalgal na utilização de gás de combustão e extração de biopolímeros para desenvolvimento de nanofibras," Programa de Pós Graduação em Engenharia e Ciência de Alimentos, Rio Grande, 2009.

[69] F. S. Figueira, *Purificação de C-ficocianina e sua incorporação em nanofibras [Tese de doutorado]*, Programa de Pós Graduação em Engenharia e Ciência de Alimentos, Rio Grande, Brazil, 2014.

[70] D. Steffens, D. Leonardi, P. R. L. Soster et al., "Development of a new nanofiber scaffold for use with stem cells in a third degree burn animal model," *BURNS*, 2014.

[71] S. Jung, D. S. Kim, J. H. Ju, and H. S. Shin, "Assessment of *Spirulina*-PCL nanofiber for the regeneration of dermal fibroblast layers," *In Vitro Cellular and Developmental Biology*, vol. 49, no. 1, pp. 27–33, 2013.

[72] V. B. Bhat and K. M. Madyastha, "Scavenging of peroxynitrite by phycocyanin and phycocyanobilin from *Spirulina platensis*: protection against oxidative damage to DNA," *Biochemical and Biophysical Research Communications*, vol. 285, no. 2, pp. 262–266, 2001.

[73] M. C. Reddy, J. Subhashini, S. V. K. Mahipal et al., "C-Phycocyanin, a selective cyclooxygenase-2 inhibitor, induces apoptosis in lipopolysaccharide-stimulated RAW 264.7 macrophages," *Biochemical and Biophysical Research Communications*, vol. 304, no. 2, pp. 385–392, 2003.

Hindawi Publishing Corporation
BioMed Research International
Volume 2014, Article ID 685426, 9 pages
http://dx.doi.org/10.1155/2014/685426

*Research Article*

# Blood Vessel-Derived Acellular Matrix for Vascular Graft Application

**Luigi Dall'Olmo,[1] Ilenia Zanusso,[2] Rosa Di Liddo,[2] Tatiana Chioato,[2] Thomas Bertalot,[2] Enrica Guidi,[2] and Maria Teresa Conconi[2]**

[1] *Istituto Oncologico Veneto, 35131 Padua, Italy*
[2] *Department of Pharmaceutical and Pharmacological Sciences, University of Padua, Via Marzolo 5, 35131 Padua, Italy*

Correspondence should be addressed to Maria Teresa Conconi; mariateresa.conconi@unipd.it

Received 21 March 2014; Revised 12 June 2014; Accepted 7 July 2014; Published 16 July 2014

Academic Editor: Luca Urbani



To overcome the issues connected to the use of autologous vascular grafts and artificial materials for reconstruction of small diameter (<6 mm) blood vessels, this study aimed to develop acellular matrix- (AM-) based vascular grafts. Rat iliac arteries were decellularized by a detergent-enzymatic treatment, whereas endothelial cells (ECs) were obtained through enzymatic digestion of rat skin followed by immunomagnetic separation of CD31-positive cells. Sixteen female Lewis rats (8 weeks old) received only AM or previously *in vitro* reendothelialized AM as abdominal aorta interposition grafts (about 1 cm). The detergent-enzymatic treatment completely removed the cellular part of vessels and both MHC class I and class II antigens. One month after surgery, the luminal surface of implanted AMs was partially covered by ECs and several platelets adhered in the areas lacking cell coverage. Intimal hyperplasia, already detected after 1 month, increased at 3 months. On the contrary, all grafts composed by AM and ECs were completely covered at 1 month and their structure was similar to that of native vessels at 3 months. Taken together, our findings show that prostheses composed of AM preseeded with ECs could be a promising approach for the replacement of blood vessels.

## 1. Introduction

Cardiovascular diseases (CVDs) represent the leading cause of death in the western countries [1]. Since pharmacological treatment mainly consisting in antiplatelet drugs and cholesterol-lowering agents (statins) has been proven to be often not sufficient [2], the implantation of a vascular graft may be needed. Although autologous vessels, such as the internal mammary artery, radial artery, or the saphenous vein, are considered the golden standard for replacement of malfunctioning or diseased blood vessels, their availability is limited especially in elderly patients [3]. Synthetic materials, such as Dacron and expanded polytetrafluoroethylene (ePTFE), perform reasonably in high-flow, low-resistance conditions and they can be used successfully to substitute large diameter vessels [4]. Nevertheless, they are not as suitable for small diameter (<6 mm) arterial grafts due to their thrombogenicity [5]. Thus, the development of an effective vascular graft, possessing biomechanical properties matching those of native vessel, has become one of the main targets of tissue engineering.

Three approaches have been designed for vascular regeneration: (i) biodegradable synthetic polymer-based constructs, (ii) cell self-assembly blood vessels, and (iii) decellularized tissue grafts.

Several polymers have been used to obtain tissue-engineered blood vessels (TEBVs): poly(dimethylsiloxane), poly(caprolactone), poly(methyl methacrylate), poly-L-lactic acid (PLLA), polyglycolic acid, poly(glycerol sebacate), and polyvinyl alcohol (PVA) [6, 7]. Notably, Shin'oka et al. [8] carried out the first human clinical study enrolling 42 patients who underwent cavopulmonary connection with a TEBV composed of a copolymer of $\varepsilon$-polycaprolactone-polylactic acid reinforced with woven polyglycolic acid previously seeded with autologous bone marrow-derived mononuclear cells. Although some grafts presented stenosis, long-term results at 2 years indicated that TEBV functioned well without any aneurysm or graft rupture.

Another approach for the fabrication of TEBVs is cell self-assembly developed by L'Heureux and colleagues [9] who used entirely autologous cells cultured *in vitro*. Sheets of smooth muscular cells (SMCs) and fibroblasts were grown to overconfluence and then assembled over a mandrel to form a tubular structure that was cultured for 6–8 weeks. During this incubation period, the autologous cells arranged themselves circumferentially producing large amounts of extracellular matrix (ECM). Recently, promising results were obtained after implantation of these TEBVs into 10 patients receiving hemodialysis with failed arteriovenous fistulas [10, 11]. Although self-assembly grafts possess excellent mechanical properties and nonimmunogenic nature, a very long culture period (about 8–10 weeks) is required to obtain an implantable construct.

Finally, decellularized tissues, named also acellular matrices (AMs), can be obtained from various anatomical sites through several procedures involving both physical and chemical agents, such as surfactants and enzymes [12]. These biomaterials possess a preformed structurally organized ECM containing angiogenic growth factors, such as b-FGF and VEGF [13, 14], and lacking immunogenic issues. Small intestinal submucosa (SIS), porcine carotid artery, aorta, and even canine carotid arteries have been evaluated using animal models [15, 16]. Beside the potential risk of viral transmission from animal tissue, the implantation of decellularized xenografts gave disappointing results. Indeed, the treatment of patients with decellularized bovine ureters resulted in high failure rate probably due to the presence of residual immunogenic contaminants, such as galactose-alpha-1,3-galactose (alpha gal) [17]. Thus, the use of homologous AMs seems to be a more suitable approach for vascular replacement.

Overall, the major drawbacks connected to described TEBVs are thrombogenicity, the occurrence of intimal hyperplasia, the progressive atherosclerotic degeneration, and the time required for culturing the cells. Starting from these considerations, the present study developed AM-based vascular grafts composed of AMs derived from iliac arteries and skin microvascular ECs and evaluated their effectiveness as abdominal aorta interposition grafts in Lewis rats.

## 2. Materials and Methods

*2.1. Materials.* Phosphate-buffered saline (PBS) tablets were purchased from Gibco Invitrogen Corp. (Paisley, UK). Rabbit monoclonal anti-MHC I and II and rabbit polyclonal anti-von Willebrand factor primary antibodies were provided by Abcam (Cambridge, UK). Horse pan-specific secondary antibody, DAB Peroxidase Substrate, Fluorescein Avidin DCS, and Vectashield Mounting Medium were from Vector Laboratories (Burlingame, CA, USA). Collagenase B and Dispase II were obtained from Roche Applied Science (Indianapolis, IN, USA). The Endothelial Cell Growth Medium MV2 was purchased from PromoCell GmbH (Heidelberg, Germany). Cell strainer, tissue culture-treated dishes, and fibronectin were from BD Biosciences (San Jose, CA, USA). Mouse monoclonal anti-rat-CD31 antibody was provided by Millipore (Billerica, MA, USA). Dynabeads M-450 were obtained from Life Technologies (Monza, Italia). Movat pentachromic stain kit was from Diapath S.p.A. (Martinengo, Italy). Contramal was purchased by Grünenthal (Aachen, Germany), whereas Terramicina was from Phibro Animal Health Corporation (Teaneck, NJ, USA). All other chemicals and reagents were provided by Sigma-Aldrich (St. Louis, MO, USA).

*2.2. Animals.* All procedures described and animal protocols were approved by the Institutional Animal Care Committee of the University of Padua and by the Italian Health Department. Lewis rats (8 weeks old, 200–300 g body weight) were purchased from Charles-River (Como, Italy). Male animals were sacrificed using $CO_2$ inhalation and iliac arteries as well as dermis were collected and rinsed with PBS. *In vivo* experiments were carried out on female rats.

*2.3. Acellular Matrices.* AMs were prepared by Meezan et al. method [18] with minor modifications. Briefly, iliac arteries were processed with distilled water for 72 h at 4°C, 4% sodium deoxycholate for 4 h, and 2,000 kU deoxyribonuclease I (DNase-I) in 1 M NaCl for 3 h. The treatment was repeated twice till the cells were completely removed. The endothelium was detached incubating the vessels with collagenase IV (0.05% in PBS) at 37°C for 1 min. To verify the lack of cells, AMs were fixed with 10% formalin in PBS, paraffin-embedded, and stained with hematoxylin/eosin (H/E). On the other hand, the absence of cellular membrane residuals was evaluated by immunoistochemistry. Briefly, slices were treated with hydrogen peroxide for 30 min at room temperature (RT) and nonspecific binding sites were blocked with 10% bovine serum albumin (BSA) in PBS for 20 min at RT. Samples were incubated for 60 min with rabbit monoclonal anti-MHC I and II primary antibodies (1 : 500 in 4% BSA in PBS) and then with the horse pan-specific secondary antibody (1 : 8 in 4% BSA in PBS) for 30 min at RT. The reaction was developed with DAB Peroxidase Substrate following the manufacturer's instruction. Finally, nuclei were counterstained with hematoxylin. Negative controls were obtained by omitting the primary antibody. Alternatively, AMs were fixed with 4% glutaraldehyde in 0.1 M cacodylate buffer (pH 7.2) for 24 h and dehydrated with 70% and 90% ethanol (2 h each) and 100% ethanol overnight. After critical point drying and gold sputtering, samples were examined by a scanning electron microscope (SEM; Stereoscan-205 S, Cambridge, UK) using a standard protocol.

*2.4. Cell Cultures.* Dermis, obtained from the abdomen of male rats, was rinsed in PBS, minced, and treated with 0.25% Collagenase B and 0.25% Dispase II for 1 h at 37°C. The digested tissue was filtered through a 100 $\mu$m cell strainer. Cell suspension was centrifuged and resuspended in culture medium MV2. Cells were then seeded on fibronectin-(1 $\mu g/cm^2$) coated dishes and cultured at 37°C with 5% $CO_2$. To obtain pure skin microvascular ECs, cultures grown to 80% confluence were immunoseparated using Dynabeads M-450 previously coated with the mouse monoclonal anti-rat-CD31 antibody following manufacturer's instruction [19]. Briefly, cells were incubated with magnetic beads for 30 min

at 4°C (5 beads/cell). ECs bound to the coated beads were collected with a magnetic particle concentrator and unbounded cells were removed by means of 2 washes with culture medium. Finally, ECs were seeded on fibronectin-coated dishes, cultured with MV2 medium, and used until the 4th passage. The isolated cells were characterized by immunofluorescence performing with rabbit polyclonal anti-von Willebrand factor (1 : 400). Briefly, cells were fixed with 4% formalin for 10 min at 4°C, washed in PBS, and incubated at RT for 1 h with 10% horse serum in PBS and, for 1 h, with the primary antibody. After rinsing with PBS, cells were treated with the horse pan-specific secondary antibody (1 : 8) for 30 min and with Fluorescein Avidin DCS 1 : 500 in HEPES 10 mM and NaCl 0.15 M for 10 min. Samples were mounted with mounting medium with DAPI.

*2.5. Cultures of ECs on AMs.* Under static conditions, ECs ($4 \times 10^5/cm^2$) were seeded onto the luminal surface of AMs, previously incubated with MV2 medium for 3 h at 37°C. Cultures were maintained for 72 h in MV2 medium and then fixed for morphological analysis or *in vivo* implanted.

*2.6. In Vivo Experiments.* Female Lewis rats (8 weeks old) were divided into two groups according to the kind of the implanted graft: group 1 AMs ($n = 7$) and group 2 AMs plus ECs ($n = 9$). Under isoflurane anesthesia (3% isoflurane carried by oxygen, 1 L/min), the abdominal area was shaved and aseptically prepared using povidone-iodine (Betadine). The muscles were exposed with a 3 cm abdominal incision and, after peritoneal incision, animals received analgesic (5 mg/Kg Tramadol, Contramal) intraperitoneally. The abdominal aorta was exposed and isolated and, after clamping the vessel, a segment of aorta was excised and the graft (about 1 cm in length) was anastomosed proximally and distally end-to-end using continuous 10.0 polypropylene sutures. Animals received antibiotic (Terramicina, 60 mg/kg) on the 3rd and 6th days after surgery and Contramal for 3 days postoperatively. No anticoagulants or antiplatelets were administered postoperatively. Animals were sacrificed by $CO_2$ inhalation either 1 (group 1 $n = 4$; group 2 $n = 4$) or 3 months (group 1 $n = 3$; group 2 $n = 5$) after implantation. The implants were recovered and each sample was divided into two pieces: one was fixed with 4% glutaraldehyde in 0.1 M cacodylate buffer for SEM and processed as described above and one was fixed in 10% neutral buffered formalin and paraffin-embedded. Five $\mu$m thick sections were treated with Movat pentachromic stain kit according to the manufacturer's instruction. This stain produces purple-black elastic fibers and nuclei, blue to green mucins, red muscle, and red fibrinoid against a yellow background with collagen.

## 3. Results and Discussion

The ideal biomaterial for the generation of TEBVs should not only possess the mechanical properties of the native vessels but also promote *in vivo* a regenerative response through the induction of host cell ingrowth. In this context, AMs, obtained by a detergent-enzymatic treatment, have been proven to support *in vitro* adhesion, growth, and function of several cell types [20–22]. Furthermore, the decellularization process induces the loss of the major histocompatibility complex markers but maintains angiogenic factors, such as b-FGF and TGF-$\beta$ [13, 23, 24]. Thus, AMs can present angiogenic activity, an important factor for the *in vivo* integration of the tissue substitutes. Indeed, *in vivo* AMs act as a template allowing the host cell ingrowth and they are remodeled in a living tissue [25, 25–27]. Moreover, they represent preformed structures whose length and gauges can be chosen according to the dimension of the segment to be repaired. Another advantage is the possibility to have easy and unlimited availability of inexpensive grafts containing tissue-specific proteins. Herein, two cycles of detergent-enzymatic treatment were needed to completely remove cells from iliac arteries (Figure 1). To detach the endothelial layer (Figure 1(a)), still present at the end of the first cycle, a treatment with collagenase IV was needed between the two decellularization cycles (Figure 1(d)). The structure of the native vessels was well preserved in AMs that lacked both MHC I (Figure 1(e)) and II (Figure 1(f)) cell membrane antigens, normally present in native tissue (Figures 1(b) and 1(c)).

To guarantee an *in vivo* long-term patency of TEBVs, intimal hyperplasia and graft occlusion must be avoided. To achieve this goal, a continuous lining of ECs on the luminal surface of TEBVs seems to be essential since it represents a physical barrier that is able to prevent platelet adhesion and the activation of the coagulation cascade [28]. Furthermore, cell seeding reduces the overall influx of macrophages and the magnitude of M1 activation, avoiding scar formation [29]. These effects, in turn, lead to a functional remodeling of the vessel wall. In particular, elastic fibers play a pivotal role as they determine the mechanical properties of both high and small resistance vessels, thus preventing stenosis [30].

Autologous ECs harvested from blood vessel, such as veins, are terminally differentiated, have limited proliferation potential, and lose their function during *in vitro* expansion [31]. Alternatively, bone marrow-derived mononuclear mesenchymal stromal cells (BM-MSCs) [32] and endothelial progenitor cells (EPCs) [33, 34] have been used to make grafts hemocompatible. Nevertheless, the use of these cells can be limited by their low number in the adult tissues, low proliferative rate, and the invasive procedures needed to obtain them, leading to morbidity for the donors. Furthermore, BM-MSCs may induce calcification and thrombus formation [35]. In this work, microvascular ECs were obtained from skin biopsy; that is, a moderately invasive procedure that avoids the need to remove healthy vessels. ECs presented a polygonal shape (Figure 2(a)) and maintained the endothelial phenotype till the fourth culture passage as demonstrated by the expression of von Willebrand factor (Figure 2(b)). Furthermore, at 72 h from seeding onto AMs, they formed an almost continuous monolayer on the luminal surface of AMs (Figures 2(c) and 2(d)) and maintained their immunoreactivity to anti-CD31 antibody (data not shown). Notably, starting from a $1\,cm^2$ skin fragment, $6 \times 10^6$ ECs were obtained in about 10 days, allowing the production of an implantable graft within

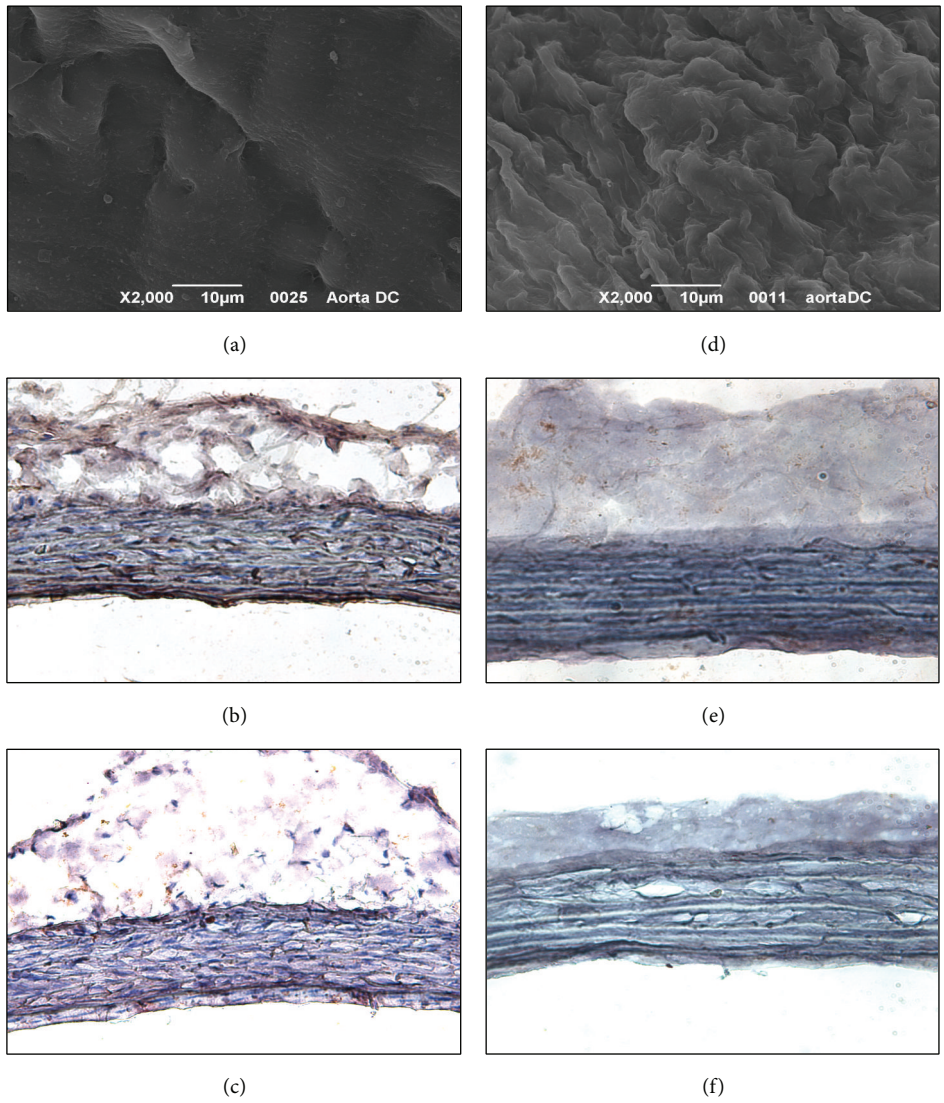


Figure 1: Iliac arteries before (a–c) and after (d–f) the decellularization treatment. (a), (d) SEM micrographs of the luminal sides. Immunoreactivity against MHC I (b, e) and II (c, f) antigens stains brown (magnification ×200).

less than two weeks. This period may represent a clinically relevant time frame. Other vascular regeneration techniques already used in clinical practice take about 4–6 weeks to generate TEBVs [4].

As expected, the implantation of only AMs into the abdominal aorta of female Lewis rats gave unsatisfactory results. Although all animals survived, at both 1 and 3 months (Figures 3(a) and 3(b)), explanted grafts presented higher external diameters than those of host vessels. One month after surgery, only the borders of the patch were reendothelialized (Figure 4(a)), whereas, in the other areas, several platelets adhered to the exposed collagen fibers (Figure 4(b)). Only one animal did not present thrombi inside the implanted AM. At 3 months, the luminal surface was almost completely covered by ECs (Figures 4(c) and 4(d)) and no thrombi were detected. At both time points, although elastic fibers were well organized, neointimal hyperplasia and thickening of the adventitial layer were evident (Figures 5(a) and 5(b)). Furthermore, the adventitia of implanted AM grafts presented a more fibrous structure than that observed in the native aorta (Figure 5(e)). The latter evidence agrees with the findings of Assmann et al. [36], who transplanted homologous decellularized aortic conduits in the infrarenal aorta of rats. Although the grafts remained patent for 8 weeks, hyperplastic tissue formation and implant microcalcification occurred. Neointimal hyperplasia was also detected in decellularized and heparinized grafts implanted in dogs as carotid artery bypass grafts [16].

The *in vitro* coverage of the luminal side of AMs with skin microvascular ECs greatly improved the outcomes of the reconstructive surgery avoiding thrombus formation and allowing good patency. It has been already demonstrated that autologous cells, rather than to mask platelets adhesion sites, may produce soluble factors that are able to enroll the cells

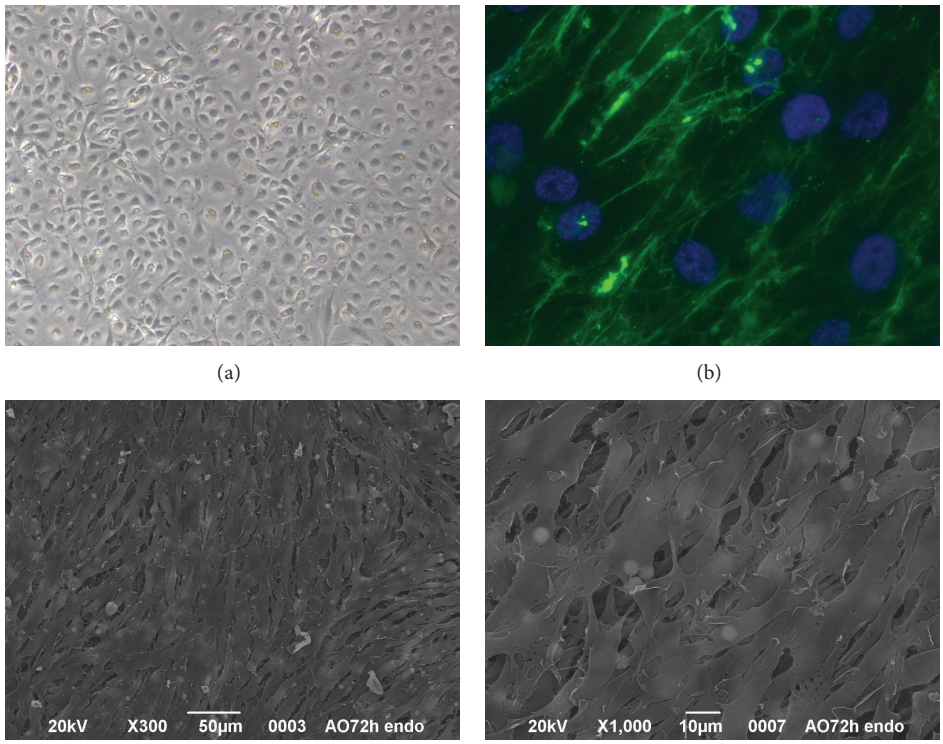


(a) (b)

(c) (d)

Figure 2: Cultures of skin microvascular ECs on tissue culture treated plates (a, b) and AMs (c, d). (a) Phase-contrast microscopy (magnification ×100). (b) Immunofluorescence carried out using anti-von Willebrand factor antibody (magnification ×400). (c), (d) SEM micrographs of ECs/AM cultures at 72 h from seeding.

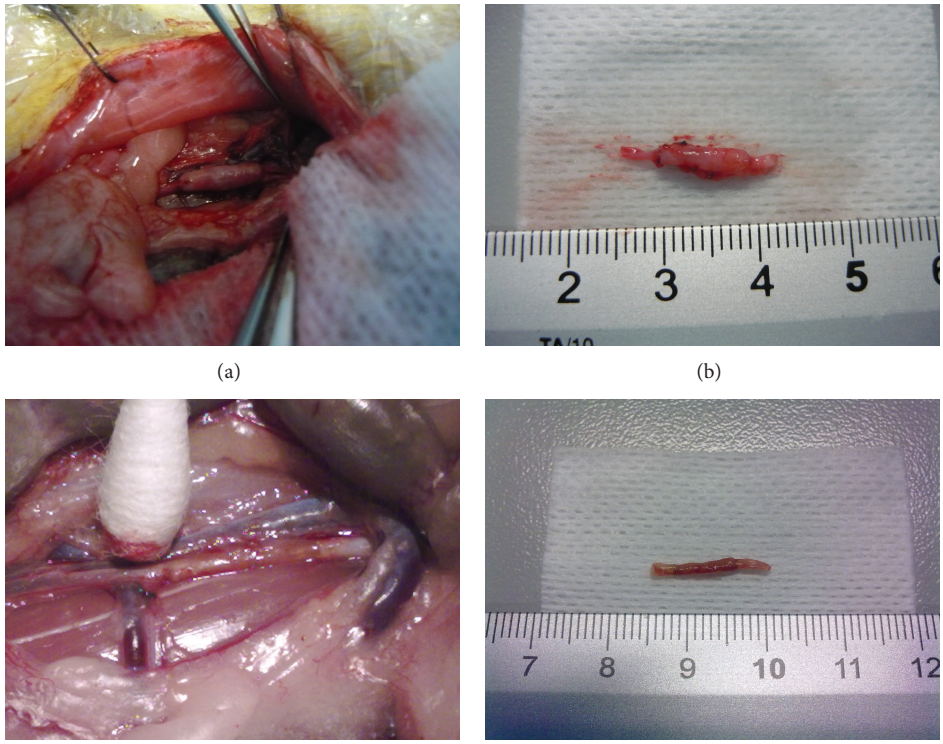


(a) (b)

(c) (d)

Figure 3: Implants composed of AMs (a, b) and ECs and AMs (c, d) 3 months after surgery.

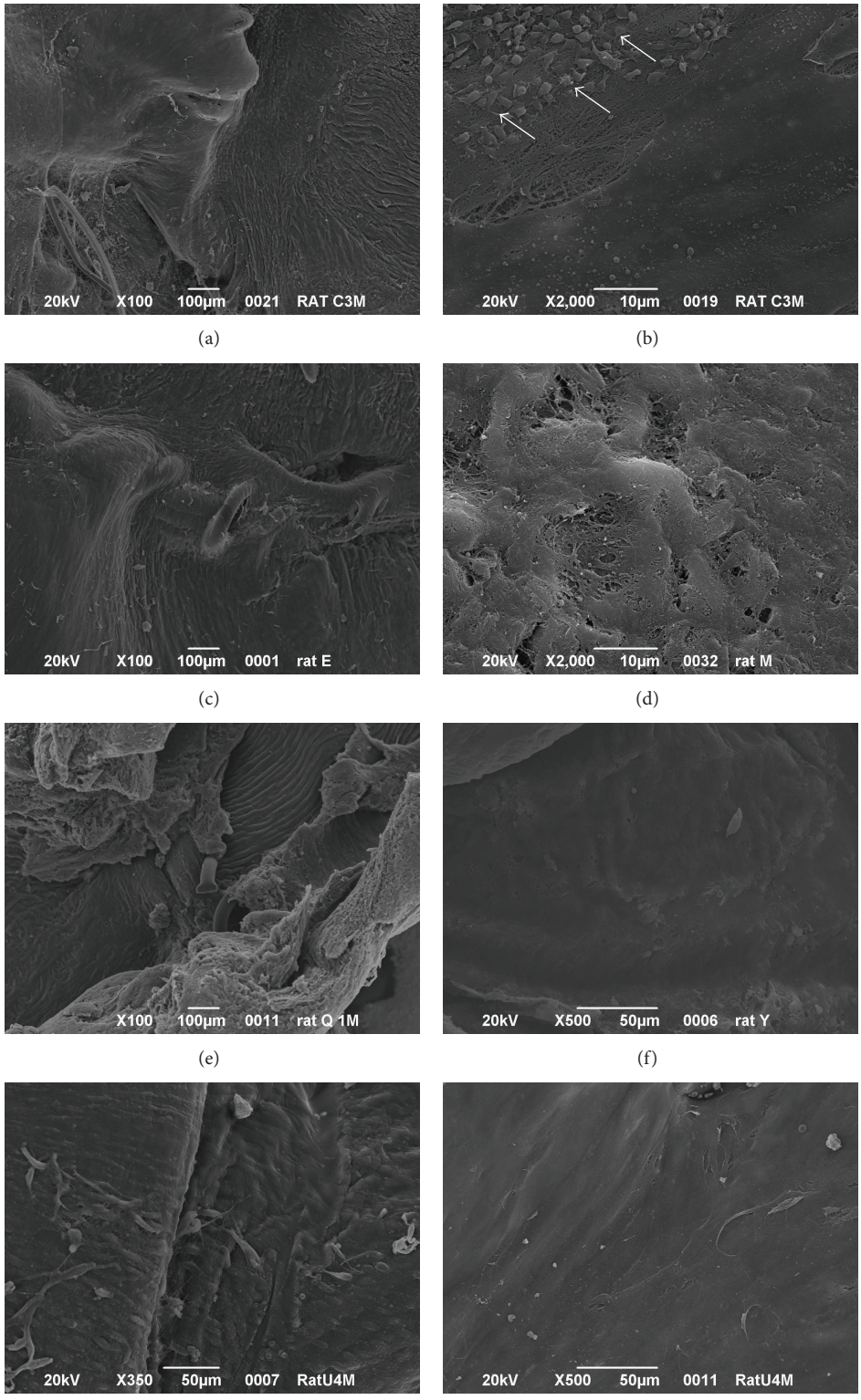


Figure 4: SEM micrographs of the luminal sides of AMs (a–d) and ECs/AM grafts (e–h) at 1 (a, b, e, f) and 3 (c, d, g, h) months after surgery. Arrows indicate area covered by platelets.

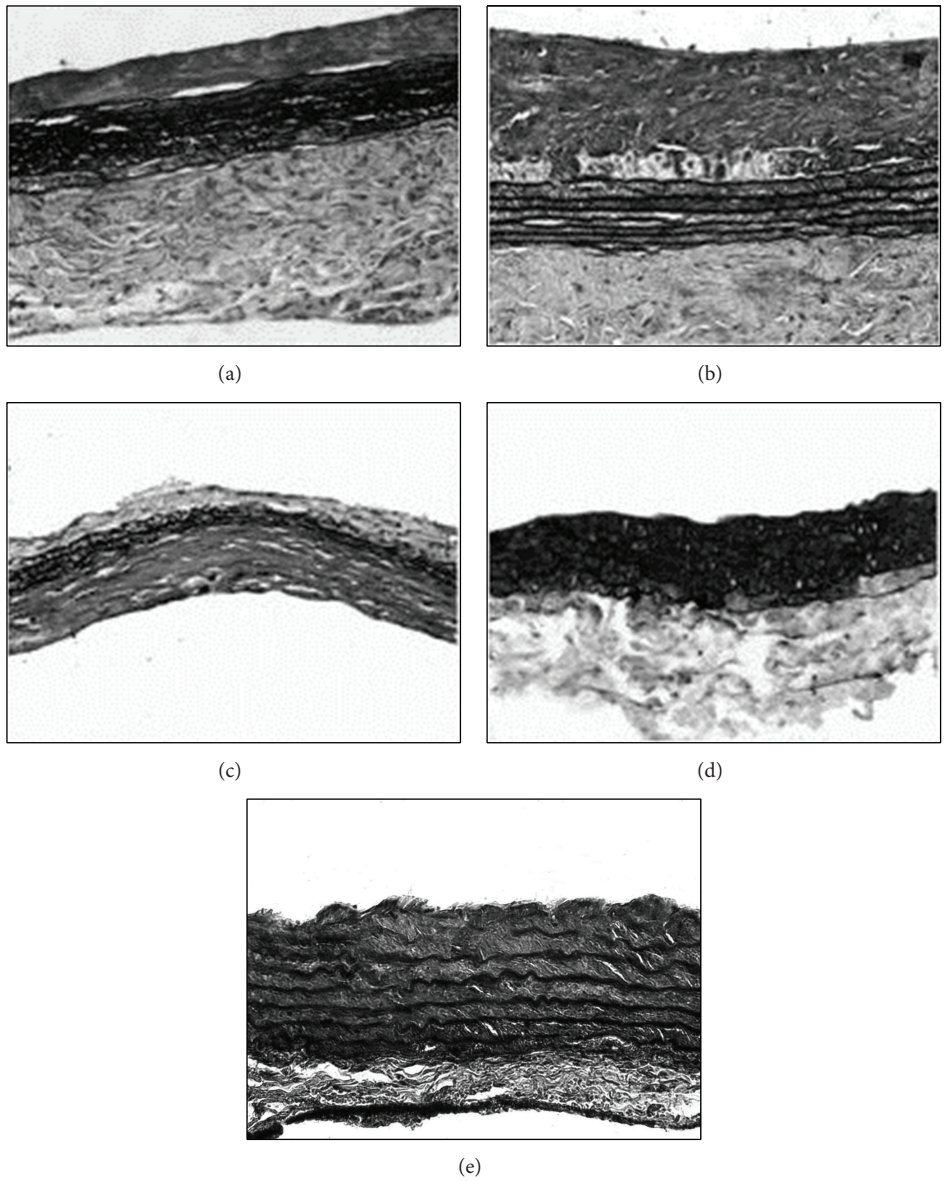


Figure 5: Movat staining of AMs (a, b) and ECs/AM (c, d) grafts after 1 (a–c) and 3 (b–d) months from surgery (magnification ×200). (e) Native aorta.

from the neighbouring host tissues [37]. Furthermore, the seeded cells may lead to the homing of circulating monocytes [29] that, in turn, release the monocyte chemotactic protein-1, stimulating the regeneration of the blood vessel [38]. Although it has not been verified whether the seeded ECs were present on the implanted grafts, we can suppose that the initial endothelial coverage could be transient and progressively replaced by the host cells [39]. At both time points, the external diameter of the explanted grafts was similar to the one of host aorta (Figures 3(c) and 3(d)). One month from surgery, all luminal surfaces were completely reendothelialized and no signs of platelet adhesion were visible (Figures 4(e)–4(h)). The implanted grafts appeared to be remodelled during the time (Figures 5(c) and 5(d)). Indeed, at 1 month, histological analysis revealed a moderate hyperplasia of the tunica intima that disappeared at 3 months. Furthermore, the thickness of the elastic layer increased over the time. Similar results were obtained by Leyh et al. [40] who implanted TEBVs composed of homologous decellularized arteries with or without autologous ECs in the pulmonary circulation of sheep. The *in vitro* reendothelialized conduits performed well for as long as 6 months, whereas the lack of ECs led to aneurysm formation.

## 4. Conclusions

Herein, we show that AM-based TEBVs lead to unsatisfactory results since the lack of ECs contributes to graft thrombogenicity and promotes intimal proliferation. One month after surgery, the luminal surface of implanted AMs was partially

covered by ECs and several platelets adhered in the areas lacking cell coverage. Intimal hyperplasia, already detected after 1 month, increased at 3 months. On the contrary, the *in vitro* reendothelialized AMs led to well-performing vascular conduits whose structure resembles that of the host vessel. The ECs lining the luminal surface of the grafts function as a barrier preventing the platelet adhesion on extracellular matrix, and they may influence, in a paracrine manner, the regeneration process by recruiting the host cells and modulating the inflammatory response. In agreement with this statement, our results demonstrated that only the implanted ECs seeded grafts were progressively changed with a thickening of the tunica media. Thus, the cellular component of the graft allows AMs to act as a temporary template that can be correctly remodelled by the host cells in a functional tissue.

## Conflict of Interests

The authors declare that there is no conflict of interests regarding the publication of this paper.

## Authors' Contribution

Luigi Dall'Olmo and Ilenia Zanusso equally contributed to this paper and should be considered co-first authors.

## Acknowledgments

This research was supported by Regione Veneto (Italy). The authors thank Mr. Mariano Schiavon for the laboratory assistance.

## References

[1] A. T. Hirsch, M. A. Allison, A. S. Gomes et al., "A call to action: women and peripheral artery disease: a scientific statement from the American Heart Association," *Circulation*, vol. 125, no. 11, pp. 1449–1472, 2012.

[2] J. G. Nemeno-Guanzon, S. Lee, J. R. Berg et al., "Trends in tissue engineering for blood vessels," *Journal of Biomedicine and Biotechnology*, vol. 2012, Article ID 956345, 2012.

[3] V. Piccone, "Alternative techniques in coronary artery reconstruction," in *Modern Vascular Grafts*, P. N. Sawyer, Ed., pp. 253–260, McGraw-Hill, New York, NY, USA, 1987.

[4] L. P. Neff, B. W. Tillman, S. K. Yazdani et al., "Vascular smooth muscle enhances functionality of tissue-engineered blood vessels in vivo," *Journal of Vascular Surgery*, vol. 53, no. 2, pp. 426–434, 2011.

[5] A. C. Thomas, G. R. Campbell, and J. H. Campbell, "Advances in vascular tissue engineering," *Cardiovascular Pathology*, vol. 12, no. 5, pp. 271–276, 2003.

[6] H. S. Hung, H. C. Chen, C. H. Tsai, and S. Z. Lin, "Novel approach by nanobiomaterials in vascular tissue engineering," *Cell Transplantation*, vol. 20, no. 1, pp. 63–70, 2011.

[7] M. T. Conconi, L. Borgio, R. Di Liddo et al., "Evaluation of vascular graft based on polyvinyl alcohol cryogels," *Molecular Medicine Reports*, 2014.

[8] T. Shin'oka, G. Matsumura, N. Hibino et al., "Midterm clinical result of tissue-engineered vascular autografts seeded with autologous bone marrow cells," *The Journal of Thoracic and Cardiovascular Surgery*, vol. 29, pp. 1330–1338, 2005.

[9] N. L'Heureux, S. Pâquet, R. Labbé, L. Germain, and F. A. Auger, "A completely biological tissue-engineered human blood vessel," *The FASEB Journal*, vol. 12, no. 1, pp. 47–56, 1998.

[10] N. L'Heureux, S. Paquet, R. Labbe, L. Germain, and F. A. Auger, "Tissue-engineered blood vessel for adult arterial revascularization," *The New England Journal of Medicine*, vol. 357, pp. 1451–1453, 2007.

[11] T. N. McAllister, M. Maruszewski, S. A. Garrido et al., "Effectiveness of haemodialysis access with an autologous tissue-engineered vascular graft: a multicentre cohort study," *The Lancet*, vol. 373, no. 9673, pp. 1440–1446, 2009.

[12] T. W. Gilbert, T. L. Sellaro, and S. F. Badylak, "Decellularization of tissues and organs," *Biomaterials*, vol. 27, no. 19, pp. 3675–3683, 2006.

[13] M. T. Conconi, B. Nico, D. Mangieri et al., "Angiogenic response induced by acellular aortic matrix in vivo," *Anatomical Record A: Discoveries in Molecular, Cellular, and Evolutionary Biology*, vol. 281, no. 2, pp. 1303–1307, 2004.

[14] J. P. Hodde, R. D. Record, H. A. Liang, and S. F. Badylak, "Vascular endothelial growth factor in porcine-derived extracellular matrix," *Endothelium*, vol. 8, no. 1, pp. 11–24, 2001.

[15] D. R. Clarke, R. M. Lust, Y. S. Sun, K. S. Black, and J. D. Ollerenshaw, "Transformation of nonvascular acellular tissue matrices into durable vascular conduits," *Annals of Thoracic Surgery*, vol. 71, no. 5, pp. S433–S436, 2001.

[16] B. S. Conklin, E. R. Richter, K. L. Kreutziger, D.-S. Zhong, and C. Chen, "Development and evaluation of a novel decellularized vascular xenograft," *Medical Engineering and Physics*, vol. 24, no. 3, pp. 173–183, 2002.

[17] J. I. Spark, S. Yeluri, C. Derham, Y. T. Wong, and D. Leitch, "Incomplete cellular depopulation may explain the high failure rate of bovine ureteric grafts," *British Journal of Surgery*, vol. 95, no. 5, pp. 582–585, 2008.

[18] E. Meezan, J. T. Hjelle, K. Brendel, and E. C. Carlson, "A simple, versatile, nondisruptive method for the isolation of morphologically and chemically pure basement membranes from several tissues," *Life Sciences*, vol. 17, no. 11, pp. 1721–1732, 1975.

[19] M. P. Pusztaszeri, W. Seelentag, and F. T. Bosman, "Immunohistochemical expression of endothelial markers CD31, CD34, von Willebrand factor, and Fli-1 in normal human tissues," *Journal of Histochemistry and Cytochemistry*, vol. 54, no. 4, pp. 385–395, 2006.

[20] P. Burra, S. Tomat, M. T. Conconi et al., "Acellular liver matrix improves the survival and functions of isolated rat hepatocytes cultured in vitro," *International journal of molecular medicine*, vol. 14, no. 4, pp. 511–515, 2004.

[21] M. Dettin, M. T. Conconi, R. Gambaretto et al., "Effect of synthetic peptides on osteoblast adhesion," *Biomaterials*, vol. 26, no. 22, pp. 4507–4515, 2005.

[22] M. T. Conconi, P. de Coppi, R. di Liddo et al., "Tracheal matrices, obtained by a detergent-enzymatic method, support in vitro the adhesion of chondrocytes and tracheal epithelial cells," *Transplant International*, vol. 18, no. 6, pp. 727–734, 2005.

[23] D. Ribatti, M. T. Conconi, B. Nico et al., "Angiogenic response induced by acellular brain scaffolds grafted onto the chick embryo chorioallantoic membrane," *Brain Research*, vol. 989, no. 1, pp. 9–15, 2003.

[24] M. T. Coconi, B. Nico, P. Rebuffat et al., "Angiogenic response induced by acellular femoral matrix *in vivo*," *Journal of Anatomy*, vol. 207, no. 1, pp. 79–83, 2005.

[25] M. Marzaro, S. Vigolo, B. Oselladore et al., "In vitro and in vivo proposal of an artificial esophagus," *Journal of Biomedical Materials Research A*, vol. 77, no. 4, pp. 795–801, 2006.

[26] M. T. Conconi, F. Rocco, R. Spinazzi et al., "Biological fate of tissue-engineered porcine valvular conduits xenotransplanted in the sheep thoracic aorta," *International Journal of Molecular Medicine*, vol. 14, no. 6, pp. 1043–1048, 2004.

[27] P. Macchiarini, P. Jungebluth, T. Go et al., "Clinical transplantation of a tissue-engineered airway," *The Lancet*, vol. 372, no. 9655, pp. 2023–2030, 2008.

[28] D. Pankajakshan and D. K. Agrawal, "Scaffolds in tissue engineering of blood vessels," *Canadian Journal of Physiology and Pharmacology*, vol. 88, no. 9, pp. 855–873, 2010.

[29] N. Hibino, T. Yi, D. R. Duncan et al., "A critical role for macrophages in neovessel formation and the development of stenosis in tissue-engineered vascular grafts," *The FASEB Journal*, vol. 25, no. 12, pp. 4253–4263, 2011.

[30] J. Ferruzzi, M. J. Collins, A. T. Yeh, and J. D. Humphrey, "Mechanical assessment of elastin integrity in fibrillin-1-deficient carotid arteries: implications for Marfan syndrome," *Cardiovascular Research*, vol. 92, no. 2, pp. 287–295, 2011.

[31] G. Grenier, M. Rémy-Zolghadri, R. Guignard et al., "Isolation and culture of the three vascular cell types from a small vein biopsy sample," *In Vitro Cellular & Developmental Biology—Animal*, vol. 39, no. 3-4, pp. 131–139, 2003.

[32] Y. Zhao, S. Zhang, J. Zhou et al., "The development of a tissue-engineered artery using decellularized scaffold and autologous ovine mesenchymal stem cells," *Biomaterials*, vol. 31, no. 2, pp. 296–307, 2010.

[33] B. W. Tillman, S. K. Yazdani, L. P. Neff et al., "Bioengineered vascular access maintains structural integrity in response to arteriovenous flow and repeated needle puncture," *Journal of Vascular Surgery*, vol. 56, no. 3, pp. 783–793, 2012.

[34] M. Zhou, Z. Liu, C. Liu et al., "Tissue engineering of small-diameter vascular grafts by endothelial progenitor cells seeding heparin-coated decellularized scaffolds," *Journal of Biomedical Materials Research B: Applied Biomaterials*, vol. 100, no. 1, pp. 111–120, 2012.

[35] Y. Yoon, J. Park, T. Tkebuchava, C. Luedeman, and D. W. Losordo, "Unexpected severe calcification after transplantation of bone marrow cells in acute myocardial infarction," *Circulation*, vol. 109, no. 25, pp. 3154–3157, 2004.

[36] A. Assmann, P. Akhyari, C. Delfs et al., "Development of a growing rat model for the in vivo assessment of engineered aortic conduits," *Journal of Surgical Research*, vol. 176, no. 2, pp. 367–375, 2012.

[37] J. Y. Liu, D. D. Swartz, H. F. Peng, S. F. Gugino, J. A. Russell, and S. T. Andreadis, "Functional tissue-engineered blood vessels from bone marrow progenitor cells," *Cardiovascular Research*, vol. 75, no. 3, pp. 618–628, 2007.

[38] J. D. Roha, R. Sawh-Martinez, M. P. Brennan et al., "Tissue-engineered vascular grafts transform into mature blood vessels via an inflammation-mediated process of vascular remodeling," *Proceedings of the National Academy of Sciences of the United States of America*, vol. 107, no. 10, pp. 4669–4674, 2010.

[39] M. A. Cleary, E. Geiger, C. Grady, C. Best, Y. Naito, and C. Breuer, "Vascular tissue engineering: the next generation," *Trends in Molecular Medicine*, vol. 18, no. 7, pp. 394–404, 2012.

[40] R. G. Leyh, M. Wilhelmi, P. Rebe, S. Ciboutari, A. Haverich, and H. Mertsching, "Tissue engineering of viable pulmonary arteries for surgical correction of congenital heart defects," *Annals of Thoracic Surgery*, vol. 81, no. 4, pp. 1466–1471, 2006.

Hindawi Publishing Corporation
BioMed Research International
Volume 2014, Article ID 161437, 8 pages
http://dx.doi.org/10.1155/2014/161437

*Research Article*

# Image-Based Three-Dimensional Analysis to Characterize the Texture of Porous Scaffolds

**Diana Massai,[1] Francesco Pennella,[1] Piergiorgio Gentile,[1,2] Diego Gallo,[1] Gianluca Ciardelli,[1] Cristina Bignardi,[1] Alberto Audenino,[1] and Umberto Morbiducci[1]**

[1] *Department of Mechanical and Aerospace Engineering, Politecnico di Torino, Corso Duca degli Abruzzi 24, 10129 Turin, Italy*
[2] *Centre for Biomaterials & Tissue Engineering, Department of Adult Dental Care, School of Clinical Dentistry, University of Sheffield, Sheffield S10 2TA, UK*

Correspondence should be addressed to Umberto Morbiducci; umberto.morbiducci@polito.it

Received 28 March 2014; Accepted 8 May 2014; Published 5 June 2014

Academic Editor: Silvia Baiguera



The aim of the present study is to characterize the microstructure of composite scaffolds for bone tissue regeneration containing different ratios of chitosan/gelatin blend and bioactive glasses. Starting from realistic 3D models of the scaffolds reconstructed from micro-CT images, the level of heterogeneity of scaffold architecture is evaluated performing a lacunarity analysis. The results demonstrate that the presence of the bioactive glass component affects not only macroscopic features such as porosity, but mainly scaffold microarchitecture giving rise to structural heterogeneity, which could have an impact on the local cell-scaffold interaction and scaffold performances. The adopted approach allows to investigate the scale-dependent pore distribution within the scaffold and the related structural heterogeneity features, providing a comprehensive characterization of the scaffold texture.

## 1. Introduction

Tissue engineering scaffolds are designed to provide a biomimetic three-dimensional (3D) architecture that mimics the native extracellular matrix (ECM), in order to guarantee adequate mechanical support and to promote cell colonization, migration, and proliferation. In parallel, such an architecture must assure an adequate oxygen and nutrient diffusion and the removal of metabolic wastes [1, 2].

Both mechanical properties and the above mentioned transport phenomena are strictly dependent on scaffold structure, with porosity, pore size, and specific surface area that play an essential role in cell migration, tissue in-growth, and cell attachment, respectively [3]. Moreover, interconnectivity and distribution of pores strongly affect tissue regeneration [4].

It is widely accepted that highly porous scaffolds with uncontrolled architecture do not recapitulate the desired features of the native ECM/tissue [5], which contrarily assures, with a 3D interconnected and homogeneous pore network, spatially uniform cell distribution, cell survival, proliferation, and migration [6].

In native tissue, structure and function are highly interrelated, therefore an in-depth analysis of the texture of porous scaffolds could allow us to get more insight into the comprehension of the impact that the scaffold architecture has in conditioning (1) not only the cellular environment and cell-cell interactions but also (2) the local cell-structure interactions. It is then clear the relevance of scaffolds microarchitecture when the final aim is to design and build effective functional substitutes [5].

The need to characterize the texture of an object at different scales and to quantitatively assess its spatial patterns is a critical issue for a huge amount of processes in many research fields, from landscape ecology [7] to the analysis of microvascular remodeling [8] and to the study of water movement in relation to soil macroporosity [9], and, in general, for all those porous media that exhibit significant physical heterogeneities, leading to the development of a wide number of metrics. However, most of these metrics suffer from the limitation that different spatial patterns can be depicted for any single value of the respective metric [7]. For example, Mandelbrot recognized that objects with identical fractal dimensions can have greatly different appearances [10], and

experience has demonstrated that the classical fractal dimensions are not sufficient to describe uniquely the interstitial geometry of porous media [11]. Indeed, although porous media, and porous scaffolds as well, could be considered as fractal structures, the fractal dimension alone is not sufficient for characterizing scaffolds architecture, since it describes how much space is filled but does not indicate how the space is filled by the object [8].

To overcome this limitation, a new concept, termed lacunarity, was introduced by Mandelbrot [10]. Lacunarity measures the deviation of a geometric object from the translational invariance or homogeneity [12] and can be used to describe the distribution of gap or pore sizes within the studied object [8], characterised by higher lacunarity values if pore sizes are distributed over a greater range. Lacunarity can be adopted to distinguish objects with similar fractal dimensions [8] but can also be used independently to describe spatial patterns [13]. In other words, as translational invariance is a highly scale-dependent property (i.e., objects which are homogeneous at a certain scale could be characterized by heterogeneity at a different scale) [7], lacunarity, which can be considered a scale-dependent measure of heterogeneity, represents an effective tool to study the scale-dependent pore distribution patterns within a scaffold and the related randomness spatial scale.

The aim of the present study is to characterize the microstructure of three bioactive glass/polymer composite scaffolds for bone tissue regeneration in order to get insight into their microarchitecture and the related randomness scale. Starting from realistic 3D models of the scaffolds reconstructed from micro-CT images, the level of heterogeneity of scaffolds architecture is evaluated performing an analysis of lacunarity. Moreover, since the scaffolds under investigation are characterized by different porosity, the relative lacunarity function is adopted for a suitable comparison to exclude the influence of the porosity.

## 2. Materials and Methods

All the single steps of the workflow, from scaffolds preparation to micro-CT image analysis, image segmentation, 3D model reconstruction, evaluation of porosity, and evaluation of pore structure distribution will be detailed in this section.

*2.1. Scaffold Fabrication.* A detailed description of the adopted scaffolds can be found in [14]. Briefly, porous scaffolds were made of blends of chitosan/gelatin (CG), for supporting cell adhesion and proliferation, containing different amounts of bioactive glasses (BG), which are inorganic materials stimulating the biomineralization, and were fabricated by freeze-drying. Foams with three different weight ratios (BG/CG) between the components (S1: 0/100 w/w; S2: 40/60 w/w; S3: 70/30 w/w) were prepared. Details on mechanical properties, biocompatibility, and bioactivity of these scaffolds are described in previous study [14].

*2.2. Micro-CT-Based 3D Scaffold Geometry Reconstruction.* Micro-CT images were used to reconstruct 3D models of the scaffolds. The SkyScan 1072 (Aartselaar, Belgium) micro-CT scanner (248 A current, 40 kV voltage) was used to perform the CT scanning of the manufactured scaffolds. Image slices with isotropic voxels were acquired and a spatial resolution of 8.7 $\mu$m was achieved.

Micro-CT image segmentation was performed by applying the open public domain Java image processing software *ImageJ* (http://imagej.nih.gov/ij/index.html). The uncertainty in the reconstruction of scaffold models was minimized adopting several local and global segmentation strategies (exhaustive details can be found at http://rsbweb.nih.gov/ij/). The most performing segmentation strategy was identified as the one giving the maximum value of normalized cross-correlation between the Fourier phases of the original image and the segmented one as proposed elsewhere [15]. The calculation of the normalized cross-correlation, performed within MATLAB (The MathWorks, Inc., Natick, USA) environment, allowed the identification of the Niblack segmentation criterion [16] as the most performing one for scaffolds S1 and S2 and the Sauvola criterion [17] for scaffold S3.

The reconstruction of the 3D model of each scaffold was performed from the stack of the properly segmented 2D images. The size of the reconstructed cubic 3D scaffold models from region of interest (ROI) images was equal to $2.2 \times 2.2 \times 2.2\,\text{mm}^3$, corresponding to $256^3$ voxels. The 3D volume rendering of the selected ROI of the scaffolds is presented in Figure 1.

*2.3. Analysis of the Scaffold Architecture: Porosity.* As recently mentioned in Pennella et al. [18], properties of a scaffold in terms of mass transport, cell colonization, and mechanical performance can be characterized in statistical terms from its porosity, average pore size, and pore size distribution.

In a widely adopted conceptual model, the internal microstructure of a porous medium (and of a porous scaffold as well) can be characterized by partitioning the pore space into a discrete collection of individual pores, which can be rigorously defined as regions of the void space confined by solid surfaces. In this way, it is possible to define the porosity $n$ as follows:

$$n = \frac{V_V}{V_{\text{TOT}}}, \tag{1}$$

where $V_V$ is the volume of void space and $V_{\text{TOT}}$ is the total volume [15, 19].

A simple, widely adopted approach based on microscopic surface analysis of the scaffold was applied to evaluate not only porosity, but also the average pore size and superficial pore size distribution [20]. Porosity was evaluated by applying (1) to the reconstructed 3D scaffold models.

*2.4. Analysis of the Scaffold Architecture: Lacunarity.* A quantitative descriptor of lacunarity was calculated in order to measure the spatial distribution and heterogeneity of scaffold pores. After the segmentation process, each 3D scaffold model, as obtained from the stack of segmented micro-CT images, was converted into a binary map where each grid cell was denoted with zero (black cell, solid space) or one

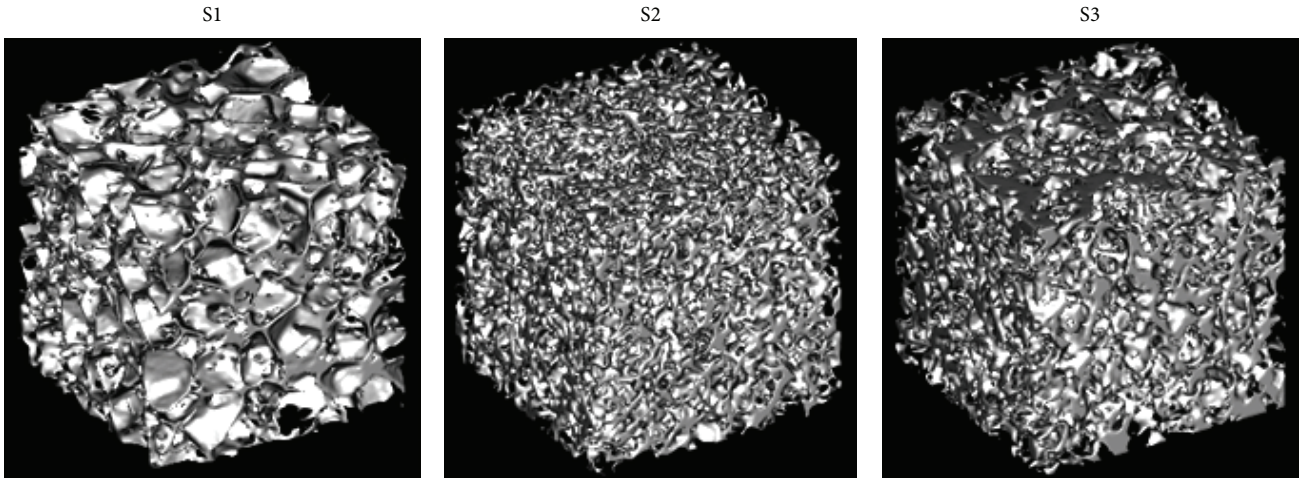


Figure 1: 3D model reconstruction from micro-CT images of (a) scaffold S1 (0/100), (b) scaffold S2 (40/60), and (c) scaffold S3 (70/30). Differences in the structure can be observed, which can be ascribed to the different composition of the scaffolds.

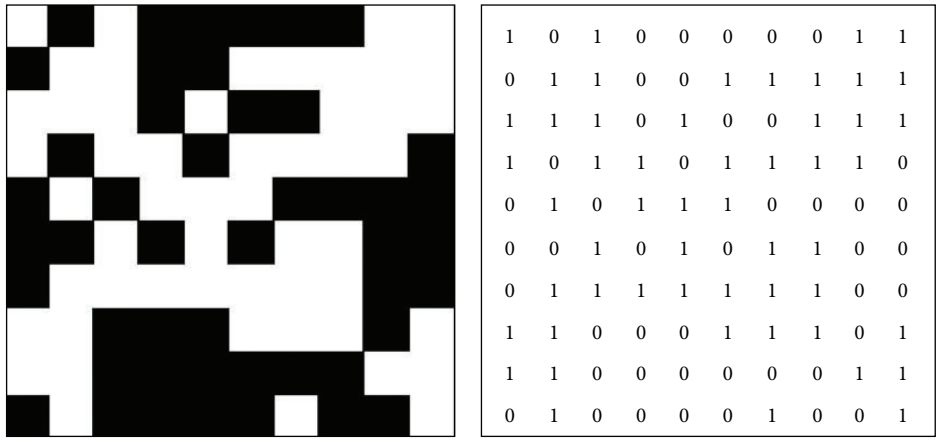


Figure 2: Synthetic 10 × 10 pixel binarized image of a two-dimensional micro-CT slice (a) and its binary representation (b).

(white cell, pore), obtaining a cube of black and white voxels. An example of a synthetic 10 × 10 pixel binarized image of a two-dimensional micro-CT slice and of its numerical binary representation is presented in Figure 2.

Lacunarity (LAC) was evaluated with the aim to provide an analysis of scaffold images in terms of (1) the overall fraction covered by the attribute of interest; (2) the presence and scale of randomness; (3) the existence of hierarchical structure.

Technically, LAC was evaluated by applying the "gliding box" algorithm [21] as reported by Plotnick et al. [7]. The following strategy was applied: (1) a cubic box of size $r$ was superimposed to the 3D scaffold model of size $M$; (2) starting from the upper left-hand corner, the box was moved one unit to the right (with a unit corresponding to the voxel size) and the number of white (pores) voxels contained within the box was counted; (3) the box was shift down one voxel size when the end of a row was reached and the process was repeated until the box was moved over all parts of the cubic 3D scaffold model.

If $N(r) = (M - r + 1)^2$ is the total number of boxes of size $r$ and $n(S, r)$ is the number of boxes of size $r$ containing $S$ white voxels, then the frequency distribution $N(r)$ can be converted into a probability distribution as follows:

$$P(S, r) = \frac{n(S, r)}{N(r)}. \tag{2}$$

LAC of the 3D scaffold model, for box size $r$, can now be defined as

$$\mathrm{LAC} = \frac{\mu_2(r)}{(\mu_1(r))^2} = \frac{\overline{S}^2(r) + \sigma_s^2(r)}{\overline{S}^2(r)} = 1 + \frac{\sigma_s^2(r)}{\overline{S}^2(r)}, \tag{3}$$

where $\mu_1$ and $\mu_2$ are the first and second moments of the distribution $P(S, r)$, respectively; and $\overline{S}(r)$ and $\sigma_s^2(r)$ are the

mean and the variance of the number of white (pore) voxels per box of size $r$, respectively.

Equation (3) shows that LAC is a function of $r$. As the size of the gliding box increases, the content of the box also increases and the probability that box contents will greatly differ from the average decreases. This is like to say that also the variance of $S(r)$ decreases (and $\mu_2$ in (3) as well) with the consequence that the same scaffold model will show lower LAC values as $r$ increases. Moreover, there is a clear dependence on LAC from the void fraction of the scaffold model (representing pores). As the mean number of voids goes to zero, the ratio $(\sigma_s^2(r)/\overline{S}^2(r))$ increases in (3), with the consequence that scaffolds with sparse pore distribution will have higher LAC than scaffolds with more dense pore maps, for the same $r$.

LAC is also sensitive to the pore size and distribution within the scaffold: for a given void fraction in the scaffold model, fewer but larger pores give rise to higher LAC values. In contrast, the LAC value of a totally regular scaffold model is equal to one, independent of the value of $r$ (the variance $\sigma_s^2(r)$ is zero at any location, because the number of white voxels within the gliding box is constant).

The above mentioned considerations clearly confirm the observation by Plotnick et al. [7] that an evaluation of lacunarity based on a single gliding box size $r$ is meaningless, when LAC is used for comparison of different scaffold models. On the contrary, the possibility to extract a whole host of information is given when LAC is calculated over a wide range of gliding box sizes. This can be done by analyzing the shape of LAC versus the gliding box size $r$ curves [7].

The scaffolds under investigation in this study are characterized by different porosity (as will be shown in Section 3), making comparison difficult. However, since the overall shape of the LAC curves depends on the degree of clustering or clumping and is independent of the value of the fraction [7], which in this case is porosity $n$ of (1), the relative lacunarity function (RLF) on a logarithmic scale was adopted to minimize the influence of different porosity on scaffolds architecture heterogeneity. According to Luo and Lin [9] RLF was calculated as follows:

$$\mathrm{RLF} = -\frac{\ln(\mathrm{LAC})}{\ln(n)}. \tag{4}$$

Using (4), the shape of the RLF versus $r$ curve and its corresponding spatial pattern could be better evaluated.

## 3. Results

The porosity values calculated from the reconstructed 3D models of the scaffolds are summarized in Table 1. As expected, porosity $n$ for scaffold S1, composed of CG alone without BG component, is greater than that for scaffolds S2 and S3. Interestingly, the porosity of scaffolds containing BG at different percentages (S2 and S3) is almost the same. This result is related to the deposition of the BG particles on the pore walls, which has the consequence of a reduction of the available void area [14].

Table 1: Porosity ($n$) values calculated over the 3D models of scaffolds S1, S2, and S3.

| Scaffold (BG/CG) | S1 (0/100) | S2 (40/60) | S3 (70/30) |
|---|---|---|---|
| $n$ (%) | 81 | 70 | 68 |

For each scaffold model, LAC and RLF were calculated for gliding box size $r$ ranging from 1 to 64.

Figure 3 shows the log-log plots of the scaffold LAC values versus $r$ for scaffolds S1, S2, and S3, respectively. It is worth noting that, in general, (1) the maximum LAC value is always found when $r$ is equal to 1 ($\ln(r) = 0$), because in this case LAC is simply a function of the void/solid fraction, that is, porosity $n$, and does not give information about pore distribution; (2) LAC is always equal to 1 ($\ln(\mathrm{LAC}) = 0$) for $r$ is equal to the maximum sample size, because in this case the variance $\sigma_s^2(r)$ in (3) is always zero; (3) away from the endpoints, in general, the shape of LAC curves differs also when the same fraction of the 3D scaffold model is occupied by voids, that is, also when scaffolds have the same porosity but different pore distribution, shape, dimension, and so forth.

From our findings, it can be observed that LAC curves are not linear (Figure 3), thus clearly indicating that scaffolds are not characterized by a fractal geometry. In fact, when a porous media is characterized by self-similarity, LAC log-log plot should be linear [7, 21]. As reported by Plotnick et al. [7], if a map has a random structure at some scale, lacunarity depends on the size $r$ of the gliding box relative to the characteristic scale of randomness. In particular, if $r$ is greater than the random scale, the variance of the void space (pores) within the gliding boxes will approach zero and LAC will be close to 1, while if $r$ is smaller than the scale of randomness, LAC will be higher than 1 pointing out heterogeneity. Considering Figures 3(a) and 3(b), it is possible to observe that for scaffolds S1 and S2 the LAC curves begin to approach a value close to 1 when $\ln(r) \approx 2$ (i.e., $r \approx 8$ voxels, corresponding to 64 $\mu$m), as highlighted by the change in the slope of the curve. This means that at scales lower than $\ln(r) \approx 2$, scaffolds S1 and S2 are characterized by an heterogeneous structure with random patterns. Moreover, both for S1 and S2, LAC approach values close to one 1 for $\ln(r) > 4$. Scaffold S3 exhibits a similar trend as for S1 and S2, but a slower LAC decrease with $r$ (Figure 3(c)), thus indicating a slightly wider scale of randomness for S3 structure.

The results in Figure 3 show that the gliding box size $r$ has approached the representative elementary volume (i.e., $r \approx 64$) of the reconstructed scaffolds [9].

As scaffolds are characterized by different porosity, in order to compare their structural heterogeneity, the RLF was calculated, and information about their randomness scale was obtained by analyzing the shapes of RLF versus $\ln(r)$ curves. The RLF curves of scaffolds S1, S2, and S3 are depicted in Figure 4.

Scaffolds S1 and S2 are characterized by the same trend, with the RLF curve of S2 being always lower than S1. This could be related to the increased wall thickness of pores in S2, a consequence of the deposition of BG particles. Concerning

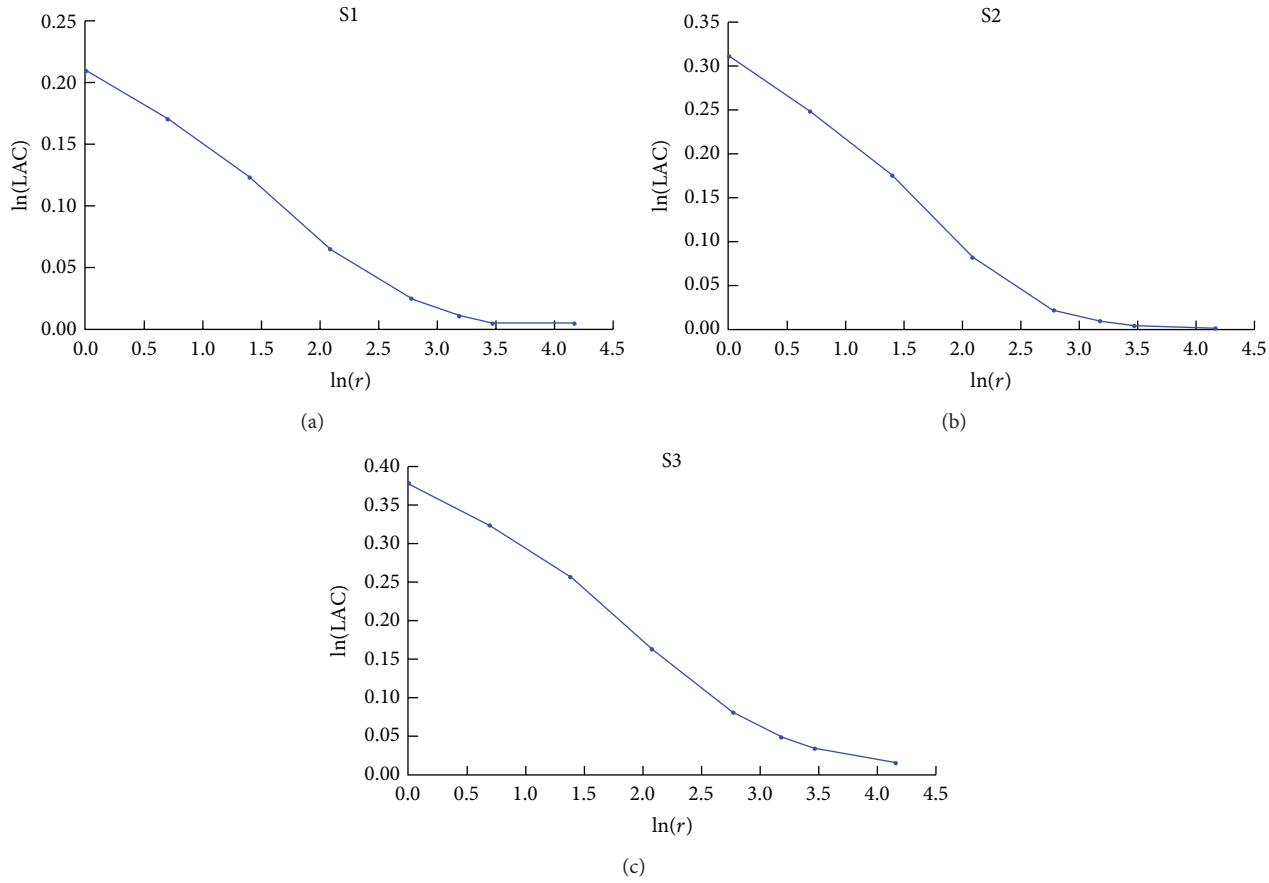


Figure 3: Log-log plot of LAC versus gliding box size $r$ calculated over the 3D model of scaffolds S1 (a), S2 (b), and S3 (c).

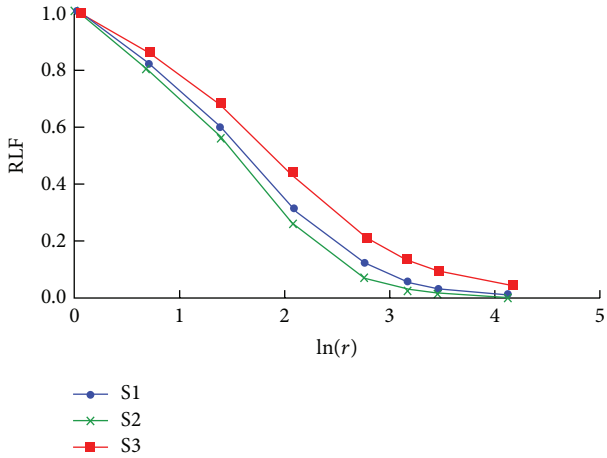


Figure 4: Log-log plot of RLF versus gliding box size $r$ calculated over the 3D models of scaffolds S1, S2, and S3.

S3, it is characterized by RLF values higher than S1 and S2, independent of $r$. This means that S3 exhibits a more marked heterogeneity than S1 and S2, which could be ascribed to its higher content of BG particles that causes micropore occlusion. To further investigate the reason for this behaviour, three (parallel) subvolumes (thickness = 520 $\mu$m), obtained from three different regions of the original reconstructed scaffold model, were considered both for S1 and S3, and on them the RLF was calculated (Figure 5).

The log-log plot of RLF versus $r$ values for the three subvolumes of S1 and S3 is displayed in Figure 6. Notably, no differences can be appreciated in the curves of the three subvolumes belonging to S1 (Figure 6(a)). On the contrary, RLF curves of the three subvolumes belonging to S3 show remarkable differences for $\ln(r) > 0.5$ (Figure 6(b)), thus confirming dissimilar spatial distribution of pores within different regions of the scaffold. More in detail, for S3 the RLF curve of subvolume 1 shows lower values than curves of subvolumes 2 and 3, indicating the presence of distributed pores and/or less pore occlusion, as also confirmed by the visual inspection of the binarized images of the pore network related to the investigated subvolumes, depicted in Figure 6(b).

## 4. Discussion

In a large part of tissue engineering approaches, the microarchitecture of porous scaffolds plays a key role in effectively guiding cell growth and tissue regeneration. The architecture is in fact among the main contributors in determining the performance of the scaffold itself in terms of both adequate mechanical support and transport of cells and compounds [1, 2].

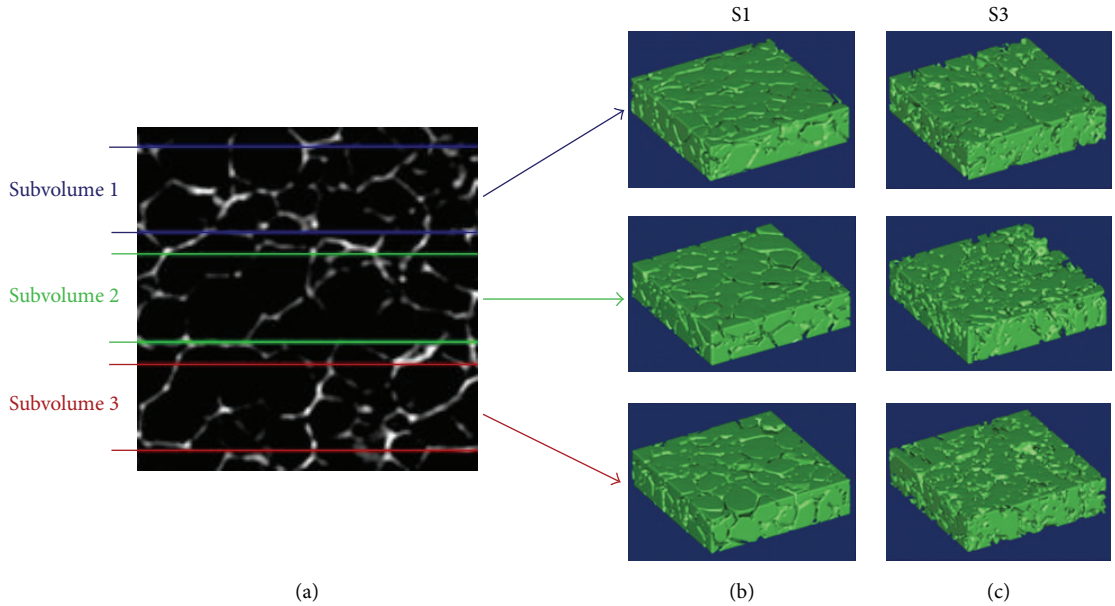


FIGURE 5: 3D reconstruction of three (parallel) subvolumes, obtained from different regions (a) of scaffold models S1 (b) and S3 (c).

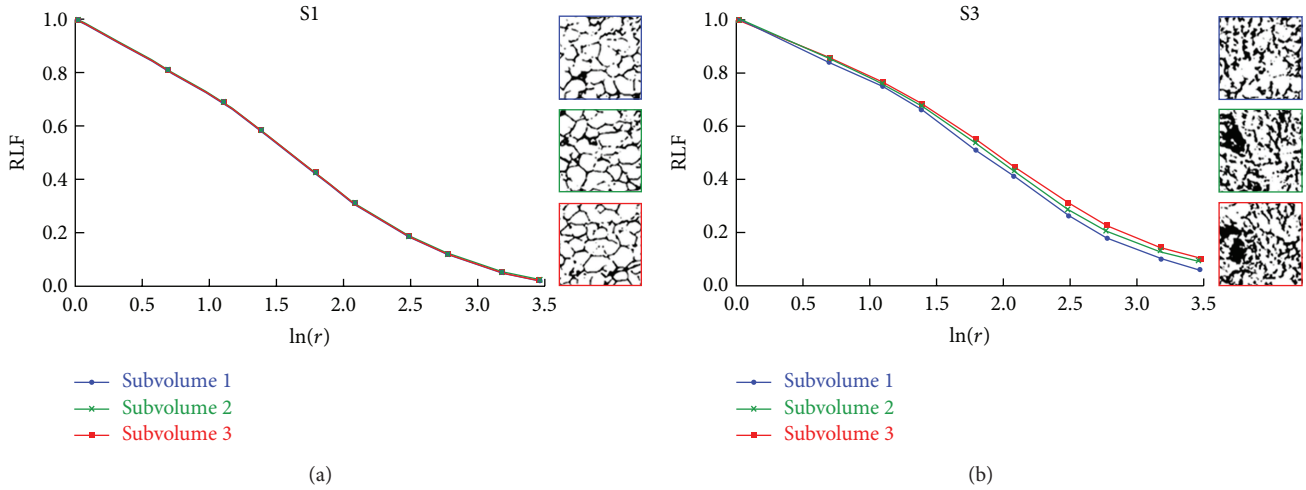


FIGURE 6: Log-log plot of RLF versus gliding box size $r$ of three different subvolumes of scaffolds S1 (a) and S3 (b). The binarized images of the pore network, related to the three subvolumes under investigation, are also shown.

It is then clear that in scaffold architecture the level of heterogeneity rather than self-similarity could have marked side effects on the quality of the engineered tissue, eventually giving also rise to scale effects.

In parallel to the development of tools for the macroscopic characterization of scaffold features (e.g., Young modulus, porosity, permeability, etc.) [18, 22], all the reasons mentioned above have lead, in recent years, to an increasing interest in (1) methods for characterizing scaffold architecture at different scales [5, 23] and in (2) quantitative descriptors of spatial emerging patterns in scaffold structure [24].

Inspired by methods applied in other disciplines [7–9], in this study a method based on lacunarity analysis was adopted for a quantitative description of the texture of three glass/polymer composite porous scaffolds for bone tissue engineering and for the identification of their randomness scale.

The effectiveness of the approach allowed to assess the spatial distribution of pores over the 3D reconstructed scaffold models and to catch heterogeneity features in the structures of the three investigated scaffolds which, due to their composition and fabrication method, lack self-similarity.

Interestingly, the findings demonstrate that the presence of the BG component affects not only porosity (S1, the scaffold composed of chitosan/gelatin alone is characterized by higher porosity than S2 and S3) but also mainly heterogeneity. In fact, the scaffold with the highest BG content, S3, presents higher spatial heterogeneity than S1 and S2, as confirmed by the RLF analysis (Figure 4). This result is independent of porosity, being S2 and S3 characterized by almost the

same porosity, which is markedly lower than S1 (Table 1). Moreover, the analysis performed on subvolumes of scaffolds S1 and S3 highlights (1) different levels of heterogeneity in different regions of S3 (Figure 6(b)), against the same levels characterizing different regions of S1 (Figure 6(a)) and (2) a scale of randomness for S3 which is slightly wider than that for S1 (Figure 6).

Previous findings on the same scaffolds showed that one consequence of the increased presence of BG in the composition of the scaffold was a structure more resistant to compression [14]. Also in this case, it is expected that heterogeneity in the microarchitecture could play a scale effect, thus contributing to the increase of the anisotropic mechanical behaviour of the scaffold.

The approach applied in this study could suffer from limitations. A possible limitation of the adopted method could be in the fact that, being the lacunarity analysis based on images, results could be markedly influenced by the adopted image resolution [11]. However, in this specific study, the high resolution (8.7 $\mu$m) of the micro-CT images is adequate with respect to the mean pore size (greater than 130 $\mu$m [14]; that is, mean pore size is 15 times higher than micro-CT image resolution) of the scaffolds under investigation. A further possible limitation can be identified in the uncertainty in the reconstruction of the 3D models, which could affect the analysis of the texture. Also in this case, we put effort in selecting, among several possible segmentation strategies (as explained in Section 2), the most appropriate one, thus minimizing the impact that this source of uncertainty could have on texture analysis.

## 5. Conclusions

In the present paper, the textures of three glass/polymer composite porous scaffolds for bone tissue engineering were characterized by adopting an image-based method based on lacunarity analysis. Our findings suggest that the texture of porous scaffolds could play a crucial role in determining the properties of the structure not only at the macroscale, but also at lower scales, where the focal relationships between cells and structure take place. The approach herein applied to engineered scaffolds could be translated to the microstructure of the native ECM of different tissues [25] in order to (1) investigate its local effects on the relationship between cell and ECM [26] and (2) design and fabricate biomimetic porous scaffolds that recapitulate the ECM architectural features of the tissue of interest [5].

In the future, 3D metrics for the analysis of spatiotemporal data as developed in ecology will be applied to 3D models of scaffolds as reconstructed from, for example, coherent anti-Stokes Raman scattering microscopy images [27], along the cell culture. In this way, the evolution of the cultured construct will be evaluated as the evolution of an "ecosystem," considering the different actors of the involved complex bioprocesses. This approach will allow to identify relationships of relevance between the level of complexity at which the system is considered and the granularity of its description, that is, the so called "contextual emergence" [28]. The proposed ecosystem evolution-like approach, applied to study the evolution of the cell-scaffold system, could provide a robust procedure which, being able to translate between descriptive levels, can be used to build up consistent level-specific criteria for reproducibility.

## Conflict of Interests

The authors declare that there is no conflict of interest regarding the publication of this paper.

## Acknowledgments

The authors would like to thank Professor C. Vitale-Brovarone and Dr. F. Baino of Politecnico di Torino, Italy, for providing the BG component and Dr. I. Pashkuleva of 3B's Group, University of Minho, Portugal, for micro-CT analysis. D. M. is granted by the Italian Ministry of University and Research (PRIN 2012 Prot. 20123E8FH4) and P. G. is granted by the UK EPSRC Centre for Innovative Manufacturing of Medical Devices, MeDe Innovation (EPSRC grant EP/K029592/1).

## References

[1] D. W. Hutmacher, "Scaffolds in tissue engineering bone and cartilage," *Biomaterials*, vol. 21, no. 24, pp. 2529–2543, 2000.

[2] S. J. Hollister, "Porous scaffold design for tissue engineering," *Nature Materials*, vol. 4, no. 7, pp. 518–524, 2005.

[3] T. S. Karande, J. L. Ong, and C. M. Agrawal, "Diffusion in musculoskeletal tissue engineering scaffolds: design issues related to porosity, permeability, architecture, and nutrient mixing," *Annals of Biomedical Engineering*, vol. 32, no. 12, pp. 1728–1743, 2004.

[4] K. Rezwan, Q. Z. Chen, J. J. Blaker, and A. R. Boccaccini, "Biodegradable and bioactive porous polymer/inorganic composite scaffolds for bone tissue engineering," *Biomaterials*, vol. 27, no. 18, pp. 3413–3431, 2006.

[5] S. N. Bhatia and C. S. Chen, "Tissue engineering at the microscale," *Biomedical Microdevices*, vol. 2, no. 2, pp. 131–144, 1999.

[6] R. Z. LeGeros and J. P. LeGeros, "Calcium phosphate biomaterials: preparation, properties, and biodegradation," in *Encyclopedia Handbook of BioMaterials and Bioengineering Part A: Materials*, D. L. Wise, D. J. Trantolo, D. E. Altobelli, M. J. Yaszemski, J. D. Gresser, and E. R. Schwartz, Eds., vol. 2, pp. 1429–1463, Marcel Dekker, 1995.

[7] R. E. Plotnick, R. H. Gardner, and R. V. O'Neill, "Lacunarity indices as measures of landscape texture," *Landscape Ecology*, vol. 8, no. 3, pp. 201–211, 1993.

[8] D. J. Gould, T. J. Vadakkan, R. A. Poche, and M. E. Dickinson, "Multifractal and lacunarity analysis of microvascular morphology and remodeling," *Microcirculation*, vol. 18, no. 2, pp. 136–151, 2011.

[9] L. Luo and H. Lin, "Lacunarity and fractal analyses of soil macropores and preferential transport using micro-X-ray computed tomography," *Vadose Zone Journal*, vol. 8, no. 1, pp. 233–241, 2009.

[10] B. B. Mandelbrot, *The Fractal Geometry of Nature*, Freeman, 1982.

[11] D. E. Pendleton, A. Dathe, and P. Baveye, "Influence of image resolution and evaluation algorithm on estimates of the lacunarity of porous media," *Physical Review E: Statistical, Nonlinear,*

*and Soft Matter Physics*, vol. 72, no. 4, part 1, Article ID 041306, 2005.

[12] Y. Gefen, Y. Meir, B. B. Mandelbrot, and A. Aharony, "Geometric implementation of hypercubic lattices with noninteger dimensionality by use of low lacunarity fractal lattices," *Physical Review Letters*, vol. 50, no. 3, pp. 145–148, 1983.

[13] R. E. Plotnick, R. H. Gardner, W. W. Hargrove, K. Prestegaard, and M. Perlmutter, "Lacunarity analysis: a general technique for the analysis of spatial patterns," *Physical Review E: Statistical Physics, Plasmas, Fluids, and Related Interdisciplinary Topics*, vol. 53, no. 5, pp. 5461–5468, 1996.

[14] P. Gentile, M. Mattioli-Belmonte, V. Chiono et al., "Bioactive glass/polymer composite scaffolds mimicking bone tissue," *Journal of Biomedical Materials Research A*, vol. 100, no. 10, pp. 2654–2667, 2012.

[15] S. Rajagopalan and R. A. Robb, "Imaged-based metrology of porous tissue engineering scaffolds," in *Medical Imaging 2006: Image Processing*, J. M. Reinhardt and J. P. W. Pluim, Eds., vol. 6144, pp. 540–550, Proceedings of the SPIE, 2006.

[16] W. Niblack, *An Introduction To Image Processing*, Prentice-Hall, Englewood Cliffs, NJ, USA, 1986.

[17] J. Sauvola, T. Seppanen, S. Haapakoski, and M. Pietikainen, "Adaptive document binarization," in *Proceedings of the 4th International Conference on Document Analysis and Recognition (ICDAR '97)*, pp. 147–152, IEEE Computer Society, August 1997.

[18] F. Pennella, G. Cerino, D. Massai et al., "A survey of methods for the evaluation of tissue engineering scaffold permeability," *Annals of Biomedical Engineering*, vol. 41, no. 10, pp. 2027–2041, 2013.

[19] J. Bear, *Dynamics of Fluids in Porous Media*, 1972.

[20] M. D. M. Innocentini, R. K. Faleiros, R. Pisani Jr., I. Thijs, J. Luyten, and S. Mullens, "Permeability of porous gelcast scaffolds for bone tissue engineering," *Journal of Porous Materials*, vol. 17, no. 5, pp. 615–627, 2010.

[21] C. Allain and M. Cloitre, "Characterizing the lacunarity of random and deterministic fractal sets," *Physical Review A*, vol. 44, no. 6, pp. 3552–3558, 1991.

[22] A. S. P. Lin, T. H. Barrows, S. H. Cartmell, and R. E. Guldberg, "Microarchitectural and mechanical characterization of oriented porous polymer scaffolds," *Biomaterials*, vol. 24, no. 3, pp. 481–489, 2003.

[23] A. Alberich-Bayarri, D. Moratal, J. L. Ivirico et al., "Microcomputed tomography and microfinite element modeling for evaluating polymer scaffolds architecture and their mechanical properties," *Journal of Biomedical Materials Research B: Applied Biomaterials*, vol. 91, no. 1, pp. 191–202, 2009.

[24] M. Y. M. Chiang, F. A. Landis, X. Wang et al., "Local thickness and anisotropy approaches to characterize pore size distribution of three-dimensional porous networks," *Tissue Engineering C: Methods*, vol. 15, no. 1, pp. 65–76, 2009.

[25] P. Krauss, C. Metzner, J. Lange, N. Lang, and B. Fabry, "Parameter-free binarization and skeletonization of fiber networks from confocal image stacks," *PLoS ONE*, vol. 7, no. 5, Article ID e36575, 2012.

[26] W. J. Polacheck, A. E. German, A. Mammoto, D. E. Ingber, and R. D. Kamm, "Mechanotransduction of fluid stresses governs 3D cell migration," *Proceedings of the National Academy of Sciences of the United States of America*, vol. 111, no. 7, pp. 2447–2452, 2014.

[27] L. Mortati, C. Divieto, and M. P. Sassi, "CARS and SHG microscopy to follow collagen production in living human corneal fibroblasts and mesenchymal stem cells in fibrin hydrogel 3D cultures," *Journal of Raman Spectroscopy*, vol. 43, no. 5, pp. 675–680, 2012.

[28] H. Atmanspacher, L. B. Lambert, G. Folkers, and P. A. Schubiger, "Relevance relations for the concept of reproducibility," *Journal of the Royal Society Interface*, vol. 11, no. 94, 2013.

Hindawi Publishing Corporation
BioMed Research International
Volume 2014, Article ID 796519, 8 pages
http://dx.doi.org/10.1155/2014/796519

*Research Article*

# Experimental Study of Diffusion Coefficients of Water through the Collagen: Apatite Porosity in Human Trabecular Bone Tissue

**Franco Marinozzi,[1] Fabiano Bini,[1] Alessandro Quintino,[2] Massimo Corcione,[2] and Andrea Marinozzi[3]**

[1] *Mechanical and Thermal Measurements Laboratory, Department of Mechanical and Aerospace Engineering, "Sapienza" University of Rome, Via Eudossiana, 18-00184 Rome, Italy*
[2] *Department of Astronautical, Electrical and Energetic Engineering, "Sapienza" University of Rome, Via Eudossiana, 18-00184 Rome, Italy*
[3] *Orthopaedics and Traumatology Area, University "Campus Bio-Medico", Via Álvaro del Portillo, 21-00128 Rome, Italy*

Correspondence should be addressed to Franco Marinozzi; franco.marinozzi@uniroma1.it

Received 28 February 2014; Revised 16 April 2014; Accepted 28 April 2014; Published 21 May 2014

Academic Editor: Costantino Del Gaudio



We firstly measured the swelling of single trabeculae from human femur heads during water imbibition. Since the swelling is caused by water diffusing from external surfaces to the core of the sample, by measuring the sample swelling over time, we obtained direct information about the transport of fluids through the intimate constituents of bone, where the mineralization process takes place. We developed an apparatus to measure the free expansion of the tissue during the imbibition. In particular, we measured the swelling along three natural axes (length $L$, width $W$, and thickness $T$) of plate-like trabeculae. For this aim, we developed a 3D analytical model of the water uptake by the sample that was performed according to Fickian transport mechanism. The results were then utilized to predict the swelling over time along the three sample directions ($L$, $W$, $T$) and the apparent diffusion coefficients $D_T$, $D_W$, and $D_L$.

## 1. Introduction

Transport phenomena within living tissues play an essential function for maintaining a proper supply of nutrients and for removing waste products. In bone tissue the transport of fluids and solutes is a concern for the bone formation and remodeling. These topics must be kept in mind when designing ECM-like scaffolds for tissue engineering to mimic the functions and structure of the biological materials [1].

Perhaps the most studied ECM with particular attention to its permeability and porosity is the bone tissue matrix. Bone is a dynamic and complex composite material with a composition of around 65 wt.% mineral phase, 25 wt.% organic, and 10 wt% water [2–8]. Referring to the volume fractions of the various parts, the bone volume (BV) is constituted by apatite minerals (33–43% BV) and organic constituents (32–44% BV) which are in turn composed of collagen type I (about 90%) and noncollagenous proteins (about 10%). The remnant is water (15–25% BV) [9] which plays a central role in the biomineralization process and contributes to the overall biomechanical properties of the biocomposite [10–12].

Water in bone may exist in three different forms: free water in pores, bound water in the collagen network (including collagen-mineral interface), and tightly bound water in the mineral phase [13, 14]. Bones with different water content display differences in stiffness and strength [15, 16]. Moreover, to describe the mechanical behavior of bone, the contribution of the bound water should be considered carefully by several viewpoints: first, the bound water in the collagen network will change the viscoelasticity of collagen phase dramatically [17, 18]; second, the bound water on the mineral-collagen interface will change the interfacial bonding properties [19]; third, water may migrate and change its local distribution

within the collagen matrix in response to stress localization, consequently introducing the nonuniform properties into the collagen phase.

Transport phenomena through the bone tissue are dictated by its hierarchical structure with four levels of porosity: collagen-apatite (~10 nm), lacunar-canalicular (~100 nm), vascular (~50 $\mu$m), and the intertrabecular porosity (~1 mm) [20]. The dimensions of the smallest pores (collagen-apatite porosity) are imposed by the intermolecular collagen bonds, that is, cross-links, the water content, and the degree of mineralization [21–24].

The water in the collagen structure was classified into 5 regimes [25] characterized by increasing water concentration from 0–0.010 g/g (regime I) to >0.5 g/g (regime V).

For the purposes of the present study it is important to point out that rehydrating the specimens from regime III causes a consistent large increase of the lateral spacing of the collagen molecules and thus produces a measurable swelling [26].

A small amount of studies was reported to our knowledge about the water dynamics and subsequent hygroexpansion in bone matrix. Diffusion coefficient [27] and water distribution [28] were measured by NMR, respectively, on rabbit and human cortical bone, while for trabecular bone few data about dimensional changes [29] and diffusion coefficient of single human trabeculae [30–33] are available.

The main scope of this work is to give experimental evidence of the fluid transport dynamics through the collagen-apatite porosity. To do that, the hygroexpansion of single human trabeculae consequent to water sorption was measured by means of a specially designed high accuracy dilatometer, and the results have been processed with the aid of a genetic algorithm.

The authors believe that this experimental investigation of transport phenomena within the bone matrix can offer a valuable support to the design of ECM-like scaffolds for bone tissue engineering. In fact, it is not sufficient for the scaffold to have the correct pore size but it should also exhibit proper connectivity to assure metabolic exchanges within the regenerating tissue.

## 2. Materials and Methods

*2.1. Specimens Preparation.* Four bone specimens of cancellous bone were extracted from human femur head withdrawn from a donor (female: age 67) suffering from moderate coxoarthritis (CA). Its caput was substituted by hip arthroplasty surgery. From preliminary dual-energy X-ray absorptiometry (DXA) a slight degree of osteopaenia was found. The bone tissue volume measured by a micro-CT apparatus [34] confirms substantially this finding. We did not use cadaveric femoral heads because it seemed important to evaluate the specimen without possible postmortem changes. After identification, the bone specimens were stored at −10°C for one month then, from the frontal-plane middle-site of the femoral head, a 10 mm thick slice was obtained for each bone specimen and stored again at −10°C for 10 hours. Subsequently, the slices were defatted by means of three complete cycles of dehydration with aqueous solutions with an increasing percentage of ethanol, 70%, 90%, and 99.9%, respectively. Between the dehydration cycles specimens were stored at −10°C for 10 hours. Bone specimen slices were then cut with a diamond saw (EXTEC Labcut 1010, Enfield CT) in order to obtain 10 × 10 × 10 mm blocks, which were further dehydrated and defatted by other three cycles with ethanol solutions at different concentrations, as previously described. Each single trabecula was dissected from a block corresponding with one of the main trabecular groups, coincident with the principal stress trajectories in the loaded femur, according to the well-known Wolff's law [35]. A dissecting microscope was used to locate uniform trabeculae which were excised with a scalpel. In order to avoid this measurement error, great care was adopted in excising a single trabecula; that is, the specimen was taken by extracting the portion located between two adjacent struts. The dimensions of the dissected trabeculae were measured with a vernier caliper (resolution 0.05 mm) prior to each test.

A total of 23 single trabeculae were initially prepared. Eight specimens presented general defects or broke up in the attempt to pin them to the test machine. Six specimens were used to gain experience with the test machine in order to obtain a preliminary estimate of the swelling behavior. Five specimens showed anomalous swelling, probably due to some microcracks created during the preparation and/or dissecting procedure, and were discarded. Thus only 4 single trabeculae were tested for the trials.

*2.2. Experimental Set-Up.* Referring to Figure 1, to measure the free expansion of the specimen during the imbibition, we developed *ad hoc* apparatus (APP) composed of a micropositioning stage (a) (M-410 DG, ±0.2 $\mu$m repeatability, Physik Instrumente, Germany) equipped by a steel rod and a strain gage load cell (b) (50 N full scale Vishay M1042-HBM, Germany). The APP was mounted in vertical position in order to accommodate a cylindrical container (c) of about 10 mL onto the free end of the load cell. Data sensed by the load cell was introduced into the strain gage amplifier (KWS 501A HBM, Germany), whereas the micropositioning is connected via RS232 serial cable to C-863 DC motor controller (Physik Instrumente, Germany).

During the start-up the steel rod was lowered on top surface of the specimen with a preload of 0.1 ± 0.01 N (mean value ± standard deviation). This preload was applied to assure proper but gentle fixation on top surface of the specimen between the load cell and the tip (d) of the pushing rod. Subsequently, the specimen was rapidly and totally submerged in distilled water.

As soon as the specimen begins to swell the micropositioning was moved upward by a feedback control system, processed by PID controller based on algorithm in NI Labview (National Instruments, Texas, USA) which actively maintains the applied preload at its constant value. The user sets a preload value due to actual demand, that is, the setpoint; as a consequence the current load cell signal acquired can be controlled to approach the set preload point. The output value of feedback loop controls the upward displacement of the micropositioning which measures the elongation in the axial direction of the trabecula caused by the hygroexpansion versus time.

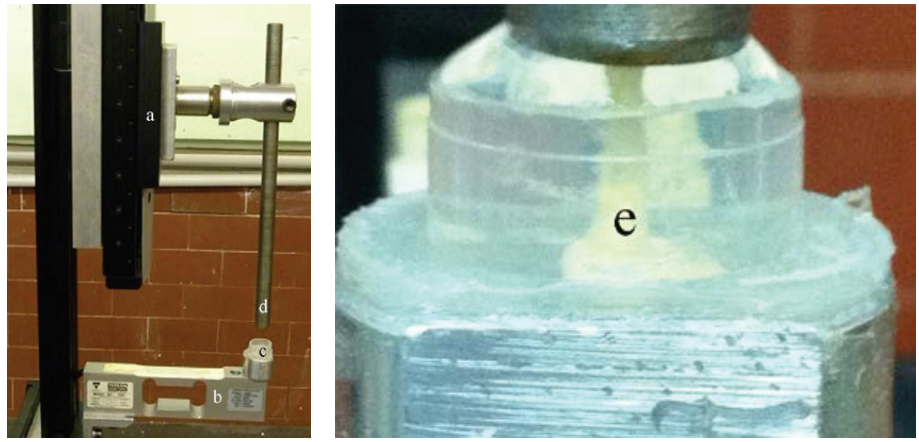


(a) (b)

Figure 1: The apparatus for the measurement of swelling of a single trabecula (e). Microtranslation stage (a); load cell (b); distilled water filled container (c); and pushing rod (d) for the imbibition of the specimen.

A total number of 12 swelling trials were performed on the four specimens along three axial directions ($L$, $W$, and $T$) of the trabecula.

The APP allowed for the measurement of the swelling along one axis at a time. In Figure 1(e) the distilled water filled container for the measurement of the swelling of the trabecular length is shown. After the execution of each trial relative to the hygroexpansion along one main axis of the trabecula (i.e., length, width, or thickness) the specimens were dried up at room temperature and humidity for 72 hours; then the trial was repeated for the other trabecular axes. Each trial was repeated five times and the mean hygroexpansion over time was computed. Standard deviation of the measured swelling dynamics was less than 5%.

The experiments were conducted at room temperature and relative humidity of $41 \pm 3\%$RH and $27 \pm 1^{\circ}$C, respectively (mean value ± standard deviation).

The two outputs signals from both the load cell and the micropositioning controller were also connected into the data acquisition system. It was built using a PXI 1031 mainframe equipped with a PXI 5122,14-bit digitizer, and PXI 8176 embedded controller (National Instruments, Texas, USA).

The data analysis software was programmed *ad hoc* and recorded in NI Labview. The graphical user interface (GUI) provides the user with complete control over all aspects of the swelling versus time. In this way, the APP operates as a high sensitivity dilatometer.

*2.3. Statistical Analysis.* All values are expressed as mean ± standard deviation. The exact Wilcoxon test was used to evaluate the differences of elongation between the axial directions of the specimens. The exact Friedman test (more than two time samples) and the exact paired Wilcoxon test (2 time samples) were applied to test for changes between time points. Two-sided $P$ values $< 0.05$ were considered statistically significant. A Bonferroni test was used to assess the changes in the elongation values for the two-tailed test. A value of $P < 0.05$ was significantly different. Statistical analysis [36] was performed using the Statistical Package for the Social Sciences for Windows (SPSS v. 20.0, Chicago, IL) program software package.

*2.4. Theoretical Framework.* The equations that describe the mass uptake over time in a porous sample of arbitrary shape immersed in a liquid [37] are analogous to that valid for the conduction of heat in solids [38]. The linear relationship between swelling and mass uptake is commonly accepted [39–47]. According to this approach, whose validity was confirmed by a comprehensive review conducted by [48], the experimental elongation data ($\Delta L_m$, $\Delta W_m$, $\Delta T_m$) measured along the principal axes $x$, $y$, and $z$ of the specimen have been fitted using the exact solution for a conventional diffusion problem in a porous three-dimensional medium. The theoretical elongations ($\Delta L$, $\Delta W$, and $\Delta T$) along $x$, $y$, and $z$ at time $t$, obtained by the application of Fick's law [38], are given by

$$\Delta L(t) = \int_{-L_x}^{L_x} \beta_x \cdot \left\{ 1 - \frac{64}{\pi^3} \sum_{n=0}^{\infty} \sum_{k=0}^{\infty} \sum_{p=0}^{\infty} \frac{(-1)^n}{2n+1} \cdot \frac{(-1)^k}{2k+1} \cdot \frac{(-1)^p}{2p+1} \cdot \cos\left[ (2n+1)\pi \frac{x}{2L_x} \right] \right.$$
$$\left. \cdot e^{-(D_x/4L_x^2)[(2n+1)\pi]^2 \cdot t} \cdot e^{-(D_y/4L_y^2)[(2k+1)\pi]^2 \cdot t} \cdot e^{-(D_z/4L_z^2)[(2p+1)\pi]^2 \cdot t} \right\} \cdot dx,$$

$$\Delta W(t) = \int_{-Ly}^{L_y} \beta_y \cdot \left\{ 1 - \frac{64}{\pi^3} \sum_{n=0}^{\infty} \sum_{k=0}^{\infty} \sum_{p=0}^{\infty} \frac{(-1)^n}{2n+1} \cdot \frac{(-1)^k}{2k+1} \cdot \frac{(-1)^p}{2p+1} \cdot \cos\left[ (2k+1)\pi \frac{y}{2L_y} \right] \right.$$

$$\cdot e^{-(D_x/4L_x^2)[(2n+1)\pi]^2\cdot t} \cdot e^{-(D_y/4L_y^2)[(2k+1)\pi]^2\cdot t} \cdot e^{-(D_z/4L_z^2)[(2p+1)\pi]^2\cdot t} \Bigg\} \cdot dy,$$

$$\Delta T(t) = \int_{-Lz}^{L_z} \beta_z \cdot \left\{ 1 - \frac{64}{\pi^3} \sum_{n=0}^{\infty} \sum_{k=0}^{\infty} \sum_{p=0}^{\infty} \frac{(-1)^n}{2n+1} \cdot \frac{(-1)^k}{2k+1} \cdot \frac{(-1)^p}{2p+1} \cdot \cos\left[ (2p+1)\pi \frac{z}{2L_z} \right] \right.$$

$$\left. \cdot e^{-(D_x/4L_x^2)[(2n+1)\pi]^2\cdot t} \cdot e^{-(D_y/4L_y^2)[(2k+1)\pi]^2\cdot t} \cdot e^{-(D_z/4L_z^2)[(2p+1)\pi]^2\cdot t} \right\} \cdot dz, \tag{1}$$

in which $D_x$, $D_y$, and $D_z$ and $\beta_x$, $\beta_y$, and $\beta_z$ are the mass diffusivities and the linear expansion coefficients along axes $x$, $y$, and $z$, respectively, whereas $2L_x$, $2L_y$, and $2L_z$ are the dimensions of the specimen, as shown in Figure 2. In this last figure the reference Cartesian coordinate system ($x$, $y$, and $z$), whose origin is located in the center of the sample, is also represented.

The determination of the values of the unknown variables $D_x$, $D_y$, and $D_z$ and $\beta_x$, $\beta_y$, and $\beta_z$, which represents the main aim of the present experimental work, is carried out by means of a genetic algorithm. As well known, genetic algorithms belong to the family of optimization methods usually called evolutionary algorithms, which can handle nonlinear problems defined on discrete search spaces in a faster way compared with other optimization methods. To this aim, a specifically developed computer code based on a genetic algorithm is used to fit a set of experimental measurements of the swelling along the three principal axes of a trabecula with $2L_x = 9$ mm, $2L_y = 2$ mm, and $2L_z = 0.5$ mm (denoted as single trabecula A).

The genetic algorithm generates the values of the unknown variables (the three mass diffusivities and the three linear expansion coefficients) that minimize the root of the mean square percentage errors between numerical results and experimental data, which is assumed as object function $\Phi$:

$$\Phi = \left( \sum_{i=1}^{N} \left\{ \frac{\left[ \left( \left( \Delta L(t_i) - \Delta L_{mi} \right) / \Delta L_{mi} \right) \times 100 \right]^2}{N} \right.\right.$$

$$+ \frac{\left[ \left( \left( \Delta W(t_i) - \Delta W_{mi} \right) / \Delta W_{mi} \right) \times 100 \right]^2}{N}$$

$$\left.\left. + \frac{\left[ \left( \left( \Delta T(t_i) - \Delta T_{mi} \right) / \Delta T_{mi} \right) \times 100 \right]^2}{N} \right\} \right)^{1/2}, \tag{2}$$

where the summation is extended to the $N$ measurements executed during time.

It is worth pointing out that although the value of each linear expansion coefficient could be obtained as the ratio between the elongation measured at steady state and the corresponding initial length, that is, $\Delta L_m/L$, $\Delta W_m/W$, and $\Delta T_m/T$, such direct calculation could lead to underestimated values if the steady state regime is not fully attained at the end of the experiment. Thus, it has seemed more correct to use such experimental values of the linear expansion coefficients to initialize the genetic algorithm and verify *a posteriori* that the results obtained are compatible with the experimental data. Similarly, the initial first-approximation values assumed for the unknown mass diffusivities ($D_x$, $D_y$, and $D_z$) are those obtained by interpolating the experimental elongation data during time using the unidimensional transient solution for the mass transfer in a porous medium [37]. For each variable, the range of existence has been set by assigning a ±40% interval around its initial value. The simulation procedure ends when the relative difference of the object function $\Phi$ given by (2) between two consecutive generations of unknown variables is smaller than the preassigned value of $10^{-2}$. To ensure that the solution found does not correspond to a local minimum, several simulations have been run by increasing the range of existence of each unknown variable around its initial value up to a ±100% interval. No significant change has been observed in the results obtained. Further details about the genetic code used in the present work can be found in [49].

## 3. Results

For the plate-like trabecula A, the values of $D_x$, $D_y$, and $D_z$ and $\beta_x$, $\beta_y$, and $\beta_z$ obtained through the genetic algorithm are reported in Table 1.

The comparison between the theoretical elongations (in mm) versus time along $x$, $y$, and $z$ of trabecula A, obtained from (1) using the values of $D_x$, $D_y$, and $D_z$ and $\beta_x$, $\beta_y$, and $\beta_z$, is listed in Table 1, and the corresponding experimental data is shown in Figure 3.

The validation of the results enumerated in Table 1 is carried out by reproducing numerically the experiments performed on three different trabeculae, denoted as B, C, and D, whose sizes along $x$, $y$, and $z$ are specified in Table 2.

The distributions of the theoretical elongations versus time, obtained using (1), and those of the corresponding experimental data are reported in Figure 4. An excellent agreement was found, that is, less than ±5% of relative error.

## 4. Discussion

The fit performed via genetic algorithm and (1) is excellent for the plate-like specimen A, as depicted in Figure 3.

By now, the average value ± standard deviation for the apparent diffusion coefficient $3.56 \cdot 10^{-11} \pm 0.78 \cdot 10^{-11}$ ($m^2\ s^{-1}$)

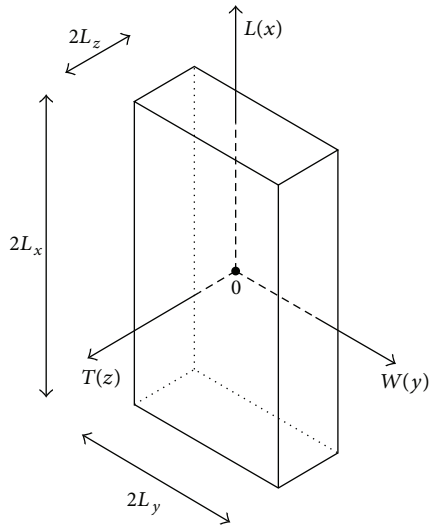


Figure 2: Sketch of the specimen geometry.

Table 1: Apparent diffusion coefficient and linear expansion coefficients for specimen A.

| Directions | Apparent diffusion coefficients ($m^2 \cdot s^{-1}$) | Linear expansion coefficients |
|---|---|---|
| Length ($2L_x$) | $D_x = 1.03 \cdot 10^{-9}$ | $\beta_x = 0.00195$ |
| Width ($2L_y$) | $D_y = 1.26 \cdot 10^{-10}$ | $\beta_y = 0.0053$ |
| Thickness ($2L_z$) | $D_z = 1.16 \cdot 10^{-11}$ | $\beta_z = 0.0107$ |

Table 2: Single trabeculae sizes.

| Single trabecula | Length—$2L_x$ (mm) | Width—$2L_y$ (mm) | Thickness—$2L_z$ (mm) |
|---|---|---|---|
| B | 7.9 | 2.6 | 2.5 |
| C | 6.3 | 2.3 | 0.5 |
| D | 7.2 | 2.1 | 1.7 |

was measured using NMR for four cortical bone specimens from rabbit tibia by [27]. The analysis of the discrepancies with respect to similar studies is beyond the scope of this work and should be investigated considering the different arrangement of the lamellae in trabecular or in osteonal cortical bone [50–52]. Also different initial and final water content are likely to affect the measured swelling by [22]. However a simple description could be proposed to find some match of our results with those described in [27]. Cortical bone is organized as a twisted and rotated plywood structure [50, 52] whereas in the trabecular bone tissue the collagen is aligned along the trabecular main axis [53]. The mass flux $F$ along the direction $r$ according to Fick's law is expressed as a function of the concentration gradient $dC/dr$ and the diffusion coefficient $D_r$:

$$F_r = -D_r \frac{dC}{dr}. \quad (3)$$

If along an axis the mass transport is equally subject to three different diffusion rates $D_1$, $D_2$, and $D_3$, such as

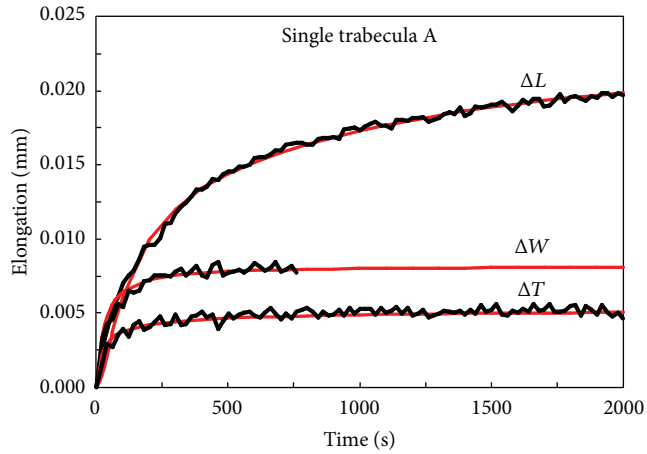


Figure 3: Comparisons between theoretical results (red line) and experimental data for single trabecula A.

what could happen through a twisted and rotated plywood structure, the overall apparent diffusion coefficient $D_o$ can be computed as follows:

$$D_o^{-1} = D_1^{-1} + D_2^{-1} + D_3^{-1}. \quad (4)$$

In our case, substituting $D_1$, $D_2$, and $D_3$ with $D_x$, $D_y$, and $D_z$ of Table 1 yields $D_o = 1.05 \cdot 10^{-11}$, in fair agreement with that of [27].

An important finding was represented by the different behaviour exhibited by plate-like versus rod-like specimens. In particular, using $D_x$, $D_y$, and $D_z$ found for specimen A does not allow a correct prediction of the swelling dynamics for rod-like trabeculae such as specimens B and D (Table 2) along some axis. This circumstance could be explained with a dissimilar nanostructure of the collagen-apatite porosity within the cross section, with respect to that of plate-like trabeculae. This in turn could be due to a marked anisotropy of the alignment of the apatite crystals caused by local loading conditions that, after remodelling, yielded a different momentum of inertia and thus flexural stiffness with respect to the plate-like trabeculae.

Regarding the measured linear expansion coefficients, the minor dimensional change along the axial direction is evident, which corresponds to the axis of the mineralized collagen fibrils, while the major swelling comes out along the thickness and width directions. This fairly agrees with the results of similar studies [54, 55].

## 5. Conclusion

We have illustrated the measurement of the swelling of single trabeculae from human femur heads during water imbibition. Moreover, since the swelling is caused by water diffusing from external surfaces to the core of the sample, by measuring the sample swelling versus time, we have obtained direct information about the transport of fluids through the intimate constituents of bone.

Our technique, based on the measurement of swelling, appeared actually sensitive on the water diffusion through the

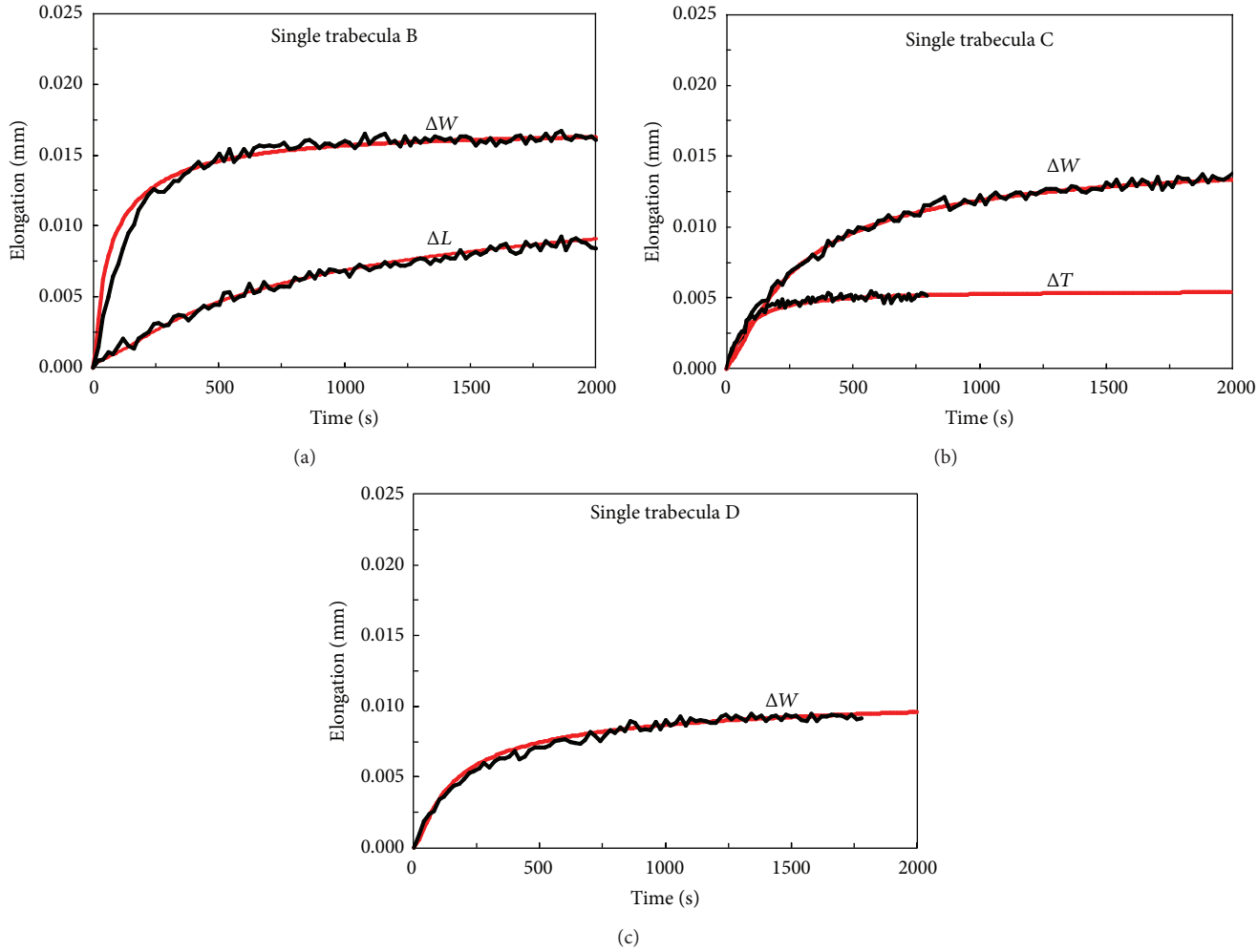


Figure 4: Comparisons between theoretical results (red line) and experimental data for single trabeculae (a) B, (b) C, and (c) D.

collagen bone matrix. As a consequence it may be argued that, in pathological tissue, deviations from normal fine structure reflecting in abnormal arrangements of collagen fibrils could be detected.

An important issue dealing with the present method is the quite cumbersome measurement of the specimen size since single trabeculae are often irregularly shaped yielding relatively dispersed results. However, these preliminary results are encouraging and suggest that further analysis on a consistent number of specimens could give a fundamental insight into the microstructure of bone tissue, depending on anatomical sites as well as normal or pathologic conditions.

To our knowledge, our study is the first measurement of the three apparent diffusion coefficient along each of the principal axis of human single trabeculae, revealing a marked anisotropy of transport phenomena within the Collagen Apatite bone matrix. In particular, the great difference among the measured diffusion coefficients $D_x$, $D_y$, and $D_z$ could provide additional in-depth data on fibre arrangement in the lamellar bone system in order to give further evidence of the relationship between the orientations of the fibre bundles.

In conclusion, since metabolic activities, adhesion, migration, and thus a proper growth of cells require proper nutrient diffusion that is in turn affected by cell-matrix interactions [1], we believe that the present work can be a valuable support to the design of ECM-like scaffolds for bone tissue engineering to optimize the transport phenomena and the mechanical properties of bone substitutes.

## Conflict of Interests

The authors declare that there is no conflict of interests regarding the publication of this paper.

## References

[1] S. C. Owen and M. S. Shoichet, "Design of three-dimensional biomimetic scaffolds," *Journal of Biomedical Materials Research A*, vol. 94, no. 4, pp. 1321–1331, 2010.

[2] J. E. Eastoe and B. Eastoe, "The organic constituents of mammalian compact bone," *Biochemical Journal*, vol. 57, no. 3, pp. 453–459, 1954.

[3] L. W. Fisher and J. D. Termine, "Noncollagenous proteins influencing the local mechanisms of calcification," *Clinical Orthopaedics & Related Research*, vol. 200, pp. 362–385, 1985.

[4] H. A. Lowenstam and S. Weiner, *On Biomineralization*, Oxford University Press, New York, NY, USA, 1989.

[5] R. B. Martin, D. Burr, and N. Sharkey, *Skeletal Tissue Mechanics*, Springer, New York, NY, USA, 1998.

[6] J. D. Currey, P. Zioupos, P. Davies, and A. Casinos, "Mechanical properties of nacre and highly mineralized bone," *Proceedings of the Royal Society B: Biological Sciences*, vol. 268, no. 1462, pp. 107–111, 2001.

[7] S. V. Dorozhkin and M. Epple, "Biological and medical significance of calcium phosphates," *Angewandte Chemie International Edition*, vol. 41, no. 17, pp. 3130–3146, 2002.

[8] J. D. Currey, "Role of collagen and other organics in the mechanical properties of bone," *Osteoporosis International*, vol. 14, supplement 5, pp. 29–36, 2003.

[9] J. D. Currey, "Biomechanics of mineralized skeletons," in *Skeletal Biomineralization: Patterns, Processes and Evolutionary Trends*, J. G. Carter, Ed., vol. 1, Van Nostrand Reinhold, New York, NY, USA, 1990.

[10] M. J. Olszta, X. Cheng, S. S. Jee et al., "Bone structure and formation: a new perspective," *Materials Science and Engineering R: Reports*, vol. 58, no. 3–5, pp. 77–116, 2007.

[11] A. J. Malcolm, "Metabolic bone disease," *Current Diagnostic Pathology*, vol. 8, no. 1, pp. 19–25, 2002.

[12] J. Yan, "Elastic-plastic fracture mechanics of compact bone," in *Materials Science & Engineering*, University of Florida, Gainesville, Fla, USA, 2005.

[13] X. Wang and S. Puram, "The toughness of cortical bone and its relationship with age," *Annals of Biomedical Engineering*, vol. 32, no. 1, pp. 123–135, 2004.

[14] S. Moelbert, B. Normand, and P. De Los Rios, "Kosmotropes and chaotropes: modelling preferential exclusion, binding and aggregate stability," *Biophysical Chemistry*, vol. 112, no. 1, pp. 45–57, 2004.

[15] J. S. Nyman, A. Roy, X. Shen, R. L. Acuna, J. H. Tyler, and X. Wang, "The influence of water removal on the strength and toughness of cortical bone," *Journal of Biomechanics*, vol. 39, no. 5, pp. 931–938, 2006.

[16] J. W. Smith and R. Walmsley, "Factors affecting the elasticity of bone," *Journal of Anatomy*, vol. 93, part 4, pp. 503–523, 1959.

[17] N. Sasaki and A. Enyo, "Viscoelastic properties of bone as a function of water content," *Journal of Biomechanics*, vol. 28, no. 7, pp. 809–815, 1995.

[18] J. Yamashita, B. R. Furman, H. R. Rawls, X. D. Wang, and C. M. Agrawal, "The use of dynamic mechanical analysis to assess the viscoelastic properties of human cortical bone," *Journal of Biomedical Materials Research*, vol. 58, no. 1, pp. 47–53, 2001.

[19] T. P. Knowles, A. W. Fitzpatrick, S. Meehan et al., "Role of intermolecular forces in defining material properties of protein nanofibrils," *Science*, vol. 318, no. 5858, pp. 1900–1903, 2007.

[20] S. C. Cowin, "Bone poroelasticity," *Journal of Biomechanics*, vol. 32, no. 3, pp. 217–238, 1999.

[21] S. Lees, "A mixed packing model for bone collagen," *Calcified Tissue International*, vol. 33, no. 6, pp. 591–602, 1981.

[22] S. Lees, J. D. Heeley, and P. F. Cleary, "Some properties of the organic matrix of a bovine cortical bone sample in various media," *Calcified Tissue International*, vol. 33, no. 1, pp. 83–86, 1981.

[23] S. Lees, M. Pineri, and M. Escoubes, "A generalized packing model for type I collagen," *International Journal of Biological Macromolecules*, vol. 6, no. 3, pp. 133–136, 1984.

[24] S. Lees, "Considerations regarding the structure of the mammalian mineralized osteoid from viewpoint of the generalized packing model," *Connective Tissue Research*, vol. 16, no. 4, pp. 281–303, 1987.

[25] M. H. Pineri, M. Escoubes, and G. Roche, "Water—collagen interactions: calorimetric and mechanical experiments," *Biopolymers*, vol. 17, no. 12, pp. 2799–2815, 1978.

[26] S. Nomura, A. Hiltner, J. B. Lando, and E. Baer, "Interaction of water with native collagen," *Biopolymers*, vol. 16, no. 2, pp. 231–246, 1977.

[27] M. A. Fernández-Seara, S. L. Wehrli, and F. W. Wehrli, "Diffusion of exchangeable water in cortical bone studied by nuclear magnetic resonance," *Biophysical Journal*, vol. 82, part 1, pp. 522–529, 2002.

[28] Q. Ni, J. S. Nyman, X. Wang, A. De Los Santos, and D. P. Nicolella, "Assessment of water distribution changes in human cortical bone by nuclear magnetic resonance," *Measurement Science and Technology*, vol. 18, no. 3, pp. 715–723, 2007.

[29] F. Marinozzi, F. Bini, and A. Marinozzi, "Evidence of entropic elasticity of human bone trabeculae at low strains," *Journal of Biomechanics*, vol. 44, no. 5, pp. 988–991, 2011.

[30] F. Marinozzi, F. Bini, and A. Marinozzi, "Water uptake and swelling in single trabeculæ from human femur head," *Biomatter*, vol. 4, no. 1, Article ID e28237, 5 pages.

[31] F. Marinozzi, F. Bini, and A. Marinozzi, "Hygroscopic swelling in single trabeculæ from human femur head," *Special Issue of the European Cells and Materials*, vol. 26, supplement 6, p. 109, 2013.

[32] F. Marinozzi, F. Bini, A. Marinozzi et al., "Experimental and theoretical analysis of water uptake and swelling kinetics of trabecular tissue from human femur head: some preliminary results," in *Proceedings of the 5th Biot Conference on Poromechanics (BIOT '13)*, pp. 1119–1127, Vienna, Austria, July 2013.

[33] W. B. Lievers, V. Lee, S. M. Arsenault, S. D. Waldman, and A. K. Pilkey, "Specimen size effect in the volumetric shrinkage of cancellous bone measured at two levels of dehydration," *Journal of Biomechanics*, vol. 40, no. 9, pp. 1903–1909, 2007.

[34] F. Marinozzi, F. Bini, A. Marinozzi et al., "Technique for bone volume measurement from human femur head samples by classification of micro-CT image histograms," *Annali dell'Istituto Superiore di Sanità*, vol. 49, no. 3, pp. 300–305, 2013.

[35] F. Bini, A. Marinozzi, F. Marinozzi, and F. Patanè, "Microtensile measurements of single trabeculae stiffness in human femur," *Journal of Biomechanics*, vol. 35, no. 11, pp. 1515–1519, 2002.

[36] M. Hollander and D. A. Wolfe, *Nonparametric Statistical Methods*, John Wiley & Sons, New York, NY, USA, 1973.

[37] J. Crank, *Mathematics of Diffusion*, Oxford University Press, New York, NY, USA, 1975.

[38] H. S. Carslaw and J. C. Jager, *Conduction of Heat in Solids*, Clarendon Press, Oxford, UK, 1959.

[39] T. Higuchi, "Mechanism of sustained-action medication. Theoretical analysis of rate of release of solid drugs dispersed in solid matrices," *Journal of Pharmaceutical Sciences*, vol. 52, no. 12, pp. 1145–1149, 1963.

[40] N. Wang and J. G. Brennan, "Changes in structure, density and porosity of potato during dehydration," *Journal of Food Engineering*, vol. 24, no. 1, pp. 61–76, 1995.

[41] E. H. Wong, R. Rajoo, S. W. Koh, and T. B. Lim, "The mechanics and impact of hygroscopic swelling of polymeric materials in electronic packaging," *Journal of Electronic Packaging*, vol. 124, no. 2, pp. 122–126, 2002.

[42] H. Ardebili, E. H. Wong, and M. Pecht, "Hygroscopic swelling and sorption characteristics of epoxy molding compounds used in electronic packaging," *IEEE Transactions on Components and Packaging Technologies*, vol. 26, no. 1, pp. 206–214, 2003.

[43] E. Stellrecht, B. Han, and M. G. Pecht, "Characterization of hygroscopic swelling behavior of mold compounds and plastic packages," *IEEE Transactions on Components and Packaging Technologies*, vol. 27, no. 3, pp. 499–506, 2004.

[44] H. Shirangi, J. Auersperg, M. Koyuncu, H. Walter, W. H. Müller, and B. Michel, "Characterization of dual-stage moisture diffusion, residual moisture content and hygroscopic swelling of epoxy molding compounds," in *Proceedings of the International Conference on Thermal, Mechanical and Multi-Physics Simulation and Experiments in Microelectronics and Micro-Systems (EuroSimE '08)*, pp. 455–462, Freiburg, Germany, April 2008.

[45] L. A. Bulavin and O. Y. Aktan, "Molecular mechanisms of water diffusion in collagen-like structures," *Ukrainian Journal of Physics*, vol. 54, no. 6, pp. 575–578, 2009.

[46] J. Yoon, S. Cai, Z. Suo, and R. C. Hayward, "Poroelastic swelling kinetics of thin hydrogel layers: comparison of theory and experiment," *Soft Matter*, vol. 6, no. 23, pp. 6004–6012, 2010.

[47] K. Huanbutta, P. Sriamornsak, S. Limmatvapirat et al., "Swelling kinetics of spray-dried chitosan acetate assessed by magnetic resonance imaging and their relation to drug release kinetics of chitosan matrix tablets," *European Journal of Pharmaceutics and Biopharmaceutics*, vol. 77, no. 2, pp. 320–326, 2011.

[48] L. Mayor and A. M. Sereno, "Modelling shrinkage during convective drying of food materials: a review," *Journal of Food Engineering*, vol. 61, no. 3, pp. 373–386, 2004.

[49] M. Corcione and L. Fontana, "Optimal design of outdoor lighting systems by genetic algorithms," *Lighting Research & Technology*, vol. 35, no. 3, pp. 261–277, 2003.

[50] M. M. Giraud-Guille, "Twisted plywood architecture of collagen fibrils in human compact bone osteons," *Calcified Tissue International*, vol. 42, no. 3, pp. 167–180, 1988.

[51] A. Ascenzi and A. Benvenuti, "Orientation of collagen fibers at the boundary between two successive osteonic lamellae and its mechanical interpretation," *Journal of Biomechanics*, vol. 19, no. 6, pp. 455–463, 1986.

[52] S. Weiner, T. Arad, I. Sabanay, and W. Traub, "Rotated plywood structure of primary lamellar bone in the rat: orientations of collagen fibril arrays," *Bone*, vol. 20, no. 6, pp. 509–514, 1997.

[53] D. Jaschouz, O. Paris, P. Roschger, H.-S. Hwang, and P. Fratzl, "Pole figure analysis of mineral nanoparticle orientation in individual trabecula of human vertebral bone," *Journal of Applied Crystallography*, vol. 36, no. 3, pp. 494–498, 2003.

[54] J. B. Finlay and W. R. Hardie, "Anisotropic contraction of cortical bone caused by dehydration of samples of the bovine femur in vitro," *Proceedings of the Institution of Mechanical Engineers H*, vol. 208, no. 1, pp. 27–32, 1994.

[55] F. S. Utku, E. Klein, H. Saybasili, C. A. Yucesoy, and S. Weiner, "Probing the role of water in lamellar bone by dehydration in the environmental scanning electron microscope," *Journal of Structural Biology*, vol. 162, no. 3, pp. 361–367, 2008.

Hindawi Publishing Corporation
BioMed Research International
Volume 2014, Article ID 756078, 10 pages
http://dx.doi.org/10.1155/2014/756078

*Review Article*

# Extracellular Matrix Modulates Angiogenesis in Physiological and Pathological Conditions

**Anna Neve,[1] Francesco Paolo Cantatore,[1] Nicola Maruotti,[1] Addolorata Corrado,[1] and Domenico Ribatti[2,3]**

[1] *Rheumatology Clinic, Department of Medical and Surgical Sciences, University of Foggia, Ospedale "Col. D'Avanzo", 71121 Foggia, Italy*
[2] *Department of Basic Medical Sciences, Neurosciences and Sensory Organs, Section of Human Anatomy and Histology, University of Bari Medical School, 70124 Bari, Italy*
[3] *National Cancer Institute "Giovanni Paolo", 70124 Bari, Italy*

Correspondence should be addressed to Domenico Ribatti; domenico.ribatti@uniba.it

Received 16 January 2014; Accepted 27 February 2014; Published 18 May 2014

Academic Editor: Silvia Baiguera



Angiogenesis is a multistep process driven by a wide range of positive and negative regulatory factors. Extracellular matrix (ECM) plays a crucial role in the regulation of this process. The degradation of ECM, occurring in response to an angiogenic stimulus, leads to degradation or partial modification of matrix molecules, release of soluble factors, and exposure of cryptic sites with pro- and/or antiangiogenic activity. ECM molecules and fragments, resulting from proteolysis, can also act directly as inflammatory stimuli, and this can explain the exacerbated angiogenesis that drives and maintains several inflammatory diseases. In this review we have summarized some of the more recent literature data concerning the molecular control of ECM in angiogenesis in both physiological and pathological conditions.

## 1. Introduction

The extracellular matrix (ECM) is the noncellular component present within all tissues and organs, consisting of a variety of structural and signalling molecules secreted from differentiated mesenchymal cells including chondrocytes and fibroblasts and with biochemical, biomechanical, and structural properties critical for the development of organs.

The ECM provides mechanical adhesive support for the cellular constituents, directs their morphological organization, and influences physiological functions, by binding growth factors and interacting with cell-surface receptors. Two biochemically and morphologically differentiated entities have been identified: the interstitial matrix and the extracellular basement membranes (BMs). The first one is mainly composed of fibrillar and nonfibrillar collagens, elastic fibers, and glycosaminoglycan- (GAG-) containing noncollagenous glycoproteins (hyaluronan and proteoglycans) (Figure 1(a)). The BMs are highly specialized extracellular matrix sheets underlining epithelial or endothelial cells, consisting of collagen IV, laminins, entactin, and heparan sulfate proteoglycans (Figure 1(b)), which affect cell shape, gene expression, proliferation, migration, and apoptosis.

The ECM is a highly dynamic structure, undergoing continuous remodelling, which consists in the deposition, degradation, and modification of its components. An abnormal ECM dynamic leads to pathological processes including tissue fibrosis and cancer.

The three-dimensional (3D) and computational *in vitro* studies [1, 2] clearly demonstrate that besides its remodelling ECM controls and regulates physiological and pathological angiogenesis [3] at several levels by several ways.

Angiogenesis has been studied by means of several *in vitro* and *in vivo* models, including endothelial cell cultures, chick embryo chorioallantoic membrane (CAM) assay [4], and ocular models [5]. Angiogenesis is a multistep process that generally begins when the endothelial cells switch from the "quiescent" to the "angiogenic phenotype" in response to

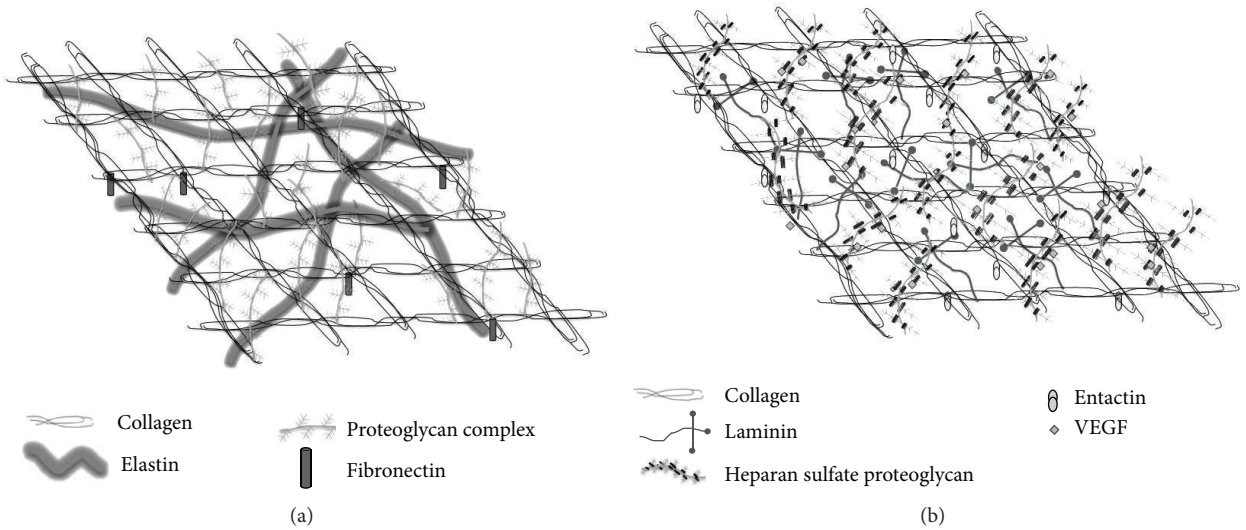


Figure 1: A schematic drawing of the extracellular matrix molecular organization. The interstitial matrix is mainly composed of collagen, fibronectin, elastin, and proteoglycans (a). The extracellular basement membrane mainly consists of collagen IV, laminin, entactin, and heparan sulfate proteoglycans which bind to VEGF (b).

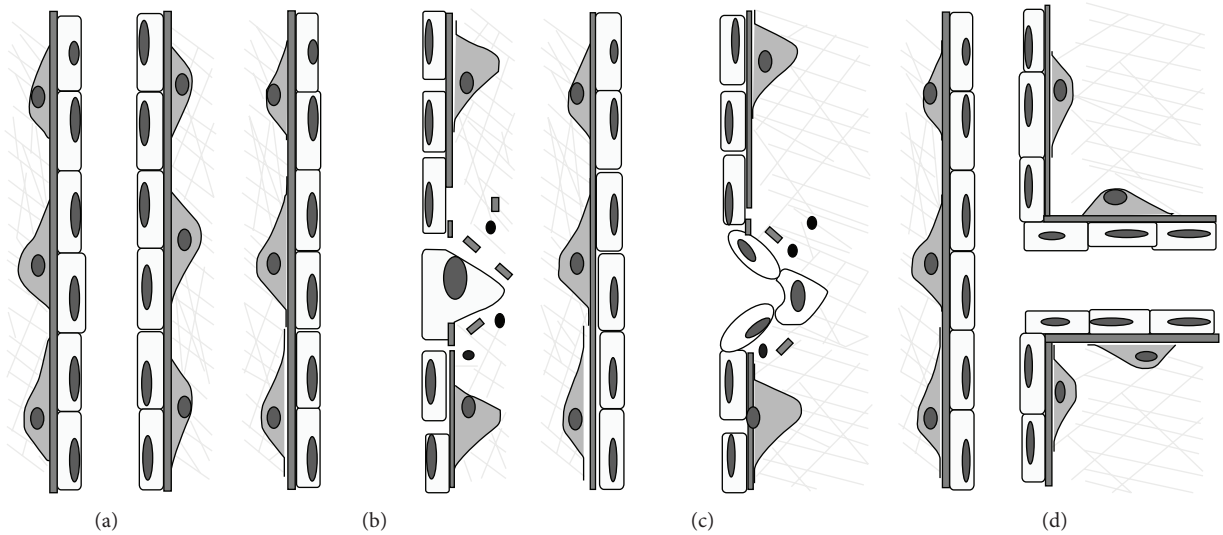


Figure 2: After stimulation with angiogenic factors of a quiescent vessel (a), the degradation of the basement membrane, pericyte detachment, and loosening of endothelial cell junctions occur (b). Endothelial cells begin to proliferate, migrate, and take part in formation of an immature capillary structure and deposition of a new complex basement membrane (c). Finally, pericytes are recruited thereby providing stabilization for the new vessel (d).

angiogenic stimuli [6, 7] (Figure 2). Subsequently, enzymatic degradation of capillary BM occurs and vascular permeability increases leading to extravasation of blood proteins and their accumulation into interstitial collagen matrix to form a new, provisional ECM. Then, endothelial cells begin to proliferate, invade the ECM, and take part in the formation of an immature capillary structure and deposition of a new complex BM. Finally, pericytes are recruited, thereby providing stabilization for the new vessels. The soluble growth factors, membrane-bound proteins, cell-matrix and cell-cell interactions, and hemodynamic forces all act in concert to control and influence angiogenesis, and the balanced activity between specific angiogenic molecules which can initiate this process and specific inhibitory molecules which can stop it are thought to be critical for an optimal angiogenic response.

Through adhesive interactions with integrins expressed on the endothelial cells surface, the ECM orchestrates complex signalling cascades within the cells and affects many fundamental aspects of their biology, including proliferation, migration, cytoskeletal organization, cell shape, survival, and ultimately blood vessel stabilization. Moreover, matrix molecules or fragments that show pro- and antiangiogenic

Table 1: ECM molecules and fragments with proangiogenic and antiangiogenic activity.

| Proangiogenic | Antiangiogenic |
|---|---|
| *Intact molecules* | *Fragments* |
| Collagen I | |
| Collagen III | Arresten |
| Collagen IV | Canstatin |
| Collagen XV | Tumstatin |
| Collagen XVIII | Restin |
| Fibrillin | Endostatin |
| Fibulin-1 | Anastellin |
| Fibrin/fibrinogen | Heparin binding fragments |
| Fibronectin | Endorepellin |
| Glypican-1 | Endostatin |
| Laminin-1 | Elastin derived peptides |
| Laminin 8 | *Transient molecules* |
| Perlecan | Thrombospondin-1 |
| Tenascin C | Thrombospondin-2 |
| Tenascin X | |
| Vitronectin | |
| Decorin | |
| *Fragments* | |
| Fragment E (fibrin) | |

activity (Table 1) are critical in the onset of angiogenesis and angiogenic cytokines which directly bind matrix and require proteolytic processing to become active [8].

## 2. ECM Components Involved in Angiogenesis

*2.1. ECM Molecules.* *In vivo* studies in knockout mice for BMs genes (fibronectin, laminin, collagen IV, and perlecan) revealed significant cardiovascular dysfunctions [9–11]. In detail, several studies bear out the hypothesis that blood vessels formation and survival are connected with collagen synthesis and deposition in BM [12, 13]. Endothelial cell adhesion to ECM, via integrins-collagen I interaction, leads to activation and/or suppression of multiple signalling pathways. In human dermal microvascular endothelial cells, isolated from neonatal foreskins and anchored to collagen I, as well as in a mouse model of skin angiogenesis involving subdermal injection of Matrigel together with immortalized human cells stably transfected with VEGF165, the interaction of collagen I with $\alpha 1\beta 1$, $\alpha 2\beta 1$, $\alpha v\beta 3$, and $\alpha v\beta 5$ integrins on cell surfaces induces the activation of MAP kinase pathway which, in turn, supports endothelial cells survival and suppresses apoptosis [14]. In the same *in vitro* model, other investigators demonstrated that integrins $\alpha 1\beta 1$ and $\alpha 2\beta 1$ binding to collagen I induced suppression of cAMP-dependent PKA, following reorganization of actin fibers and changes in cell shape [15]. In mouse skin model that used VEGF-expressing cells together with packaging cells producing retroviruses encoding RhoA GTPase mutants, the endothelial cells adhesion to collagen I selectively induced activation of Src and Rho and suppression of Rac activity, which, in turn, disrupt intercellular junctions [16]. Interestingly, collagen I also contributes to coalescence of pinocytic intracellular vacuoles, which is an essential step for lumen formation [17, 18].

Type IV collagen, the main protein component of all BMs, has a crucial role in endothelial cell proliferation and cell behaviour [19]. An *in vitro* study that analysed angiogenic and nonangiogenic culture systems demonstrated the dependence of angiogenesis on secretion and subsequent extracellular deposition of collagen type IV [20].

Laminin of BM appears to be involved prevalently in the regulation of the late stages of angiogenesis: it is responsible for cessation of endothelial cells proliferation and pericytes recruitment and vessels stabilization through Notch signalling activation [21]. By using antibodies directed to laminin receptor, it has been demonstrated that laminin can activate proteinases and contribute to matrix degradation [22].

Fibronectin is a widely distributed glycoprotein and is a component of plasma in a soluble dimeric form and of cell surface and ECM in a dimeric and multimeric form and is localized in ECM underlying endothelial cells. The arginine-glycine-aspartic acid (RGD) motif was the first sequence of fibronectin found to possess cell-adhesive properties [23] and the use of the microfluidic shear devices suggested that endothelial cells adhere to fibronectin stronger than type I collagen [24]. The binding of RGD sequence to the integrins $\alpha 5\beta 1$ and $\alpha v\beta 3$ in endothelial cells initiates the polymerization of fibronectin locally synthesized [25], which, in turn, regulates cell growth as demonstrated in cultures of mouse embryonic cells that lack endogenous fibronectin [26], regulates cytoskeletal organization [27], and stabilizes cell-matrix adhesion [28]. Additionally, fibronectin controls endothelial cell survival during angiogenesis *in vivo* by suppressing the activity of PKA [29]. Plasma fibronectin incorporated in the serum-free collagen gel culture of rat aorta induced a selective dose-dependent elongation of microvessels, without affecting mitotic activity of cells [30].

*2.2. ECM Fragments: Matrikines and Matricryptic Sites.* In the early stage of angiogenesis, the degradation of ECM occurs in response to angiogenic stimuli. As a consequence, matrix molecules are degraded or partially modified, soluble factors are released, and cryptic sites are exposed.

In 1960, the presence of small peptides derived from degradation of connective tissue glycoproteins was demonstrated for the first time [31]. Maquart et al. [32] introduced the term "matrikines" to designate peptides produced from degradation of ECM components, as result of enzymatic activity of proteinases produced by connective tissue cells. The same term has been then adopted to describe peptides derived by partial proteolysis of ECM surrounding microvessels. Endothelial cells produce proteinases, whose activation is responsible for degradation and liberation of matrix fragments which, in turn, can regulate cellular activity by binding specific cells receptors and by activating intracellular signalling pathways.

The term "matricryptic sites" has been coined to describe the biologically active sites that are not exposed in the mature,

secreted form of ECM molecules but which become exposed after structural or conformational alterations [33].

Two classes of proteolytic enzymes appear to be mainly involved in the matrix degradation: plasminogen activator (PA)/plasmin system and matrix metalloproteinases (MMPs). The plasminogen activator/plasmin system is an enzymatic cascade involved in the control of fibrin degradation, matrix turnover, and cell invasion. The physiological activators urokinase-type PA or tissue-type PA mediate the conversion of the inactive plasma zymogen, plasminogen, to the serine protease plasmin. The latter belongs to the large serine proteinase family and can act directly or indirectly, by cleaving numerous ECM proteins, including fibronectin, laminin, thrombospondin, and von Willebrand factor [34], by activating MMPs [35], or by liberating growth factors and cytokines sequestered within the ECM [36, 37].

MMPs belong to the family of zinc endopeptidases and can exist in both membrane-bound (MT-MMPs) and soluble forms. The latter are secreted as inactive proenzymes and their activation occurs in the extracellular compartment. MMPs are produced by a variety of cells, including epithelial cells, fibroblasts, inflammatory cells, and endothelial cells, and their activity is inhibited by the family of tissue inhibitors of metalloproteinase (TIMPs) [38]. At least, five MMPs are involved in angiogenesis: MMP-1, -2, -3, -7, and -9 are upregulated in endothelial cells in a variety of physiological and pathological settings [35].

Many of matrikines and matricryptic sites, resulting from PA/plasmin system and MMPs activity, are important physiologic angiogenesis inhibitors. Among these, endostatin has been extensively studied. It is a proteolytic fragment of the C-terminal noncollagenous domain of collagen XVIII, isolated from the conditioned media of a nonmetastatic murine hemangioendothelioma cell line [39]. Its role as a local inhibitor of angiogenesis has been demonstrated *in vitro* and *in vivo* [39, 40]; nevertheless, the evidence that lack of endostatin does not affect angiogenesis in major organs suggests that this fragment is not a critical regulator of angiogenesis [41]. Endostatin acts by inhibiting endothelial cells proliferation and migration [39] and by blocking G1/S phase transition and apoptosis of cells [42, 43]. Immunoblotting analysis of endostatin treated murine brain endothelial cells revealed that endostatin induces activation of phosphatases or other regulatory signalling proteins, which may interfere with FGF effects on endothelial cells; nevertheless, this occurs only if endostatin binds to the endothelial cell surface via heparan-sulfate proteoglycans [44, 45]. Moreover, endostatin inhibits VEGF-induced endothelial cell migration in a dose-dependent manner [46].

Tumstatin, canstatin, and arresten are derived from degradation of $\alpha$3, $\alpha$2, and $\alpha$1 chain, respectively, of type IV collagen. Tumstatin, generated by MMP-9 proteolysis [47], binds to endothelial cells via $\alpha v\beta_3$ integrin [48]. Its antiangiogenic activity is restricted to amino acids 54–132 within the 244 amino acid complete sequence [49]. *In vitro* studies showed that tumstatin peptide negatively regulates endothelial cells proliferation and induces apoptosis [50] through inhibition of protein synthesis [51]. Canstatin in an antiangiogenic fragment derived from NC1 domain of the $\alpha$2 chain of type IV collagen [52]. Recombinant canstatin selectively inhibits endothelial cells proliferation and tube formation in a dose-dependent manner [53]. Moreover, in human umbilical vein endothelial cells, canstatin inhibits the phosphorylation of Akt and focal adhesion kinase, induces Fas ligand expression, and activates caspase-dependent apoptotic pathways [54]; all these activities are mediated by interaction with $\alpha v\beta_3$ and $\alpha v\beta_5$ integrins on the surface of endothelial cells [55]. Arresten binds to $\alpha 1\beta 1$ integrin and heparan sulphate proteoglycans and exerts its antiangiogenic effect in endothelial cells via inhibition of MAPK signalling [56, 57]. Arresten inhibits, in a dose-dependent manner, the proliferation of mouse retinal endothelial cells cultured on type IV collagen and stimulated with fibroblast growth factor-2 (FGF-2) [58]. *In vivo*, arresten significantly inhibits neovascularization in Matrigel plug assays [59].

Tetrastatin, pentastatin, and hexastatin are derived from degradation of type IV collagen, from $\alpha$4, $\alpha$5, and $\alpha$6 chain, respectively. Tetrastatin and pentastatin lack antiangiogenic activity in the CAM assay [48]; nevertheless, *in vitro* they affect angiogenesis by interacting with human endothelial cells and potently inhibiting their migration [60]. On the other hand, hexastatin administration resulted in inhibition of angiogenesis in the CAM [48] and in Matrigel plug assay [61]. Additionally, through the non-RGD-dependent $\alpha v\beta 3$ binding sites, hexastatin significantly inhibits endothelial cell proliferation [61].

Endorepellin is derived from perlecan [62] and by interacting with the $\alpha 2\beta 1$ integrin receptor triggers a signalling cascade that leads to disruption of the endothelial actin cytoskeleton [63]. Endorepellin affects angiogenesis by interacting with the VEGF receptor through its laminin G-like, leading to the downstream of VEGF signalling [64, 65].

*2.3. Angiogenic Factors.* The role of VEGF as major inducer of angiogenesis is well recognized [66]. VEGF induces expression of $\alpha 1\beta 1$ and $\alpha 2\beta 1$ integrins in microvascular endothelial cells [67], endothelial cell migration, and proliferation [68, 69]. VEGF is not stored intracellularly but it bounds the cell surface or ECM and various MMPs [70] and PA [71] can generate diffusible, non-heparin-binding fragments. Two classes of VEGF binding sites have been identified on fibronectin: one constitutively available and the other whose availability is modulated by the conformational state of fibronectin, which, in turn, depends on heparin interaction [72, 73].

FGF-2 stimulates survival, proliferation, migration, and differentiation of endothelial cells both *in vitro* and *in vivo* and binds with high affinity to heparan sulfate proteoglycans located on the surface of most cells and within the ECM [74]. Heparan sulfate proteoglycans, particularly perlecan, modulate the binding of FGF-2 to its specific tyrosine kinase receptors [75] and protect the growth factor from proteolytic degradation by extracellular proteinases [76].

The proangiogenic activity of transforming growth factor beta 1 (TGF-$\beta$1) has been demonstrated in new-born mice [77] and in the CAM assay [78] and it has been confirmed in TGF-$\beta$1 knockout mice [79]. However, *in vitro* studies suggested that activity of TGF-$\beta$1 is strictly dependent on

composition and organization of the ECM: TGF-$\beta$1 treatment elicits the formation of calcium and magnesium dependent tube-like structures, mimicking angiogenesis, in three-dimensional cultures [80], whereas it induces endothelial cells apoptosis in two-dimensional cultures [81]. TGF-$\beta$1 upregulates the VEGF expression and the interaction with its receptor in endothelial cells and this mechanism induces endothelial cell apoptosis and angiogenesis *in vitro* and *in vivo* [82, 83].

## 3. ECM as a Link between Angiogenesis and Inflammation

Angiogenesis and inflammation are distinct processes that can occur independently of each other, although in some cases they are codependent. Angiogenesis can stimulate and intensify the inflammatory response by providing nutrients and oxygen in inflammatory sites, and some angiogenic factors exert proinflammatory activity. Conversely, in chronic inflammation, inflammatory cells produce cytokines and growth factors that may affect endothelial cell functions.

Angiogenesis and inflammation are associated with nuclear factor kappa-B (NF-$\kappa$B) and angiopoietin- (Ang-) Tie2 signalling pathways. NF-$\kappa$B is an inducible transcription factor, whose activation regulates the expression of genes for proinflammatory cytokines, chemokines, and enzymes that generate mediators of inflammation. There is also evidence that this transcription factor is involved in the regulation of migration, proliferation and survival of endothelial cells [84], and expression of MMPs [85]. Ang-1 is secreted and incorporated into and sequestered by the ECM. By binding Tie-2 receptor expressed in endothelial cells, it does not affect the cells proliferation; however, it stimulates endothelial cells migration, sprouting, and survival and promotes recruitment of the pericytes and smooth muscle cells [86]. Mice lacking of Ang-1 and Tie-2 showed defective remodelling and maturation of the vasculature, whereas the transgenic mice overexpressing Ang-1 displayed increased vascularization suggesting a role in the formation of blood vessels during development [87]. Additionally, Ang-1 has been shown to inhibit vascular permeability and exert anti-inflammatory effects [88]. It has been demonstrated that Ang-1 can act also in nonendothelial cells, including monocytes via p38 and Erk1/2 phosphorylation and macrophages inducing their switch toward a proinflammatory phenotype [89]. Unlike Ang-1, its antagonist, Ang-2, is not incorporated into ECM and disrupts blood vessel formation in the mouse embryo [90]. Stored in endothelial Weibel-Palade bodies, Ang-2 is rapidly released in response to exogenous stimuli and promotes inflammation [91].

Angiogenesis and inflammation share ECM remodelling which, in turn, directly and indirectly influences both processes. ECM molecules and fragments, resulting from proteolysis, can act directly as inflammatory stimuli; they can influence immune cell activation and survival and proper tissue repair as well as each step of angiogenesis, as previously described.

Inflammatory cells produce a large amount of MMPs, which activate cytokines and chemokines through cleavage, regulate inflammatory cells response, and notably contribute to ECM degradation. Analysis of RNA levels expression in mononuclear cells isolated from venous blood of normal volunteers revealed that they highly express several forms of MMPs [92]. Expression of MMPs can be selectively induced by binding of bacteria to toll-like receptor 2 in monocytes and CD14, toll-like receptor 2, and toll-like receptor 1 in macrophages and is strictly dependent on the stage of cellular differentiation [93, 94].

The role of inflammation in tumor development is not less negligible: an inflammatory microenvironment can increase mutation rates and enhance the proliferation of cancer cells, contributing to tumor initiation, and innate and adaptive immune system cells can infiltrate the tumor sites, release growth and survival factors, and facilitate angiogenesis, tumor growth, invasion, and metastasis by themselves or by inducing other effector molecules. The increase of several immune cell-derived factors, such as interleukin-1 (IL-1), IL-6, IL-8, IL-10, and tumor necrosis factor alpha (TNF-$\alpha$), has been described in tumor microenvironment: they sustain inflammatory process, contribute to tumor progression, and also exert proangiogenic activity [95, 96].

Osteopontin (OPN), a multifunctional ECM phosphoprotein-containing and RGD integrin binding domain, is limited to the bone, kidney, and epithelial linings and is secreted in body fluids including milk, blood, and urine in normal conditions, whereas it is upregulated at sites of inflammation and tissue remodelling. Chakraborty et al. [97] provided both *in vitro* and *in vivo* experimental evidences that OPN regulates Brk/NF-$\kappa$B/ATF-4 signalling cascades which, in turn, upregulates the VEGF expression and tumor angiogenesis through autocrine and paracrine mechanisms in breast cancer system.

Inflammatory cells release MMPs involved in the release of angiogenic factors, such as VEGF and FGF-2, and cryptic antiangiogenic factors. VEGF derived from matrix stores, as a result of MMP-9, is implicated in the angiogenic switch and tumor growth [98].

Rheumatoid arthritis (RA) is an autoimmune disease characterized by chronic inflammation of synovial joints and destruction of cartilage and bone, as well as by systemic extra-articular inflammation. The synovium that normally is relatively acellular and with scattered blood vessels, results hyperplastic, rich of inflammatory cells and high vascularized in RA. The new vessels besides provide nutrients and oxygen, also sustain the inflammation by being a source of cytokines, chemokines, and proteases [99], facilitate the ingress of inflammatory cells into the synovium, and, therefore, stimulate pannus formation. At the same time, infiltrated inflammatory cells stimulate angiogenic process, by upregulating proangiogenic factors [100, 101] and activating NF-$\kappa$B. Upregulation of Angs-Tie 2 [102] and VEGF [103] detected in chronic inflamed synovium and serum of RA patients emphasizes the interdependence of inflammation and angiogenesis in RA. VEGF may act as a proinflammatory mediator and as an angiogenic stimulator in RA joints: it induces the production of chemokines by endothelial cells, such as MCP-1 and IL-8 [104], which, in turn, recruit monocytes in synovial membranes. Several clinical studies

demonstrated high levels of MMPs, directly involved in ECM degradation, in the systemic circulation and synovial fluid of patients with RA and their correlation with clinical activity [105, 106].

Osteoarthritis (OA) is a disease characterized by degeneration of cartilage and its underlying bone within a joint as well as bony overgrowth. Even if OA has been commonly described as "noninflammatory" disorder, in order to distinguish it from inflammatory arthritis, evidence is now accumulating that synovitis occurs and exacerbates structural damage [107, 108]. The inflammation contributes directly to angiogenesis, observed in the synovium of osteoarthritic joints [107], and these two processes contribute to pain and damage. Hypoxia, a common feature of the inflamed synovial environment, and IL-1 stimulate VEGF expression in synovial fibroblasts [109]. Also TNF-$\alpha$, which promotes angiogenesis *in vivo* [110] and regulates the expression of MMP-9 and MMP-1 [111], is involved in OA. Thus, angiogenesis may exacerbate inflammation in OA, by facilitating inflammatory cell infiltration [111].

Psoriasis is a chronic inflammatory disease of skin and small joints characterized by excessive growth of the epidermal keratinocytes, inflammatory cell accumulation, and excessive dermal angiogenesis. Psoriasis is characterized by the overproduction of interferon gamma (INF-$\gamma$), TNF-$\alpha$, and IL-17 [112]. TNF-$\alpha$ induced upregulation of IL-24 and activation of signal transducer and activator of transcription 3 (STAT3) signalling in mice keratinocytes [113]. IL-9 contributes to the development of psoriatic lesions, by inducing Th17-related inflammation and by promoting angiogenesis [114]. Keratinocytes in the psoriatic skin lesions are a source of proangiogenic cytokines, such as VEGF, whose levels have been shown to be dramatically elevated in human psoriatic skin [115] and correlate with increased levels of inflammatory cytokines and MMPs [116] and with degree of psoriasis severity [117]. Additionally, keratinocytes isolated from psoriatic skin show a strongly reduced expression of thrombospondin-1, an endogenous inhibitor of angiogenesis. Enzyme immunoassay [118] and immunohistochemistry analysis [119] revealed that keratinocytes in psoriasis express and produce MMP-1 and MMP-19, which are decreased by anti-TNF-alpha [120].

Ocular angiogenesis is an important cause for severe loss of vision in several disorders, such as age-related macular degeneration, diabetic retinopathy, retinal artery or vein occlusion, and retinopathy of prematurity. Even if the mechanism that leads to abnormal growth of new vessels in eyes remains to be elucidated, it is related to inflammation. VEGF, as well as IL-6, IL-8, and IL-10, monocyte chemoattractant protein-1 levels are higher in patients with ocular diseases, when compared with normal subjects, and significantly decreased after administration of bevacizumab, a humanized anti-VEGF monoclonal IgG1 antibody [121, 122]. VEGF intravitreal injection induced upregulation of intercellular adhesion molecule in endothelial cells and, consequently, the local adhesion of leucocytes and vascular permeability [123]. Injection of FGF into the vitreous cavity did not show the same effect of FGF mobilized by degradation of the matrix by proteolytic enzymes [123]. Conversely, macrophage depletion in mice reduced the choroidal neovascularization and was associated with decreased macrophage infiltration and VEGF protein [124].

## 4. Concluding Remarks

Overall, the literature data analyzed in this review demonstrate that, in addition to providing basic support for cells, ECM is also a critical component that allows the intercellular crosstalk and stores several important mediators which, in turn, regulate several cellular and connective components functions, including angiogenesis.

The progressive increase of knowledge concerning the cellular and extracellular mechanisms that regulate angiogenesis in normal and pathological conditions may provide the potential basis for the development of new therapeutic approaches against abnormal angiogenesis that contributes to the pathogenesis of several disorders.

## Conflict of Interests

The authors declare that there is no conflict of interests regarding the publication of this paper.

## References

[1] C. Fang, Y. G. Man, F. Cuttitta et al., "Novel phenotypic fluorescent three-dimensional co-culture platforms for recapitulating tumor in vivo progression and for personalized therapy," *Journal of Cancer*, vol. 4, no. 9, pp. 755–763, 2013.

[2] L. T. Edgar, S. C. Sibole, C. J. Underwood, J. E. Guilkey, and J. A. Weiss, "A computational model of in vitro angiogenesis based on extracellular matrix fibre orientation," *Computer Methods in Biomechanics and Biomedical Engineering*, vol. 16, no. 7, pp. 790–801, 2013.

[3] J. Folkman, "Tumor angiogenesis: therapeutic implications," *New England Journal of Medicine*, vol. 285, no. 21, pp. 1182–1186, 1971.

[4] D. Ribatti, "Chicken chorioallantoic membrane angiogenesis model," *Methods in Molecular Biology*, vol. 843, pp. 47–57, 2012.

[5] S. R. Montezuma, D. Vavvas, and J. W. Miller, "Review of the ocular angiogenesis animal models," *Seminars in Ophthalmology*, vol. 24, no. 2, pp. 52–61, 2009.

[6] D. Ribatti, B. Nico, and E. Crivellato, "Morphological and molecular aspects of physiological vascular morphogenesis," *Angiogenesis*, vol. 12, no. 1, pp. 101–111, 2009.

[7] M. Bastaki, E. E. Nelli, P. Dell'Era et al., "Basic fibroblast growth factor-induced angiogenic phenotype in mouse endothelium. A study of aortic and microvascular endothelial cell lines," *Arteriosclerosis, Thrombosis, and Vascular Biology*, vol. 17, no. 3, pp. 454–464, 1997.

[8] V. W. M. van Hinsbergh and P. Koolwijk, "Endothelial sprouting and angiogenesis: matrix metalloproteinases in the lead," *Cardiovascular Research*, vol. 78, no. 2, pp. 203–212, 2008.

[9] J. Thyboll, J. Kortesmaa, R. Cao et al., "Deletion of the laminin $\alpha$4 chain leads to impaired microvessel maturation," *Molecular and Cellular Biology*, vol. 22, no. 4, pp. 1194–1202, 2002.

[10] S. Astrof, D. Crowley, and R. O. Hynes, "Multiple cardiovascular defects caused by the absence of alternatively spliced segments

of fibronectin," *Developmental Biology*, vol. 311, no. 1, pp. 11–24, 2007.

[11] E. Pöschl, U. Schlötzer-Schrehardt, B. Brachvogel, K. Saito, Y. Ninomiya, and U. Mayer, "Collagen IV is essential for basement membrane stability but dispensable for initiation of its assembly during early development," *Development*, vol. 131, no. 7, pp. 1619–1628, 2004.

[12] M. E. Maragoudakis, E. Missirlis, G. D. Karakiulakis, M. Sarmonica, M. Bastakis, and N. Tsopanoglou, "Basement membrane biosynthesis as a target for developing inhibitors of angiogenesis with anti-tumor properties," *Kidney International*, vol. 43, no. 1, pp. 147–150, 1993.

[13] S. M. Sweeney, G. DiLullo, S. J. Slater et al., "Angiogenesis in collagen I requires $\alpha 2\beta 1$ ligation of a GFP*GER sequence and possibly p38 MAPK activation and focal adhesion disassembly," *Journal of Biological Chemistry*, vol. 278, no. 33, pp. 30516–30524, 2003.

[14] C. A. Perruzzi, A. R. de Fougerolles, V. E. Koteliansky, M. C. Whelan, W. F. Westlin, and D. R. Senger, "Functional overlap and cooperativity among $\alpha$v and $\beta$1 integrin subfamilies during skin angiogenesis," *Journal of Investigative Dermatology*, vol. 120, no. 6, pp. 1100–1109, 2003.

[15] M. C. Whelan and D. R. Senger, "Collagen I initiates endothelial cell morphogenesis by inducing actin polymerization through suppression of cyclic AMP and protein kinase A," *Journal of Biological Chemistry*, vol. 278, no. 1, pp. 327–334, 2003.

[16] M. V. Hoang, M. C. Whelan, and D. R. Senger, "Rho activity critically and selectively regulates endothelial cell organization during angiogenesis," *Proceedings of the National Academy of Sciences of the United States of America*, vol. 101, no. 7, pp. 1874–1879, 2004.

[17] M. Kamei, W. Brian Saunders, K. J. Bayless, L. Dye, G. E. Davis, and B. M. Weinstein, "Endothelial tubes assemble from intracellular vacuoles in vivo," *Nature*, vol. 442, no. 7101, pp. 453–456, 2006.

[18] A. N. Stratman, W. B. Saunders, A. Sacharidou et al., "Endothelial cell lumen and vascular guidance tunnel formation requires MT1-MMP-dependent proteolysis in 3-dimensional collagen matrices," *Blood*, vol. 114, no. 2, pp. 237–247, 2009.

[19] J. A. Madri, "Extracellular matrix modulation of vascular cell behaviour," *Transplant Immunology*, vol. 5, no. 3, pp. 179–183, 1997.

[20] M. Bahramsoltani, I. Slosarek, W. de Spiegelaere, and J. Plendl, "Angiogenesis and collagen type IV expression in different endothelial cell culture systems," *Anatomia, Histologia, Embryologia*, vol. 43, no. 2, pp. 103–115, 2014.

[21] S. Estrach, L. Cailleteau, C. A. Franco et al., "Laminin-binding integrins induce Dll4 expression and notch signaling in endothelial cells," *Circulation Research*, vol. 109, no. 2, pp. 172–182, 2011.

[22] R. Khusal, B. ca Costa Dias, K. Moodley et al., "In vitro inhibition of angiogenesis by antibodies directed against the 37kDa/67kDa laminin receptor," *PLoS ONE*, vol. 8, no. 3, Article ID e58888, 2013.

[23] M. D. Pierschbacher and E. Ruoslahti, "Cell attachment activity of fibronectin can be duplicated by small synthetic fragments of the molecule," *Nature*, vol. 309, no. 5963, pp. 30–33, 1984.

[24] E. W. K. Young, A. R. Wheeler, and C. A. Simmons, "Matrix-dependent adhesion of vascular and valvular endothelial cells in microfluidic channels," *Lab on a Chip*, vol. 7, no. 12, pp. 1759–1766, 2007.

[25] S. Bourdoulous, G. Orend, D. A. MacKenna, R. Pasqualini, and E. Ruoslahti, "Fibronectin matrix regulates activation of RHO and CDC42 GTPases and cell cycle progression," *Journal of Cell Biology*, vol. 143, no. 1, pp. 267–276, 1998.

[26] J. Sottile and D. C. Hocking, "Fibronectin polymerization regulates the composition and stability of extracellular matrix fibrils and cell-matrix adhesions," *Molecular Biology of the Cell*, vol. 13, no. 10, pp. 3546–3559, 2002.

[27] J. Sottile, D. C. Hocking, and P. J. Swiatek, "Fibronectin matrix assembly enhances adhesion-dependent cell growth," *Journal of Cell Science*, vol. 111, no. 19, pp. 2933–2943, 1998.

[28] D. C. Hocking, J. Sottile, and K. J. Langenbach, "Stimulation of integrin-mediated cell contractility by fibronectin," *Journal of Biological Chemistry*, vol. 275, no. 14, pp. 10673–10682, 2000.

[29] S. Kim, M. Bakre, H. Yin, and J. A. Varner, "Inhibition of endothelial cell survival and angiogenesis by protein kinase A," *Journal of Clinical Investigation*, vol. 110, no. 7, pp. 933–941, 2002.

[30] R. F. Nicosia, E. Bonanno, and M. Smith, "Fibronectin promotes the elongation of microvessels during angiogenesis in vitro," *Journal of Cellular Physiology*, vol. 154, no. 3, pp. 654–661, 1993.

[31] L. Robert and B. Robert, "Structural glycoproteins, their metabolism in normal and pathological connective tissue," *Bibliotheca Nutritio et Dieta*, vol. 13, pp. 123–130, 1969.

[32] F. X. Maquart, A. Siméon, S. Pasco, and J. C. Monboisse, "Regulation of cell activity by the extracellular matrix: the concept of matrikines," *Journal de la Societe de Biologie*, vol. 193, no. 4-5, pp. 423–428, 1999.

[33] G. E. Davis, K. J. Bayless, M. J. Davis, and G. A. Meininger, "Regulation of tissue injury responses by the exposure of matricryptic sites within extracellular matrix molecules," *American Journal of Pathology*, vol. 156, no. 5, pp. 1489–1498, 2000.

[34] A. Bonnefoy and C. Legrand, "Proteolysis of subendothelial adhesive glycoproteins (fibronectin, thrombospondin, and von Willebrand factor) by plasmin, leukocyte cathepsin G, and elastase," *Thrombosis Research*, vol. 98, no. 4, pp. 323–332, 2000.

[35] G. E. Davis, K. A. Pintar Allen, R. Salazar, and S. A. Maxwell, "Matrix metalloproteinase-1 and -9 activation by plasmin regulates a novel endothelial cell-mediated mechanism of collagen gel contraction and capillary tube regression in three-dimensional collagen matrices," *Journal of Cell Science*, vol. 114, no. 5, pp. 917–930, 2001.

[36] O. Saksela, D. Moscatelli, A. Sommer, and D. B. Rifkin, "Endothelial cell-derived heparan sulfate binds basic fibroblast growth factor and protects it from proteolytic degradation," *Journal of Cell Biology*, vol. 107, no. 2, pp. 743–751, 1988.

[37] S. J. George, J. L. Johnson, M. A. Smith, and C. L. Jackson, "Plasmin-mediated fibroblast growth factor-2 mobilisation supports smooth muscle cell proliferation in human saphenous vein," *Journal of Vascular Research*, vol. 38, no. 5, pp. 492–501, 2001.

[38] D. E. Gomez, D. F. Alonso, H. Yoshiji, and U. P. Thorgeirsson, "Tissue inhibitors of metalloproteinases: structure, regulation and biological functions," *European Journal of Cell Biology*, vol. 74, no. 2, pp. 111–122, 1997.

[39] M. S. O'Reilly, T. Boehm, Y. Shing et al., "Endostatin: an endogenous inhibitor of angiogenesis and tumor growth," *Cell*, vol. 88, no. 2, pp. 277–285, 1997.

[40] A. G. Marneros and B. R. Olsen, "The role of collagen-derived proteolytic fragments in angiogenesis," *Matrix Biology*, vol. 20, no. 5-6, pp. 337–345, 2001.

[41] N. Fukai, L. Eklund, A. G. Marneros et al., "Lack of collagen XVIII/endostatin results in eye abnormalities," *EMBO Journal*, vol. 21, no. 7, pp. 1535–1544, 2002.

[42] M. Dhanabal, R. Ramchandran, M. J. F. Waterman et al., "Endostatin induces endothelial cell apoptosis," *Journal of Biological Chemistry*, vol. 274, no. 17, pp. 11721–11726, 1999.

[43] M. Dhanabal, R. Volk, R. Ramchandran, M. Simons, and V. P. Sukhatme, "Cloning, expression, and in vitro activity of human endostatin," *Biochemical and Biophysical Research Communications*, vol. 258, no. 2, pp. 345–352, 1999.

[44] J. Dixelius, H. Larsson, T. Sasaki et al., "Endostatin-induced tyrosine kinase signaling through the Shb adaptor protein regulates endothelial cell apoptosis," *Blood*, vol. 95, no. 11, pp. 3403–3411, 2000.

[45] T. Sasaki, H. Larsson, J. Kreuger et al., "Structural basis and potential role of heparin/heparan sulfate binding to the angiogenesis inhibitor endostatin," *EMBO Journal*, vol. 18, no. 22, pp. 6240–6248, 1999.

[46] N. Yamaguchi, B. Anand-Apte, M. Lee et al., "Endostatin inhibits VEGF-induced endothelial cell migration and tumor growth independently of zinc binding," *EMBO Journal*, vol. 18, no. 16, pp. 4414–4423, 1999.

[47] Y. Hamano, M. Zeisberg, H. Sugimoto et al., "Physiological levels of tumstatin, a fragment of collagen IV $\alpha 3$ chain, are generated by MMP-9 proteolysis and suppress angiogenesis via $\alpha V\beta 3$ integrin," *Cancer Cell*, vol. 3, no. 6, pp. 589–601, 2003.

[48] E. Petitclerc, A. Boutaud, A. Prestayko et al., "New functions for non-collagenous domains of human collagen type IV. Novel integrin ligands inhibiting angiogenesis and tumor growth in vivo," *Journal of Biological Chemistry*, vol. 275, no. 11, pp. 8051–8061, 2000.

[49] Y. Maeshima, M. Manfredi, C. Reimerli et al., "Identification of the anti-angiogenic site within vascular basement membrane-derived tumstatin," *Journal of Biological Chemistry*, vol. 276, no. 18, pp. 15240–15248, 2001.

[50] G.-M. Zhang, Y.-M. Zhang, S.-B. Fu et al., "Effects of cloned tumstatin-related and angiogenesis-inhibitory peptides on proliferation and apoptosis of endothelial cells," *Chinese Medical Journal*, vol. 121, no. 22, pp. 2324–2330, 2008.

[51] Y. Maeshima, A. Sudhakar, J. C. Lively et al., "Tumstatin, an endothelial cell-specific inhibitor of protein synthesis," *Science*, vol. 295, no. 5552, pp. 140–143, 2002.

[52] G. D. Kamphaus, P. C. Colorado, D. J. Panka et al., "Canstatin, a novel matrix-derived inhibitor of angiogenesis and tumor growth," *Journal of Biological Chemistry*, vol. 275, no. 2, pp. 1209–1215, 2000.

[53] G.-A. He, J.-X. Luo, T.-Y. Zhang, F.-Y. Wang, and R.-F. Li, "Canstatin-N fragment inhibits in vitro endothelial cell proliferation and suppresses in vivo tumor growth," *Biochemical and Biophysical Research Communications*, vol. 312, no. 3, pp. 801–805, 2003.

[54] D. J. Panka and J. W. Mier, "Canstatin inhibits Akt activation and induces Fas-dependent apoptosis in endothelial cells," *Journal of Biological Chemistry*, vol. 278, no. 39, pp. 37632–37636, 2003.

[55] C. Magnon, A. Galaup, B. Mullan et al., "Canstatin acts on endothelial and tumor cells via mitochondrial damage initiated through interaction with alphavbeta3 and alphavbeta5 integrins," *Cancer Research*, vol. 65, no. 10, pp. 4353–4361, 2005.

[56] A. Sudhakar, P. Nyberg, V. G. Keshamouni et al., "Human $\alpha 1$ type IV collagen NC1 domain exhibits distinct antiangiogenic activity mediated by $\alpha 1\beta 1$ integrin," *Journal of Clinical Investigation*, vol. 115, no. 10, pp. 2801–2810, 2005.

[57] P. C. Colorado, A. Torre, G. Kamphaus et al., "Anti-angiogenic cues from vascular basement membrane collagen," *Cancer Research*, vol. 60, no. 9, pp. 2520–2526, 2000.

[58] C. S. Boosani, N. Nalabothula, N. Sheibani, and A. Sudhakar, "Inhibitory effects of arresten on bFGF-induced proliferation, migration, and matrix metalloproteinase-2 activation in mouse retinal endothelial cells impact of arresten on mouse retinal Endothelial Cells," *Current Eye Research*, vol. 35, no. 1, pp. 45–55, 2010.

[59] P. Nyberg, L. Xie, H. Sugimoto et al., "Characterization of the anti-angiogenic properties of arresten, an $\alpha 1\beta 1$ integrin-dependent collagen-derived tumor suppressor," *Experimental Cell Research*, vol. 314, no. 18, pp. 3292–3305, 2008.

[60] E. D. Karagiannis and A. S. Popel, "Identification of novel short peptides derived from the $\alpha 4$, $\alpha 5$, and $\alpha 6$ fibrils of type IV collagen with anti-angiogenic properties," *Biochemical and Biophysical Research Communications*, vol. 354, no. 2, pp. 434–439, 2007.

[61] T. M. Mundel, A.-M. Yliniemi, Y. Maeshima, H. Sugimoto, M. Kieran, and R. Kalluri, "Type IV collagen $\alpha 6$ chain-derived noncollagenous domain 1 ($\alpha 6$(IV)NC1) inhibits angiogenesis and tumor growth," *International Journal of Cancer*, vol. 122, no. 8, pp. 1738–1744, 2008.

[62] M. Mongiat, S. M. Sweeney, J. D. San Antonio, J. Fu, and R. V. Iozzo, "Endorepellin, a novel inhibitor of angiogenesis derived from the C terminus of perlecan," *Journal of Biological Chemistry*, vol. 278, no. 6, pp. 4238–4249, 2003.

[63] G. Bix, J. Fu, E. M. Gonzalez et al., "Endorepellin causes endothelial cell disassembly of actin cytoskeleton and focal adhesions through $\alpha 2\beta 1$ integrin," *Journal of Cell Biology*, vol. 166, no. 1, pp. 97–109, 2004.

[64] A. Goyal, C. Poluzzi, C. D. Willis, J. Smythies, A. Shellard, and T. Neill, "Endorepellin affects angiogenesis by antagonizing diverse vascular endothelial growth factor receptor 2 (VEGFR2)-evoked signaling pathways: transcriptional repression of hypoxia-inducible factor 1a and VEGFA and concurrent inhibition of nuclear factor of activated T cell 1 (NFAT1) activation," *Journal of Biological Chemistry*, vol. 287, no. 52, pp. 43543–43556, 2012.

[65] C. D. Willis, C. Poluzzi, M. Mongiat, and R. V. Iozzo, "Endorepellin laminin-like globular 1/2 domains bind Ig3-5 of vascular endothelial growth factor (VEGF) receptor 2 and block pro-angiogenic signaling by VEGFA in endothelial cells," *FEBS Journal*, vol. 280, no. 10, pp. 2271–2284, 2013.

[66] D. Ribatti, A. Vacca, and M. Presta, "The discovery of angiogenic factors: a historical review," *General Pharmacology: Vascular System*, vol. 35, no. 5, pp. 227–231, 2000.

[67] D. R. Senger, K. P. Claffey, J. E. Benes, C. A. Perruzzi, A. P. Sergiou, and M. Detmar, "Angiogenesis promoted by vascular endothelial growth factor: regulation through alpha1beta1 and alpha2beta1 integrins," *Proceedings of the National Academy of Sciences of the United States of America*, vol. 94, no. 25, pp. 13612–13617, 1997.

[68] D. R. Senger, S. R. Ledbetter, K. P. Claffey et al., "Stimulation of endothelial cell migration by vascular permeability factor/vascular endothelial growth factor through cooperative mechanisms involving the alphavbeta3 integrin, osteopontin, and thrombin," *American Journal of Pathology*, vol. 149, no. 1, pp. 293–305, 1996.

[69] S. Wang, X. Li, M. Parra, E. Verdin, R. Bassel-Duby, and E. N. Olson, "Control of endothelial cell proliferation and migration by VEGF signaling to histone deacetylase 7," *Proceedings of the*

*National Academy of Sciences of the United States of America*, vol. 105, no. 22, pp. 7738–7743, 2008.

[70] S. Lee, S. M. Jilan, G. V. Nikolova, D. Carpizo, and M. Luisa Iruela-Arispe, "Processing of VEGF-A by matrix metalloproteinases regulates bioavailability and vascular patterning in tumors," *Journal of Cell Biology*, vol. 169, no. 4, pp. 681–691, 2005.

[71] B. A. Keyt, L. T. Berleau, and H. V. Nguyen, "The carboxyl-terminal domain (111–165) of vascular endothelial growth factor is critical for its mitogenic potency," *Journal of Biological Chemistry*, vol. 271, no. 13, pp. 7788–7795, 1996.

[72] M. Mitsi, K. Forsten-Williams, M. Gopalakrishnan, and M. A. Nugent, "A catalytic role of heparin within the extracellular matrix," *Journal of Biological Chemistry*, vol. 283, no. 50, pp. 34796–34807, 2008.

[73] M. Mitsi, Z. Hong, C. E. Costello, and M. A. Nugent, "Heparin-mediated conformational changes in fibronectin expose vascular endothelial growth factor binding sites," *Biochemistry*, vol. 45, no. 34, pp. 10319–10328, 2006.

[74] R. Ishai-Michaeli, C. M. Svahn, M. Weber et al., "Importance of size and sulfation of heparin in release of basic fibroblast growth factor from the vascular endothelium and extracellular matrix," *Biochemistry*, vol. 31, no. 7, pp. 2080–2088, 1992.

[75] D. Aviezer, E. Levy, M. Safran et al., "Differential structural requirements of heparin and heparan sulfate proteoglycans that promote binding of basic fibroblast growth factor to its receptor," *Journal of Biological Chemistry*, vol. 269, no. 1, pp. 114–121, 1994.

[76] O. Saksela and D. B. Rifkin, "Release of basic fibroblast growth factor-heparan sulfate complexes from endothelial cells by plasminogen activator-mediated proteolytic activity," *Journal of Cell Biology*, vol. 110, no. 3, pp. 767–775, 1990.

[77] A. B. Roberts, M. B. Sporn, and R. K. Assoian, "Transforming growth factor type $\beta$: rapid induction of fibrosis and angiogenesis in vivo and stimulation of collagen formation in vitro," *Proceedings of the National Academy of Sciences of the United States of America*, vol. 83, no. 12, pp. 4167–4171, 1986.

[78] E. Y. Yang and H. L. Moses, "Transforming growth factor $\beta$1-induced changes in cell migration, proliferation, and angiogenesis in the chicken chorioallantoic membrane," *Journal of Cell Biology*, vol. 111, no. 2, pp. 731–741, 1990.

[79] M. C. Dickson, J. S. Martin, F. M. Cousins, A. B. Kulkarni, S. Karlsson, and R. J. Akhurst, "Defective haematopoiesis and vasculogenesis in transforming growth factor-$\beta$1 knock out mice," *Development*, vol. 121, no. 6, pp. 1845–1854, 1995.

[80] J. R. Merwin, J. M. Anderson, O. Kocher, C. M. van Itallie, and J. A. Madri, "Transforming growth factor beta1 modulates extracellular matrix organization and cell-cell junctional complex formation during in vitro angiogenesis," *Journal of Cellular Physiology*, vol. 142, no. 1, pp. 117–128, 1990.

[81] M. Frater-Schroder, W. Risau, and R. Hallmann, "Tumor necrosis factor type $\alpha$, a potent inhibitor of endothelial cell growth in vitro, is angiogenic in vivo," *Proceedings of the National Academy of Sciences of the United States of America*, vol. 84, no. 15, pp. 5277–5281, 1987.

[82] G. Ferrari, B. D. Cook, V. Terushkin, G. Pintucci, and P. Mignatti, "Transforming growth factor-beta 1 (TGF-$\beta$1) induces angiogenesis through vascular endothelial growth factor (VEGF)-mediated apoptosis," *Journal of Cellular Physiology*, vol. 219, no. 2, pp. 449–458, 2009.

[83] G. Ferrari, G. Pintucci, G. Seghezzi, K. Hyman, A. C. Galloway, and P. Mignatti, "VEGF, a prosurvival factor, acts in concert with TGF-$\beta$1 to induce endothelial cell apoptosis," *Proceedings of the National Academy of Sciences of the United States of America*, vol. 103, no. 46, pp. 17260–17265, 2006.

[84] T. Kisseleva, L. Song, M. Vorontchikhina, N. Feirt, J. Kitajewski, and C. Schindler, "NF-$\kappa$B regulation of endothelial cell function during LPS-induced toxemia and cancer," *Journal of Clinical Investigation*, vol. 116, no. 11, pp. 2955–2963, 2006.

[85] H.-M. Ko, J.-H. Kang, J.-H. Choi, S. J. Park, S. Bai, and S.-Y. Im, "Platelet-activating factor induces matrix metalloproteinase-9 expression through Ca2+- or PI3K-dependent signaling pathway in a human vascular endothelial cell line," *FEBS Letters*, vol. 579, no. 28, pp. 6451–6458, 2005.

[86] Y. Xu and Q. Yu, "Angiopoietin-1, unlike angiopoietin-2, is incorporated into the extracellular matrix via its linker peptide region," *Journal of Biological Chemistry*, vol. 276, no. 37, pp. 34990–34998, 2001.

[87] C. Suri, P. F. Jones, S. Patan et al., "Requisite role of angiopoietin-1, a ligand for the TIE2 receptor, during embryonic angiogenesis," *Cell*, vol. 87, no. 7, pp. 1171–1180, 1996.

[88] L. Pizurki, Z. Zhou, K. Glynos, C. Roussos, and A. Papapetropoulos, "Angiopoietin-1 inhibits endothelial permeability, neutrophil adherence and IL-8 production," *British Journal of Pharmacology*, vol. 139, no. 2, pp. 329–336, 2003.

[89] S. H. Seok, J. I. Heo, J. H. Hwang et al., "Angiopoietin-1 elicits pro-inflammatory responses in monocytes and differentiating macrophages," *Molecules and Cells*, vol. 35, no. 6, pp. 550–556, 2013.

[90] P. C. Maisonpierre, C. Suri, P. F. Jones et al., "Angiopoietin-2, a natural antagonist for Tie2 that disrupts in vivo angiogenesis," *Science*, vol. 277, no. 5322, pp. 55–60, 1997.

[91] U. Fiedler, Y. Reiss, M. Scharpfenecker et al., "Angiopoietin-2 sensitizes endothelial cells to TNF-$\alpha$ and has a crucial role in the induction of inflammation," *Nature Medicine*, vol. 12, no. 2, pp. 235–239, 2006.

[92] A. Bar-Or, R. K. Nuttall, M. Duddy et al., "Analyses of all matrix metalloproteinase members in leukocytes emphasize monocytes as major inflammatory mediators in multiple sclerosis," *Brain*, vol. 126, no. 12, pp. 2738–2749, 2003.

[93] J. A. Gebbia, J. L. Coleman, and J. L. Benach, "Selective induction of matrix metalloproteinases by Borrelia burgdorferi via toll-like receptor 2 in monocytes," *Journal of Infectious Diseases*, vol. 189, no. 1, pp. 113–119, 2004.

[94] E. Elass, L. Aubry, M. Masson et al., "Mycobacterial lipomannan induces matrix metalloproteinase-9 expression in human macrophagic cells through a toll-like receptor 1 (TLR1)/TLR2- and CD14-dependent mechanism," *Infection and Immunity*, vol. 73, no. 10, pp. 7064–7068, 2005.

[95] H. Kai, Y. Kitadai, M. Kodama et al., "Involvement of proinflammatory cytokines IL-1$\beta$ and IL-6 in progression of human gastric carcinoma," *Anticancer Research*, vol. 25, no. 2, pp. 709–713, 2005.

[96] M. M. Mohamed, E. A. El-Ghonaimy, M. A. Nouh, R. J. Schneider, B. F. Sloane, and M. El-Shinawi, "Cytokines secreted by macrophages isolated from tumor microenvironment of inflammatory breast cancer patients possess chemotactic properties," *International Journal of Biochemistry and Cell Biology*, vol. 46, pp. 138–147, 2014.

[97] G. Chakraborty, S. Jain, and G. C. Kundu, "Osteopontin promotes vascular endothelial growth factor-dependent breast tumor growth and angiogenesis via autocrine and paracrine mechanisms," *Cancer Research*, vol. 68, no. 1, pp. 152–161, 2008.

[98] G. Bergers, R. Brekken, G. McMahon et al., "Matrix metalloproteinase-9 triggers the angiogenic switch during carcinogenesis," *Nature Cell Biology*, vol. 2, no. 10, pp. 737–744, 2000.

[99] C. M. Storgard, D. G. Stupack, A. Jonczyk, S. L. Goodman, R. I. Fox, and D. A. Cheresh, "Decreased angiogenesis and arthritic disease in rabbits treated with an $\alpha v\beta 3$ antagonist," *Journal of Clinical Investigation*, vol. 103, no. 1, pp. 47–54, 1999.

[100] H. Nakahara, J. Song, M. Sugimoto et al., "Anti-interleukin-6 receptor antibody therapy reduces vascular endothelial growth factor production in rheumatoid arthritis," *Arthritis & Rheumatism*, vol. 48, no. 6, pp. 1521–1529, 2003.

[101] J. M. Woods, A. Mogollon, M. A. Amin, R. J. Martinez, and A. E. Koch, "The role of COX-2 in angiogenesis and rheumatoid arthritis," *Experimental and Molecular Pathology*, vol. 74, no. 3, pp. 282–290, 2003.

[102] B. B. Scott, P. F. Zaratin, A. Colombo, M. J. Hansbury, J. D. Winkler, and J. R. Jackson, "Constitutive expression of angiopoietin-1 and -2 and modulation of their expression by inflammatory cytokines in rheumatoid arthritis synovial fibroblasts," *Journal of Rheumatology*, vol. 29, no. 2, pp. 230–239, 2002.

[103] S. Ballara, P. C. Taylor, P. Reusch et al., "Raised serum vascular endothelial growth factor levels are associated with destructive change in inflammatory arthritis," *Arthritis & Rheumatology*, vol. 44, no. 9, pp. 2055–2064, 2001.

[104] T. Marumo, V. B. Schini-Kerth, and R. Busse, "Vascular endothelial growth factor activates nuclear factor-$\kappa$B and induces monocyte chemoattractant protein-1 in bovine retinal endothelial cells," *Diabetes*, vol. 48, no. 5, pp. 1131–1137, 1999.

[105] I. Tchetverikov, H. K. Ronday, B. Van El et al., "MMP profile in paired serum and synovial fluid samples of patients with rheumatoid arthritis," *Annals of the Rheumatic Diseases*, vol. 63, no. 7, pp. 881–883, 2004.

[106] G. Keyszer, I. Lambiri, R. Nagel et al., "Circulating levels of matrix metalloproteinases MMP-3 and MMP-1, tissue inhibitor of metalloproteinases 1 (TIMP-1), and MMP-1/TIMP-1 complex in rheumatic disease. Correlation with clinical activity of rheumatoid arthritis versus other surrogate markers," *Journal of Rheumatology*, vol. 26, no. 2, pp. 251–258, 1999.

[107] L. Haywood, D. F. McWilliams, C. I. Pearson et al., "Inflammation and angiogenesis in osteoarthritis," *Arthritis & Rheumatism*, vol. 48, no. 8, pp. 2173–2177, 2003.

[108] Y. Henrotin, C. Lambert, and P. Richette, "Importance of synovitis in osteoarthritis: evidence for the use of glycosaminoglycans against synovial inflammation," *Seminars in Arthritis and Rheumatism*, vol. 43, no. 5, pp. 579–587, 2014.

[109] J. R. Jackson, J. A. Minton, M. L. Ho, N. Wei, and J. D. Winkler, "Expression of vascular endothelial growth factor in synovial fibroblasts is induced by hypoxia and interleukin 1beta," *Journal of Rheumatology*, vol. 24, pp. 1253–1259, 1997.

[110] M. Frater-Schroder, G. Muller, W. Birchmeier, and P. Bohlen, "Transforming growth factor-beta inhibits endothelial cell proliferation," *Biochemical and Biophysical Research Communications*, vol. 137, no. 1, pp. 295–302, 1986.

[111] W. Lehmann, C. M. Edgar, K. Wang et al., "Tumor necrosis factor alpha (TNF-$\alpha$) coordinately regulates the expression of specific matrix metalloproteinases (MMPS) and angiogenic factors during fracture healing," *Bone*, vol. 36, no. 2, pp. 300–310, 2005.

[112] A. E. Koch, J. C. Burrows, G. K. Haines, T. M. Carlos, J. M. Harlan, and S. J. Leibovich, "Immunolocalization of endothelial and leukocyte adhesion molecules in human rheumatoid and osteoarthritic synovial tissues," *Laboratory Investigation*, vol. 64, no. 3, pp. 313–320, 1991.

[113] B. J. Nickoloff, R. S. Mitra, J. Varani, V. M. Dixit, and P. J. Polverini, "Aberrant production of interleukin-8 and thrombospondin-1 by psoriatic keratinocytes mediates angiogenesis," *American Journal of Pathology*, vol. 144, no. 4, pp. 820–828, 1994.

[114] S. Kumari, M. C. Bonnet, M. H. Ulvmar et al., "Tumor necrosis factor receptor signaling in keratinocytes triggers interleukin-24-dependent psoriasis-like skin inflammation in mice," *Immunity*, vol. 39, no. 5, pp. 899–911, 2013.

[115] T. P. Singh, M. P. Schön, K. Wallbrecht, A. Gruber-Wackernagel, X. J. Wang, and P. Wolf, "Involvement of IL-9 in Th17-associated inflammation and angiogenesis of psoriasis," *PLoS ONE*, vol. 8, no. 1, Article ID e51752, 2013.

[116] M. Bhushan, B. McLaughlin, J. B. Weiss, and C. E. M. Griffiths, "Levels of endothelial cell stimulating angiogenesis factor and vascular endothelial growth factor are elevated in psoriasis," *British Journal of Dermatology*, vol. 141, no. 6, pp. 1054–1060, 1999.

[117] O. Simonetti, G. Lucarini, G. Goteri et al., "VEGF is likely a key factor in the link between inflammation and angiogenesis in psoriasis: results of an immunohistochemical study," *International Journal of Immunopathology and Pharmacology*, vol. 19, no. 4, pp. 751–760, 2006.

[118] A. Nofal, I. Al-Makhzangy, E. Attwa, A. Nassar, and A. Abdalmoati, "Vascular endothelial growth factor in psoriasis: an indicator of disease severity and control," *Journal of the European Academy of Dermatology and Venereology*, vol. 23, no. 7, pp. 803–806, 2009.

[119] I. Flisiak, H. Myśliwiec, and B. Chodynicka, "Effect of psoriasis treatment on plasma concentrations of metalloproteinase-1 and tissue inhibitor of metalloproteinases-1," *Journal of the European Academy of Dermatology and Venereology*, vol. 19, no. 4, pp. 418–421, 2005.

[120] S. Suomela, A.-L. Kariniemi, U. Impola et al., "Matrix metalloproteinase-19 is expressed by keratinocytes in psoriasis," *Acta Dermato-Venereologica*, vol. 83, no. 2, pp. 108–114, 2003.

[121] P. Cordiali-Fei, E. Trento, G. D'Agosto et al., "Decreased levels of metalloproteinase-9 and angiogenic factors in skin lesions of patients with psoriatic arthritis after therapy with anti-TNF-$\alpha$," *Journal of Autoimmune Diseases*, vol. 3, article 5, 2006.

[122] M. Funk, K. Kriechbaum, F. Prager et al., "Intraocular concentrations of growth factors and cytokines in retinal vein occlusion and the effect of therapy with bevacizumab," *Investigative Ophthalmology and Visual Science*, vol. 50, no. 3, pp. 1025–1032, 2009.

[123] M. Funk, G. Schmidinger, N. Maar et al., "Angiogenic and inflammatory markers in the intraocular fluid of eyes with diabetic macular edema and influence of therapy with bevacizumab," *Retina*, vol. 30, no. 9, pp. 1412–1419, 2010.

[124] S. Ishida, T. Usui, K. Yamashiro et al., "VEGF164-mediated inflammation is required for pathological, but not physiological, ischemia-induced retinal neovascularization," *Journal of Experimental Medicine*, vol. 198, no. 3, pp. 483–489, 2003.

Hindawi Publishing Corporation
BioMed Research International
Volume 2014, Article ID 652432, 11 pages
http://dx.doi.org/10.1155/2014/652432

*Research Article*

# Novel Scaffolds Fabricated Using Oleuropein for Bone Tissue Engineering

**Hui Fan,[1,2] Junfeng Hui,[1,2] Zhiguang Duan,[1,2] Daidi Fan,[1,2] Yu Mi,[1,2] Jianjun Deng,[1,2] and Hui Li[1,2]**

[1] *Shaanxi Key Laboratory of Degradable Biomedical Materials, School of Chemical Engineering, Northwest University, 229 Taibai North Road, Xi'an 710069, China*
[2] *Shaanxi R&D Center of Biomaterials and Fermentation Engineering, School of Chemical Engineering, Northwest University, Xi'an 710069, China*

Correspondence should be addressed to Daidi Fan; fandaidi@nwu.edu.cn and Yu Mi; mi_yu@nwu.edu.cn

Received 13 December 2013; Revised 10 March 2014; Accepted 29 March 2014; Published 13 May 2014

Academic Editor: Costantino Del Gaudio



We investigated the feasibility of oleuropein as a cross-linking agent for fabricating three-dimensional (3D) porous composite scaffolds for bone tissue engineering. Human-like collagen (HLC) and nanohydroxyapatite (n-HAp) were used to fabricate the composite scaffold by way of cross-linking. The mechanical tests revealed superior properties for the cross-linked scaffolds compared to the uncross-linked scaffolds. The as-obtained composite scaffold had a 3D porous structure with pores ranging from 120 to 300 $\mu$m and a porosity of $73.6 \pm 2.3\%$. The cross-linked scaffolds were seeded with MC3T3-E1 Subclone 14 mouse osteoblasts. Fluorescence staining, the Cell Counting Kit-8 (CCK-8) assay, and scanning electron microscopy (SEM) indicated that the scaffolds enhanced cell adhesion and proliferation. Our results indicate the potential of these scaffolds for bone tissue engineering.

## 1. Introduction

The need for bone grafts to repair skeletal defects caused by trauma or bone neoplasia has been constantly increasing in recent years. Currently, autologous bone grafts and allografts are the main options for bone replacement. Although autologous bone grafts are ideal for osteoinduction and osteogenesis, they require secondary surgery, are available in very limited supplies, and can lead to donor site morbidity [1, 2]. In addition, allografts can potentially result in disease transmission and immune responses. All of these factors limit their application in bone reconstruction. To overcome these limitations, various bone tissue engineering strategies have been proposed. The ideal scaffold for use as a transplant not only has good biocompatibility, appropriate mechanical properties, and a well-matched degradation rate [3–5] but also has an appropriate pore size and high interconnectivity to promote cells attachment, proliferation, and bone repair [6–10].

To provide a biocompatible and bioactive environment for new bone formation, a wide variety of materials have been used to mimic the bone-forming components. As the main structural element in skin, bone, tendon, cartilage, blood vessels, and heart valves, collagen has been widely used in tissue engineering. Human-like collagen (HLC) is a recombinant collagen expressed by recombinant *Escherichia coli* BL21 [11], which contains a modified cDNA reverse-transcribed from human collagen mRNA. Due to the water solubility, workability, low immunogenicity, biocompatibility, and biodegradability of HLC, this material has been successfully used for vascular scaffolds [12, 13], artificial bone [14], hydrogels [15], and skin tissues [16]. As the major components of human natural bone, nanohydroxyapatite (n-HAp) possesses excellent biocompatibility, osteoconductivity, and bioactivity and lacks antigenicity and cytotoxicity. Thus, n-HAp is an outstanding biomaterial for guided bone regeneration [17, 18].

In addition, the cross-linking technique can increase the mechanical properties of the scaffolds. Chemical cross-linking agents, such as carbodiimide or glutaraldehyde, have been studied extensively for biomedical applications. However, their high cytotoxicity may influence the biocompatibility of the scaffolds [19]. Thus, the development of a natural noncytotoxic cross-linking agent is urgently needed. Simple phenolic compounds derived from plants have been studied for cross-linking proteins [20]. However, little attention has been focused on polyphenol as a cross-linking agent for bone tissue engineering. Furthermore, oleuropein, a polyphenol belonging to the secoiridoid class, the most representative catecholic components of olives, possesses high antioxidation ability due to its ability to scavenge superoxide radicals. Antioxidant nutrients might reduce the production of free radicals, contributing to bone resorption and enhancing bone formation. It has been demonstrated that oleuropein elicits protective effects on bone [21].

In this study, oleuropein was employed as a cross-linking agent for bone tissue engineering using cross-linked composite HLC/n-HAp scaffolds. The characteristics and mechanical properties of the scaffolds and their ability to promote cell adhesion and proliferation were investigated.

## 2. Materials and Methods

*2.1. Materials.* HLC was supplied from Juzi Biogene Technology Co. Ltd. (97,000 Da, Xi'an, China) and n-HAp was supplied by Epri Nano Materials Ltd. Co. (20 nm, Nanjing, China). Oleuropein was supplied by Wedar Ltd. Co. (Shanghai, China). MC3T3-E1 cells were obtained from Biok&KM Co. Ltd. (Jiangsu, China). Trypsin (250 units/mg) was obtained from Amresco (Solon, OH, USA). Minimum essential medium (MEM) and fetal bovine serum (FBS) were purchased from Hyclone (Logan, UT, USA). The Cell Counting Kit-8 (CCK-8) was obtained from Keygen Biological Technology Development Co. Ltd. (KGA317, Nanjing, China). All other reagents and solvents were of analytical grade.

*2.2. Preparation of Composite HLC/n-HAp Scaffolds.* HLC was dissolved in deionized distilled water at a concentration of 4.8% (w/v) by gentle stirring at room temperature for 30 min. The n-HAp (HLC/n-HAp ratio = 1 : 2, 1 : 3, 1 : 4, 1 : 5, and 1 : 6 (w/w)) was then dispersed in the HLC solution. The HLC/n-HAp mixture was transferred into a mold, which was successively frozen at 4°C for 20 min, −20°C for 1 h, and −70°C for 3 h. After lyophilization in a vacuum freeze-dryer (FD 5–10, SIM, USA) for 48 h at 6.7–13.3 Pa (50–100 mTorr), the as-obtained scaffolds were cross-linked using an oleuropein ethanol-water solution (concentration of 0.5%, 1%, 1.5%, 2%, 2.5%, and 3% (w/v) and 90% ethanol) at 37°C for 36 h. The scaffolds were then washed under running deionized distilled water for 3 h to remove the ethanol and again lyophilized for 48 h. The scaffolds were applied to subsequent experiments.

*2.3. Scanning Electron Microscopy (SEM).* The surface morphologies of the composite HLC/n-HAp scaffolds were examined by scanning electron microscopy (Hitachi S-570, Japan). Before imaging, the scaffolds were cut into pieces with a razor blade, which were mounted on aluminum stubs and sputter-coated with gold.

*2.4. Mechanical Properties of the HLC/n-HAp Scaffolds.* The mechanical property of the composite HLC/n-HAp scaffolds was determined by measurement of the compression strength and Young's modulus using an INSTRON 5565 Materials Testing System with a 5000 N load cell. To test the longitudinal compression strength, the loading rate was 1 mm/min. Five samples were measured for each group. Cylindrical samples were prepared with diameters of 10 mm and lengths of 30 mm.

*2.5. X-Ray Diffraction (XRD).* The crystalline phase of the scaffold was analyzed by X-ray diffraction (Rigaku D/max-3C, Japan). The phases were identified by comparison to the n-HAp X-ray diffractograms. The scaffold was ground to a powder and analyzed. The XRD data were acquired using a voltage of 40 kV at a rate of 2°/min and angle range of 10–60°.

*2.6. Fourier Transform Infrared Spectra (FTIR).* The chemical structures of the composite HLC/n-HAp scaffold, HLC, and n-HAp were characterized using a Fourier transform infrared spectrophotometer (EQUINOX-55, Bruker Corporation, Germany) using the KBr method. FTIR spectra were collected from 4000 to 500 $cm^{-1}$.

*2.7. Thermogravimetric Analysis (TGA).* The thermal stability of the composite scaffolds was evaluated by thermogravimetric analysis (STA449C, Netzsch) with a heating rate of 3°C/min from 30°C to 600°C.

*2.8. Scaffold Porosity.* The porosity of the scaffold was measured by liquid displacement, as calculated according to $P = (W_1 - W_0)/\rho V_0$, where $W_1$ is the wet weight of the scaffold after it is immersed in the dehydrated alcohol for 48 h until it is saturated, $W_0$ is the dry weight of the scaffold, $\rho$ is the density of the dehydrated alcohol, and $V_0$ is the volume of the scaffold. Three parallel samples were tested.

*2.9. Cell Seeding and Culture.* MC3T3-E1 Subclone 14 mouse osteoblasts were used to evaluate cell proliferation and morphology on the scaffolds. MC3T3-E1 cells were cultured in minimum essential medium (MEM) including 10% heat-inactivated FBS in a 95% relative humidity atmosphere of 5% $CO_2$ at 37°C. The composite scaffolds were cut into circular disks of 10 mm diameter and 3 mm height. The pieces were placed in 48-well culture plates and sterilized by $Co_{60}$ irradiation. Before cell seeding, the scaffolds were prewetted with MEM for 24 h to displace air from the scaffolds. The MC3T3-E1 cells were digested by trypsin/EDTA solution and suspended in MEM at a concentration of $1 \times 10^6$ cell/mL. A total of 50 $\mu$L of cell suspension was seeded onto each scaffold

surface. The seeded scaffolds were incubated at 37°C with 5% $CO_2$ to allow cells to attach. After 4 h, an additional 1 mL of medium was added to each well. The culture medium was refreshed every two days. After 3, 7, and 14 days, the cell-scaffold constructs were analyzed.

*2.10. Cell Viability and Proliferation.* Evaluation of the cell viability and proliferation on the scaffolds was performed by fluorescence staining and the CCK-8 assay. For fluorescence staining, each cell-scaffold was carefully washed with PBS and the nuclei were stained with 4′,6-diamidino-2-phenylindole (DAPI) solution (1 : 1000 DAPI in PBS) for 10 min. The cell-scaffolds were analyzed using a fluorescence microscope (TS100, Nikon, Japan). For the CCK-8 assay, the cell-seeded scaffolds were transferred to new 48-well plates and incubated with 1 mL fresh MEM medium containing 10 $\mu$L CCK-8 at 37°C with 5% $CO_2$ for 3 h. An unseeded scaffold was used as a control. A total of 100 $\mu$L of reaction liquid was transferred to a 96-well plate to measure the absorbance at 450 nm using a microplate reader (Power Wave XS2, Gene Company, USA). Scaffolds with medium but without cells were used to assess the background absorbance. The degree of cell proliferation was determined after 3, 7, and 14 days of culture. Five cell-scaffold constructs were tested each time.

*2.11. Morphological Analysis.* Scanning electron microscopy was used to observe the morphology of cells adhered to the scaffolds. After 7 and 14 days of culture, the cell-seeded scaffolds were rinsed with PBS and fixed with 2.5% glutaraldehyde in phosphate buffer (pH 7.4) at 4°C for 4 h. The scaffolds were dehydrated in increasing concentrations of ethanol (30%, 50%, 70%, 90%, 95%, and 100%) and critically point-dried. The dried cell-scaffolds were mounted on aluminum stubs and sputter-coated with gold for SEM.

*2.12. Statistical Analysis.* The data were analyzed using the Statistical Analysis System (SAS 9.0) package software for analysis of variance using Duncan's test. All experiments were carried out in triplicate. Significance was established at $P \leq 0.05$.

## 3. Results

*3.1. Effects of Processing Parameters on the Properties of Scaffolds.* The porosity for the different samples is reported in Table 1. With the ratio of HLC to n-HAp decreasing from 1 : 2 to 1 : 6, the porosity of the scaffolds decreased from approximately 89.3±4.1% to 51.57±1.5%. This was coincident with the SEM images of the different samples, as shown in Figure 1. The samples with ratios of 1 : 2, 1 : 3, and 1 : 4 had homogeneous pores that were interconnected. The samples with ratios of 1 : 5 and 1 : 6 had weakly interconnected pores that were inhomogeneous. The effects of different composites and the oleuropein concentration on the compressive strength and Young's modulus were investigated. As shown in Figure 2(a), increasing the n-HAp content of the scaffolds to 80 wt.% increased the compressive strength and Young's modulus to 2.97±0.19 MPa and 43.03±6.17 MPa, respectively.

Table 1: Porosity of the composite scaffolds with different n-HAp contents.

| HLC : n-HAp ratio (w/w) | Porosity (%) |
|---|---|
| 1 : 2 | 89.3 ± 4.1 |
| 1 : 3 | 81.2 ± 2.8 |
| 1 : 4 | 73.6 ± 2.3 |
| 1 : 5 | 60.8 ± 2.0 |
| 1 : 6 | 51.6 ± 1.5 |

When the n-HAp content of the scaffolds was more than 80 wt.%, the brittleness of the scaffolds increased significantly. As shown in Figure 2(b), when the concentration of oleuropein solution reached 2% (w/v), the compressive strength and Young's modulus reached maximums of 2.97 ± 0.19 MPa and 43.03 ± 6.17 MPa, respectively. The composite scaffold with a porosity of 73.6 ± 2.3 and a compressive strength of 2.97 ± 0.19 was used for subsequent characterization and cell culture. The effect of the sterilization procedure by $Co_{60}$ irradiation on the HLC/n-HAp scaffold (HLC : n-HAp = 1 : 4, with concentration of oleuropein being 2%) was also investigated.

*3.2. Morphology of the HLC/n-HAp Composite Scaffolds.* The macroscopic view and the morphology of the HLC/n-HAp scaffolds are shown in Figures 3 and 4, respectively. The scaffolds (before and after $Co_{60}$ irradiation) had 3D porous structures with homogeneous pores ranging from 120 to 300 $\mu$m and the porosity was 73.6 ± 2.3%. The pores were interconnected, which might be helpful for water and nutrient transport. On the walls of the macropores there were smaller pores, with pore sizes less than 6 $\mu$m. The $Co_{60}$ irradiation sterilization procedure did not have any obvious influence on the scaffold morphology.

*3.3. Characterization of the HLC/n-HAp Composite Scaffolds.* Compression tests were conducted to assess the mechanical performance of the scaffolds. The compressive strength of the HLC/n-HAp scaffolds was enhanced by cross-linking, which indicated that the cross-linking process contributed to the superior mechanical properties of the scaffolds. Figure 5(a) shows the mechanical properties of the scaffolds before and after the sterilization by $Co_{60}$ irradiation. There was no obvious difference in the mechanical properties of the scaffold after sterilization.

As shown in Figure 5(b), the composite scaffolds displayed sharp and intense diffraction peaks at 25.8°, 31.8°, 33°, 34°, 39.8°, 46.7°, and 49.4°, which confirmed the presence of hydroxyapatite.

Figure 5(c) shows the FT-IR spectra of the scaffolds (before and after $Co_{60}$ irradiation), along with the spectra for n-HAp and HLC. In the n-HAp spectra, an absorption band associated with the –OH stretching vibration mode is clearly seen at 3436 $cm^{-1}$. The peaks at approximately 1039, 602, and 567 $cm^{-1}$ were assigned to $PO_4^{3-}$. The characteristic absorption peaks of HLC were 3429, 1650, and 1237 $cm^{-1}$, which were attributed to the N–H stretching vibration peaks,

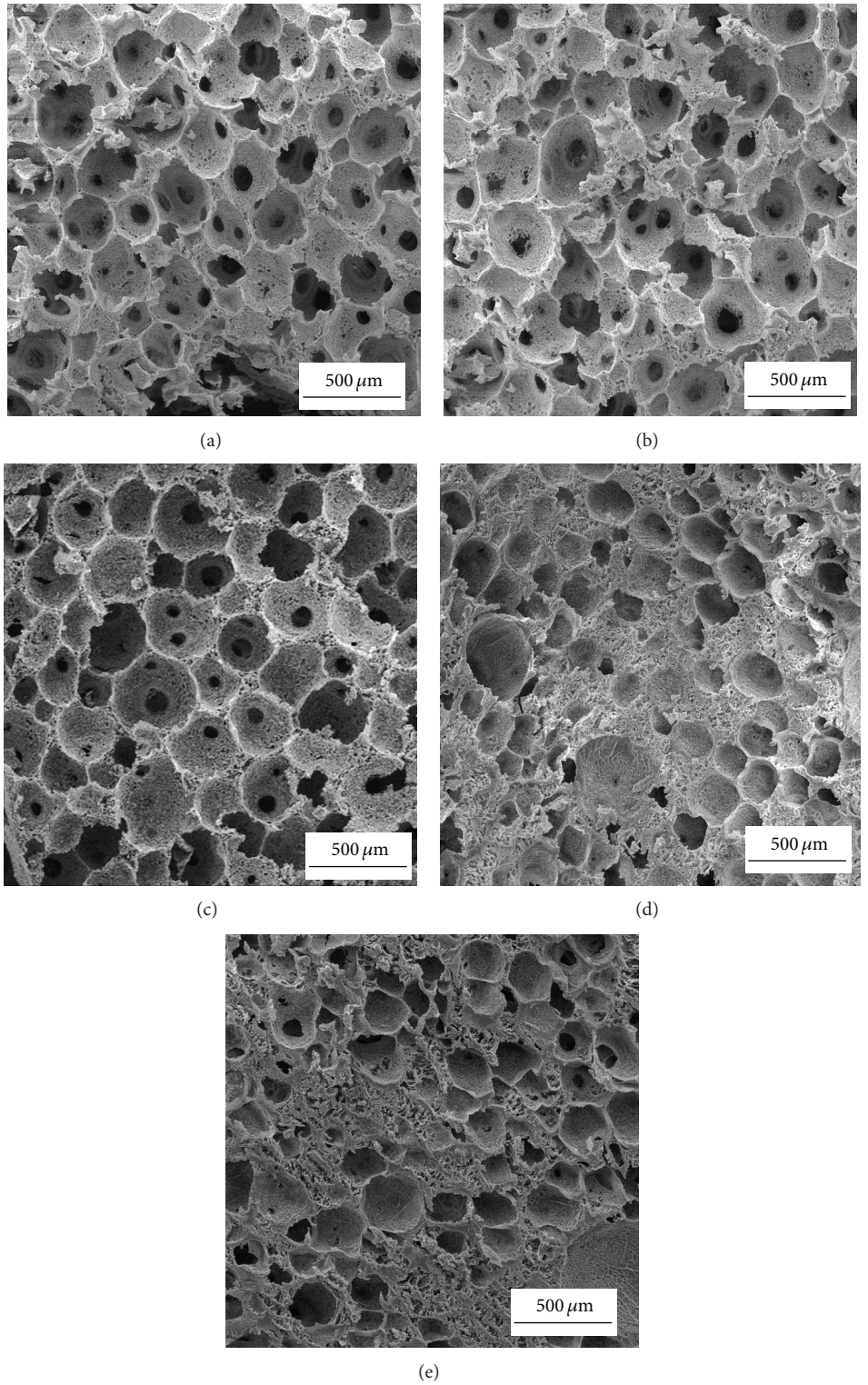


Figure 1: SEM images of different samples. The ratio of HLC/n-HAp is 1 : 2 (a), 1 : 3 (b), 1 : 4 (c), 1 : 5 (d), and 1 : 6 (e).

C=O peaks, and the combined peaks between the C–N stretching vibration and N–H bending vibration, respectively. These characteristic absorption peaks were also found in the spectra of the composite scaffolds. The scaffolds showed the same characteristic absorption peaks before and after $Co_{60}$ irradiation.

As observed from the TGA curve (Figure 5(d)), there were two main decreases in the mass of the HLC and

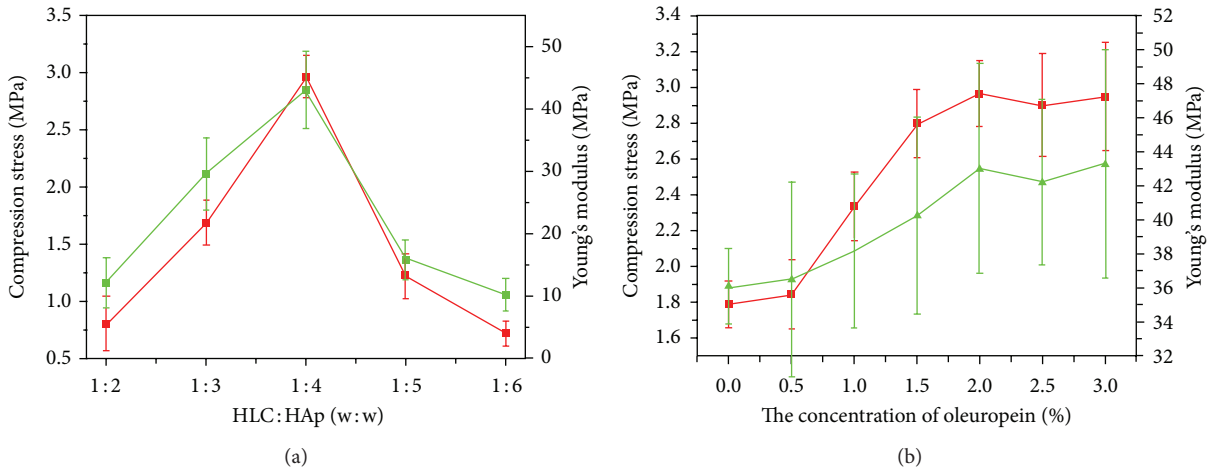


Figure 2: Compressive strength (red) and Young's modulus (green) for the different samples. (a) The composite scaffolds were formed with different n-HAp contents using a 2% solution of oleuropein. (b) The scaffolds were formed with different concentration of oleuropein at an HlC/n-HAp ratio of 1 : 4.

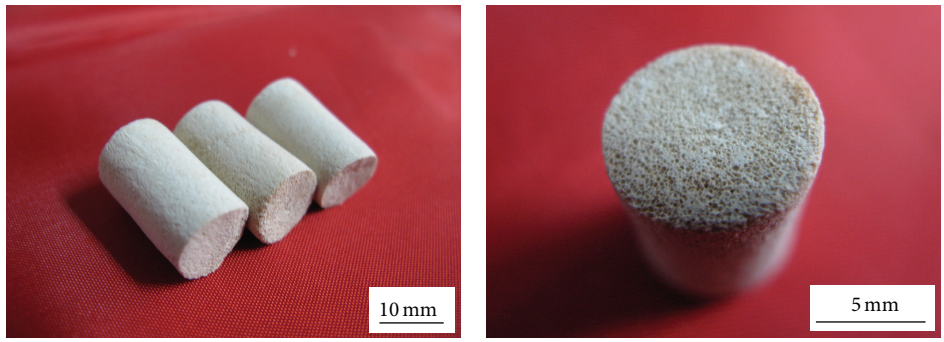


Figure 3: Images of (a) HLC/n-HAp scaffolds and (b) cross-sections with homogeneous pores.

HLC/n-HAp scaffolds (before and after $Co_{60}$ irradiation). The n-HAp did not have any obvious weight loss. The weight loss for the HLC and the scaffolds below 120°C could be attributed to the loss of freely bound water. From 250°C to 600°C, the significant decrease in the mass could be attributed to the decomposition of HLC. Thermal degradation of HLC began at 250°C, while the onset of thermal degradation for the scaffolds was approximately 300°C. The electrostatic interaction between HLC and n-HAp, as well as the cross-linking procedure, resulted in an altered thermal degradation profile. The $Co_{60}$ irradiation had no obvious influence on the thermal stability of the scaffolds.

*3.4. Cell Viability and Proliferation.* We evaluated the viability and proliferation of MC3T3-E1 cells on the as-prepared scaffolds. Figure 6 shows fluorescence images of the cell-scaffolds incubated for 7 and 14 days. With increasing culture time, more area was covered by the cells. It was clear that the MC3T3-E1 cells adhered and proliferated well. As shown in Figure 7, the CCK-8 assay revealed that the absorbance values increased significantly with culture time. This suggested that the pores and the surfaces of the scaffolds enhanced cell adhesion and proliferation. These results further indicate that the HLC/n-HAp scaffolds are nontoxic and biocompatible.

*3.5. Cell Morphology.* SEM images of the cells grown on the scaffolds are shown in Figure 8. A greater number of MC3T3-E1 cells were observed to attach, spread, and proliferate at 7 and 14 days on the scaffolds. After 7 days of incubation, almost all of the scaffold surfaces were covered with spherical cells. The cells extended more cellular protrusions and connected with each other by way of these structures. After 14 days in culture, the cells produced a large amount of extracellular matrix (ECM), in which the cells were embedded.

## 4. Discussion

A new strategy to fabricate biodegradable scaffolds with more than two components with different physicochemical properties was proposed for bone tissue engineering, when a one-component scaffold cannot suffice [22, 23]. In this study, an HLC/n-HAp scaffold was fabricated, which preserved the

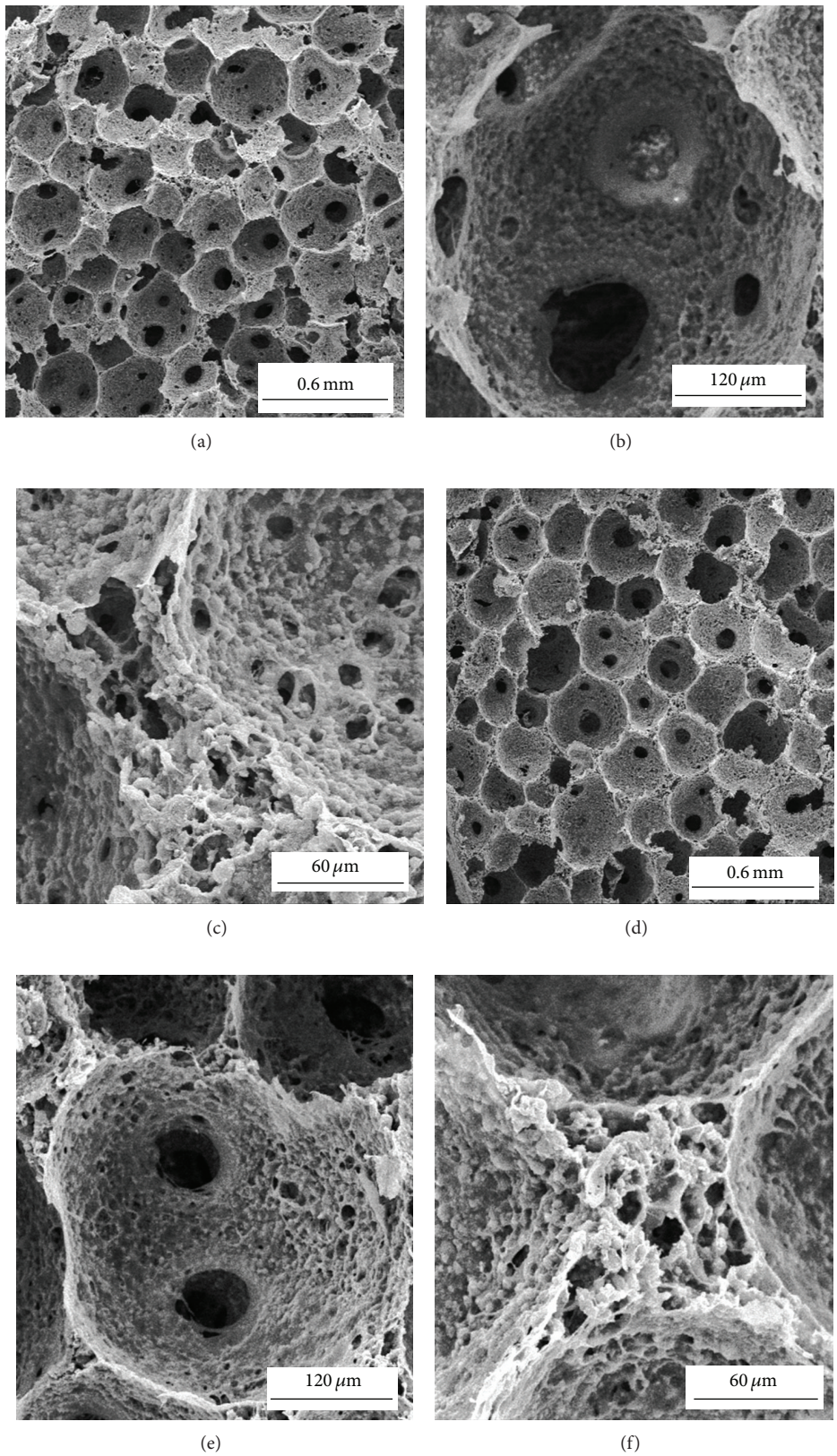


Figure 4: SEM images of the cross-sectional surfaces of the HLC/n-HAp scaffolds before ((a), (b), and (c)) and after ((d), (e), and (f)) $Co_{60}$ irradiation. ((a), (d)) The scaffolds display interconnected pores ranging in size from 120 to 300 $\mu$m. ((b), (e)) A typical macroporous microstructure for the scaffolds. ((c), (f)) The pore walls in the scaffold.

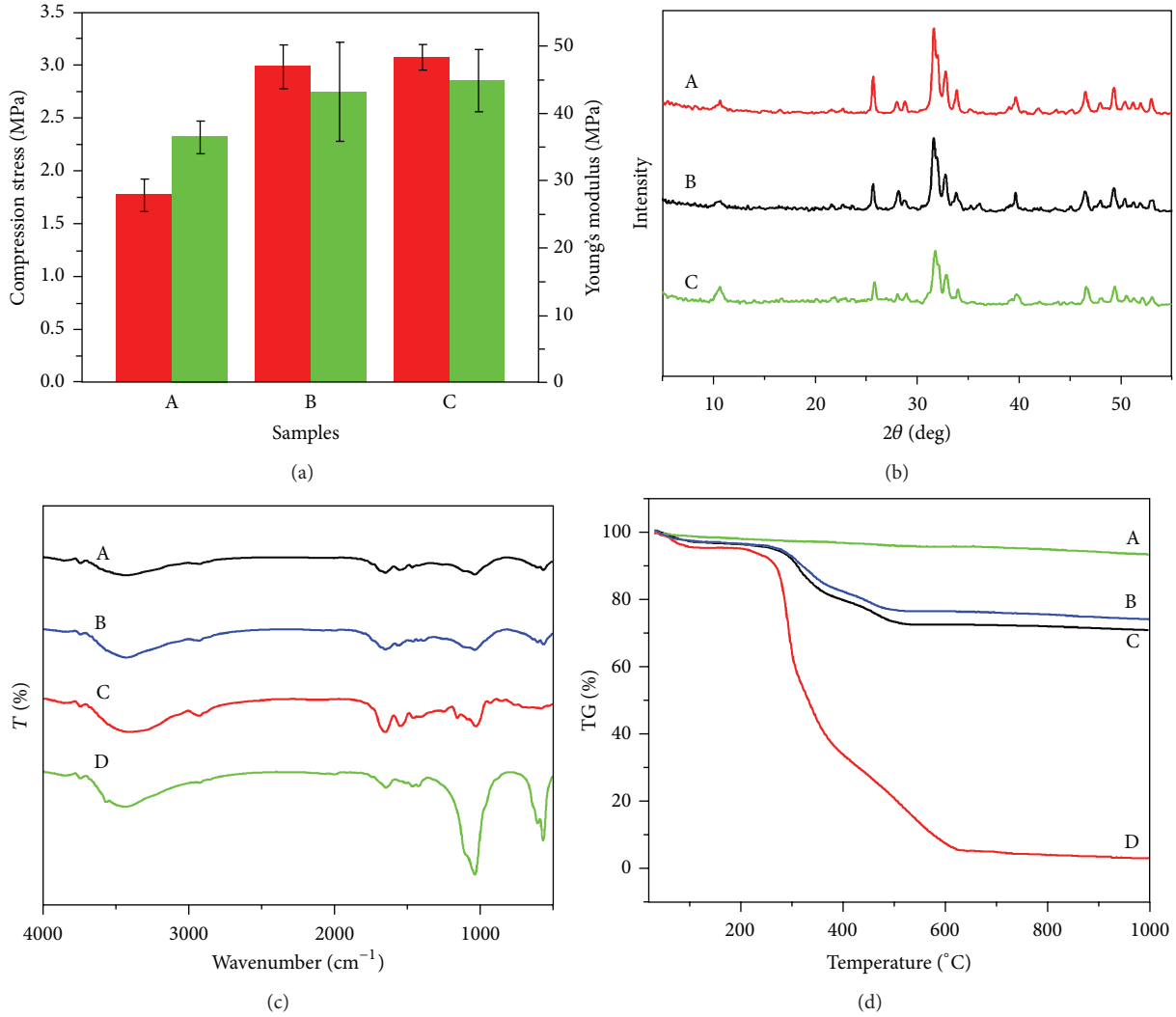


Figure 5: HLC/n-HAp scaffolds characterization. (a) Compressive strength (in red) and Young's modulus (in green) of the scaffolds (A) after and (B) before the cross-linking procedure and (B) before and (C) after $Co_{60}$ irradiation. (b) XRD patterns for (A) the n-HAp, HLC/n-HAp scaffolds (B) before and (C) after $Co_{60}$ irradiation. (c) FT-IR spectra for the HLC/n-HAp scaffolds (A) before, (B) after $Co_{60}$ irradiation, (C) for HLC, and (D) for n-HAp. (d) TGA curves for the (A) n-HAp, HLC/n-HAp scaffolds (B) after, (C) before $Co_{60}$ irradiation, and (D) for HLC.

biological characteristics of the HLC and the mechanical properties and osteoconductivity of the n-HAp. We fabricated highly porous 3D structure scaffolds with homogeneous and interconnected pores by slow cooling and vacuum freeze-drying. These water-soluble scaffolds were transformed into water-insoluble scaffolds using the natural cross-linking agent oleuropein. After cross-linking, another freeze-drying step was performed.

In bone tissue engineering, it is important to have the appropriate pore sizes for cell adhesion and tissue reconstruction. The pore size greatly affects the cellular activity. Even subtle changes in pore size may have significant effects on cell adhesion [24]. It has been reported that small pore sizes can limit cell migration and colonization [25, 26], vascular ingrowth, and nutrient and water transfer [27]. Furthermore, smaller pore sizes can influence the cell distribution in the scaffolds. However, if the pore size is too large, it can influence cell adhesion. Large pore sizes affect the construct and mechanical properties of the scaffolds. Moreover, it is difficult to create a suitable environment for the production of ECM in scaffolds with large pore sizes [28]. Freeze-drying has proved to be a gentle drying method that can be used to obtain scaffolds with appropriate pore size and interconnectivity [29]. As shown in Figures 3(b) and 4, the pores of the HLC/n-HAp scaffolds are homogeneous and interconnected. The SEM images (Figure 8) indicate that cells are contained within the scaffold pores, forming bridges over the pores (Figure 8(e)). The cells connected with neighboring cells by way of the pore structures. The HLC/n-HAp scaffolds promoted MC3T3-E1 ECM production, which is essential for bone formation.

An ideal tissue engineering scaffold provides sufficient mechanical properties and high porosity, both of which are key determinant factors for implantation. Proper mechanical

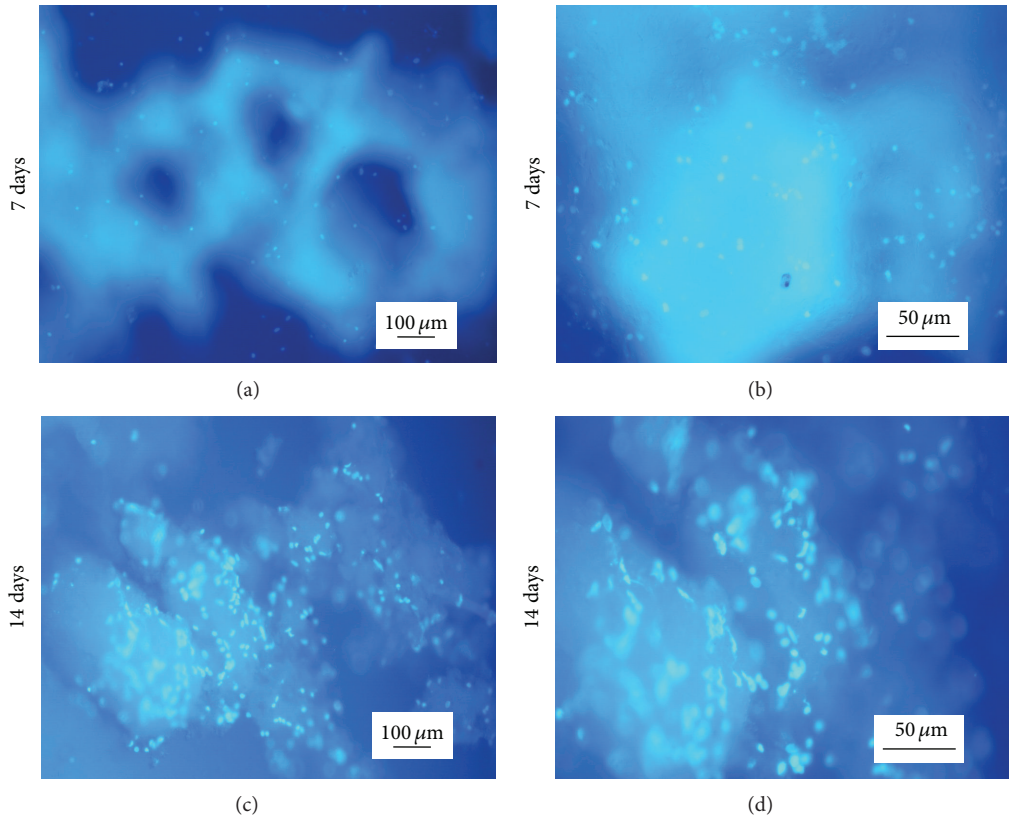


Figure 6: Fluorescence images of MC3T3-E1 cells cultured on the HLC/n-HAp scaffolds for ((a), (b)) 7 days and ((c), (d)) 14 days. ((a), (c)) Low magnification views of the cell-scaffolds. ((b), (d)) Magnified views of the cells on the pore walls of the scaffolds. The scale bars in the left column and right column represent 100 $\mu$m and 50 $\mu$m, respectively.

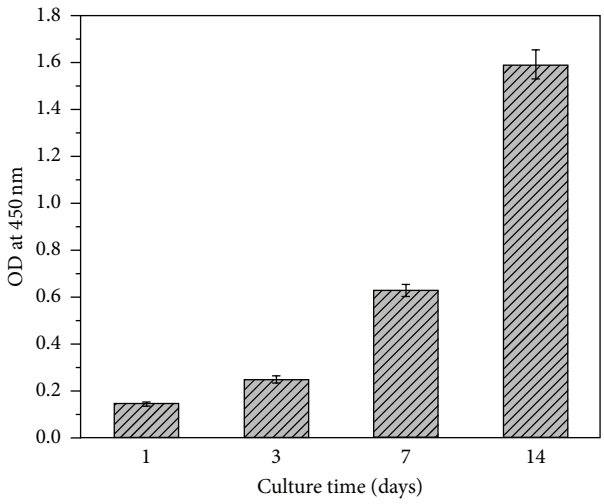


Figure 7: CCK-8 assay for attachment and proliferation of MC3T3-E1 cells on the HLC/n-HAp scaffolds over various incubation periods. Error bars represent means ± SD ($n = 5$).

properties and porosity are needed to supply temporary support for vascularization and tissue ingrowth [30]. However, exceedingly high porosity can reduce the mechanical property of the scaffolds. The compressive strength is also closely tied to the proportion of inorganic and organic ingredients [31]. In this case, an HLC and n-HAp ratio of 1 : 4 was employed to obtain a better scaffold with a porosity of 73.6 ± 2.3% and a mechanical strength of 3 MPa. In addition, the cross-linking process further contributed to the mechanical properties, as shown in Figure 5(a).

The rate and quality of new tissue formation are greatly affected by the initial cell adhesion to the scaffolds. Cell adhesion is influenced by the scaffold surface characteristics, such as the surface chemical composition, surface topography, surface multicavities, and roughness [32]. Higher initial cell adhesion requires adhesion proteins that are abundant in the serum. The n-HAp nanoscale crystals have a high binding affinity to the serum proteins [33]. When a higher degree of proteins is absorbed on the scaffold surface, it could provide more attachment sites for the cells. In this study, the use of nanoscale n-HAp greatly promoted cell adhesion. In addition, the surface roughness (Figures 4(c) and 4(f)) could improve cell-biomaterial response, adding cellular adhesion, growth, migration, and differentiation. The cell spreading and proliferation significantly increase on rough surfaces, compared to smoother surfaces [32]. As shown in the SEM images, the cells established close contact with the scaffold surface, displaying spherical morphologies (Figures 8(c) and 8(f)) with numerous filopodia and lamellipodia (Figures 8(d), 8(e), and 8(f)).

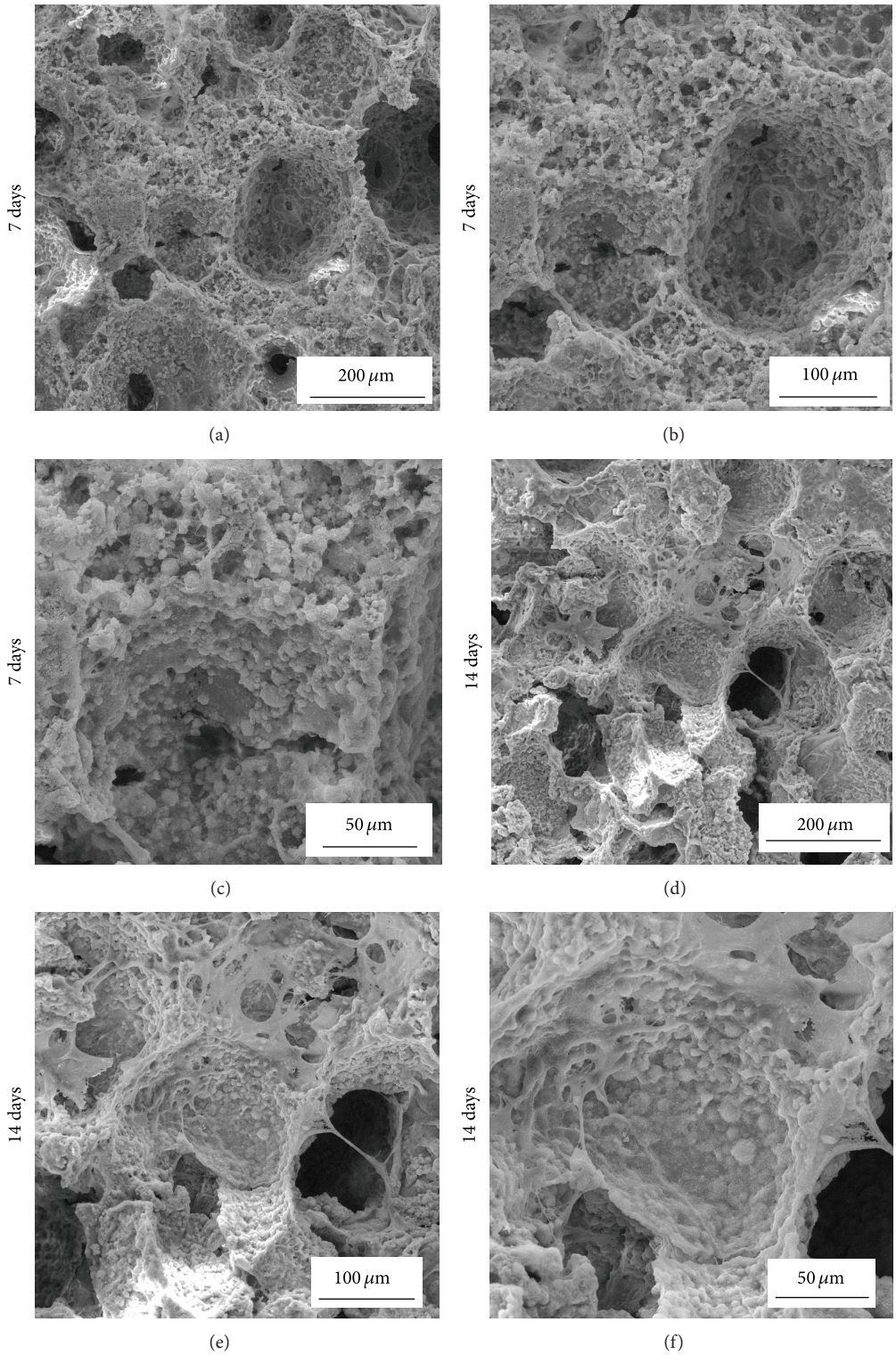


Figure 8: SEM images of MC3T3-E1 cells cultured on the HLC/n-HAp scaffolds for 7 ((a), (b), and (c)) and 14 ((d), (e), and (f)) days. The scale bars in the left column, middle column, and right column represent 200 $\mu$m, 100 $\mu$m, and 50 $\mu$m, respectively.

Cytotoxicity must be evaluated for all scaffolds used in bone tissue engineering. In this study, the natural cross-linking agent oleuropein was used. The most common cross-linking agents, glutaraldehyde and carbodiimide, are cytotoxic and may negatively affect the cells [34]. In our study, the natural cross-linking agent, oleuropein, was assessed using the CCK-8 assay. As shown in Figure 7, the composite HLC/n-HAp scaffolds are biocompatible and can thus serve as suitable materials for biomedical applications.

## 5. Conclusion

A composite HLC/n-HAp system with interconnected pores was prepared by cross-linking. The as-prepared scaffolds were characterized using SEM, XRD, FTIR, and TGA. In addition, the porosity, compressive strength, cytotoxicity, cell adhesion, and proliferation of the scaffolds were investigated. The scaffolds had interconnected pores ranging from 120 to 300 $\mu$m. The cells attached well to the pore walls, extending cellular protrusions and producing large amounts of ECM. The HLC/n-HAp scaffolds were noncytotoxic and biocompatible. The scaffolds preserved the outstanding biological characteristics of HLC and the excellent osteoconductivity of n-HAp. Therefore, the HLC/n-HAp scaffolds obtained by oleuropein cross-linking have potential for use in bone tissue engineering.

## Conflict of Interests

The authors declare that there is no conflict of interests regarding the publication of this paper.

## Authors' Contribution

Hui Fan and Junfeng Hui are co-first authors; they contributed equally to this paper.

## Acknowledgments

This study was financially supported by the National Natural Science Foundation of China (21276210, 21106112, 21106111, 21106114, 31000019, 21206135, and 21376190); the National High Technology Research and Development Program of China (863 Program, 2014AA02108); the Shaanxi Provincial Scientific Technology Research and Development Program (2007K06-03, 2011JE003, 2012JQ2019, 2012KJXX-28, 2013KJXX-28, and 2011JQ4026); and the Scientific Research Program of Shaanxi Provincial Department of Education, China (12JK0449, 13JS106, 13JS105, 13JS104, and 2013JK0696).

## References

[1] R. Z. LeGeros, "Calcium phosphate-based osteoinductive materials," *Chemical Reviews*, vol. 108, no. 11, pp. 4742–4753, 2008.

[2] W. G. de Long Jr., T. A. Einhorn, K. Koval et al., "Bone grafts and bone graft substitutes in orthopaedic trauma surgery: a critical analysis," *Journal of Bone and Joint Surgery A*, vol. 89, no. 3, pp. 649–658, 2007.

[3] V. Mouriño and A. R. Boccaccini, "Bone tissue engineering therapeutics: controlled drug delivery in three-dimensional scaffolds," *Journal of the Royal Society Interface*, vol. 7, no. 43, pp. 209–227, 2010.

[4] J. F. A. Valente, T. A. M. Valente, P. Alves, P. Ferreira, A. P. Silva, and I. J. Correia, "Alginate based scaffolds for bone tissue engineering," *Materials Science and Engineering C*, vol. 32, no. 8, pp. 2596–2603, 2012.

[5] H. Seyednejad, D. Gawlitta, W. J. A. Dhert, C. F. van Nostrum, T. Vermonden, and W. E. Hennink, "Preparation and characterization of a three-dimensional printed scaffold based on a functionalized polyester for bone tissue engineering applications," *Acta Biomaterialia*, vol. 7, no. 5, pp. 1999–2006, 2011.

[6] G. Wei and P. X. Ma, "Structure and properties of nano-hydroxyapatite/polymer composite scaffolds for bone tissue engineering," *Biomaterials*, vol. 25, no. 19, pp. 4749–4757, 2004.

[7] K. S. Jack, S. Velayudhan, P. Luckman, M. Trau, L. Grøndahl, and J. Cooper-White, "The fabrication and characterization of biodegradable HA/PHBV nanoparticle-polymer composite scaffolds," *Acta Biomaterialia*, vol. 5, no. 7, pp. 2657–2667, 2009.

[8] D. W. Hutmacher, "Scaffolds in tissue engineering bone and cartilage," *Biomaterials*, vol. 21, no. 24, pp. 2529–2543, 2000.

[9] J. R. Jones and L. L. Hench, "Regeneration of trabecular bone using porous ceramics," *Current Opinion in Solid State and Materials Science*, vol. 7, no. 4-5, pp. 301–307, 2003.

[10] V. Karageorgiou and D. Kaplan, "Porosity of 3D biomaterial scaffolds and osteogenesis," *Biomaterials*, vol. 26, no. 27, pp. 5474–5491, 2005.

[11] X. Hua, D. Fan, Y. Luo et al., "Kinetics of high cell density fed-batch culture of recombinant escherichia coli producing human-like collagen," *Chinese Journal of Chemical Engineering*, vol. 14, no. 2, pp. 242–247, 2006.

[12] C. Zhu, D. Fan, X. Ma et al., "Effects of chitosan on properties of novel human-like collagen/chitosan hybrid vascular scaffold," *Journal of Bioactive and Compatible Polymers*, vol. 24, no. 6, pp. 560–576, 2009.

[13] C. Zhu, D. Fan, Z. Duan et al., "Initial investigation of novel human-like collagen/chitosan scaffold for vascular tissue engineering," *Journal of Biomedical Materials Research A*, vol. 89, no. 3, pp. 829–840, 2009.

[14] Y. Wang, F. Z. Cui, K. Hu, X. D. Zhu, and D. D. Fan, "Bone regeneration by using scaffold based on mineralized recombinant collagen," *Journal of Biomedical Materials Research B: Applied Biomaterials*, vol. 86, no. 1, pp. 29–35, 2008.

[15] X. Li, X. Ma, D. Fan, and C. Zhu, "New suitable for tissue reconstruction injectable chitosan/collagen-based hydrogels," *Soft Matter*, vol. 8, no. 14, pp. 3781–3790, 2012.

[16] K. Hu, F. Cui, Q. Lv et al., "Preparation of fibroin/recombinant human-like collagen scaffold to promote fibroblasts compatibility," *Journal of Biomedical Materials Research A*, vol. 84, no. 2, pp. 483–490, 2008.

[17] P. N. de Aza, Z. B. Luklinska, C. Santos, F. Guitian, and S. de Aza, "Mechanism of bone-like formation on a bioactive implant in vivo," *Biomaterials*, vol. 24, no. 8, pp. 1437–1445, 2003.

[18] T. Livingston, P. Ducheyne, and J. Garino, "In vivo evaluation of a bioactive scaffold for bone tissue engineering," *Journal of Biomedical Materials Research*, vol. 62, no. 1, pp. 1–13, 2002.

[19] R. O. Beauchamp Jr., M. B. G. St. Clair, T. R. Fennell, D. O. Clarke, K. T. Morgan, and F. W. Kari, "A critical review of the toxicology of glutaraldehyde," *Critical Reviews in Toxicology*, vol. 22, no. 3-4, pp. 143–174, 1992.

[20] J. C. Isenburg, N. V. Karamchandani, D. T. Simionescu, and N. R. Vyavahare, "Structural requirements for stabilization of vascular elastin by polyphenolic tannins," *Biomaterials*, vol. 27, no. 19, pp. 3645–3651, 2006.

[21] C. Puel, A. Quintin, A. Agalias et al., "Olive oil and its main phenolic micronutrient (oleuropein) prevent inflammation-induced bone loss in the ovariectomised rat," *British Journal of Nutrition*, vol. 92, no. 1, pp. 119–127, 2004.

[22] K. Rezwan, Q. Z. Chen, J. J. Blaker, and A. R. Boccaccini, "Biodegradable and bioactive porous polymer/inorganic composite scaffolds for bone tissue engineering," *Biomaterials*, vol. 27, no. 18, pp. 3413–3431, 2006.

[23] C. Xu, P. Su, X. Chen et al., "Biocompatibility and osteogenesis of biomimetic Bioglass-Collagen-Phosphatidylserine composite scaffolds for bone tissue engineering," *Biomaterials*, vol. 32, no. 4, pp. 1051–1058, 2011.

[24] C. M. Murphy, M. G. Haugh, and F. J. O'Brien, "The effect of mean pore size on cell attachment, proliferation and migration in collagen-glycosaminoglycan scaffolds for bone tissue engineering," *Biomaterials*, vol. 31, no. 3, pp. 461–466, 2010.

[25] E. D. Boland, J. A. Matthews, K. J. Pawlowski, D. G. Simpson, G. E. Wnek, and G. L. Bowlin, "Electrospinning collagen and elastin: preliminary vascular tissue engineering," *Frontiers in Bioscience*, vol. 9, pp. 1422–1432, 2004.

[26] A. S. Badami, M. R. Kreke, M. S. Thompson, J. S. Riffle, and A. S. Goldstein, "Effect of fiber diameter on spreading, proliferation, and differentiation of osteoblastic cells on electrospun poly(lactic acid) substrates," *Biomaterials*, vol. 27, no. 4, pp. 596–606, 2006.

[27] J. H. Brauker, V. E. Carr-Brendel, L. A. Martinson, J. Crudele, W. D. Johnston, and R. C. Johnson, "Neovascularization of synthetic membranes directed by membrane microarchitecture," *Journal of Biomedical Materials Research*, vol. 29, no. 12, pp. 1517–1524, 1995.

[28] S. Grad, L. Kupcsik, K. Gorna, S. Gogolewski, and M. Alini, "The use of biodegradable polyurethane scaffolds for cartilage tissue engineering: potential and limitations," *Biomaterials*, vol. 24, no. 28, pp. 5163–5171, 2003.

[29] J. S. Mao, L. G. Zhao, Y. J. Yin, and K. D. Yao, "Structure and properties of bilayer chitosan-gelatin scaffolds," *Biomaterials*, vol. 24, no. 6, pp. 1067–1074, 2003.

[30] A. Nemati Hayati, S. M. Hosseinalipour, H. R. Rezaie, and M. A. Shokrgozar, "Characterization ofpoly(3-hydroxybutyrate)/nano-hydroxyapatite composite scaffolds fabricated without the use of organic solvents for bone tissue engineering applications," *Materials Science and Engineering C*, vol. 32, no. 3, pp. 416–422, 2012.

[31] B. Li, L. Huang, X. Wang, J. Ma, and F. Xie, "Biodegradation and compressive strength of phosphorylated chitosan/chitosan/hydroxyapatite bio-composites," *Materials and Design*, vol. 32, no. 8-9, pp. 4543–4547, 2011.

[32] S. Huang and X. Fu, "Cell behavior on microparticles with different surface morphology," *Journal of Alloys and Compounds*, vol. 493, no. 1-2, pp. 246–251, 2010.

[33] H.-W. Kim, H.-E. Kim, and V. Salih, "Stimulation of osteoblast responses to biomimetic nanocomposites of gelatin-hydroxyapatite for tissue engineering scaffolds," *Biomaterials*, vol. 26, no. 25, pp. 5221–5230, 2005.

[34] J. E. Gough, C. A. Scotchford, and S. Downes, "Cytotoxicity of glutaraldehyde crosslinked collagen/poly(vinyl alcohol) films is by the mechanism of apoptosis," *Journal of Biomedical Materials Research*, vol. 61, no. 1, pp. 121–130, 2002.